EXPERIMENTAL ASSESSMENT OF SOLAR THERMAL ENERGY STORAGE IN BASALTIC ROCK FILL

Decho Phueakphum

A Thesis Submitted in Partial Fulfillment of the Requirements for the

Doctor of Philosophy of Engineering in Geotechnology

Suranaree University of Technology

Academic Year 2008

การทดสอบการกักเก็บพลังงานความร้อนจากแสงอาทิตย์
ในหินถมบะซอลต์

นายเดโช เผือกภูมิ

วิทยานิพนธ์นี้เป็นส่วนหนึ่งของการศึกษาตามหลักสูตรปริญญาวิศวกรรมศาสตรดุษฎีบัณฑิต

สาขาวิชาเทคโนโลยีธรณี

มหาวิทยาลัยเทคโนโลยีสุรนารี

ปีการศึกษา 2551

EXPERIMENTAL ASSESSMENT OF SOLAR THERMAL ENERGY STORAGE IN BASALTIC ROCK FILL

Suranaree University of Technology has approved this thesis submitted in partial fulfillment of the requirements for the Degree of Doctor of Philosophy.

Thesis Examining Committee

____

(Asst. Prof. Thara Lekuthai)

Chairperson

____

(Assoc. Prof. Dr. Kittitep Fuenkajorn)

Member (Thesis Advisor)

____

(Asst. Prof. Dr. Anant Oonsivilai)

Member

____

(Assoc. Prof. Ladda Wannakao)

Member

____

(Dr. Prachaya Tepnarong)

Member

____________________________________	____________________________________
(Prof. Dr. Pairote Sattayatham)	(Assoc. Prof. Dr. Vorapot Khompis)
Vice Rector for Academic Affairs	Dean of Institute of Engineering

เดโช เผือกภูมิ : การทดสอบการกักเก็บพลังงานความร้อนจากแสงอาทิตย์ในหินถมบะซอลต์ (EXPERIMENTAL ASSESSMENT OF SOLAR THERMAL ENERGY STORAGE IN ROCK FILLS) อาจารย์ที่ปรึกษา : รองศาสตราจารย์ ดร.กิตติเทพ เฟื่องขจร, 222 หน้า.

วัตถุประสงค์ของงานวิจัยนี้คือ เพื่อทดสอบศักยภาพระบบการกักเก็บพลังงานความร้อนจากแสงอาทิตย์ไว้ในหินถมในเวลากลางวันและนำความร้อนที่ได้มาใช้ในเวลากลางคืน ซึ่งเป็นประโยชน์สำหรับให้ความอบอุ่นแก่อาคารบ้านเรือนในพื้นที่ที่ประสบภัยหนาว และยังช่วยลดค่าใช้จ่ายด้านพลังงานแก่โรงบ่มเมล็ดพันธุ์พืช โรงเลี้ยงสัตว์ ตัวอย่างหินมากกว่า 10 ชนิดที่พบอยู่ทั่วไปในประเทศไทยได้นำมาทดสอบเพื่อหาคุณสมบัติด้านความจุความร้อนจำเพาะและสัมประสิทธิ์การส่งผ่านความร้อนเพื่อใช้เป็นข้อมูลในการคัดเลือกตัวอย่างหินที่จะมาใช้ในการออกแบบและสร้างแบบจำลองย่อส่วน ผลที่ได้พบว่าหินบะซอลต์จากจังหวัดบุรีรัมย์มีความเหมาะสมที่สุดเนื่องจากมีค่าความจุความร้อนสูงที่สุด ระบบการกักเก็บพลังงานความร้อนจากแสงอาทิตย์ถูกทดสอบโดยการสร้างแบบจำลองย่อส่วนซึ่งประกอบด้วย ระบบกักเก็บพลังงานที่สร้างโดยใช้หินบะซอลต์ย่อยและมีท่ออากาศร้อนเชื่อมต่อบริเวณส่วนบนของระบบกักเก็บเข้ากับบ้านจำลองที่สร้างจากไม้ และทำการตรวจวัดอุณหภูมิของระบบในหลายจุดตลอดฤดูหนาว ผลการตรวจวัดระบุว่าประสิทธิภาพของระบบกักเก็บขึ้นกับระดับพลังงานแสงอาทิตย์ ขนาดของท่ออากาศร้อน การสูญเสียพลังงานความร้อนในบ่อกักเก็บพลังงานและในบ้านจำลอง ระบบที่มีความเหมาะสมมากที่สุดได้แก่ ระบบที่ใช้ท่ออากาศร้อนมีขนาดเส้นผ่านศูนย์กลางมากกว่า 10.2 เซนติเมตร โดยติดตั้งให้เอียงมากกว่า 30 องศา ส่วนบนของบ่อกักเก็บพลังงานควรจะคลุมด้วยวัสดุที่เป็นฉนวนความร้อน ซึ่งสามารถทำให้อุณหภูมิในบ้านจำลองสูงขึ้นจากอุณหภูมิปกติประมาณ 5 องศาเซลเซียสเป็นอย่างน้อย อุณหภูมิที่สูงขึ้นนี้เป็นการเปรียบเทียบกับอุณหภูมินอกบ้านและอุณหภูมิของบ้านที่มีการตรวจวัดโดยไม่เปิดท่อนำความร้อน อย่างไรก็ตาม เมื่อถึงเวลา 9:00 น. อุณหภูมิในบ่อกักเก็บความร้อนยังคงสูงกว่าอุณหภูมิในบ้านจำลองอยู่มาก อาจเป็นผลมาจากการส่งผ่านความร้อนของระบบยังไม่มีประสิทธิภาพดีเท่าที่ควร ระบบกักเก็บมีประสิทธิภาพเท่ากับ 35 เปอร์เซ็นต์ และเมื่อใช้ท่ออาการร้อนที่มีเส้นผ่านศูนย์กลางเท่ากับ 10.2 เซนติเมตร จะให้อุณหภูมิในบ้านที่เพิ่มขึ้นมีค่าเทียบเท่ากับพลังงานไฟฟ้าจำนวน 203.3 kJ.hr

สมการทางคณิตศาสตร์ได้ถูกพัฒนาขึ้นเพื่อใช้เพิ่มศักยภาพของระบบด้วยการเปรียบเทียบอุณหภูมิในบ้านจำลองและบ่อกักเก็บพลังงานขณะที่มีการถ่ายเทพลังงานความร้อน อุณหภูมิที่ได้จากการคำนวณด้วยสมการดังกล่าวถูกนำไปเปรียบเทียบกับผลที่ตรวจวัดจริง ผลที่ได้พบว่ามีความใกล้เคียงและสอดคล้องกันเป็นอย่างดี และสรุปได้ว่าสมการทางคณิตศาสตร์ที่พัฒนาขึ้นนี้มีความ

น่าเชื่อถือและเหมาะสมที่จะนำไปใช้ทำนายอุณหภูมิในระบบภายใต้ตัวแปรที่หลากหลาย และจากการเปรียบเทียบผลยังพบว่าบ้านจำลองที่สร้างขึ้นมีการรั่วไหลของพลังงานความร้อนออกจากบ้านไปสู่สิ่งแวดล้อมประมาณ 10 เปอร์เซ็นต์ของพลังงานที่ได้จากบ่อกักเก็บพลังงาน ตัวแปรจากการวิเคราะห์ความอ่อนไหว ได้แก่ ปริมาตรบ้านจำลอง ปริมาตรของหินถม พื้นที่รับพลังงานแสงอาทิตย์ และขนาดของท่ออากาศร้อน ได้ถูกมาใช้ในการคำนวณประกอบคำแนะนำในการออกแบบระบบหินถม คำแนะนำในการออกแบบหินถมได้พัฒนาภายใต้เงื่อนไขที่ว่าไม่มีการรั่วไหลของบ้านจำลองและอุณหภูมิของสิ่งแวดล้อมมีค่าต่ำสุดที่เวลา 6.00 น. เท่ากับ 0 องศาเซลเซียส ผลที่ได้จากการวิเคราะห์ระบุว่าการที่หินถมมีพื้นที่รับพลังงานแสงอาทิตย์เพิ่มขึ้นจะทำให้อุณหภูมิในหินถมสูงขึ้นด้วย เนื่องจากสามารถรับพลังงานในปริมาณที่มากขึ้นด้วย นอกจากนี้ยังพบว่าความหนาของหินถมที่เหมาะสมอยู่ที่ประมาณ 30 ถึง 70 เซนติเมตร คำแนะนำในการออกแบบจะเสนอขึ้นในรูปแบบของแผนภูมิแบบให้เลือก โดยผู้ใช้ต้องระบุค่าอุณหภูมิในบ้านที่เพิ่มขึ้นและเลือกขนาดของท่อที่คาดว่าจะใช้บนแผนภูมิที่สร้างไว้ ดังนี้จะได้อัตราส่วนของปริมาตรบ้านต่อปริมาตรหินถมที่เหมาะสม

สาขาวิชา เทคโนโลยีธรณี ลายมือชื่อนักศึกษา____________________

ปีการศึกษา 2551 ลายมือชื่ออาจารย์ที่ปรึกษา________________

DECHO PHUEAKPHUM : EXPERIMENTAL ASSESSMENT OF SOLAR THERMAL ENERGY STORAGE IN ROCK FILLS. THESIS ADVISOR : ASSOC. PROF. KITTITEP FUENKAJORN, Ph.D., PE., 222 PP.

SOLAR ENERGY/STORAGE SYSTEM/ROCK FILL/SOLAR COLLECTOR/THERMAL CONDUCTIVITY/SPECIFIC HEAT

The objective of this research is to experimentally assess the performance of the solar thermal energy storage system using rock fills. The thermal energy stored during the daytime can be used to warm up housings and agricultural facilities during the night time which may result in a reduction of the required energy during the winter. Here over 10 rock types commonly found in Thailand have been tested to determine their specific heat and thermal conductivities. The results suggest that Burirum basalt is the most suitable rock for heat storage, as indicated by the highest specific heat value. The basalt fragments have been used in the pilot scale of the solar thermal storage system, comprising rock fills, housing model and connecting tubes. Temperatures have been monitored at various points in the system for two winter seasons. The results indicated that the storage system efficiency depends on the level of energy, size and inclination of hot-air tube, the heat loss through the pit and housing model. The most suitable connection between the housing and the pit is a 10.2-cm diameter hot-air tube with an inclined angle of 30°. The top of the pit should be covered with an isolation sheet. This results in a temperature increase in the housing model of 5°C over the ambient temperature. At 9:00 am of any day the temperature of the rock fills however remains higher than that of the housing model.

This indicates that the heat circulation within the system has not reached its top efficiency. The efficiency of the storage system is about 35 percent. The gained heat energy in housing model with 10.2 cm diameter hot-air tube is equivalent to the electrical energy of 203.3 kJ·hr.

The mathematical equations are used to improve the system efficiency by producing comparable temperatures in the housing and storage pit, during the heat transfer time. The heat transfer is simulated to compare with the actual temperature measured in the model. The calculated results agree with the measurements which can be concluded that the mathematical equations are reliable and suitable for the temperature predictions under different physical parameters. The heat loss from the housing model is calibrated at 10 percent of the total heat energy transfer. The variables from the sensitivity analysis including volume of the housing model, packed rock volume, collector area, and size of the hot-air tubes are considered for the design recommendations. The design guidelines of the rock-fill system have been developed under the assumptions that no heat energy leaks from the housing model and that the lowest surrounding air temperature at 6:00 pm is 0°C. The results indicate that the larger rock-fills volume and collector area give the higher temperature increase due to the rock-fills could store more heat energy. The suitable thickness of rock fills should be 30-70 cm. The user can apply the required temperature increase (ΔT) in the housing on the recommendation charts. The provided size of hot-air tube can be selected, and the housing volume to packed rock volume (V_h/V_b) ratio can be obtained.

School of Geotechnology Student's Signature_________________

Academic Year 2008 Advisor's Signature_________________

ACKNOWLEDGEMENTS

The author wishes to acknowledge the support from the Suranaree University of Technology (SUT) who has provided funding for this research.

Grateful thanks and appreciation are given to Assoc. Prof. Dr. Kittitep Fuenkajorn, thesis advisor, who lets the author work independently, but gave a critical review of this research. Many thanks are also extended to Asst. Prof. Thara Lekuthai, Asst. Prof. Dr. Anant Oonsivilai, Assoc. Prof. Ladda Wannakao, and Dr. Prachaya Tepnarong, who served on the thesis committee and commented on the manuscript.

Finally, I most gratefully acknowledge my parents and friends for all their supported throughout the period of this research.

Decho Phueakphum

TABLE OF CONTENTS

Page

TABLE OF CONTENTS (Continued)

Page

TABLE OF CONTENTS (Continued)

Page

TABLE OF CONTENTS (Continued)

Page

TABLE OF CONTENTS (Continued)

Page

TABLE OF CONTENTS (Continued)

Page

LIST OF TABLES

LIST OF FIGURES

Figure **Page**

LIST OF FIGURES (Continued)

Figure **Page**

LIST OF FIGURES (Continued)

Figure **Page**

LIST OF FIGURES (Continued)

Figure **Page**

LIST OF FIGURES (Continued)

Figure **Page**

LIST OF FIGURES (Continued)

Figure **Page**

LIST OF FIGURES (Continued)

Figure **Page**

LIST OF FIGURES (Continued)

Figure **Page**

LIST OF FIGURES (Continued)

Figure **Page**

LIST OF FIGURES (Continued)

Figure **Page**

LIST OF FIGURES (Continued)

Figure **Page**

LIST OF FIGURES (Continued)

Figure **Page**

LIST OF FIGURES (Continued)

LIST OF FIGURES (Continued)

Figure **Page**

LIST OF FIGURES (Continued)

Figure **Page**

LIST OF SYMBOLS AND ABBREVIATIONS

$\dot{m}$	=	air mass flow rate from the storage pit to the housing model
$\dot{Q}_{in,sun}$	=	energy gained from the solar irradiation (heat flux)
$\dot{Q}_{conv,r\_s}$	=	energy loss (heat flux) from the rocks surface to the air in the pit in form of convective air transfer
$\dot{Q}_{rad,r\_c}$	=	energy loss from the rock to the chamber or pit wall in form of radiation
$\dot{Q}_{rad,r\_s}$	=	energy loss from the rocks to the surrounding air in mode of radiation
$\dot{Q}_{loss3}$	=	energy loss in form of heat convection from the housing model to the surroundings
$\dot{Q}_{loss4}$	=	energy loss in form of heat radiation from the housing model to the surroundings
$\dot{Q}_{conv,r\_c}$	=	energy lost in form of heat convection from the rocks to the air in storage system
$\dot{Q}_{rad,r\_c}$	=	energy lost in form of heat radiation from the rocks to the air in storage system
$\sum \dot{Q}_{out}$	=	energy lost to the surroundings
q''	=	heat flux normal to the surface

LIST OF SYMBOLS AND ABBREVIATIONS (Continued)

$\dot{Q}_{loss2}$	=	heat loss from the air in storage system to the pit wall
$\dot{Q}_{loss1}$	=	heat loss from the air in storage system to the surrounding air
$\dot{Q}$	=	heat transfer rate
$\sum\dot{Q}_{in}$	=	income energy or solar radiation energy
$\dot{Q}_{leak}$	=	leaks of air in housing through the rift of the wall
$\dot{Q}_{emit,max}$	=	maximum rate of radiation
$\dot{Q}_{inc}$	=	rate at which radiation is incident on the surface
$\dot{Q}_{cond}$	=	rate of heat conduction
$\dot{Q}_{conv}$	=	rate of heat convection
C_{p,H_2O}	=	specific heat capacity of the water
T_r^n	=	temperature of the rock at the next time step
ρ	=	density
ρ_{air}	=	density of air
ρ_{H_2O}	=	water density
ρ_{rock}	=	density of the rock
ρ_s	=	particle density of soil solids
%leak	=	leakage of heat energy from the housing model
α	=	absorbtivity coefficient
δ	=	characteristic length

LIST OF SYMBOLS AND ABBREVIATIONS (Continued)

β	=	coefficient of volume expansion
ε	=	emissivity coefficient
ϕ	=	fraction porosity
ν	=	kinematics viscosity of air
ϕ	=	size of hot-air tube
θ	=	soil volumetric water content
σ	=	Stefan-Boltzmann constant
λ	=	thermal conductivity of material
κ	=	thermal diffusivity
β	=	volumetric thermal expansion coefficient of air
α_a	=	thermal diffusivity of the air
ΔE	=	net change in total energy of system
λ_e	=	thermal conductivity of solid/fluid system
ΔE_{CV1}	=	energy changes of the rock fragments
ΔE_{CV2}	=	energy changes of air in the storage system
ΔE_{CV3}	=	energy changes if air in the housing model
λ_f	=	thermal conductivity of fluid
λ_i	=	mineral thermal conductivity
α_r	=	absorbtivity coefficient of rocks
ε_r	=	emissivity or heat exchanger effectiveness of rock

LIST OF SYMBOLS AND ABBREVIATIONS (Continued)

α_r = thermal absorbability of rock

λ_s = thermal conductivity of solid

ν_s = volume fraction of solid

ρ_{solid} = average grain density

Δt = time interval

ΔT = temperature difference, or temperature increases

Δx = layer of constant thickness

Δx = the thickness of acrylic sheet

Δx = thickness of housing wall

A = area normal to the direction of heat transfer

A_{acr} = area of acrylic sheet

A_{cham} = area of pit wall

A_h = area of housing wall for thermal loss

A_o, A_i = cross-sectional area of tube

A_r = ratio of A_o/A_i

A_r = surface area of all rock fragments in storage system

$A_{r,top}$ = solar collection area which equivalent with the area of rocks on the top exposed to the air

A_{rad} = surface of emissivity

A_{top} = collector area

A_{top} = collector area of rock fill

LIST OF SYMBOLS AND ABBREVIATIONS (Continued)

c	=	heat capacity of material
C	=	thermal capacity of material
C_a	=	specific heat of air
C_a	=	specific heat of air in storage system
C_D	=	discharge coefficient
C_p	=	specific heat capacity rock containing with water
C_p	=	heat capacity of the storage medium
C_p	=	specific heat at constant pressure
$C_{p,solid}$	=	mean specific heat capacity of the mineral grains
C_r	=	heat capacity of rock
C_r	=	specific heat or heat capacity of rocks
c_s	=	specific heat capacities of the soil constituents
C_v	=	specific heat at constant volume
CV2	=	air in the storage system
CV3	=	air in the housing model
c_w	=	specific heat of water
D	=	diameter of ideal rock fragment
f_1	=	adjusted factor due to an effect of the surrounding air temperature
f_2	=	adjusted factor due to an effect of the leakage from the housing model
f_{ab}	=	heat loss factor from reflected radiation of rock
g	=	gravitational acceleration

LIST OF SYMBOLS AND ABBREVIATIONS (Continued)

Gr_L	=	Grashof number
H	=	elevation head of tube (different between the elevation of entrance and exit
$h_{ex,h}$	=	convective heat transfer coefficient of air outside housing
h_{exc}	=	convective heat transfer coefficient of air outside the pit or air above cover sheet
$h_{i,h}$	=	convective heat transfer coefficient of air in housing
h_{ic}	=	convective heat transfer coefficient of air in pit
h_r	=	convective heat transfer coefficient
h_r	=	convective heat transfer coefficient from rocks to air in storage system
I	=	amount of solar radiation received over a specified period of time
I_s	=	solar radiation or heat flux
k	=	thermal conductivity of the material
k	=	thermal conductivity of object in fluid.
K	=	thermal conductivity coefficient of rocks
k_{acr}	=	thermal conductivity of acrylic sheet
k_r	=	thermal conductivity of rock
k_w	=	thermal conductivity coefficient of hosing wall
m_c	=	mass of air in the storage pit
m_c	=	mass of air in storage system
m_h	=	mass of air in housing

LIST OF SYMBOLS AND ABBREVIATIONS (Continued)

m_r	=	mass of rocks in pit
m_r	=	weight of the rock fragment
M_s	=	mass of the storage medium
n_i	=	volume fraction
Nu	=	Nusselt number
P	=	air pressure
Pr	=	Prandtl number
Q	=	heat stored in the medium
Q	=	net heat transfer across system boundaries
q	=	heat transfer per unit mass
Q_{12}	=	heat transferred during the process between states 1 and 2
Q_r	=	amount of solar energy stored in the rock fill
R	=	gas constant
Ra	=	Rayleigh number
T	=	temperature
T_0	=	temperature increases when have no leakage from the housing model
t_{bed}	=	rock fill thickness
T_c	=	the temperature of air in pit
T_f	=	bulk fluid temperature away from the surface
T_h	=	temperature of air in housing
T_{max}	=	maximum temperature

LIST OF SYMBOLS AND ABBREVIATIONS (Continued)

T_{min}	=	minimum temperature
T_r	=	temperature of rocks
T_s	=	surface temperature
T_{sur}	=	surrounding air temperature
T_{sur}	=	surrounding temperature or air outside the housing
U_1	=	overall heat transfer coefficient of air in pit to surrounding air
U_2	=	overall hear transfer coefficient of air to pit wall
U_h	=	overall heat transfer coefficient of air in housing to surrounding
V_b	=	packed rock volume
V_{bed}	=	bulk volume of rock or the packed rock volume
V_c	=	volume of the storage pit
V_h	=	volume of housing model
V_i	=	volume of concentration
W	=	net work done in all forms
ε	=	void fraction of rock fill
η	=	storage efficiency
ν_a	=	volume fraction of air
ρ_r	=	density of rock

CHAPTER I

INTRODUCTION

1.1 Rationale and background

Every year, during winter, people who live in the north and northeast of Thailand have suffered from cold weather. Records from the Thai Meteorological Department (2003) show that temperature in many areas (for example, Chiang Mai, Chiang Rai, Mea Hong Son and Loei provinces) during that periods drop to nearly zero Celsius. The government and public agencies spent a large amount of funds (more than 90,374,800 Bahts for 584,988 of blankets) (Figure 1.1) to allay this problem (Department of Disaster Prevention and Mitigation, 2005). A low-cost technology is required to solve this problem or to minimize the impact of the cold weather on the human health in those regions.

An alternative solution is the application of the solar thermal energy storage system. This technology deals with selecting the media that can absorb and store heat during the daytime and release it to warm housing space during the nighttime. Rocks are one of the suitable heat storage media which have been widely used in this technology. Volcanic rocks in particular are one of the prime candidates. Results from the Department of Mineral Resources reveal that volcanic rocks distribute in many areas in Thailand. The solar thermal energy storage technology has been developed and performed successfully in many countries (Coutier and Farber, 1982;

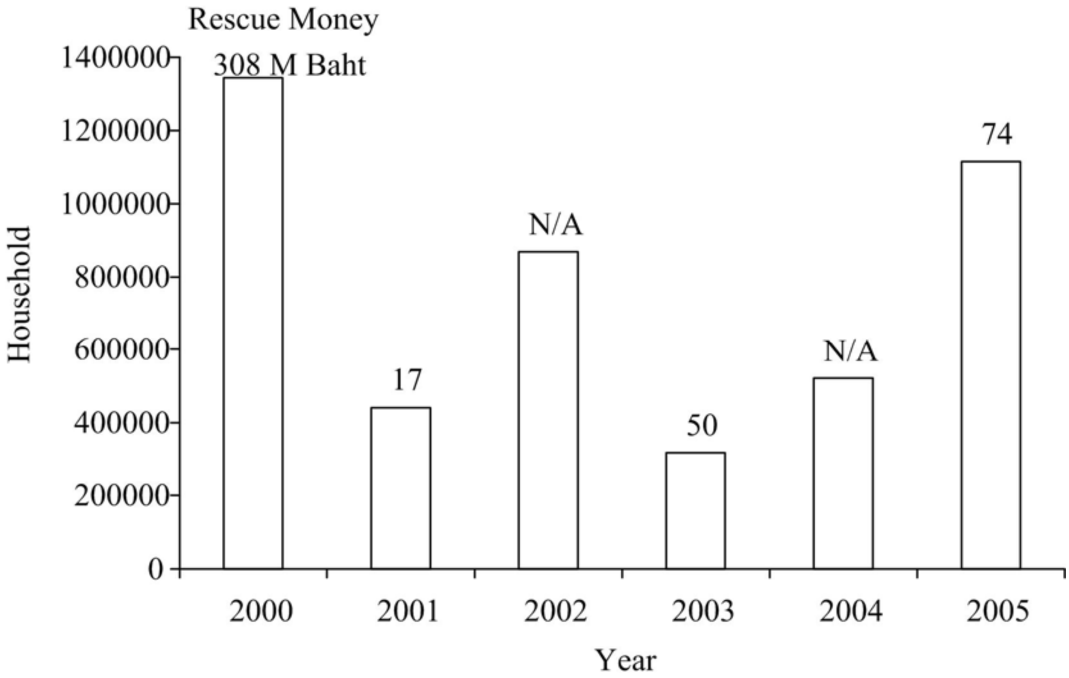

Figure 1.1 Numbers of households who suffer from cold weather from year 2000 through 2005. The numbers shown on the top of column are the rescue money from the government and public funds (Department of Disaster Prevention and Mitigation, Ministry of Interior Thailand, 2006).

Meier et al., 1991; Choudhury et al., 1995; Abbud et al., 1995 and Kurklu et al., 2003). However, instead of using rocks, those projects use solar cells or solar greenhouse dome to collect the thermal energy and the energy is subsequently transferred through the transferring equipment to the provided rock fills. This technique is, therefore, very costly to install. In order to apply this technology in Thailand, modification is needed to suit the local economics. To do so, cheap and efficient materials should be selected for thermal energy storage system. The advantage of this technology is that the source of the main energy is the sun which is not only enormous but also free. The suitable rocks are also cheap, readily available, and long-lasting and safe.

1.2 Research objective

The objective of this research is to design the optimum thermal energy storage system by using rock fills for household space warming. This research determines experimentally the transient behavior of the thermal energy storage system using a scaled-down physical model. The heat transfer is analyzed by a simple model (mathematical equation) to describe the system and comparing the results with the experimental results. The relationships are developed between the increased temperatures in household space during nighttime (difference between the temperatures in the housing and surrounding), volume of household space, and size of rock fill. The system deals with storage of heat or solar thermal energy during sunny day and releasing it to warm up household space during nighttime when the weather cools down without using external electricity or fossil fuel.

1.3 Scope and limitations of the study

The research effort mainly involves laboratory testing, mathematical modeling, construction of pilot scale solar thermal energy storage system, and development of design parameters for the system. The scope and limitations of this study include:

1) Study of the geology of igneous rocks (both intrusive and extrusive) in the north and northeast of Thailand to define the appropriate areas, for further investigation and collecting suitable rock types as storage medium. The information will be obtained from the available documents published by the government agencies and academic institutes.

2) Collection of soil and rock samples to represent the readily available natural materials in the north and northeast of Thailand.

3) The laboratory testing is performed to determine the thermal properties of rock and soil samples.

4) Mathematical equations will be developed by using the parameters obtained from laboratory testing to determine the change of temperature in storage media and housing as a function of time. Results from the mathematical calculations will be subsequently verified by comparing with the actual behavior obtained from the physical model.

5) Pilot scale solar thermal energy storage system will be constructed and monitored at the Equipment Building (F4), Suranaree University of Technology to study the system behavior, the efficiency of soil mass used as heat insulator, and the performance of the storage medium.

1.4 Research methodology

The research effort is divided into seven tasks, as follows (Figure 1.2).

1.4.1 Literature review

The literatures related to the solar thermal energy storage in rock fills will be reviewed, including 1) climate of Thailand, 2) solar energy in Thailand, 3) solar energy applications, 4) solar thermal energy storage, 5) thermal properties of rocks, 6) thermal properties of soils, 7) relevant principles of thermodynamic and heat transfer, 8) modeling of thermal system, and 9) geology of igneous rocks in Thailand.

1.4.2 Sample collection and preparation

The geological data will be used to select the areas where the samples are collected and brought to the laboratory. The rock samples will be cut and polished to the desired size and shape for thermal property testing (with dimension of 3×3×1 cm) and for petrographic study (with 1.5×3.0 cm). The soil samples are collected at the site where the pilot scale solar thermal energy storage system will be constructed.

1.4.3 Laboratory test

The laboratory testing includes physical properties test on soil samples, petrographic study on rock samples, and thermal properties test on rock and compacted soil samples.

1.4.4 Pilot scale solar thermal energy storage system

The physical modeling aims at studying the performance of the solar thermal storage system and to assess an efficiency of the system. The most suitable rock type will be used as the storage medium. Temperatures at various locations

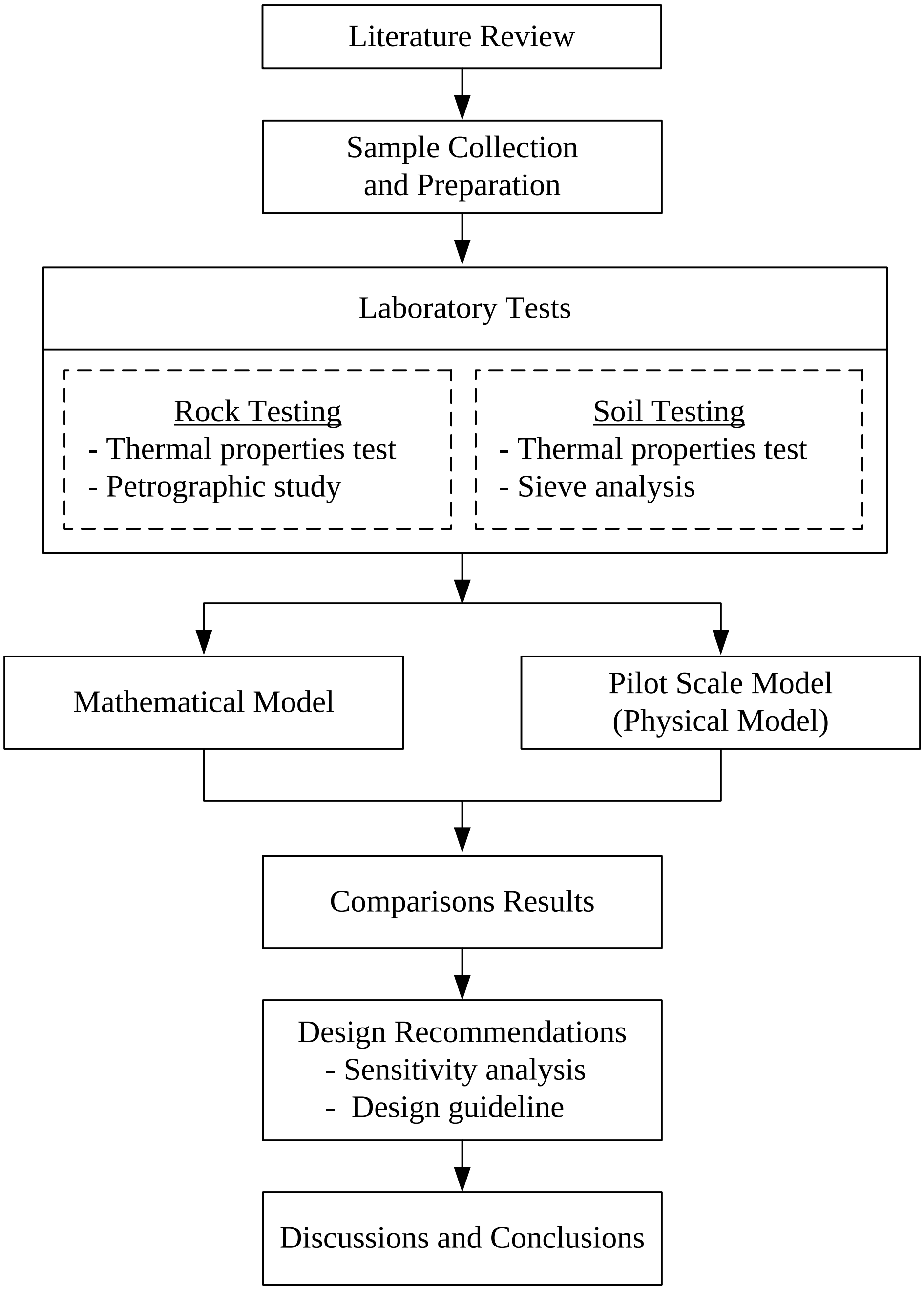

Figure 1.2 Research methodology.

within the constructed system will be monitored during the testing periods. The results will be used to assess the system performance and to compare within the mathematical model.

1.4.5 Mathematical model

The mathematical model will be developed to study the transient thermal behavior of the system. The change of temperature within rock fills, air in the storage system, and air in the housing model will be calculated as a function of time by using conservation laws to derive the governing equations which are the ordinary differential equations as a function of three modes of heat transfer. The results in this section will be used to optimize the storage system parameters, including the suitable fragment size, type of rock, cross-sectional area of hot-air tube, characteristics of rock bed, suitable depth, and energy-absorbed area.

1.4.6 Data analysis

The measurement results are used in the calibration of the mathematical model and to determine the energy loss in the system. The results from mathematical calculation will be used to establish the relationship between the volume of storage system, volume of housing space and the increase (or warmed up) of housing temperature. The parameters that are considered for the system will be determined by using the results from mathematical calculation. Sensitivity analyses will be performed.

1.4.7 Thesis writing and presentation

The thesis will be submitted at the end of the research. The results of the research will be presented at an international conference or journal.

1.5 Expected results

Results from this research can be used as a design guideline to construct the solar thermal storage system in specific area with specific purpose. The design parameters will be recommended. Installation procedure for the system will be derived. The expected efficiency of the system can be determined for specific design under a variety of varying design parameters (rock type, packed density, pit size, solar radiation collection area, etc.).

1.6 Thesis contents

Chapter I describes the objectives, the problems and rational, and the methodology of the research. Chapter II presents the results of literature review. Chapter III describes the rock and soil samples collection, preparation, and laboratory testing. Chapter IV describes the mathematical model use to calculate the changing of temperature within rock fills, the storage system, and the housing model as a function of time. Chapter V presents the construction of pilot scale solar thermal energy storage system and the result from measurement. Chapter VI compares the measured results from pilot scale solar thermal energy storage and the calculated results from mathematic model. Chapter VII presents the sensitivity analysis of the variables and the design guidelines of rock fill system. Chapter VIII concludes the research results and provides recommendations for the future research studies.

CHAPTER II

LITERATURE REVIEW

The literature review relevant to the solar thermal energy storage in rock fills to be reviewed here include: 1) climate of Thailand, 2) solar energy in Thailand, 3) solar energy applications, 4) solar thermal energy storage, 5) thermal properties of rocks, 6) thermal properties of soils, 7) relevant principles of thermodynamic and heat transfer, 8) modeling of thermal system, and 9) geology of igneous rocks in Thailand.

2.1 Climate of Thailand

Thailand is located in the tropical area between latitudes 5° 37'N to 20° 27'N and longitudes 97° 22'E to 105° 37'E (Thai Meteorological Department, 2002). The climate of Thailand is under the influence of seasonal monsoon winds. From the meteorological basis the climate of Thailand may be divided into three seasons, 1) rainy or southwest monsoon season (mid-May to mid-October), 2) summer or pre-monsoon season (mid-February to mid-May) and 3) winter or northeast monsoon season (mid-October to mid-February).

The upper part of Thailand (i.e. the northern, northeastern, central and eastern parts) usually experiences a long period of warm weather because of its inland nature and tropical latitude zone. During March to May, the hottest period of the year, the maximum temperatures usually reach 40°C or more except along coastal areas where sea breezes will moderate afternoon temperatures. The onset of rainy season also significantly reduces the temperatures from mid-May to make lower than 40°C. In winter the outbreaks of cold air from China occasionally reduce temperatures to fairly low, especially in the northern and northeastern parts where temperatures may drop below zero. In the southern part temperatures are generally mild throughout the year because of the maritime characteristic of this region. The high temperatures common to upper parts of Thailand are seldom. The diurnal and seasonal variations of temperatures are significantly less than those in the upper parts of Thailand. Figures 2.1 through 2.4 show the temperatures in the winter (November through February) of Thailand.

2.2 Solar energy in Thailand

Thailand is located near the equator where the sunshine is relatively strong and available all year round. Department of Alternative Energy Development and Efficiency (DEDE) and Silpakorn University (1999) have developed a solar radiation map using satellite images from visible channels of GMS4 and GMS5 satellites collected during 6 year-period (1993-1998) and data measured from ground base stations. Those data were used to develop a physical model to estimate average solar radiation at any required time interval and locations within the country. It was found that the distribution of solar radiation is influenced by the northeast and southwest monsoons. Highest solar radiation in most parts of the country occurs during April and May. Its value ranges between 20 and 24 MJ/m^2-day. The average daily global radiation map is illustrated in Figure 2.5 showing that about 14 percents of the total area receiving highest solar radiation of 19-20 MJ/m^2-day are in the northeast and central regions. About half of the country receives the average daily global radiation

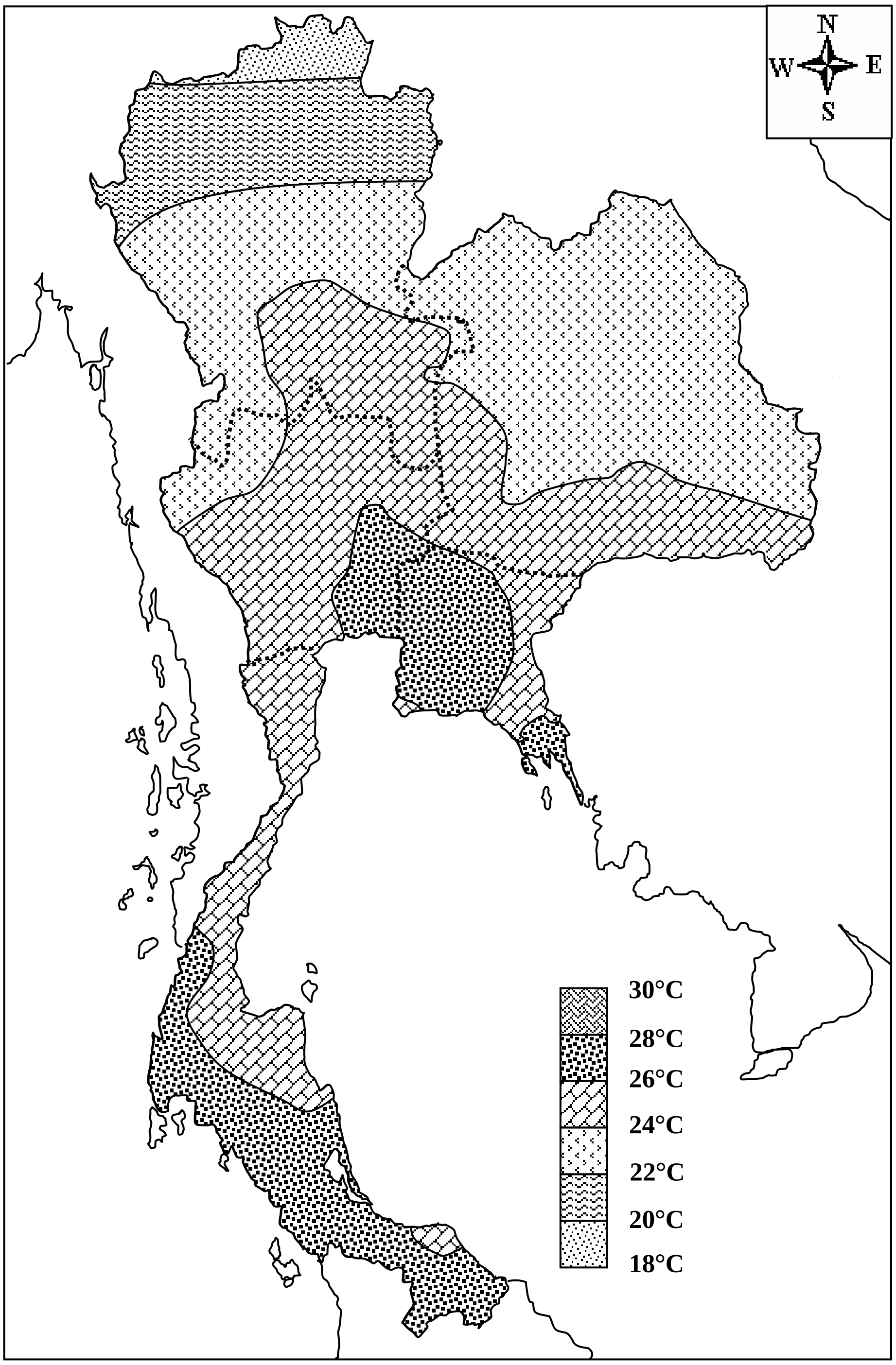

Figure 2.1 Temperature map in January (Thai Metrological Department, 2002).

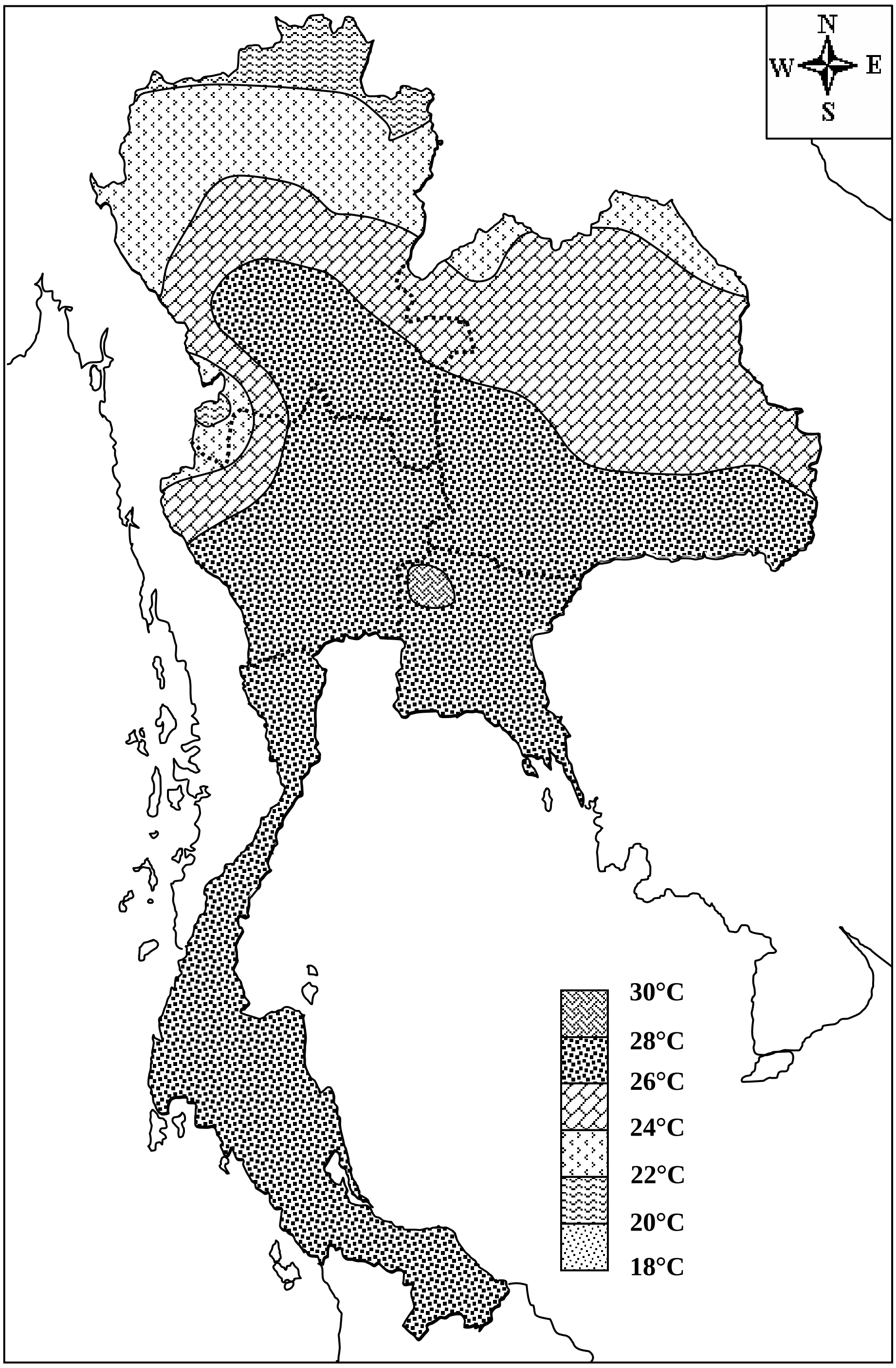

Figure 2.2 Temperature map in February (Thai Metrological Department, 2002).

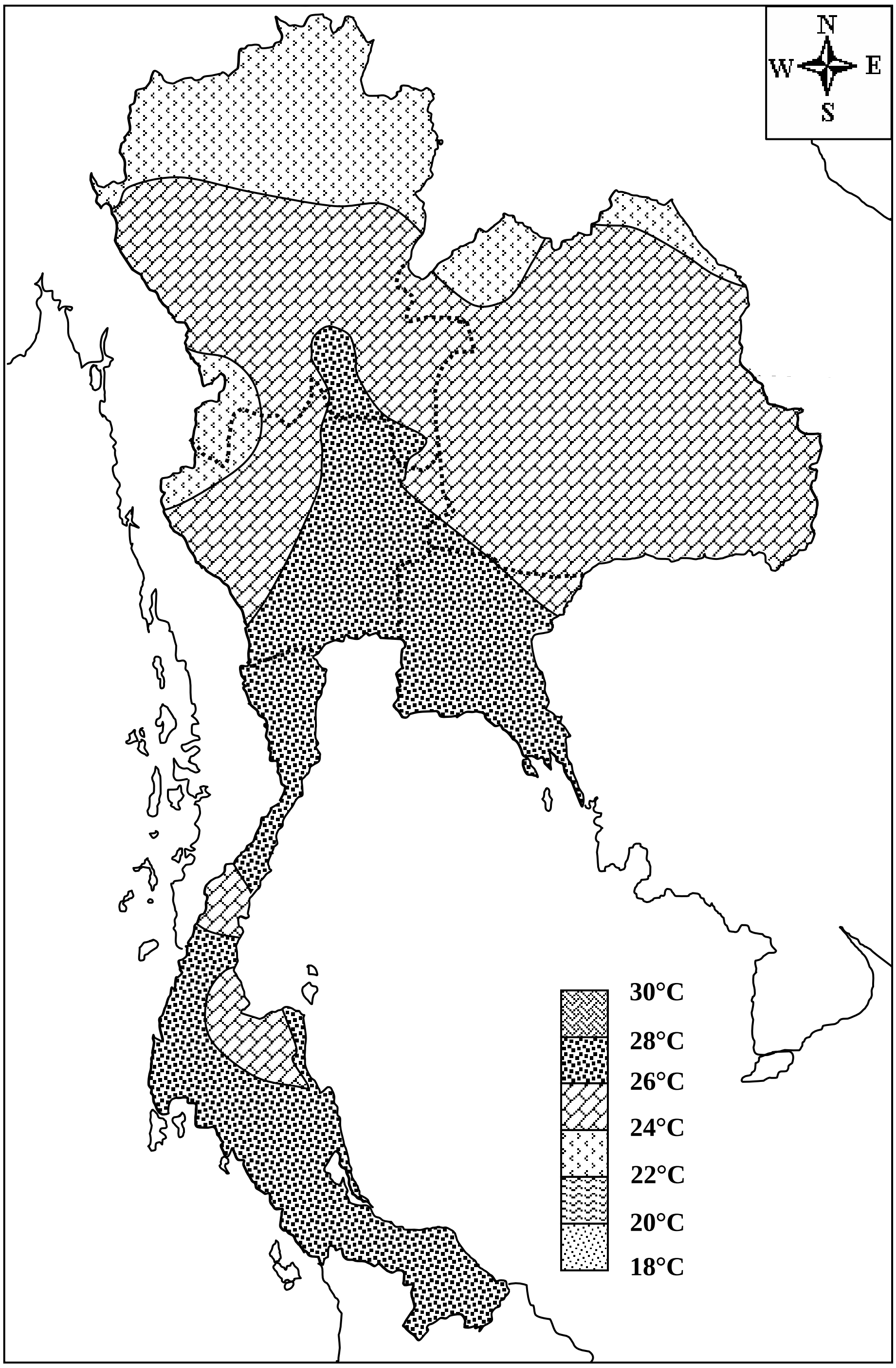

Figure 2.3 Temperature map in November (Thai Metrological Department, 2002).

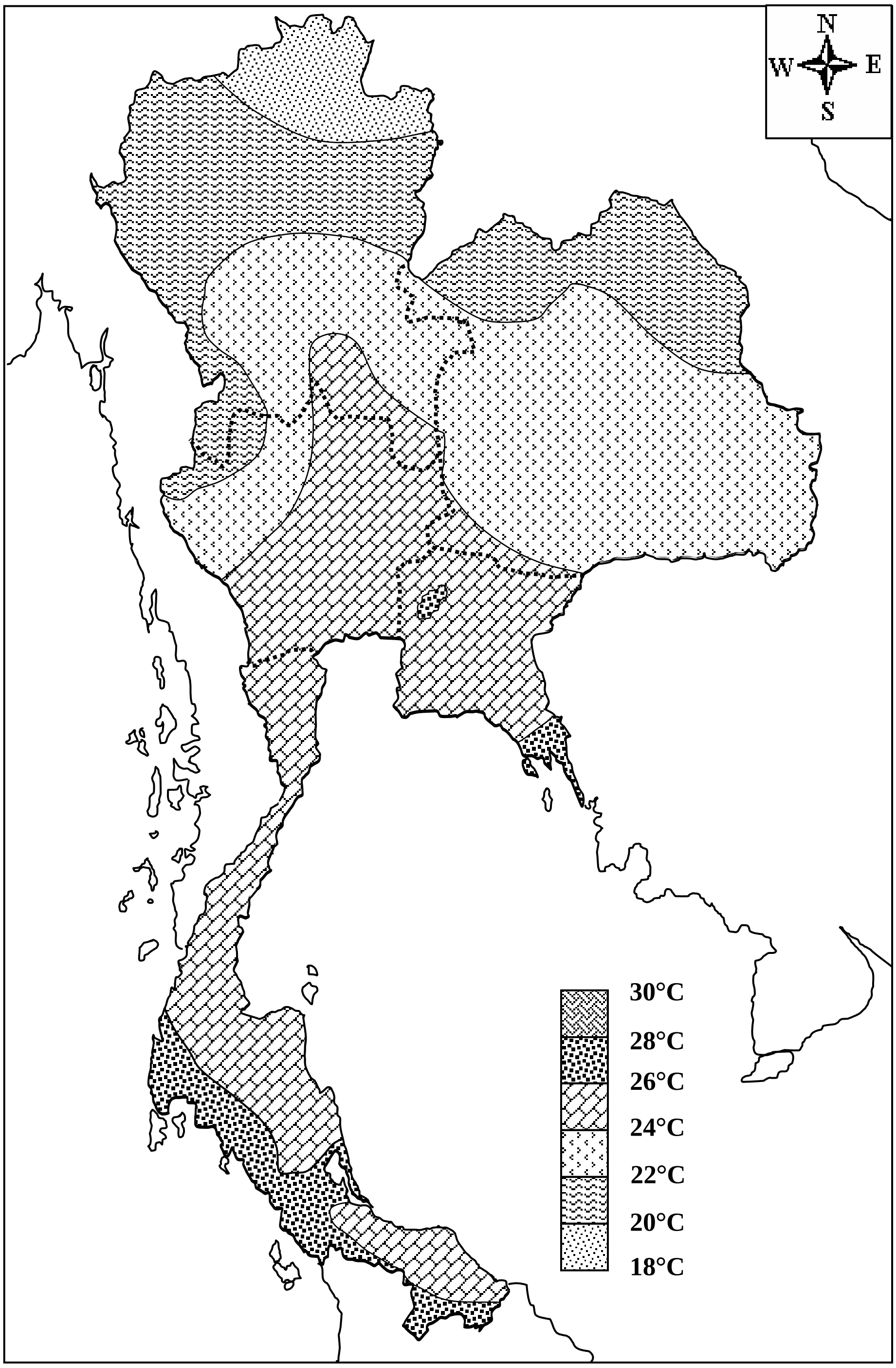

Figure 2.4 Temperature map in December (Thai Metrological Department, 2002).

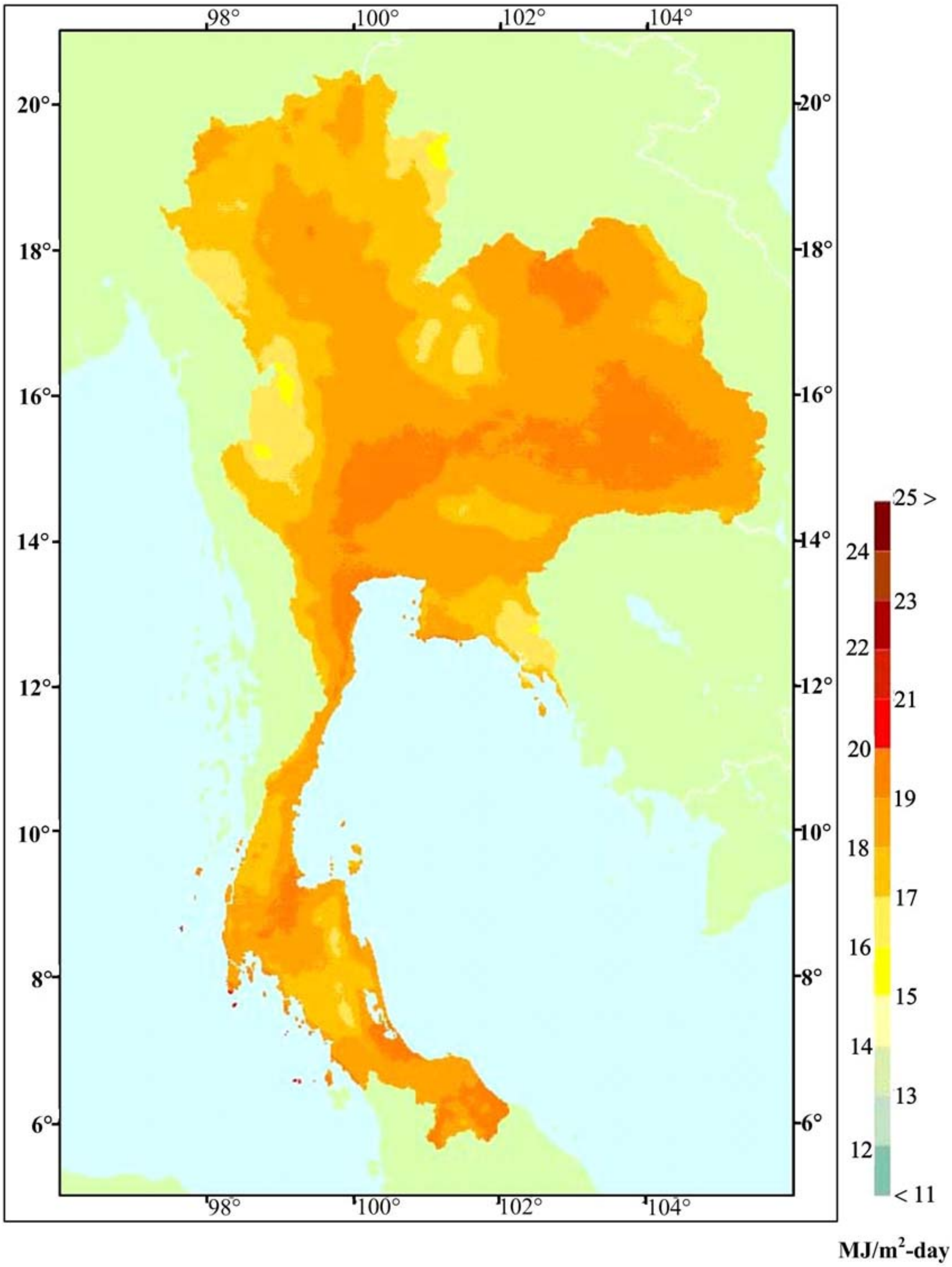

Figure 2.5 Solar energy map of Thailand (Department of Alternative Energy Development and Efficiency and Silpakorn University, 1999).

in the range of 18-19 MJ/m^2-day. Only 0.5 percent of the country receives the average daily global radiation less than 16 MJ/m^2-day. The global radiation for the whole country is 18.2 MJ/m^2-day. Figures 2.6 through 2.9 illustrate the average daily global radiation map of Thailand in January, February, November and December.

2.3 Solar energy applications

Solar thermal technology is used for collecting and converting the sun energy to thermal energy for various applications, such as water and air heating, cooking and drying, steam generation, distillation, etc. Basically a solar thermal device consists of a solar energy collector (or absorber), a heating or heat transferring medium, and a heat storage or heat tank. Solar thermal technology uses good heat conducting materials, insulation and reflectors (The Schumacher Center for Technology and Development, n.d.).

2.3.1 Water heating

There is a wide variety of solar water heaters available. The simplest is a piece of black plastic pipe, filled with water, and laid in the sun for the water to heat up. Simple solar water heaters usually comprise a series of pipes which are painted black, sitting inside an insulated box fronted with a glass panel. This is known as a solar collector. The fluid to be heated passes through the collector and into a tank for storage. The fluid can be cycled through the tank several times to raise the heat of the fluid to the required temperature. There are two common simple configurations for such a system; thermosyphon system and pumped solar water heaters. Figure 2.10 illustrates the application of solar energy as water heating.

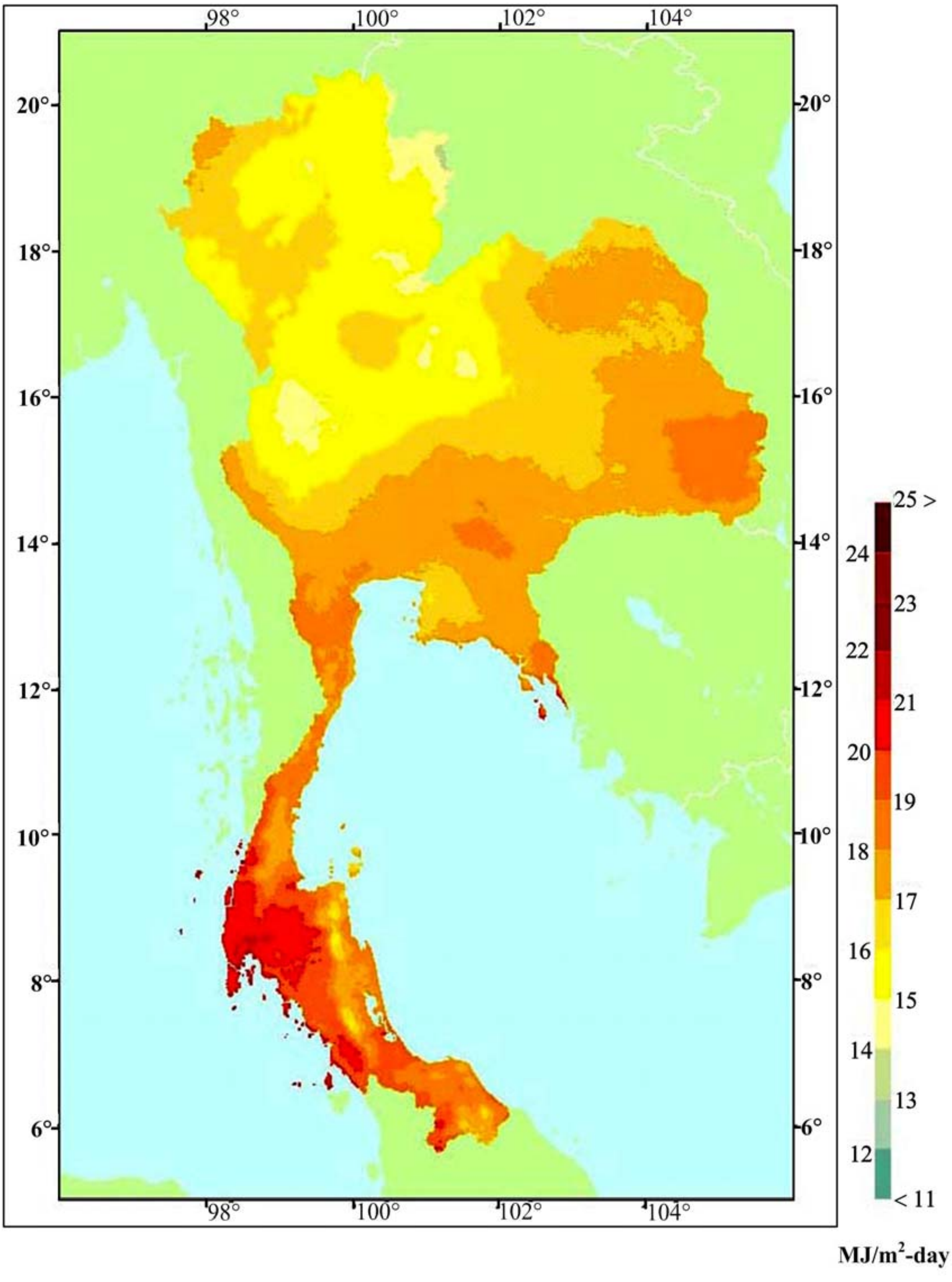

Figure 2.6 Solar energy map of Thailand in January (Department of Alternative Energy Development and Efficiency and Silpakorn University, 1999).

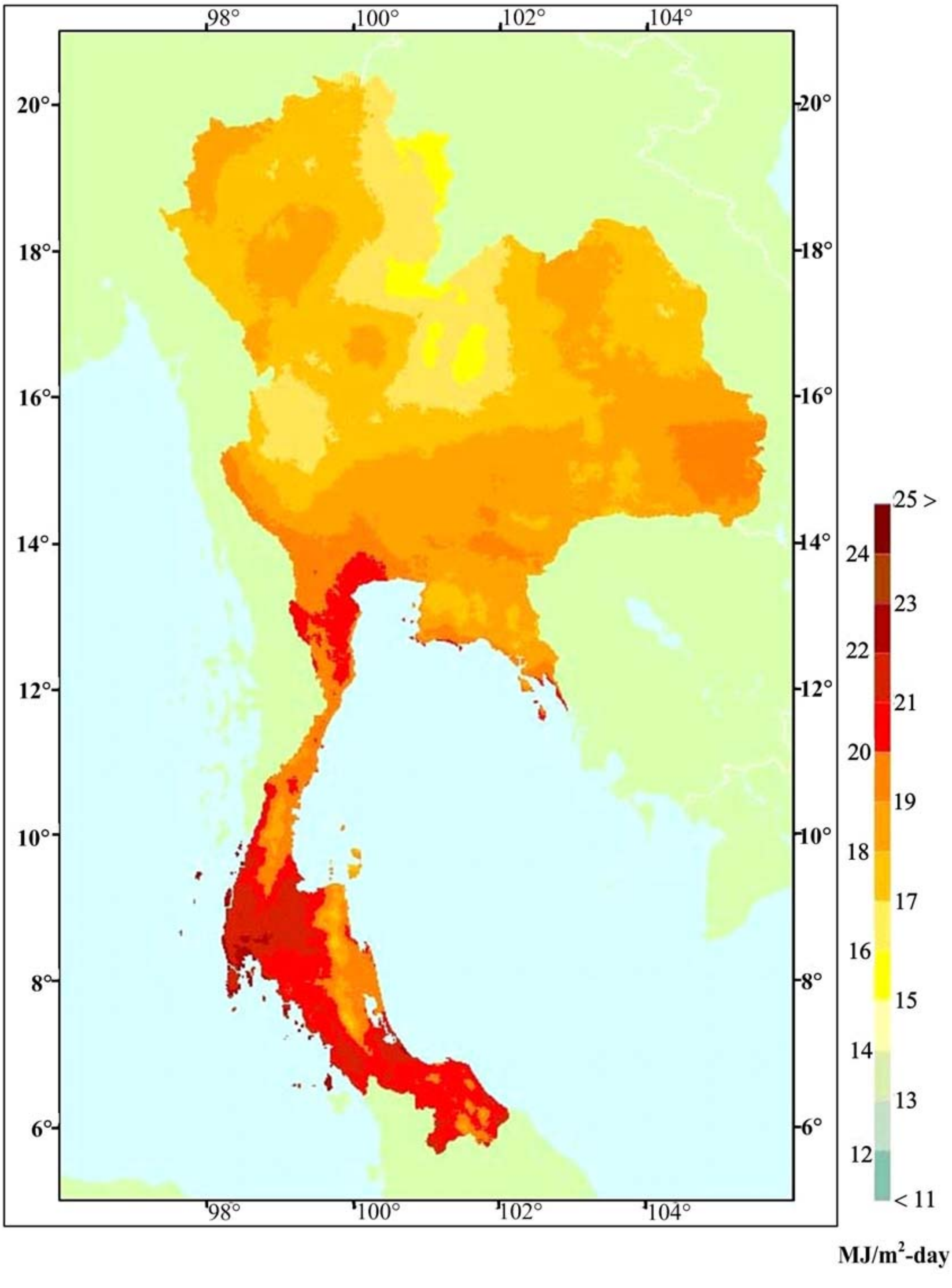

Figure 2.7 Solar energy map of Thailand in February (Department of Alternative Energy Development and Efficiency and Silpakorn University, 1999).

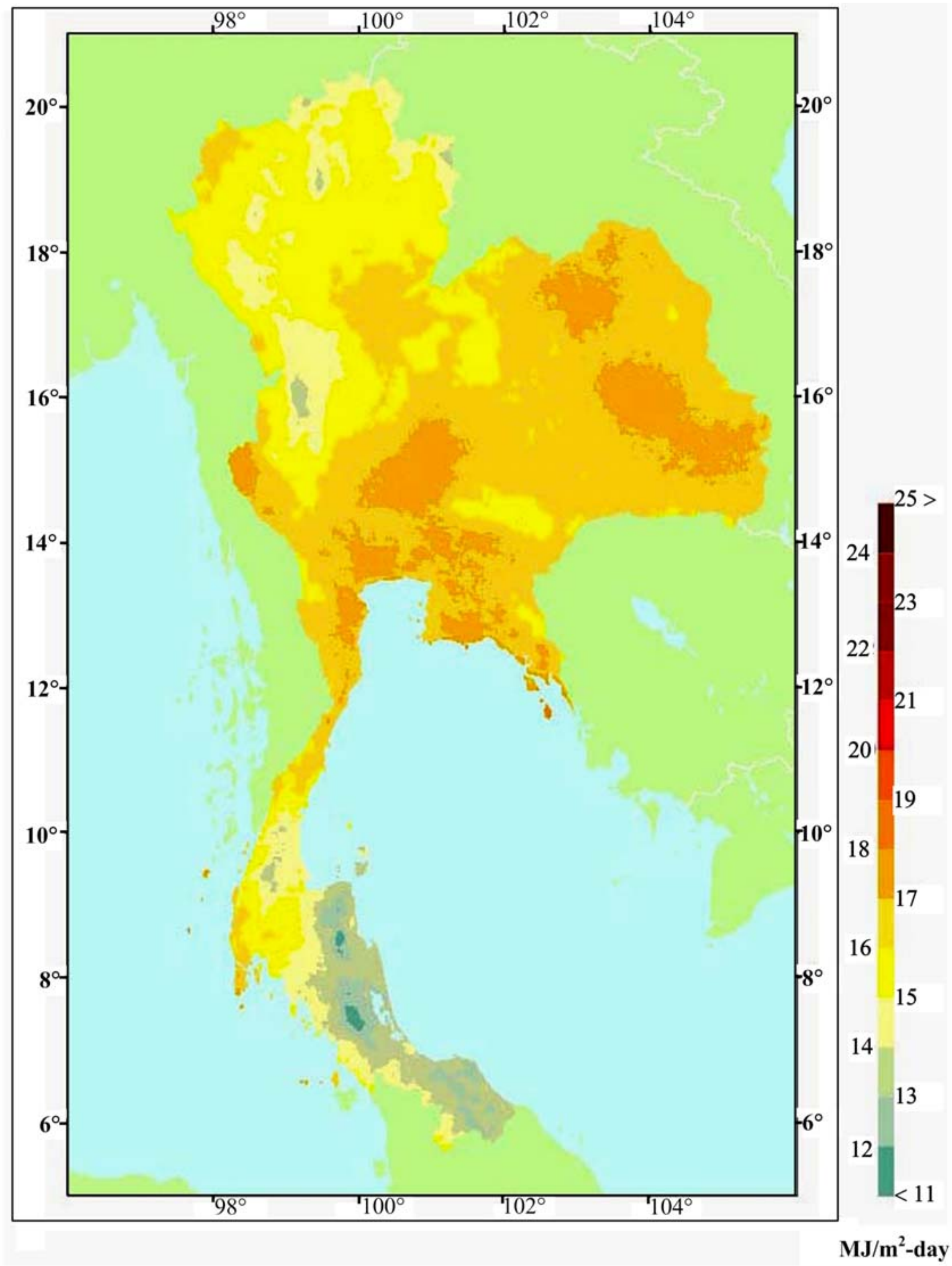

Figure 2.8 Solar energy map of Thailand in December (Department of Alternative Energy Development and Efficiency and Silpakorn University, 1999).

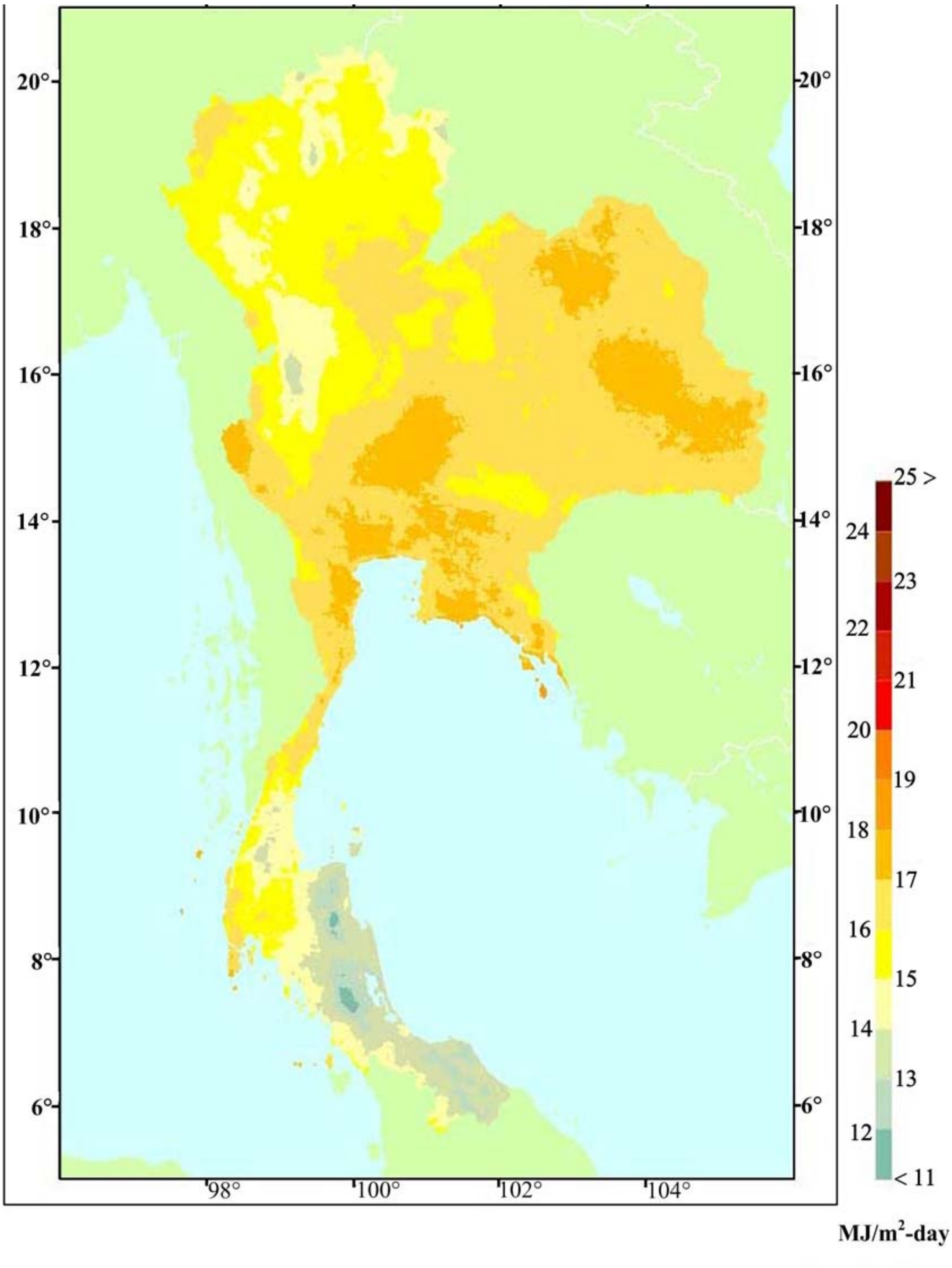

Figure 2.9 Solar energy map of Thailand: in December (Department of Alternative Energy Development and Efficiency and Silpakorn University, 1999).

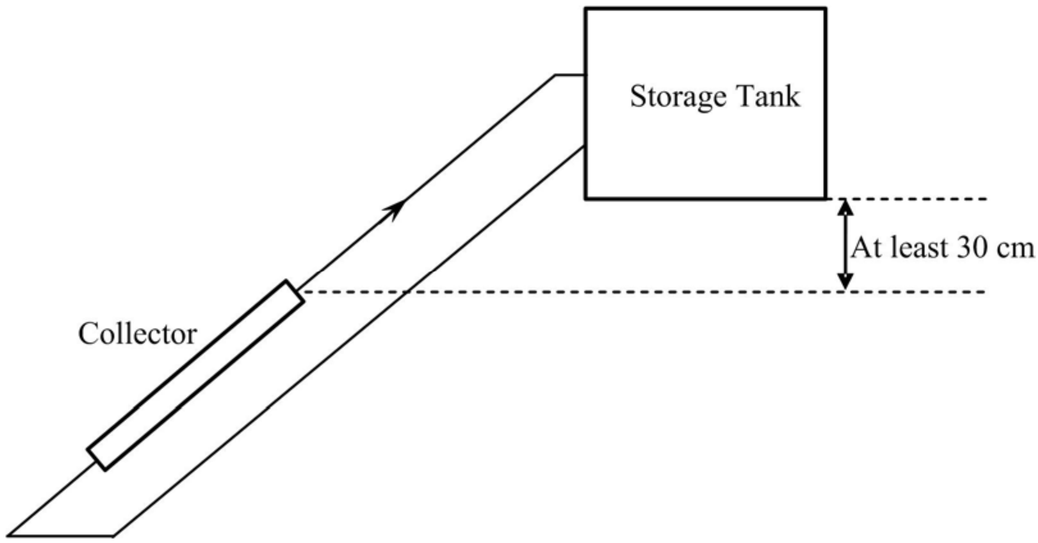

(a) Thermosyphon hot water system

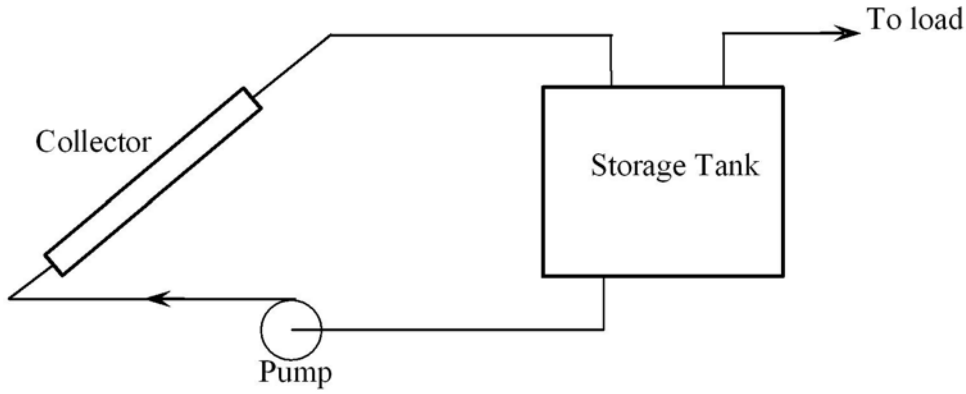

(b) Pumped hot water system

Figure 2.10 Schematic diagrams of thermosyphon hot water system (a) and pumped hot water system (b) (modified from Charters and Pryor, 1982).

2.3.2 Solar cooking

Solar cooking is a technology which has been given a lot of attention in recent years in developing countries. The basic design is that of a box with a glass cover (Figure 2.11). The box is lined with insulation and a reflective surface is applied to concentrate the heat onto the pot. The pots can be painted black to help with heat absorption. The solar radiation raises the temperature sufficiently to boil the contents in the pots.

2.3.3 Crop dying

Controlled drying is required for various crops and products, such as grain, coffee, tobacco, fruits, vegetables and fish. Their quality can be enhanced if the drying is properly carried out. Solar thermal technology can be used to assist with the drying of such products. The main principle of operation is to raise the heat of the product, which is usually held within a compartment or box, while at the same time passing air through the compartment to remove moisture. The flow of air is often promoted using the stack effect which takes advantage of the fact that hot air raises and can therefore be drawn upwards through a chimney, while drawing in cooler air from below. Alternatively a fan can be used. Figure 2.12 shows the application of solar energy as crop drying.

2.3.4 Space heating

In colder areas, space heating is often required during the winter months. Vast quantities of energy can be used to achieve this. The use of building materials with a high thermal mass (which stores heat), good insulation and large glazed areas can increase a building capacity to capture and store heat from the sun. Many technologies exist to assist with diurnal heating needs but seasonal storage is

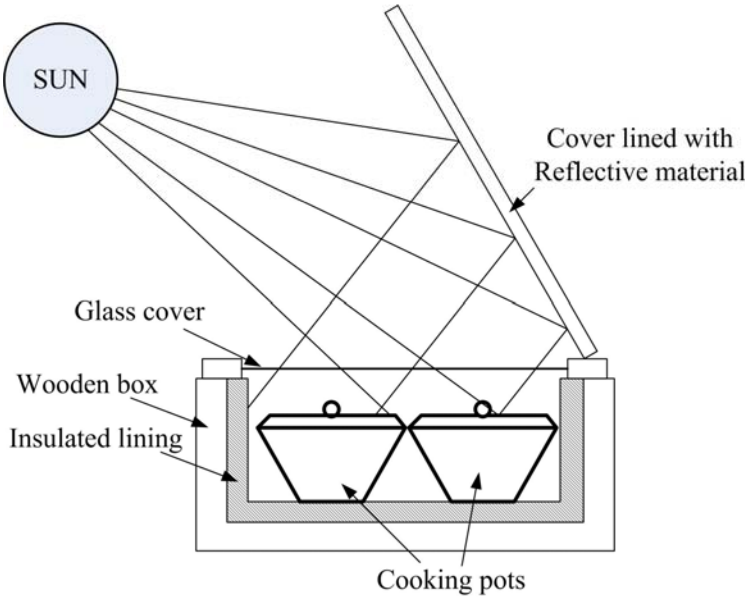

(a) Conceptual solar cooking

(b) Actual setup

Figure 2.11 Application of solar energy for cooking (Nandwani, 2006).

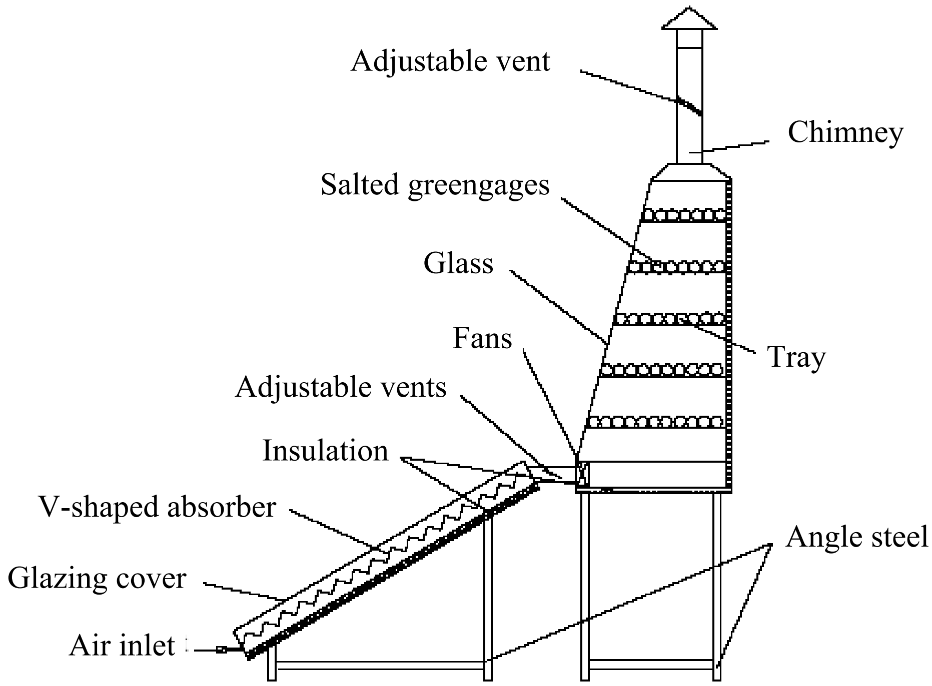

Figure 2.12 Application of solar energy for crop drying (Li et al., 2006).

more difficult and costly (Charters and Pryor, 1982). Figure 2.13 shows the application of solar energy for space heating.

2.3.5 Space cooling

The majority of the world warm climate cultures have again developed traditional, simple, elegant techniques for cooling their dwellings, often using effects promoted by passive solar phenomenon. There are many methods for minimizing heat gain. The rock pile storage unit may be used to obtain cooling in the summer. The operation of the system is shown in Figure 2.14. At night, air is blown through an evaporative cooler and then through the rock bed. The rock bed is cooler in this process so that during the day warm air from the building may be passed through the rock bed, cooled, and returned to the building. The use of evaporative cooling system is restricted to regions with cool nights and low wet bulb temperatures (Charters and Pryor, 1982).

2.3.6 Day-lighting

A simple and obvious use for solar energy is to provide light for use in buildings. Many modern buildings, office blocks and commercial premises for example, are designed in such a way that electric light has to be provided during the daytime to provide sufficient light for the activities taking place within. An obvious improvement would be to design buildings in such a way that the light of the sun can be used for this purpose. The energy savings are significant and natural lighting is often preferred to artificial electric lighting.

2.3.7 Solar thermal power stations

There are two basic types of solar thermal power station. The first is the power tower design which uses thousands of sun-tracking reflectors or heliostats

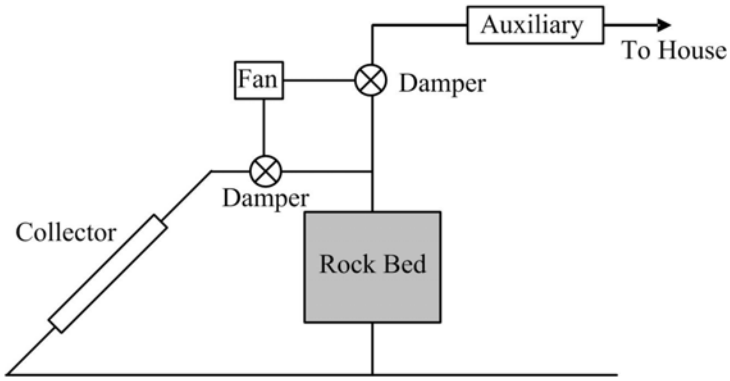

(a) Schematic diagram of solar space heating system

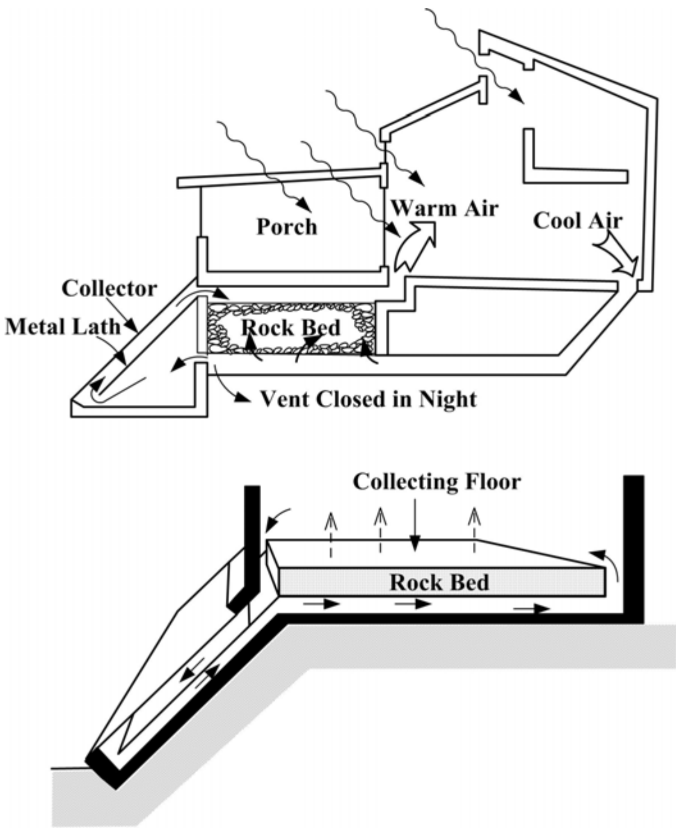

(b) Two possible configurations combined with rock bed storage

Figure 2.13 Application of solar energy for space heating. (a) Schematic diagram of a solar space hearting system (Charters and Pryor, 1982) and (b) two possible configurations in which convection loop in combined with rock bed storage (Garg et al., 1985).

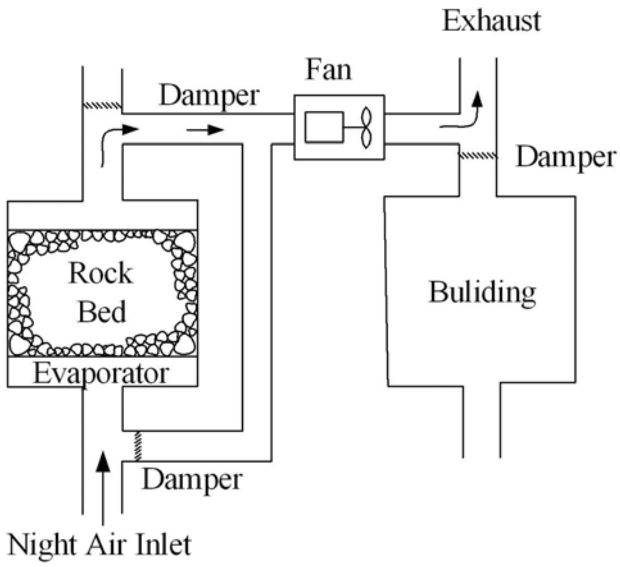

(a) Night charging of rock bed

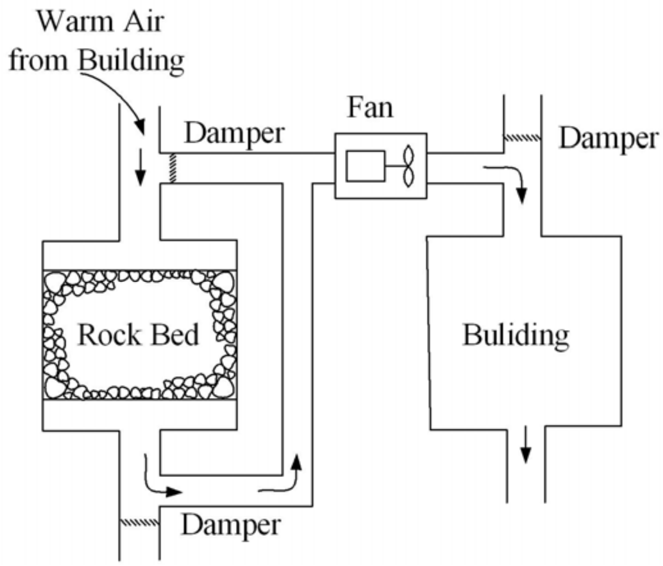

(b) Day cooling of building

Figure 2.14 Application of solar energy for day cooling of building (Charters and Prayor, 1982).

to direct and concentrate solar radiation onto a boiler located atop a tower. The temperature in the boiler rises to 500-700°C and the steam raised can be used to drive a turbine, which in turn drives an electricity producing turbine. The second type is the distributed collector system. This system uses a series of specially designed trough collectors which have an absorber tube running along their length. Large arrays of these collectors are coupled to provide high temperature water for driving a steam turbine. Figure 2.15 shows generals layout of solar thermal power stations.

2.4 Solar thermal energy storage

The main purpose of energy storage is to improve the match between the collected energy and the load. As energy is often needed at night and during cloudy periods, it is necessary to store energy when possible for use during these periods. The principle components of a thermal energy storage system are a heat storage material, a well-insulated container, and provision for efficiently adding and removing heat (Charters and Pryor, 1982).

2.4.1 Type of storage system

Charters and Pryor (1982) state that thermal energy may be stored in the forms of water storage, rock bed storage, and phase change storage systems.

Water is most common material for storing sensible heat in low and medium-temperature solar systems. A further limitation is that water cannot be used to store heat at temperature greater than 100°C unless pressure vessels are used to contain the water.

With in air based solar systems rock beds are used to store energy. The containers holding the rocks must have air spaces above and below the rocks to

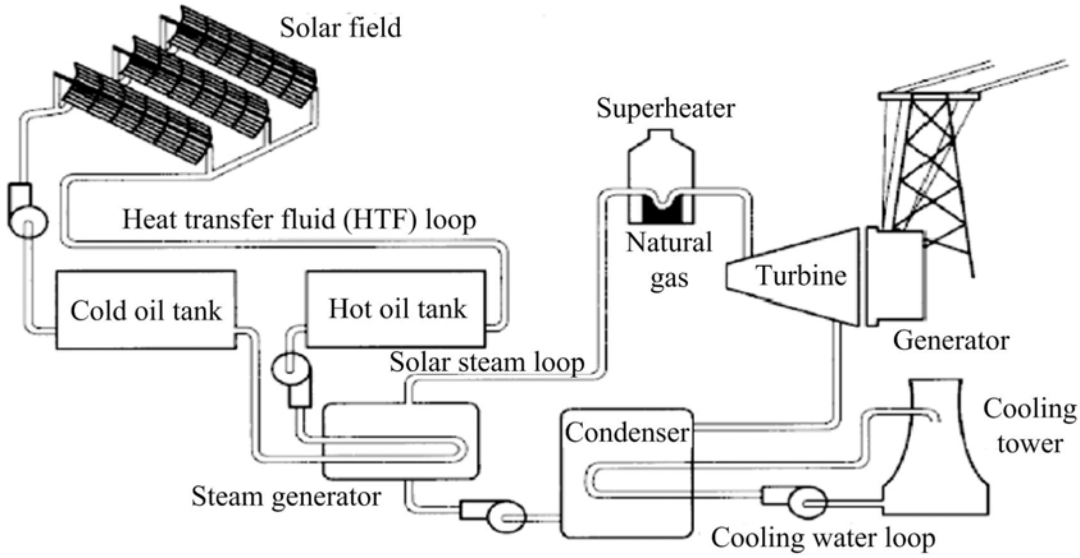

(a)

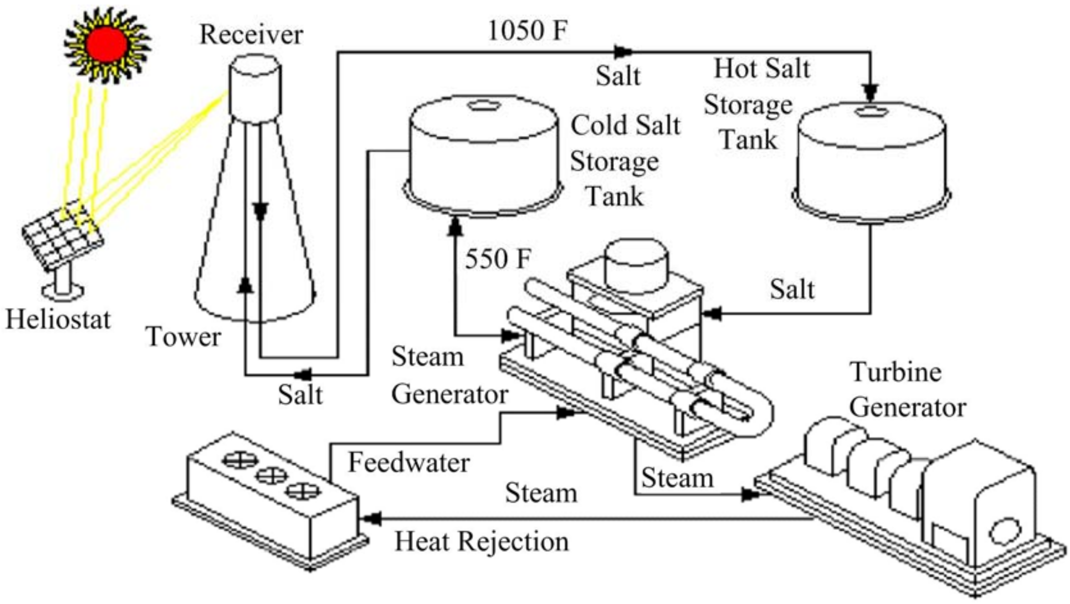

(b)

Figure 2.15 Solar thermal power stations with distributed collector system (Miri and Mraoui, 2007).

enable even air flow through the bed. Uniform distribution of air in rock beds is important. If it is not achieved air will bypass some of the rocks and the full capacity of the bed will not be utilized. Three steps can be taken to ensure uniform air distribution include (a) designing the rock bed for a vertical air flow through the rocks, (b) designing sufficiently large plenum chambers, and (c) designing the rock bed so that the pressure drop across the bed is greater than 4 mm of water.

Phase change materials can be used for solar heat storage systems because in the process of changing from solid to liquid, energy is absorbed by the material and this energy (the heat of transformation) can be released when the material returns to its solid form.

2.4.2 General considerations

The general considerations for solar thermal storage system are daily temperature range and heat capacity. The daily temperature range of the thermal stored is influenced by the amount of solar radiation, the size of the storage device, the heat capacity of the storage material, the demand for heat, and the type of system. The daily temperature range (T_{max}-T_{min}) is related to the amount of usable heat stored in the device (Q) by the equation: $Q = M_s C_p(T_{max}-T_{min})$ where M_s is the mass of the storage material in kg and C_p is the heat capacity of the storage medium in kJ kg^{-1} K^{-1}. If the temperature swing in the store is to be limited for some reason, the necessary size to achieve this can be calculated. Heat capacity is a measure of a materials ability to store sensible heat. In granular material medium such as rock bed, there are spaces between the particles and the percentage of spaces compared to the total volume is termed the void fraction. The volumetric heat capacity of such material will be depending on the void fraction. Experiments have shown that loose materials pack with a void fraction of around 30% and these loose materials behave as if their heat capacity were reduced by this same percentage (Charters and Pryor, 1982).

2.4.3 Design guidelines for rock bed storage

Salaron Corporation Solar Energy Systems (1978) suggested the design criteria for rock bed storage units as follows:

- Storage size: 0.15 - 0.25 cubic meters of rock per square meter of collector,
- Rock bed depth: 1.5-2.0 m (normally),
- Rock size: 20-40 mm (crushed rock or river gravel), the rock should be washed and clean,
- Air mass velocity through the rock fill: 0.10-0.15 m/s velocity is determined by dividing the flow rate through the box by the cross-sectional area of the rock box.

2.5 Thermal properties of rocks

Knowledge of the thermal properties of rock and soil is required to determine heat transfer in the thermal systems which use soils as the container of storage bed. The thermal properties of material depend on number of properties some of which can be time-dependent. The several terms that describe thermal properties are defined as: thermal conductivity, λ (W/m.K) is the ability of a material to transport thermal energy, thermal diffusivity, κ (m^2/s) is the ability of a material to level temperature differences, and thermal capacity, C (J/m^3.K) is the capacity of a material to store thermal energy. $C = \rho c$, ρ is density, kg/m^3, c is thermal capacity, J kg^{-1} K^{-1} (Sandburg, 1988).

2.5.1 Thermal conductivity of rocks

Measurement of thermal conductivity can be classified as in situ measurement and laboratory measurement. There are numerous steady state and transient techniques available for measuring thermal conductivity, the most prominent being the divided bar and the needle probe method. As these methods are discussed in detail in several textbooks and review articles (Beck, 1988, Somerton, 1992). In-situ thermal conductivity may be deviated significantly from laboratory test that is affected from temperature, pressure and pore-fluid. The reason for this problem is a certain scale dependence in which different aspects are involved: in-situ measurements, as a rule, represent an average over a much larger rock volume than laboratory measurements performed on small samples (Gul and Maqsood, 2006).

Thermal conductivity of formed mineral rock can be determined by using mixing law model and empirical model based on the porosity and thermal conductivity data of the mineral contents and saturation (Gul and Maqsood, 2006). Assuming that minerals with thermal conductivities (λ_i) and volume concentration (V_i) are arranged in parallel in a nonporous rock, then the thermal conductivity (λ_s) of the solid rock is,

$$\lambda_s = \frac{\sum \lambda_i V_i}{\sum V_i} \tag{2.1}$$

The variation of thermal conductivity of sedimentary and volcanic rocks is influenced on petrophysical such as porosity, metamorphic and plutonic rock is influenced on dominant mineral phase, and metamorphic rock is influenced on anisotropy (Clauser and Huenges, 1995).

a) Influence of porosity

The thermal conductivity of rocks tends to increase as the increasing of porosity. This is due to the low-conductivity fill of the void space, which can be either air or water. Mixing law models can be used to calculate the thermal conductivity of rocks which combine values of the thermal conductivities of the rock solids (λ_s) with the thermal conductivity of the fluids (λ_f) on the basis of porosity (ϕ). The porosity weighted arithmetic mean would be the equivalent of parallel arrangement of the components relative to the direction of heat flow (Clauser and Huenges, 1995);

$$\lambda_e = \lambda_f \phi + \lambda_s (1 - \phi) \tag{2.2}$$

where λ_s and λ_f are the thermal conductivities of the rock solids and the fluid, respectively. This form gives the largest values of thermal conductivity of the rock/fluid system (λ_e) of all the mixing law models. Table 2.1 summarizes the empirical models that used to determine the thermal conductivity of rock as a function of λ_s, λ_f, and ϕ.

b) Influence of temperature

The thermal conductivity varies inversely with temperature. The measurements on thermal conductivity as function of increasing temperature generally show initially a decrease with temperature. For moderate temperature range several approaches have been suggested as how to infer thermal conductivity at elevated temperatures. Based on the analysis of available tabulated data of thermal conductivity as function of temperature, Zoth and Hanel (1988) suggested the following relationship:

Table 2.1 Empirical models used to determine the thermal conductivity of rocks as a function of λ_f, λ_s, and ϕ.

Model	Expression	References
$\lambda_e = \left[\frac{\phi}{\lambda_e} + \frac{1-\phi}{\lambda_s}\right]^{-1}$	N/A	Gul and Maqsood (2006)
$\lambda_e = (1-A)\lambda_s + A\lambda_f$ where $A = \left[2^n(2^n-1)^{-1}\right]\left[1-(1+\phi)^{-n}\right]$	$n > 0$	Sugawara and Yoshizawa (1962)
$\lambda_e = \lambda_s \left[\frac{\left(\frac{2\lambda_s}{\lambda_f}+1\right) - 2\phi\left(\frac{\lambda_s}{\lambda_f}-1\right)}{\left(\frac{2\lambda_s}{\lambda_f}+1\right) + \phi\left(\frac{\lambda_s}{\lambda_f}-1\right)}\right]$	- ϕ of one of the two components does not exceed about 0.25 - $\lambda_s/\lambda_f \leq 10$.	Maxwell model (1904)
$\lambda_e = \lambda_s \left\{\frac{1-3\phi\left[1-\left(\frac{\lambda_f}{\lambda_s}\right)\right]}{2+\phi+\left(\frac{\lambda_s}{\lambda_f}\right)}\right\}$ $\lambda_e = \frac{\lambda_s\lambda_s(3+\phi)}{\phi\lambda_s + 3\lambda_f}$	- ϕ <1 vol. % - for isolated, more or less, isometric pores, a "minimum" value, - ϕ <1 vol. % - for interconnected, rock-type pores, a "maximum" value,	Walsh and Decker (1966)
$\lambda_e = \lambda_f + (1-\phi)^2\left[(\lambda_s + pS) - \lambda_f\right]$	- p is the actual percentage of the specific mineral - S is a slope constant equal to the change of λ with the specific mineral content, determined from intercept values obtained from experimental data at $(1-\phi)^2 = 1$	Robertson (1988)
$\lambda_e = (\lambda_f)^{\phi}\lambda_s^{(1-\phi)}$	N/A	Woodside and Messmer (1961)

Remarks: λ_f is the pore fluid thermal conductivity; λ_s is solid rock thermal conductivity; λ_e is porous rock thermal conductivity; and ϕ is porosity.

$$\lambda(T) = A + \frac{B}{350 + T} \tag{2.3}$$

where λ is given in W/m.K, T in °C, and the empirical constants A and B are determined from a least-squares fit to measured data for different rock types (Table 2.2).

Sass et al. (1992) also distinguish between the effects of composition and temperature. They propose a quite general empirical relation for λ as a function of λ(25°C) for crystalline rocks:

$$\lambda(T) = \frac{\lambda(0)}{1.007 + T\left(0.0036 - \dfrac{0.0072}{\lambda(0)}\right)} \tag{2.4}$$

$$\lambda(0) = \lambda(25^\circ C)\left[1.007 + 25\left(0.0037 - \frac{0.0074}{\lambda(25^\circ C)}\right)\right] \tag{2.5}$$

Seipold (1998, 2001) used different expressions for the temperature dependence of thermal conductivity. He used a large number of measurements and additional literature data to determine a linear decrease of λ(T). A temperature function can thus be written as:

$$\lambda(T) = \frac{1}{B(T - 532 \pm 45)} + 0.448 \pm 0.014 \tag{2.6}$$

where B is a coefficient which depends on rock type and T is temperature in K.

Table 2.2 Constants A and B for thermal conductivity calculation for different rock types (after Zoth and Hanel, 1988).

Rock Types	**T(°C)**	**A**	**B**
(1) Rock salt	-20-40	-2.11	2960
(2) Limestone	0-500	0.13	1073
(3) Metamorphic rock	0-1200	0.75	705
(4) Acid rock	0-1400	0.64	807
(5) Basic rock	50-1100	1.18	474
(6) Ultra-basic rock	20-1400	0.73	1293
(7) Rock type (2) through (5)	0-800	0.70	770

Remarks: $\lambda(T) = A + \frac{B}{350 + T}$, where T in °C

Vosteen and Schellschmidt (2003) proposed the empirical equation for the determination of thermal conductivity of crystalline and sedimentary rocks as a function of T and λ(0):

$$\lambda(T) = \frac{\lambda(0)}{0.99 + T\left[a - \left(\frac{b}{\lambda(0)}\right)\right]} \tag{2.7}$$

λ(0) for crystalline rock;

$$\lambda(0) = 0.53\lambda(25^\circ C) + \frac{1}{2}\sqrt{1.13\left(\lambda(25^\circ C)\right)^2 - 0.42(25^\circ C)} \tag{2.8}$$

λ(0) for sedimentary rock;

$$\lambda(0) = 0.54\lambda(25^\circ C) + \frac{1}{2}\sqrt{1.16\left(\lambda(25^\circ C)\right)^2 - 0.39(25^\circ C)} \tag{2.9}$$

with empirical constant a = 0.003 and b = 0.0042 for crystalline rocks (0< T< 500°C), a = 0.034 and b = 0.0039 for sedimentary rocks (0< T< 300°C), λ is given in W/m.K and T in °C. Figure 2.16 shows the thermal conductivity of various rock types which tested by many researchers.

2.5.2 Heat capacity of rocks

Measured heat capacities of rocks include the heat capacities of any pore fluids present in the samples analyzed. Because the specific heat capacity of water is higher than that of any mineral, the measured heat capacities of porous, wet rocks do not give a good indication of the heat capacities of the solid materials

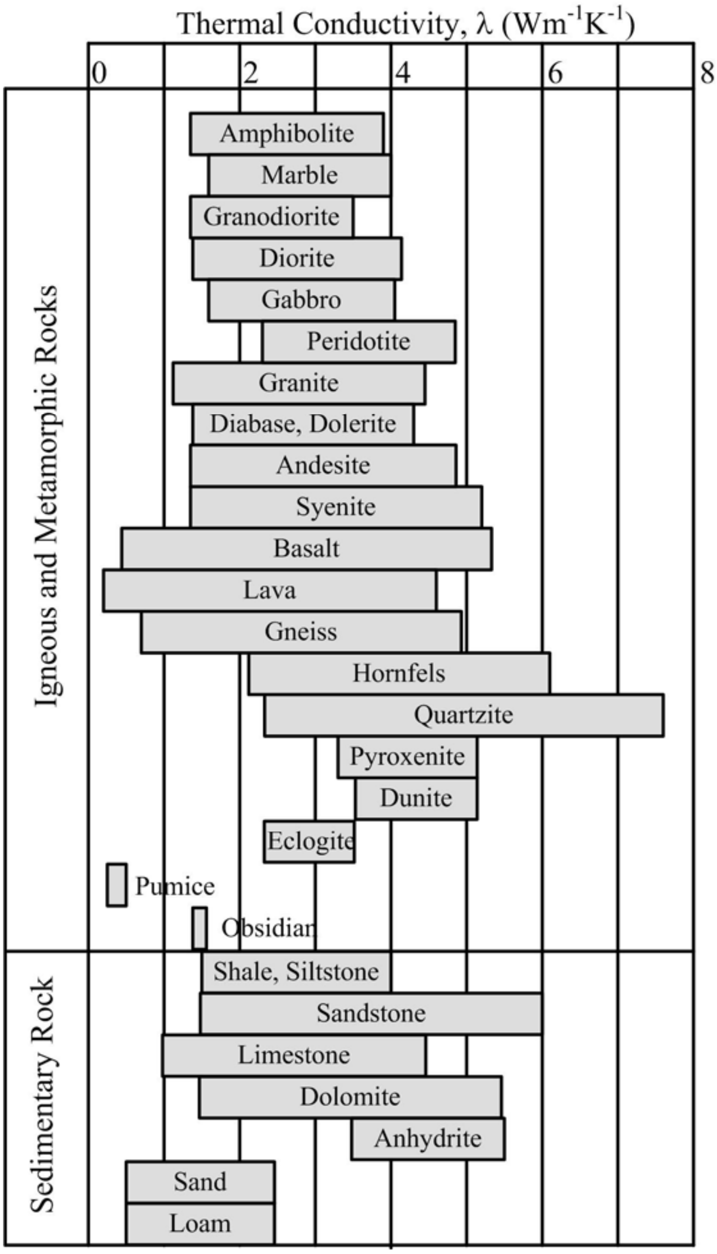

Figure 2.16 Comparison of the thermal conductivity of various rock types (Modified from Department Angewandte Geowissenschaften und Geophysik, 2006).

(Waples and Waples, 2004). Specific heat of rocks can be calculated as the arithmetic mean of the conditions from the individual mineralogical constituents and saturating fluids of the rock weighted by the volume fraction (n_i) of the N individual phases relative to the total rock volume, where $\Sigma n_i = 1$;

$$c = \sum_{i=1}^{N} n_i c_i \tag{2.10}$$

a) Influence of porosity and mineral composition

The thermal capacity of a real rock (that is a mixture of solids and liquids) normally is calculated as the weighted average of the thermal capacities of the various solids and liquids (Somerton, 1992; Scharli and Rybach, 2001). The specific heat capacity of the rock then can be calculated by dividing the thermal capacity by the density of the rock, including pore fluids. As an example, the specific heat capacity (C_p) rock for a rock containing water or ice as its only pore fluid is given by

$$C_{p,rock} = \frac{\left[\rho_{solid} C_{p,solid}(1-\phi) + \rho_{H_2O} C_{p,H_2O}\phi\right]}{\rho_{rock}} \tag{2.11}$$

where ϕ is the fractional porosity, ρ_{solid} is the average grain density, ρ_{H_2O} is the density of water or ice, ρ_{rock} is the density of the rock, and $C_{p,solid}$ and C_{p,H_2O} are the mean specific heat capacity of the mineral grains and the specific heat capacity of the water or ice, respectively. Table 2.3 summarizes the empirical equation used to calculate heat capacity of porous rock.

Table 2.3 Empirical models used to determine the thermal capacity of rocks.

Model	Expression	References
$c = 1.0263\exp(0.2697\rho)$ - for the low-density minerals	c Unite $J/cm^3.K$ ρ unite g/cm^3	Waples and Waples (2004)
$c = -0.0123\rho^4+0.399\rho^3-4.64\rho^2+22.66\rho-36.42$		
$C = -0.0000828C^4+0.00955C^3+0.505C^2-105C+4845$ - for coals	C_p is in J/kg.K C is the % carbon in the coal	Krevelen (1961)
$C_p=4184*(0.2+0.00088T+0.0015V)$		Gambill (1957)
$C_p=0.01[(A+B(V)+C(V)^2+D/(V+1)]$	A, B, C, and D is itself a quadratic function of temperature T (in K)	Richardson (1992)

b) Influence of temperature

The specific heat capacities of individual minerals and nonporous rocks increase with increasing temperature, it is useful to have equations to calculate specific heat capacity as a function of temperature. The researchers have developed empirical equations describing the temperature dependence of specific heat capacity for rocks and minerals. The original standard equation is a polynomial function, usually terminated after the quadratic term, in which the constants A, B, and C are determined empirically for each substance (Waples and Waples, 2004):

$$C_p = A + BT + CT^2 \tag{2.12}$$

For sandstones, the constants A, B, and C are 2.05, 0.00381, and 3.55, respectively (Somerton, 1992). Figure 2.17 gives heat capacity of many rock types.

2.6 Thermal properties of soils

Thermal properties of soil closed to surface are of primarily importance for determining the energy balance and heat transfer between the air and soil interface in storage system (Mongelli et al., 1971; Ochsner et al., 2001; Abu-Hamdeh and Reeder, 2000). They are strongly influenced by the soil volumetric water content (θ), volume fraction of solids (ν_s) and volume fraction of air (ν_a). Air is a poor thermal conductor and reduces the effectiveness of the solid and liquid phases to conduct heat. While the solid phase has the highest conductivity it is the variability of soil moisture that largely determines land temperatures. As such soil moisture properties and soil thermal properties are very closely linked and are often measured and reported together.

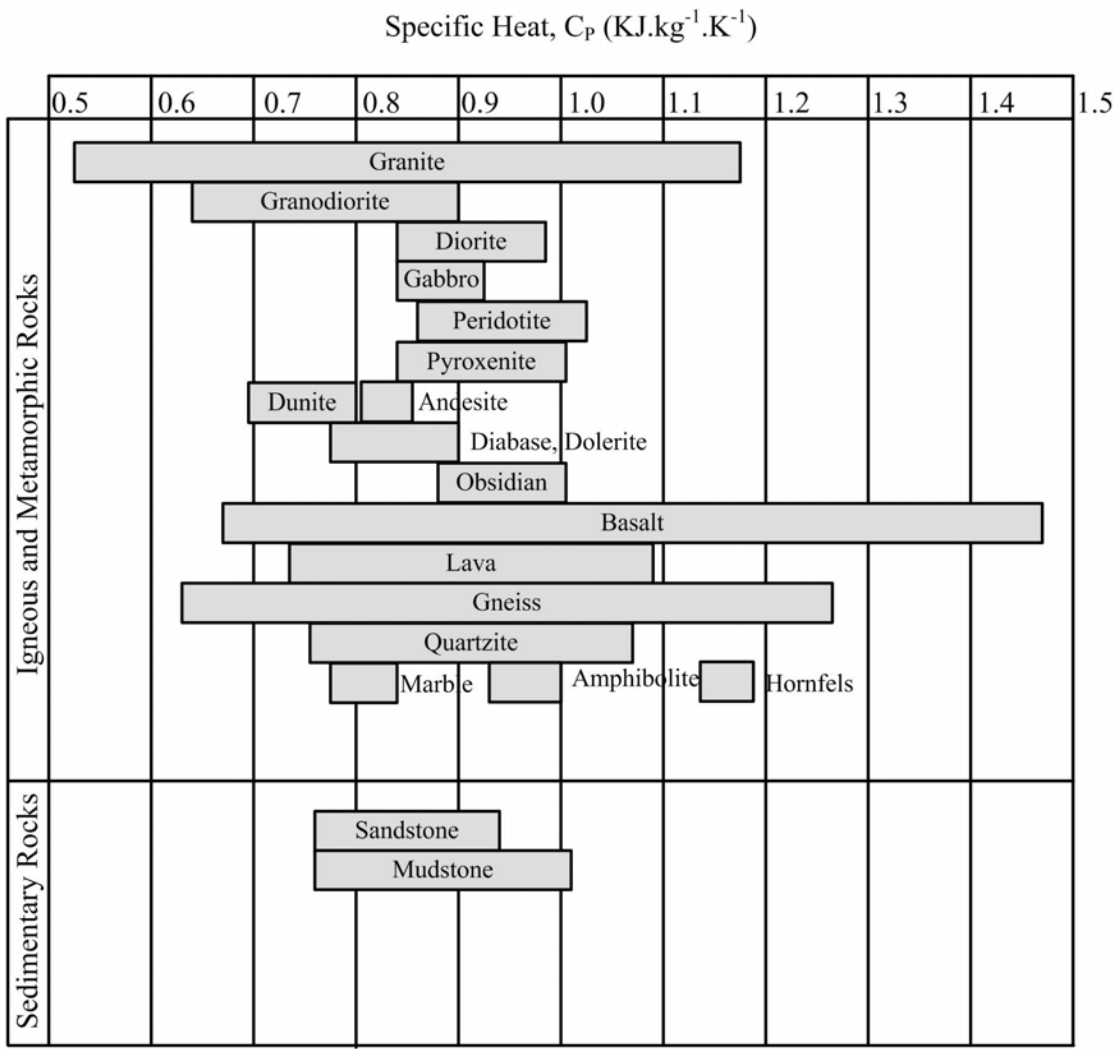

Figure 2.17 Comparison of the heat capacity of various rock types (Modified from Department Angewandte Geowissenschaften und Geophysik, 2006).

2.6.1 Thermal conductivity of soils

The thermal conductivity decreased as the increasing of porosity, increased as the increasing of water content and volume fraction of air. Many researched proposed an empirical function to calculate the soil thermal conductivity (Bilskie, 1994; Campbell and Norman, 1998; Bristow, 2002).

The procedure of DeVries (1963), λ is calculated as the weighted average of the conductivities of the carious soil constituents according to the formula

$$\lambda = \frac{\sum_{i=0}^{n} k_i \lambda_i \nu_i}{\sum_{i=0}^{n} k_i \nu_i} \tag{2.13}$$

where ν_i is the volume fraction of each constituent, λ_i is the thermal conductivity of each constituent, n is the number of soil constituents, and k_i is the weighting factors, depending on the shape and the orientation of the granules of soil constituents. Bristow (2002) proposed an empirical function to compute the soil thermal conductivity from soil water content. The parameters of the empirical function are also calculated empirically from basic soil properties.

$$\lambda_{heat} = A_\lambda + B_\lambda \theta - (A_\lambda - D_\lambda)\exp\left(-(C_\lambda \theta)^{E_\lambda} \right) \tag{2.14}$$

$$A_\lambda = \frac{0.57 + 1.73\phi_d + 0.93\phi_m}{1 - 0.74\phi_d - 0.49\phi_m} - 2.8\phi_s(1 - \phi_s)\,, \tag{2.15}$$

$$B_\lambda = 2.8\phi_s\theta\,,\ C_\lambda = 1 + 2.6\sqrt{m_c}\,,\ D_\lambda = 0.03 + 0.1\rho_s^2\,,\ E_\lambda = 4 \tag{2.16}$$

where ρ_b is density of the bulk soil (g/cm^3), θ is volumetric soil water content (m^3/m^3), ϕ_s is volume fraction of solids (m^3/m^3), ϕ_m is volume fraction of soil minerals other than quartz (m/m^3), ϕ_d is volume fraction of quartz (m/m^3), m_c is clay fraction of soil (g/g), and λ is soil thermal conductivity (W/m.K).

2.6.2 Heat capacity of soils

The heat capacity of soil is modeled as the weighted sum of heat capacities of soil constituents (Campbell and Norman, 1998). Omitting the negligible contribution of air in the soil, the equation is

$$C = \rho_s \nu_s c_s + \rho_w \nu_w \theta \tag{2.17}$$

where ρ_s is the particle density of soil solids, ρ_w is the density of water (998 kg/m^3 at 20°C), c_w is the specific heat capacity of water (4,182 J/kg.K at 20°C), and c_s is the specific heat capacities of the soil constituents.

Nassar et al. (2005) suggest that soil composes of many elements, such as, sand, air and water. Thermal capacity of soil may be determined by identifying the volumetric percent for each element in the mixture as:

$$\rho C_p = f_s(\rho C_p)_s + f_a(\rho C_p)_a + f_w(\rho C_p)_w \tag{2.18}$$

where the symbol f represents the volumetric contribution of each element in the compound, while, the subscripts s, a and w indicate the components of the soil, e.g. sand, air and water, respectively. Some of these volumetric percents are equal to unity. Then: $f_s + f_a + f_w = 1$.

2.7 Thermodynamics and heat transfer

Thermodynamics deals with the relationship between the properties of substance and their changes between two states. A thermodynamics state is defined when all the thermodynamic properties (pressure, specific volume or density, temperature, internal energy enthalpy, constant-volume and constant-pressure specific heat, and entropy) have a set of unique values. The state of the substance changes as the value of one or more thermodynamic properties change. This is called a thermodynamic process. It may be accompanied by work and/or heat transfer. Work transfer is energy transfer due to unbalance in mechanical forces. Heat transfer is energy transfer due to temperature differences (Suryanarayana and Arici, 2003).

2.7.1 Thermodynamic systems

A Thermodynamic system is defined as a quantity of matter or region in space chosen for study. The mass or region outside the system is called the surroundings. The real or imaginary surface that separates the system from its surrounding is called the boundary. Systems may be considered to be closed or open, depending on whether a fixed mass or a fixed volume in space is chosen for study.

A closed system (or a control mass) consists of a fixed amount of mass, and no mass can cross its boundary. But energy, in the form of heat and work, can cross the boundary, and the volume of closed system does not have to be fixed (Figure 2.18). If, as a special case, even energy is not allowed to cross the boundary, that system is called an isolated system.

An open system (or a control volume) is a properly selected region in space. It usually encloses a device that involves mass flow such as a compressor, turbine, or nozzle. Flow through these devices is best studies by selecting the region

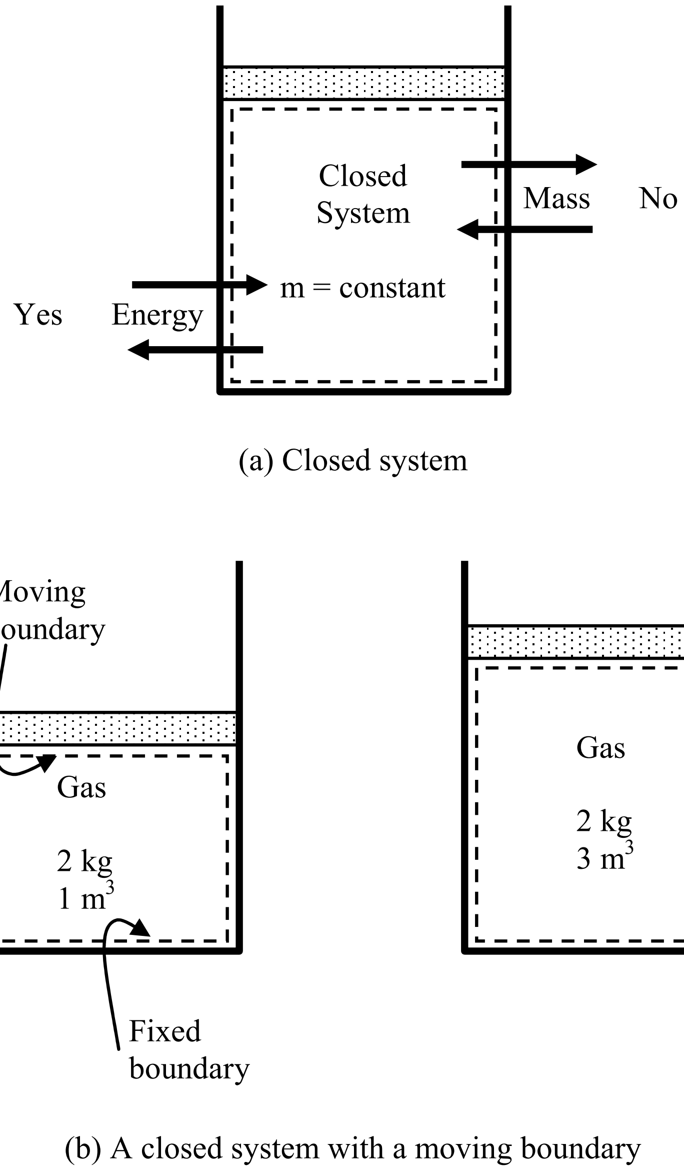

Figure 2.18 Mass and energy transfer within the closed system (Modified from Cengel, 1997).

within the device as the control volume. Both mass and energy can cross the boundary of a control volume, which is called a control surface (Figure 2.19).

2.7.2 Forms of energy

Energy can exist in numerous forms such as thermal, mechanical, kinetic, potential, electric, magnetic, chemical, and nuclear, and their sum constitutes the total energy (E) of a system. The total energy of a system on a unit mass (m) basis is denoted by e and is defined as (Cengel, 1997)

$$e = \frac{E}{m}, \text{ (KJ/kg)} \tag{2.19}$$

In thermodynamics analysis, it is often helpful to consider the various forms of energy that make up the total energy of a system in two groups: macroscopic and microscopic. The macroscopic forms of energy, on one hand, are those system processes as a whole with respect to some outside reference frame, such as kinetic energy (KE) and potential energy (PE). The microscopic forms of energy are those related to the molecular structure of a system and the degree of the molecular activity, and they are independent of outside reference frames. The sum of all the microscopic forms of energy is called the internal energy (U) of a system.

Kinetic energy is the energy that a system processes as a result of its motion relative to some reference frame. When the parts of a system move with the same velocity, the kinetic energy is expressed as (Cengel, 1997)

$$KE = \frac{mv^2}{2}, \text{ (kJ)} \tag{2.20}$$

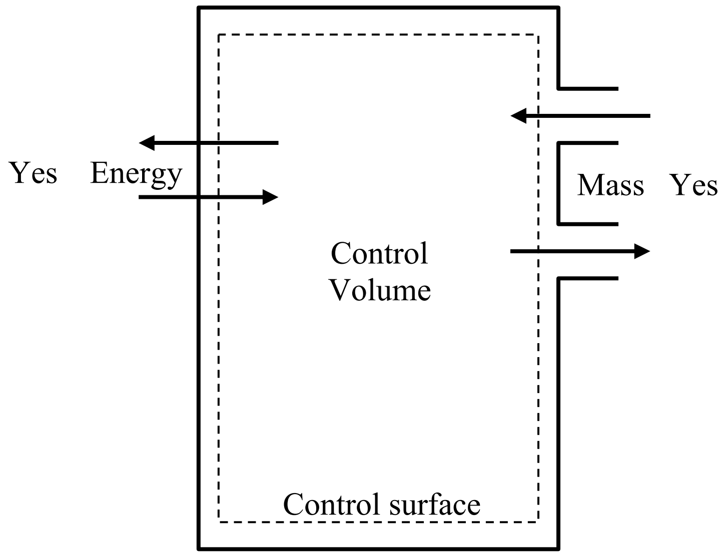

(a) Open system

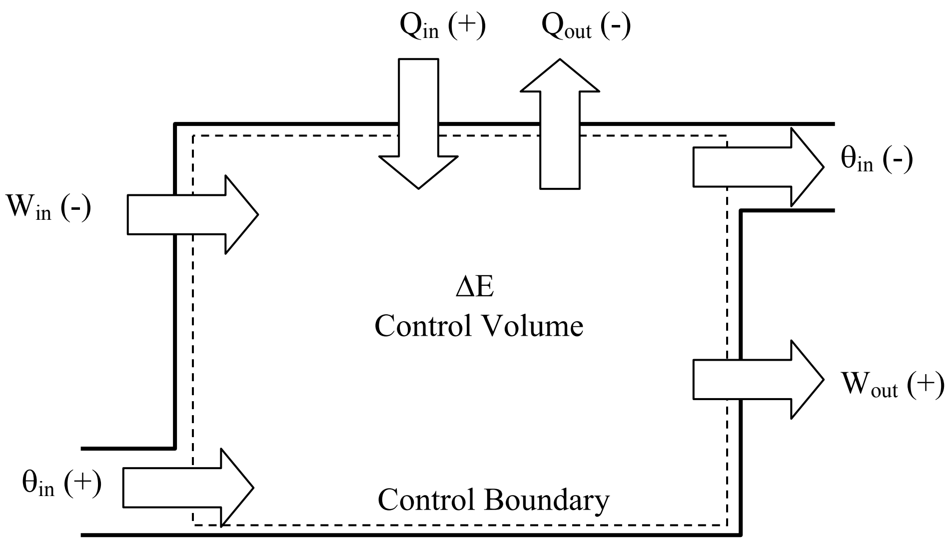

(b) An open system with one inlet and one exit.

Figure 2.19 Mass and energy transfer within the open system (Modified from Cengel, 1997).

Potential energy is the energy that a system processes as a result of its elevation in a gravitational field and is expressed as

$$PE = mgz \text{, (kJ)} \tag{2.21}$$

The magnetic, electric, and surface tension effects are significant in some specialized cases only and are not considered. In the absence of these effects, the total energy of a system consists of the kinetic, potential, and internal energies and is expressed as

$$E = U + KE + PE = U + \frac{mv^2}{2} + mgz \text{, (kJ)} \tag{2.22}$$

or, on a unit mass basis,

$$e = u + ke + pe = u + \frac{v^2}{2} + gz \tag{2.23}$$

Most closed systems remain stationary during a process and thus experience no change in their kinetic and potential energies. Closed systems whose velocity and elevation of center of gravity remain constant during a process are frequently referred to as stationary systems. The change in the total energy (ΔE) of stationary system is identical to the change in its internal energy (ΔU).

The total energy of a system can be contained or stored in a system and can be viewed as the static forms of energy. The forms of energy that are not stored in a system can be viewed as the dynamic forms of energy. The dynamic forms of energy are recognized at the system boundary as they cross it, and they represent the energy gained or lost by a system during a process. The only two forms of energy interactions associated with a closed system are heat transfer and work (Cengel, 1997).

The amount of energy needed to raise the temperature of a unit mass of a substance by one degree is called the specific heat at constant volume (C_v) for a constant-volume process and the specific heat at constant pressure (C_p) for a constant-pressure process. They are defined as

$$C_v = \left(\frac{\partial u}{\partial T}\right)_v \text{ and } C_p = \left(\frac{\partial h}{\partial T}\right)_p \tag{2.24}$$

For ideal gases u, h, C_v, and C_p are functions of temperature alone. The Δu and Δh of ideal gases can be expressed as

$$\Delta u = u_2 - u_1 = \int_1^2 C_v(T)dT \approx C_{v,av}(T_2 - T_1) \tag{2.25}$$

$$\Delta h = h_2 - h_1 = \int_1^2 C_p(T)dT \approx C_{p,av}(T_2 - T_1) \tag{2.26}$$

For ideal gases, C_v and C_p are related by

$$C_p = C_v + R, \text{ [kJ/(kg.k)]} \tag{2.27}$$

For incompressible substances (liquids and solids), both the constant-pressure and constant-volume specific heats are identical and denoted by C:

$$C_p = C_v = C, \tag{2.28}$$

The Δu and Δh of incompressible substance are given by

$$\Delta u = \int_1^2 C(T)dT \approx C_{av}(T_2 - T_1) \text{, (kJ/kg)} \tag{2.29}$$

$$\Delta h = \Delta u + v\Delta P \text{, (kJ/kg)} \tag{2.30}$$

2.7.3 Heat transfer

Suryanarayana and Arici (2003) conclude that heat is defined as the form of energy that is transferred between two systems (or a system and its surroundings) by virtue of a temperature difference. Heat transfer is energy transfer due to temperature differences. It can be classified as either diffusion or radiation. Diffusion requires a material medium. In a diffusion process the energy flux across a surface at any location can be found from knowledge of the state of the medium in the immediate vicinity of the location, and the effect of a disturbance in temperature is propagated much more slowly than in radiation. In radiative heat transfer, the energy transport does not require a material medium, and to determine the energy flux at a point, one needs to know the state of all the regions that the point sees.

Heat transfer is a surface phenomenon. The heat transfer rate across a surface is found from the relation

$$q = \int q'' dA \text{, (W/m}^2\text{)} \tag{2.31}$$

where, q'' is the heat flux normal to the surface dA. Depending on the mode, an appropriate expression relating the heat flux and temperature is inserted into Equation (2.31) to determine the total heat transfer rate (Suryanarayana and Arici, 2003).

Heat has energy units, kJ (or Btu) being the most common one. A mount of heat transferred during the process between two states (states 1 and 2) is denoted by Q_{12}, or just Q. Heat transfer per unit mass (q) is determined from

$$q = \frac{Q}{m}, \text{ (kJ/kg)} \tag{2.32}$$

Sometimes it is desirable to know the rate of heat transfer ($\dot{Q}$) instead of the total heat transferred over some time interval. The heat transfer rate has the unit kJ/s, which is equivalent to kW. When varies with time, the amount of heat transfer during a process is determined by integrating $\dot{Q}$ over the time interval of the process:

$$Q = \int_{t_1}^{t_2} \dot{Q}dt, \text{ (kJ)} \tag{2.33}$$

When $\dot{Q}$ remains constant during a process, the relation above reduces to

$$Q = \dot{Q}\Delta t, \text{ (kJ)} \tag{2.34}$$

where $\Delta t = t_2 - t_1$ is the time interval during which the process occurs.

Heat can be transferred in three different ways: conduction, convection, and radiation. All modes of heat transfer require the existence of a temperature difference, and all modes of heat transfer are from the high-temperature medium to a lower-temperature one (Cengel, 1997; 2003).

Conduction is the transfer of energy from the more energetic particles of substance to the adjacent less energetic ones as a result of interactions between the particles. It can take place in solids, liquids, or gases. In gases and liquids, conduction is due to the collisions of molecules during their random motion. In solids, it is due to the combination of vibrations of the molecules in a lattice and the energy transport by free electrons. It is observed that the rate of heat conduction ($\dot{Q}_{cond}$) through a layer of constant thickness (Δx) is proportional to the temperature difference (ΔT) across the layer and the area (A) normal to the direction of heat transfer, and is inversely proportional to the thickness of the layer. Therefore,

$$\dot{Q}_{cond} = kA\frac{\Delta T}{\Delta x}, \text{ (W)} \tag{2.35}$$

where the constant of proportionality k is the thermal conductivity of the material which is a measure of the ability of a material to conduct heat. In the limiting case of $\Delta x \rightarrow 0$, the Equation (2.35) reduces to the differential form:

$$\dot{Q}_{cond} = -kA\frac{dt}{dx}, \text{ (W)} \tag{2.36}$$

which is known as Fourier's law of heat conduction. It indicates that the rate of heat conduction in a direction is proportional to the temperature gradient in the direction. Heat is conducted in the direction of decreasing temperature, and the temperature gradient becomes negative sing is added in Equation (2.35) to make heat transfer in the positive x direction a positive quantity (Cengel, 1997; 2003).

Convection is the mode of energy transfer between a solid surface and the adjacent liquid or gas which is in motion, and it involves the combined effects of conduction and fluid motion. The convection is called forced convection if the fluid is forced to flow in a tube or over a surface by external means such as a fan, pump, or the wind. In contrast, convection is call free (or natural) convection if the fluid motion is caused by buoyancy forces that are induced by density differences due to the variation of temperature in the fluid. The rate of heat transfer by convection ($\dot{Q}_{conv}$) is determined from Newton's law of cooling, which is expressed as

$$\dot{Q}_{conv} = hA(T_s - T_f), \text{(W)} \tag{2.37}$$

where h is the convection heat transfer coefficient, A is the surface area through which heat transfer takes place, T_s is the surface temperature, and T_f is bulk fluid temperature away from the surface. At the surface, the fluid temperature equals the surface temperature of the solid (Cengel, 1997; 2003). For natural convection heat transfer, h can be determined from Equation (2.38):

$$h = \left(\frac{k}{\delta}\right)\mathrm{Nu} \tag{2.38}$$

where, Nu is Nusselt number, the simple relations for the average Nu for various on the geometries are given in Table 2.4,

δ is characteristic length, and

k is thermal conductivity of object in fluid.

For spherical shape;

$$\mathrm{Nu} = 2 + \frac{0.589\mathrm{Ra}^{1/4}}{\left[1 + \left(\frac{0.469}{\mathrm{Pr}}\right)^{9/16}\right]^{4/9}} \tag{2.39}$$

Table 2.4 Nusselt number (Cengel, 1998).

Geometry	Characteristic length δ	Range of Ra	Nu
Vertical plate 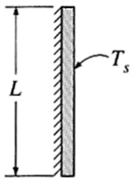	L	10^4–10^9 10^9–10^{13} Entire range	$\text{Nu} = 0.59\text{Ra}^{1/4}$ $\text{Nu} = 0.1\text{Ra}^{1/3}$ $\text{Nu} = \left\{0.825 + \frac{0.387\text{Ra}^{1/6}}{(1 + (0.492/\text{Pr})^{9/16})^{8/27}}\right\}^2$ (complex but more accurate)
Inclined plate 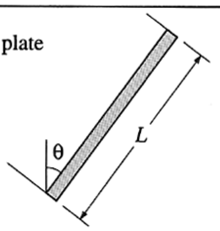	L		Use vertical plate equations as a first degree of approximation. Replace g by $g\cos\theta$ for $\text{Ra} < 10^9$
Horizontal plate (Surface area A and perimeter p) (*a*) Upper surface of a hot plate (or lower surface of a cold plate) 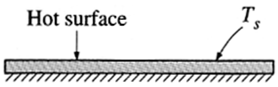 (*b*) Lower surface of a hot plate (or upper surface of a cold plate) 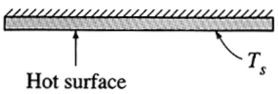	A/p	10^4–10^7 10^7–10^{11} 10^5–10^{11}	$\text{Nu} = 0.54\text{Ra}^{1/4}$ $\text{Nu} = 0.15\text{Ra}^{1/3}$ $\text{Nu} = 0.27\text{Ra}^{1/4}$
Sphere 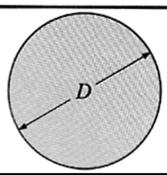	$\frac{1}{2}\pi D$	$\text{Ra} \le 10^{11}$ ($\text{Pr} \ge 0.7$)	$\text{Nu} = 2 + \frac{0.589\text{Ra}^{1/4}}{(1 + (0.469/\text{Pr})^{9/16})^{4/9}}$

where, Pr is Prandtl number (= 0.71 for dry air at atmospheric pressure and temperature ranging from 0 through 300 °C)

Ra is Rayleigh number, which is the product of the Grashof (Gr_L) and Prandtl numbers;

$$Ra = Gr_L \, Pr = \frac{g\beta(T_s - T_\infty)\delta^3}{\nu^2} \cdot Pr \tag{2.40}$$

where, ν is kinematics viscosity of air, $15.7\times10^{6} \le \nu \le 19.4\times10^{6}$ for temperature ranging from 20 through 60°C (Raznjevic, 1976). β is coefficient of volume expansion (β= 1/T).

Radiation is the energy emitted by matter in the form of electromagnetic waves (or photons) as a result of the changes in the electronic configurations of the atoms or molecules. The transfer energy by radiation does not require the presence of an intervening medium. Energy transfer by radiation is fastest (at speed of light) and it suffers no attenuation in a vacuum. Radiation is a volumetric phenomena, and all solids, liquids, and gases emit, absorb, or transmit radiation to varying degrees. However, radiation is usually considered to be a surface phenomenon for solids that are opaque to thermal radiation such as metals, wood, and rocks since the radiation emitted by interior regions of such material can never reach the surface, and radiation incident on such bodies is usually absorbed within a few microns from the surface. The maximum rate of radiation ($\dot{Q}_{emit,max}$) that can be emitted from a surface at an absolute temperature T_s is given by the Stefan-Boltzmann, law as

$$\dot{Q}_{emit,max} = \sigma A T_s^4 \text{, (W)} \tag{2.41}$$

where A is the surface area and σ = 5.67×10^{-8} W/(m^2.K^4) is the Stefan-Boltzmann constant. The idealized surface which emits radiation at this maximum rate is called a blackbody, and the radiation emitted by real surfaces is less than the radiation emitted by a blackbody at the same temperature and it expressed as

$$\dot{Q}_{emit} = \varepsilon\sigma A T_s^4 \text{, (W)} \tag{2.42}$$

where ε is the emissivity of the surface. The property emissivity, whose value is in the range $0\leq\varepsilon\leq1$, is a measure of how closely a surface approximates a blackbody for which $\varepsilon = 1$.

Another important radiation property of a surface is its absorbtivity (α) which is the fraction of the radiation energy incident on the surface that is absorbed by the surface. Like emissivity, its value is in the rage $0\leq\alpha\leq1$. A blackbody is perfect absorbs ($\alpha = 1$) as well as a perfect emitter. Both α and ε of surface depend on the temperature and the wavelength of the radiation. Kirchhoff's law of radiation states that the emissivity and the absorbtivity of a surface are equal at the same temperature and wavelength. In the most practical applications, the dependence of α and ε on the temperature and wave length is ignored, and the average absorbtivity of a surface is taken to be equal to its average emissivity. The rate at which a surface absorbs radiation is determined from (Figure 2.20)

$$\dot{Q}_{abs} = \alpha\dot{Q}_{inc} \text{, (W)} \tag{2.43}$$

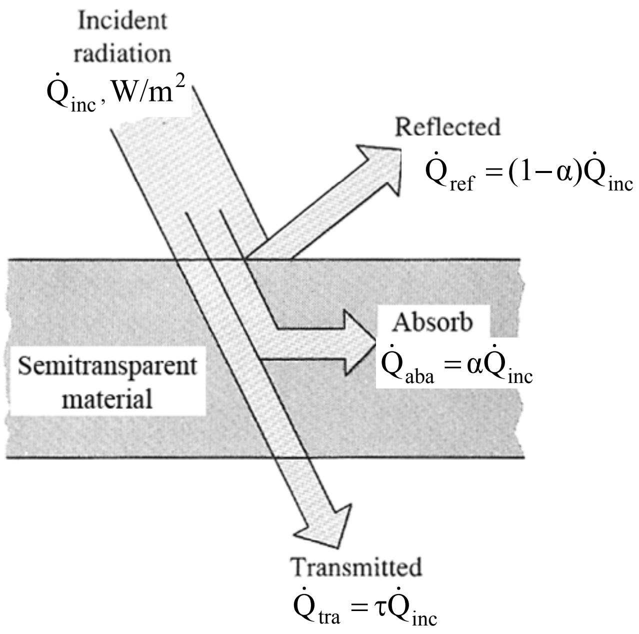

Figure 2.20 Absorption of radiation incident on an opaque surface of absorbtivity (Cengel, 2003).

where $\dot{Q}_{inc}$ is the rate at which radiation is incident on the surface and α is the absorbtivity of the surface. For opaque (nontransparent) surfaces, the portion of incident radiation that is not absorbed by the surface is reflected back.

The difference between the rates of radiation emitted by the surface and the radiation absorbed is the net radiation heat transfer. In general, the determination of the net rate of heat transfer by radiation between two surfaces is a complicated matter since it depends in the properties of the surface, their orientation relative to each other, and the interaction of the medium between the surfaces with radiation. In special case of a relatively small surface of emissivity (ε) and surface area (A) at absolute temperature (T_s) that is completely enclosed by much larger surface at absolute temperature (T_{surr}) separated by gas (such as air) that does not interact with radiation, the net rate of radiation heat transfer between these two surfaces is determined from (Figure 2.21)

$$\dot{Q}_{rad} = \varepsilon\sigma A(T_s^4 - T_{surr}^4)\text{, (W)} \tag{2.44}$$

In this special case, the emissivity and the surface area of the surrounding surface do not have any effect on the net radiation heat transfer.

2.7.4 Conservation of energy principle

Cengel (1997) concludes that the first law of thermodynamics, or the conservation of energy principle for a closed system or fixed mass, may be expressed as follows:

$$\begin{bmatrix} \text{net energy transfer} \\ \text{to (or form) the system} \\ \text{as heat and work} \end{bmatrix} = \begin{bmatrix} \text{net increase (or decrease)} \\ \text{in the total energy} \\ \text{of system} \end{bmatrix}$$

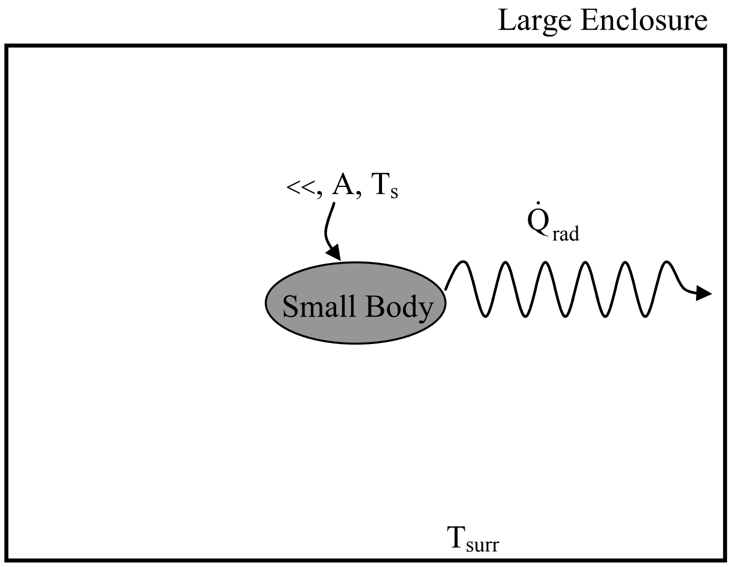

Figure 2.21 Radiation heat transfer between a body and the inner surfaces of a much larger enclosure which completely surrounds it (Cengel, 1997).

or $Q - W = \Delta E$, (kJ) (2.45)

where
- Q is net heat transfer across system boundaries (= ΣQ_{in} - Σ_{out})
- W is net work done in all forms (= ΣW_{out} - ΣW_{in})
- ΔE is net change in total energy of system

Then the change of total energy of a system during a process can be expressed as the sum of the changes in its internal, kinetic, and potential energies:

$$\Delta E = \Delta U + \Delta KE + \Delta PE \text{, (kJ)} \quad (2.46)$$

Substituting Equation (2.46) into Equation (2.45);

$$Q - W = \Delta U + \Delta KE + \Delta PE \text{, (kJ)} \quad (2.47)$$

where $\Delta U = m(u_2 - u_1)$, $\Delta KE = \frac{1}{2} m(v_2^2 - v_1^2)$, and $\Delta PE = mg(z_2 - z_1)$

For stationary closed systems, the changes in kinetic and potential energies are negligible (that is, $\Delta KE = \Delta PE = 0$), and the first-law relation reduces to

$$Q - W = \Delta U \quad (2.48)$$

The rate form of the first law is obtained by dividing Equation (2.45) by the time interval Δt and taking the limit as $\Delta t \rightarrow 0$. This yield

$$\dot{Q} - \dot{W} = \frac{dE}{dt} \text{, (kW)} \quad (2.49)$$

Equation (2.49) can be expressed in differential form as

$$\delta Q - \delta W = dE \text{, (kJ)} \qquad (2.50)$$

2.8 Modeling of thermal system

Jaluria (1998) discusses the modeling of thermal systems, a crucial element in the design and optimization process. Because of complexity of typical system, it is essential to simplify the analysis so that the inputs needed for design can be obtained with the desired accuracy without spending exorbitant time and effort in computations or experiments. The model also allows one to minimize the number of parameters that govern a given system or process and to generalize the results so that they may be used for a wide range of conditions and design. Several types of models are considered, particularly analog, mathematical, physical, and numerical. Analog models are of limited value since such models themselves must be ultimately solved by mathematical and numerical modeling. The mathematical model, both theoretical model, derived on the basis of physical insight, and empirical model, which simply curve fit available data, are considered, since both of these lead to mathematical equations that characterize the behavior of a given system. Curve fitting is discussed in detail, following physical modeling, since it is used to develop equations from experimental data as well as from numerical results.

2.8.1 Mathematical modeling

Mathematical modeling is at the very core of modeling of thermal system because it brings out the basic considerations with respect to given system, focusing on the dominant mechanisms and neglecting less important aspects. It simplifies the problem by using approximations and idealizations. Conservation laws are used to derive the governing equations, which may be algebraic equation, integral equation, ordinary differential equations, partial differential equations, or combination of these. The governing equations are often further simplified by dropping terms that are relatively small, often employing nondimensionalization of the equations to determine which term are negligible (Jaluria, 1998).

2.8.2 Physical modeling

Physical modeling refers to the process of developing a model that is similar in shape and geometry to the given component or system. The given system is often represented by scaled-down version in which experiments are performed to provide information that is not easily available through mathematical modeling. Dimensional analysis is employed to determine the important dimensionless groups that govern the behavior of the given system so as to reduce the experimental effort. These parameters are also used to establish similitude between the model and the actual system or prototype. Various kinds of similarity are outlined, including geometric, kinematics, dynamic, thermal, and mass transfer similarly. The conditions needed for these types of similarity are presented (Jaluria, 1998).

2.8.3 Numerical modeling

For most practical thermal systems, numerical methods are essential for obtaining a solution to the governing equations because of the inherent complexity in those systems. This complexity arises for the nonlinear nature of transport mechanisms, complicated domains and boundary conditions, material property variations, coupling between flow and heat transfer mechanisms, the transient and distributed nature of most processes, and the wide range of energy sources. Numerical modeling involves selecting the appropriate method for the solution; for instance, the finite-difference or the finite-element method; discretizing the mathematical equations to put them in a form suitable for digital computation; choosing appropriate numerical parameters, such as grid size, time step, etc.; developing the numerical code; and obtaining the numerical solution. Additional inputs on material properties, heat transfer coefficients, component characteristic, etc., are entered as part of the numerical model. The validation of the numerical results is then carried out to ensure that the numerical scheme yields accurate results than closely approximate the behavior of the actual physical system. The numerical scheme for the solution of the equations that describe the flow and heat transfer in a solar energy storage system, for instance, represents a numerical model of this system (Jaluria, 1998).

2.9 Geology of igneous rocks in Thailand

There are many types of igneous rocks found in Thailand formed during Paleozoic to Cenozoic Era and can be divided into 3 zones or 3 major belts according to their appearance 1) the Eastern Belt; 2) the Central Belt; and 3) the Western Belt. Most of the rocks are granite and volcanic rocks. Some mafic and ultramafic rocks occur as a narrow belt along geological suture crossed Nan-Uttaradit-Nakhon Ratchasima-Sa Kaeo-Prachin Buri and Narathiwat (Klompe, 1962; Pitakpaivan, 1969; and Suensilpong and Putthapiban, 1978).

Igneous rocks in the north and in the upper part of the west consists either intrusive rocks or extrusive rocks. The intrusive rocks are granite and gneissic granite. The rocks occur in 3 minor belts; 1) the east belt extending from west of Chiang Rai to Phayao, Nan and Uttaradit, the rock is porphyritic granite formed as small pluton around 208±4 to 213±10 million years ago; 2) the middle belt extending from west of Chiang Mai to Lampang and Tak, the rocks are foliated batholiths granite with locally metamorphic granite formed 212±12 to 236±5 million years ago (approximately); 3) the west belt granite formed as a chain of small photons intruded through paleozoic rock and some granites in the middle part, the granites show porphyritic texture to slightly course-grain texture and the age is about 130±4 million years. The extrusive rocks distribute in large area from east of Chiang Rai trough Phayao, Lampang, Phrae and Tak. Most of the rocks are rhyolite, andesite, rhyolitic tuff, andesitic tuff, basalts and some of gabbros and pyroxenite, ages of the extrusive rock are from Silurian to Jurassic Periods. Ages of basalts found in 3 districts of Lampang, Maeta, Kohka and Sobphra, are from 500,000 to 800,000 years. Whereas ages of basalts found in Chiang Rai at Ban Changkean in Theung District is approximately 1.7±0.12 million years and ages of basalt found in Phrae province at Ban Bokaew in Denchai district is approximately 5.64±0.28 million years (approximately) (German Geological Mission to Thailand Report, 1972).

Basalt is another source of extrusive rock or volcanic rock formed by cooling of melting rock, or so-called Lava flows out of the earth surface through joints or volcanic vents. Most of basalt colors are black, gray, green or blackish purple. Their textures vary from fine grained to coarse grained and most of them are vesicular basalt. The rock forming minerals are plagioclase, feldspar, olivine and pyroxene. Only rarely quartz is found. The corundum bearing basalts are found in Kanchanaburi, Phrae, Lampang, Chantaburi, Trad and Si Sa Ket. The rest basalts are corundum-less basalt distributed in many areas in Chiang Rai, Lampang. Petchaboon, Lop Buri, Nakhon Ratchasrima, Chon Buri, Saraburi, Uttaradit, Burirum, Ubon Ratchathani and Surin (Department of Primary Industries and Mines, 2004).

According to Department Mineral Resources (2003), the reserved storage of basalts in Thailand is as follows: Burirum – 82,689,240 metric tons, Nakhon Ratchasrima – 18,217,425 metric tons, Trad – 22,346,619 metric tons, Petchaboon – 11,300,700 metric tons, and Surin – 15,345,494 metric tons (Department Mineral Resources, 2003).

CHAPTER III

LABORATORY TEST

This chapter presents the laboratory testing on rocks and soil. Rock samples are tested to determine the thermal conductivity and heat capacity. These parameters will be used as input for the mathematical equation (presented in next chapter). Soil sample is tested to determine the grain size distribution and to indicate the type of soil.

3.1 Types of rock and soil

Most of rocks used in this study are collected in the northern, northeastern, and central part of Thailand. The selection criteria are that the rocks cover a large variety as much as possible, and that the sample collection is convenient and repeatable. Rock samples were collected from ten different locations, which represented the most commonly encountered rocks in the construction and mining industries in Thailand. They can be categorized here into six groups: four sandstones, three granites, two rock salts, marble, limestone, and basalt. Soil sample was collected in the area of Suranaree University of Technology where the pilot scale solar thermal energy storage will be constructed. Table 3.1 gives rock name and geologic formation or unit to which they belong, and location from which they are obtained. Figure 3.1 shows the area where the rock and soil specimens are obtained for the laboratory testing.

Table 3.1 Locations and rock unit/or formation of rocks.

No.	Materials	Locations	Rock Unit/or Formation
1	Compacted Soil	Suranaree University of Technology/Nakhon Ratchasrima province	Clayey Sand
2	Saraburi Marble	Saraburi province	Saraburi Group
3	Burirum Basalt	Muang district/ Burirum province	Burirum Basalt Unit
4	Lopburi Limestone	Lopburi province	Saraburi Group
5	Phu Kradung Sandstone	Pakchong district/ Nakhon Ratchasrima province	Phu Kradung Formation
6	Phu Phan Sandstone	Sricue district Nakhon Ratchasrima province	Phu Phan Formation
7	Phra Wihan Sandstone	Sricue district Nakhon Ratchasrima province	Phra Wihan Formation
8	Sao Khua Sandstone	Dankhuntod district Nakhon Ratchasrima province	Sao Khua Formation
9	Chinese Granite	China	N/A
10	Tak Granite	Tak province	Eastern Belt Granite/ Tak Batholith
11	Vietnamese Granite	Vietnam	N/A
12	Middle Salt Unit	Phra Thongcom sub-district/ Nakhon Ratchasrima province	Khorat Basin/Maha Sarakham Formation
13	Lower Salt Unit	Phra Thongcom sub-district/ Nakhon Ratchasrima province	Khorat Basin/Maha Sarakham Formation

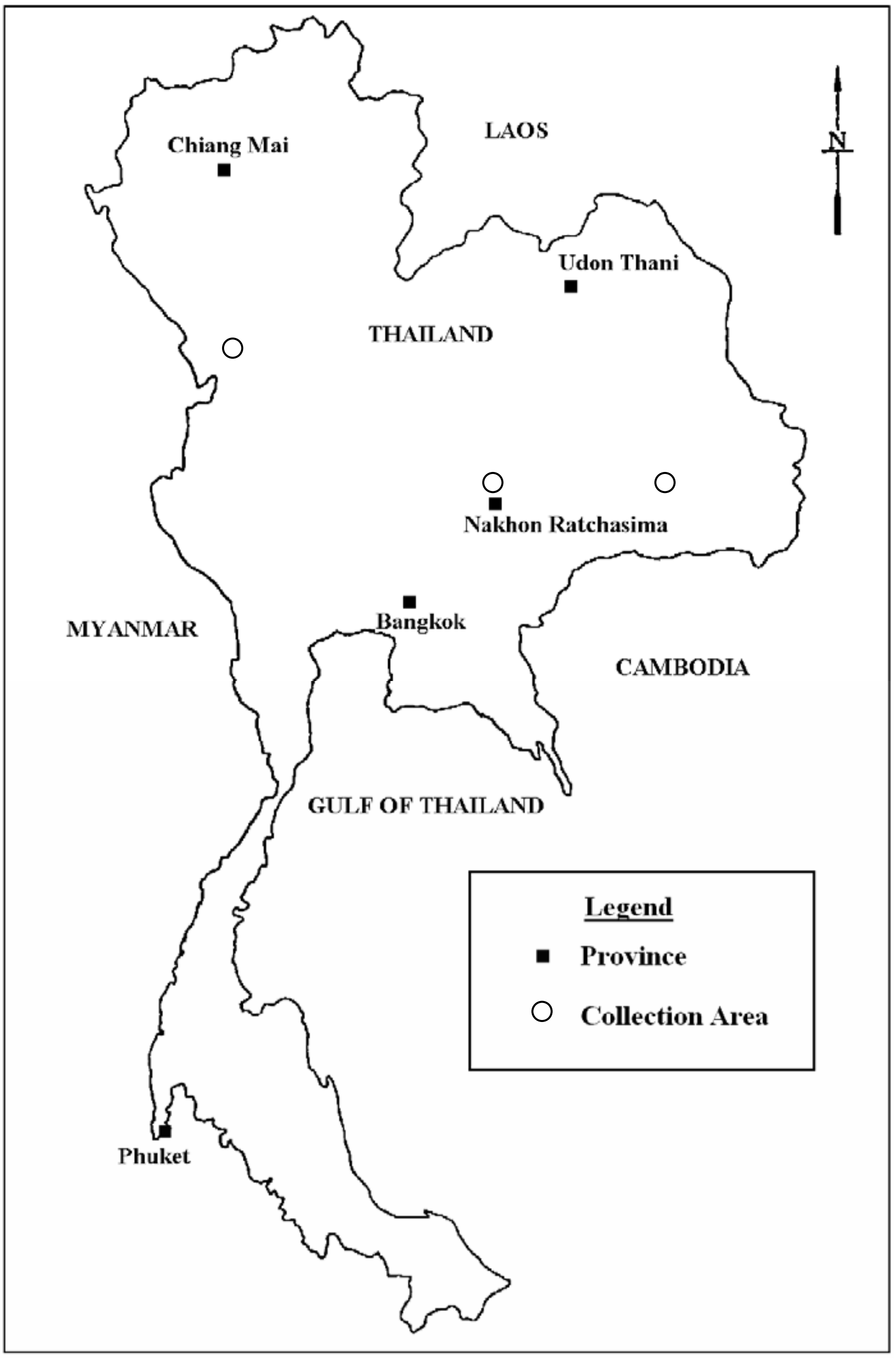

Figure 3.1 Location map of the area where the rock specimens are obtained for the laboratory testing.

3.1.1 Soil samples

Soil sample is collected in the area on the west side of F.4 building, Suranaree University of Technology, where the pilot-scaled solar thermal energy storage will be constructed. They are poor sorting with conglomerates inside fine grained particles.

3.1.2 Rock samples

1) Sandstones: The sandstone samples are collected from four locations in Nakhon Ratchasima province. These samples are Phu Kradung sandstone, Phu Phan sandstone, Phra Wihan sandstone, and Sao Khua sandstone. Phu Kradung sandstone is collected from Pakchong district. It has fine grained, grayish green color and slightly reacted with HCl. Phu Phan sandstone is collected from Sricue district. It has fine grained, brownish yellow color, with quartz and feldspar dominated with a few mica, well sorted, angular, and not reacted with HCl. Phra Wihan sandstone is collected from Sricue district. It has fine grained, brownish white color with scattered black, quartz and feldspar dominated with less mica, well sorted, angular, not reacted with HCl. Sao Khua sandstone is collect from Dankhuntod district. It has fine grained, appearing red color, with feldspar and quartz dominated with less mica, well sorted, angular, not reacted with HCl.

2) Granites: Granites are collected from three locations including Tak granite, Chinese granite, and Vietnamese granite. Tak granite is the eastern belt granite. It is gray, fine grained with grain size approximately 4 to 5 mm. The essential minerals in the Tak granite are plagioclase and quartz. Chinese granite is white, coarse grain with grained size approximately 5 mm. This granite comprises plagioclase and quartz. Vietnamese granite is reddish-pink,

fine grained with grain size approximately 2 to 5 mm. The common minerals in this granite are quartz and feldspar.

3) Rock salts: The specimens used here belong to the middle and lower salt member of the Maha Sarakham formation in the Khorat Basin. They are obtained from 54-mm diameter cores drilled from the depth ranging between 320 m and 350 m at Non Thai district, Nakhon Ratchasima province. The middle salt is smoky white with grain size approximately 5 mm comprising one percent of anhydrite and one percent of clay mineral. The lower salt is clean with colorless with grain size around 5 mm and with 1 percent of clay mineral.

4) Marbles: These samples are collected from Saraburi and Lopburi provinces. Saraburi marble is white, fine grained calcite (2-mm average grain size). Lopburi marble is brown-yellow and fine grained. Both Saraburi and Lopburi marbles strongly react with HCl.

5) Limestone: These samples are collected from Saraburi province. They belong to limestone in Saraburi group. They are dark gray and fine grained.

6) Basalt: Basalt samples are Burirum basalt unit which collected from the area of Hinratch Mining Company, Muang district, Burirum province. They are grayish-black, densed with a few vesicles (less than 1%). No olivine crystal observed.

3.2 Sample preparation

There are 3 types of laboratory test including petrographic study of rocks, grain size distribution of soil and thermal properties test rocks.

For petrographic analysis, ten thin sections of representative samples are prepared from each rock type. The specimen size is 2×3 cm with a thickness of less than 1 mm.

For thermal property determination, rock samples are cut by cutting machine (Figure 3.2) and soil sample (which are disturbed during collecting) are compacted to obtain the specimens with dimension of 1×3×3 cm (two pieces for each sample). The rock surfaces are polished to obtain the smooth surfaces. Figure 3.3 shows some rock and soil specimens prepared for the thermal property testing.

Granular soils are washed to separate the course and fine grained soil. The course grained soil contained on sieve no.200 and fine grained soil is removed through washing (suspended in water). They are dried in oven under temperature at 110°C for 12 hours. Then the dry samples are tested by sieve analysis and hydrometer testing to determine grain size distribution.

3.3 Physical property of soil

Soil samples are tested by sieve analysis and hydrometer test to classify soil type. The test procedure follows the ASTM standard (ASTM D422). Hydrometer test is used for fine grains Figure 3.4a) and sieve analysis for course grains (Figure 3.4b). Figures 3.5 through 3.8 show the relationship between percent finer and sieve openings of soil sample numbers A1, A2, B1 and B3. Tables 3.2 and 3.3 summaries the percentage by weight of gravel and pebble, sand, silt, and clay when classifying based on Wentworth’s scale (Wentworth, 1922) and Unified Soil Classification System (ASTM D2487-00). Figures 3.9 and 3.10 illustrate soil sample after sieve analysis. From the results, soil sample used in this research can be classified as clayey sand.

Figure 3.2 Rock sample is cut to obtain the desired geometry and size.

Figure 3.3 Rock and soil specimens prepared for the thermal property determination.

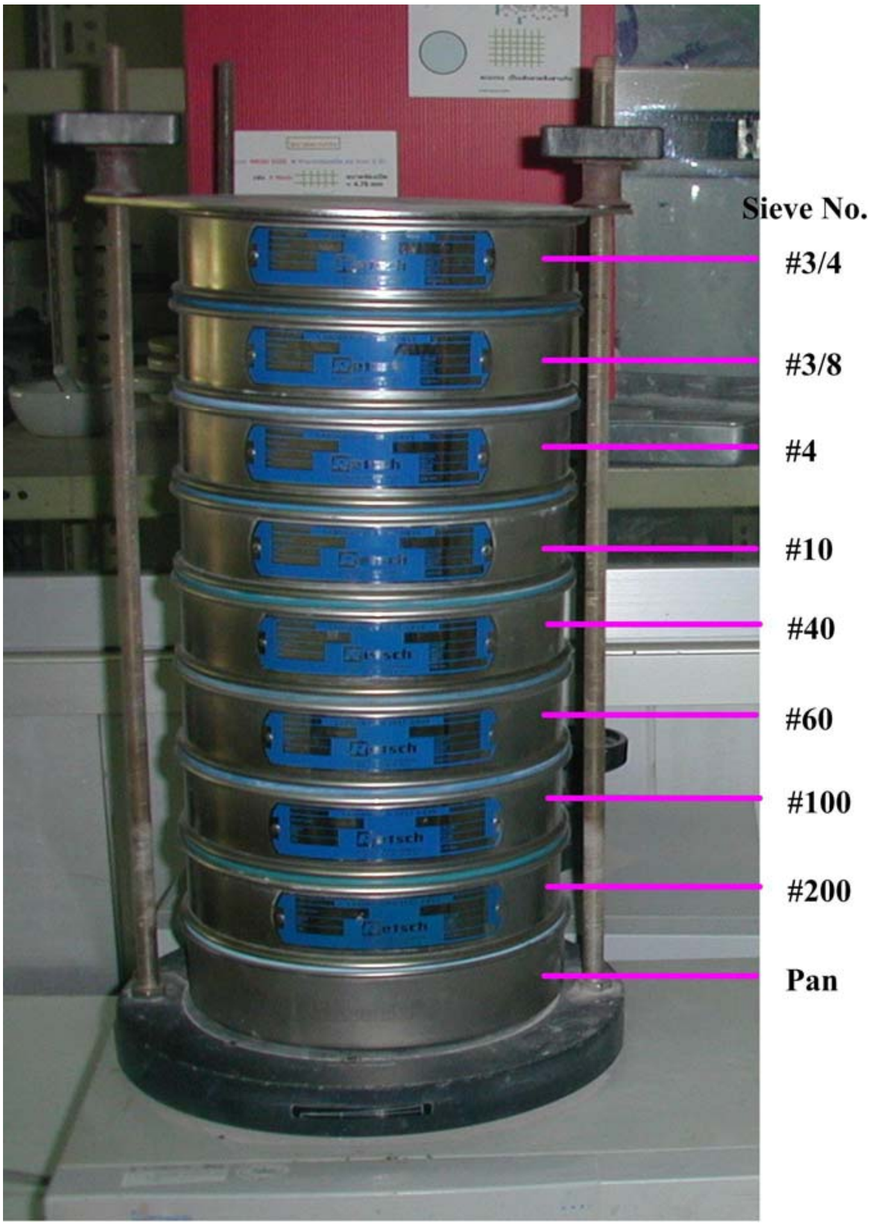

Figure 3.4 Sieves used in particle size distribution analysis.

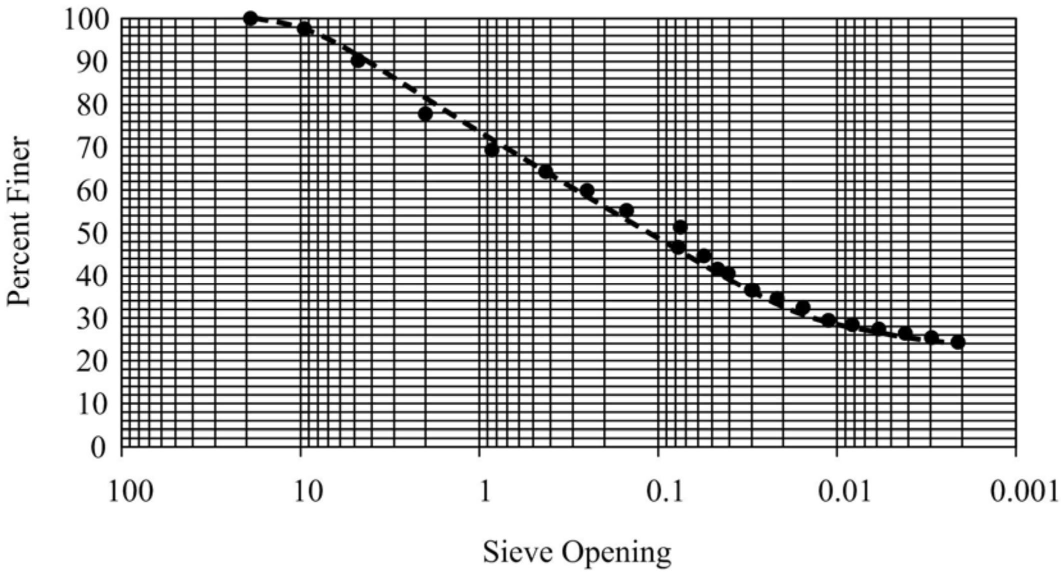

Figure 3.5 Relationship between sieve opening and percent finer from sieve analysis and hydrometer test of soil sample no. A1.

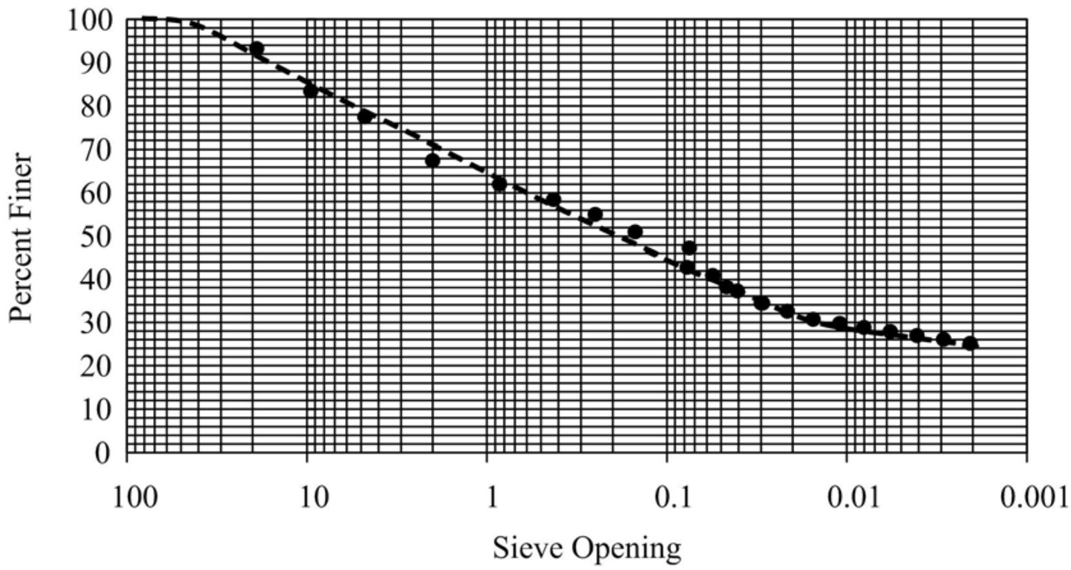

Figure 3.6 Relationship between sieve opening and percent finer from sieve analysis and hydrometer test of soil sample no. A2.

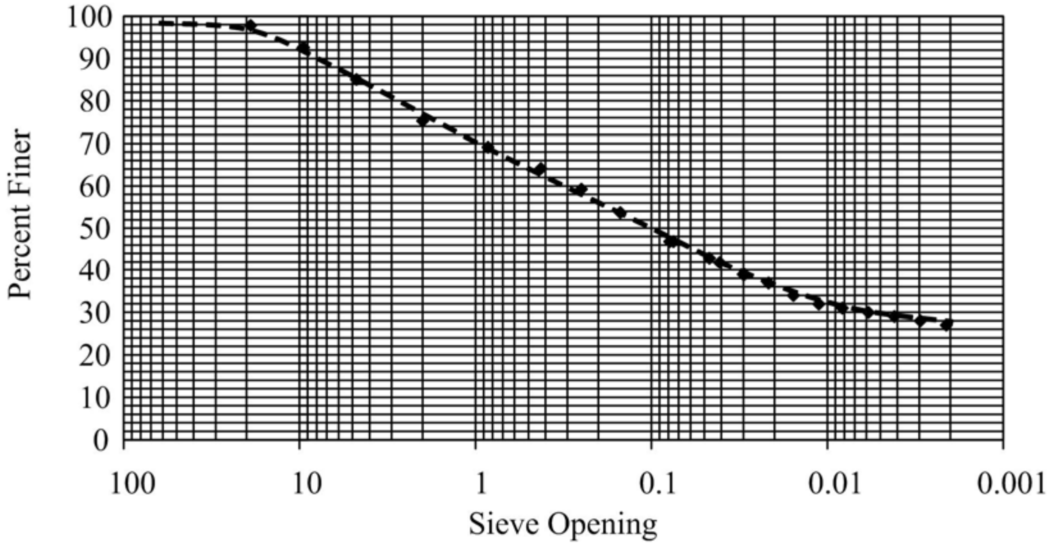

Figure 3.7 Relationship between sieve opening and percent finer from sieve analysis and hydrometer test of soil sample no. B1.

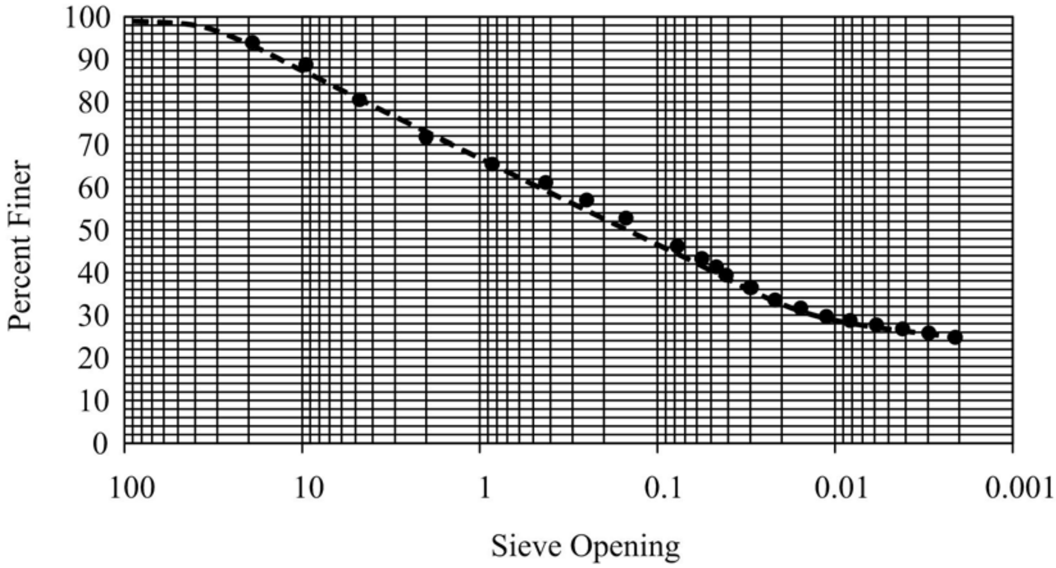

Figure 3.8 Relationship between sieve opening and percent finer from sieve analysis and hydrometer test of soil sample no. B2.

Table 3.2 Percentage of gravel, sand, silt and clay composed in soils sample which classify based on Wentworth's scale (Wentworth, 1922).

Sample No.	Gravel & Pebble (%)	Sand (%)	Silt (%)	Clay (%)
A1	22	33	19	26
A2	33	25	15	27
B1	25	29	17	29
B2	28	28	16	28

Table 3.3 Percentage of gravel, sand, silt and clay composed in soils sample which classify based on Unified Soil Classification System (ASTM D2487-00).

Sample No.	Gravel (%)	Sand (%)	Silt and Clay (%)
A1	10	39	51
A2	23	30	47
B1	15	35	50
B2	19	32	49

(a)

(b)

Figure 3.9 Soil samples no. A1 (a) and A2 (b) after tested by sieve analysis.

(a)

(b)

Figure 3.10 Soil samples no. B1 (a) and B2 (b) after tested by sieve analysis.

3.4 Petrographic analysis

Thin sections of representative samples are prepared from each rock type for the petrographic analysis. The mineral compositions and grain (crystal) sizes are determined. Table 3.4 gives rock names are brief mineral compositions.

3.5 Thermal properties test

Thermal constants analyser (hot disk) (Figure 3.11) is used to determine the thermal property of rocks and compacted soil samples. Thermal properties of the tested rocks are summarized in Table 3.5. Basalt shows maximum value of specific heat which has advantage for use as storage medium. Basalt shows the highest values of heat capacity (3.30 MJ/m3.K) in comparisons with other rocks tested here. It means that basalt can absorb and store more heart energy. Figure 3.12 shows the relationships between thermal conductivity of rocks and their density. Figure 3.13 shows the relationship between heat capacity of rocks and their density.

The thermal conductivity and heat capacity of rock tend to be independent of their density because rocks contain various mineral compositions (each minerals show difference in thermal properties). Rocks behave differently as compared to homogeneous materials, such as steels, ceramic and aluminums. For these homogeneous materials, the density has a relation with thermal conductivity and heat capacity.

From the previous study, basalt can be found in the northern and the northeastern parts of Thailand, the laboratory results indicate therefore basalt samples will be used to construct the collector in the pilot scale thermal storage system in this research. Figures 3.14 and 3.15 show the comparison of the thermal conductivity and heat capacity of rocks tested here with other sources.

Table 3.4 Brief descriptions of rock samples obtained from ten source locations.

Rock Types	Mineral composition	Description	Rock Name
Burirum Basalt	pyroxene 50% and plagioclase 50%	Aphanitic basalt, very dark grey to black in colour, densed with a few vesicles (less than 1%), no olivine crystal observed	Aphanitic basalt
Vietnamese Granite	orthoclase 75%, quartz 10%, plagioclase 10% and amphibole 7%	Felsic phaneritic granite, appearing pink, crystals of minerals can be seen by naked eyes, fine grained with average size of 2-5 mm in length, quartz is generally smaller than feldspar, orthoclase phenocryst (> 1cm) also present	Composition of high percentage orthoclase and less than 20% quartz refers to “quartz syenite”
Tak Granite	plagioclase 40%, quartz 30%, orthoclase 5%, amphibole 3% and biotite 2%	Felsic phaneritic granite, appearing grey with black and white spotted, crystals of minerals can be seen by eyes, fine grained with average size of 4-5 mm., quartz and feldspar are equally of the same size	Composition of plagioclase and quartz rich (70%), less than 10% mafic minerals refers to “plagio-granite”
Chinese Granite	plagioclase 70%, quartz 15%, orthoclase 7%, amphibole 5% and biotite 3%	Intermediate phaneritic granite, appearing white with scattered black, crystals of minerals can be seen by eyes, coarse grained, quartz and feldspar generally of equal size, average size of more than 5 mm, plagioclase crystals reach 1 cm, showing striations	Composition of plagioclase rich (70%), less than 20% quartz, and less than 10% mafic minerals refers to “quartz monzonite”
Middle Salt	halite 98%, anhydrite 1%, clay mineral 1%	Smoky color, Average grain size 5 mm	“rock salt”
Lower Salt	halite 99%, clay mineral 1%	Colorless, Average grain size 5 mm	“rock salt”

Table 3.4 Brief descriptions of rock samples obtained from ten source locations (cont.).

Rock Types	Mineral composition	Description	Rock Name
Saraburi Marble	calcite 100%	Meta-sedimentary rock, appearing yellowish brown, non granular, non foliated, showing original texture of limestone with metamorphosed fossils and rock fragments, strongly reacts with HCL without powdering Discussion: The rock should have been overcome the low grade metamorphism according to undestroyed original texture. Calcite is still retained. Original rock was moderately abundant fossiliferous limestone, containing 40% fossils, 10% intraclasts with micrite matrix, also called "sparce biomicrite"	Limestone marble
Lopburi Marble	calcite 100%	Granular marble, appearing white, calcite grains can be seen by eye, average size of 2 mm, equidimensional, mineral grains crumbled by hand, strongly reacts with HCL without powdering Discussion: The original rock can be any limestone but it was overcome low-high temperature-intermediate pressure metamorphism. Calcite is still retained in the rock which reacts strongly with HCL. Though shape of calcite crystals are interlocking and changed to be more rounded. It is easy to be crumbled by hand	According to the reaction with HCL without powdering, this rock is designated as "limestone marble"
Sao Khua Sandstone	feldspar 70%, quartz 18%, mica 7%, rock fragment 3%, and other 2%	Fine grained sandstone, appearing red, feldspar and quartz dominated with less mica, well sorted, angular, not react with HCL. Discussion: Red colour may point to occurrence of oxidization by Fe-oxide	The composition of feldspar rich without gravel suggests to "arkosic feldspathic sandstone"

Table 3.4 Brief description of rock samples obtained from ten source locations (cont.).

Rock Types	Mineral composition	Description	Rock Name
Lopburi Marble	100% calcite	Granular marble, appearing white, calcite grains can be seen by eye, average size of 2 mm, equidimensional, mineral grains crumbled by hand, strongly reacts with HCL without powdering Discussion: The original rock can be any limestone but it was overcome low-high temperature-intermediate pressure metamorphism. Calcite is still retained in the rock which reacts strongly with HCL. Though shape of calcite crystals are interlocking and changed to be more rounded. It is easy to be crumbled by hand	According to the reaction with HCL without powdering, this rock is designated as "limestone marble"
Phu Kradung Sandstone	lithic fragment 70%, quartz 18%, mica 7%, feldspar 3%, and other 2%	Fine grained sandstone, grayish green, lithic fragment and quartz dominated with less mica, well sorted, angular, slightly reacts with HCL	The rich of lithic fragment and reaction with HCL suggest "calcareous lithic sandstone"
Phu Phan Sandstone	quartz 72%, feldspar 20%, rock fragment 3%, mica 3%, and other 2%	Fine grained sandstone, brownish yellow, quartz and feldspar dominated with a few mica, well sorted, angular, not react with HCL Discussion: Brownish yellow colour may originate from limonite, Fe-oxide mineral	The rock is composed mainly of quartz that suggests "quartz sandstone"
Phra Wihan Sandstone	quartz 75%, feldspar 15%, mica 7%, and lithic fragment 3%	Fine grained sandstone, brownish white with scattered black, quartz and feldspar dominated with less mica, well sorted, angular, not react with HCL	The rich of quartz and feldspar suggests "white quartz sandstone"

Figure 3.11 Thermal Constants Analyser (Hot Disk).

Table 3.5 Thermal properties of rocks and soil.

Rock Type	Density (g/cm^3)	Thermal Conductivity (W/ m K)*	Heat Capacity (MJ/m^3 K)*
Compacted Soil	-	1.19 ± 0.00	2.43 ± 0.01
Saraburi Marble	2.58	3.01 ± 0.00	2.91 ± 0.05
Burirum Basalt	2.81	1.70 ± 0.05	3.30 ± 0.71
Lopburi Limestone	2.64	2.93 ± 0.00	2.54 ± 0.01
Phu Kradung Sandstone	2.54	4.02 ± 0.01	1.80 ± 0.03
Phu Phan Sandstone	2.26	2.69 ± 0.01	2.00 ± 0.04
Phra Wihan Sandstone	2.33	3.75 ± 0.00	1.77 ± 0.02
Sao Khua Sandstone	2.33	2.06 ± 0.01	1.79 ± 0.02
Chinese Granite	2.64	3.16 ± 0.00	1.69 ± 0.01
Tak Granite	2.62	2.84 ± 0.00	2.21 ± 0.01
Vietnamese Granite	2.62	3.26 ± 0.00	2.04 ± 0.03
Middle Salt	2.16	5.80 ± 0.01	1.83 ± 0.01
Lower Salt	2.19	5.51 ± 0.01	2.54 ± 0.01

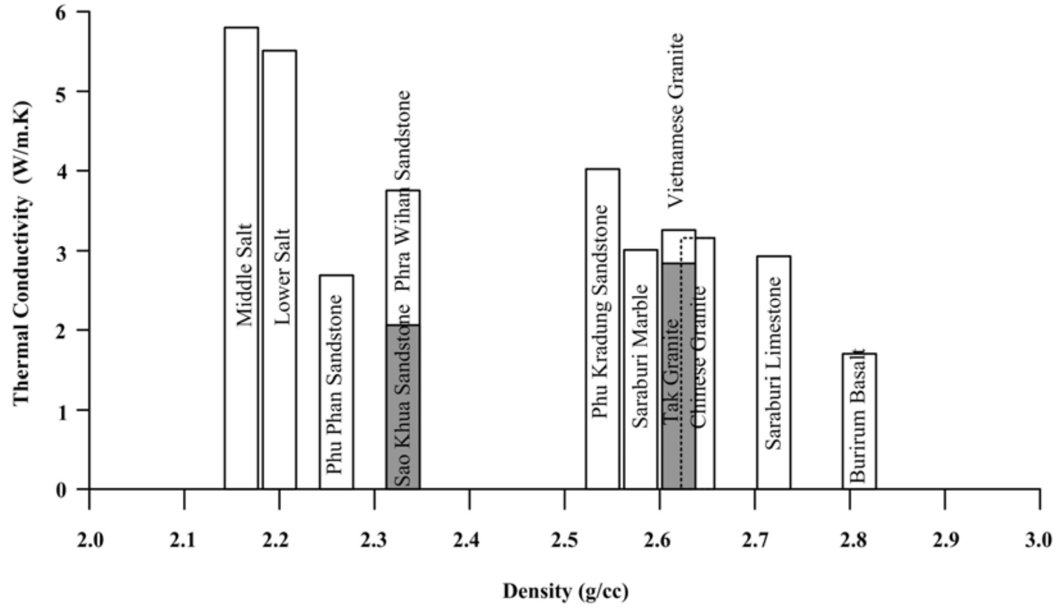

Figure 3.12 Thermal conductivity of rocks plotted as a function of their density.

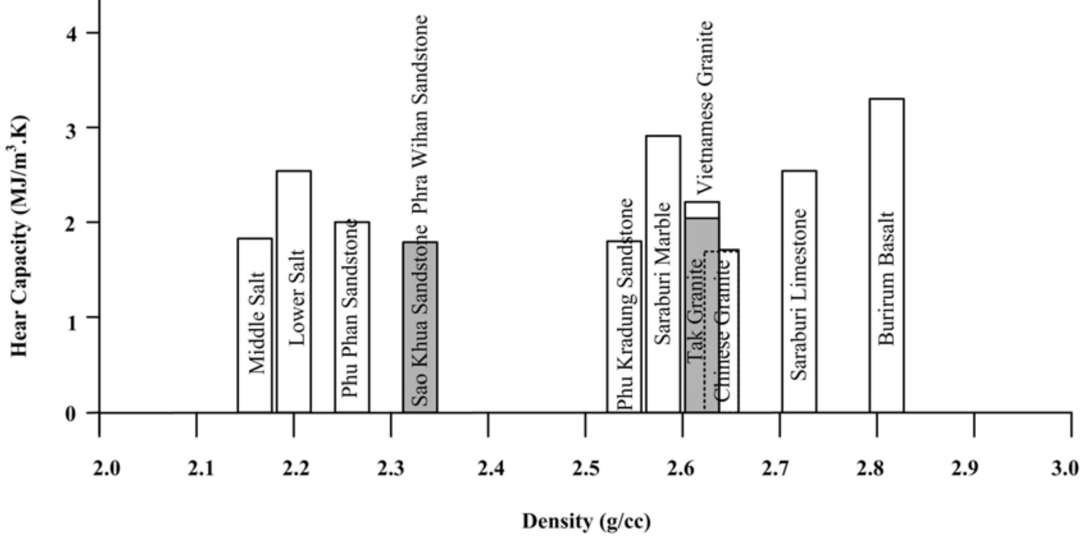

Figure 3.13 Heat capacity of rocks plotted as a function of their density.

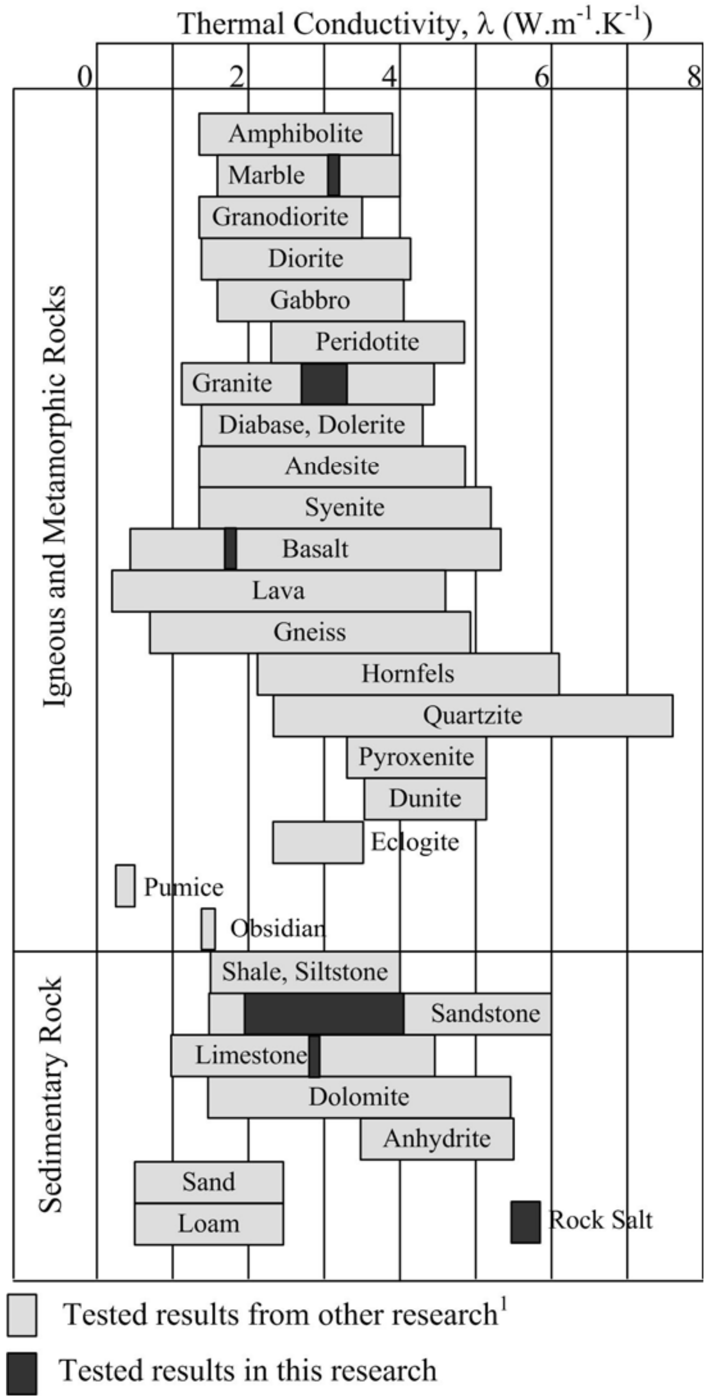

Figure 3.14 The thermal conductivity of rocks tested here and from other research ([1]Department Angewandte Geowissenschaften und Geophysik, 2006).

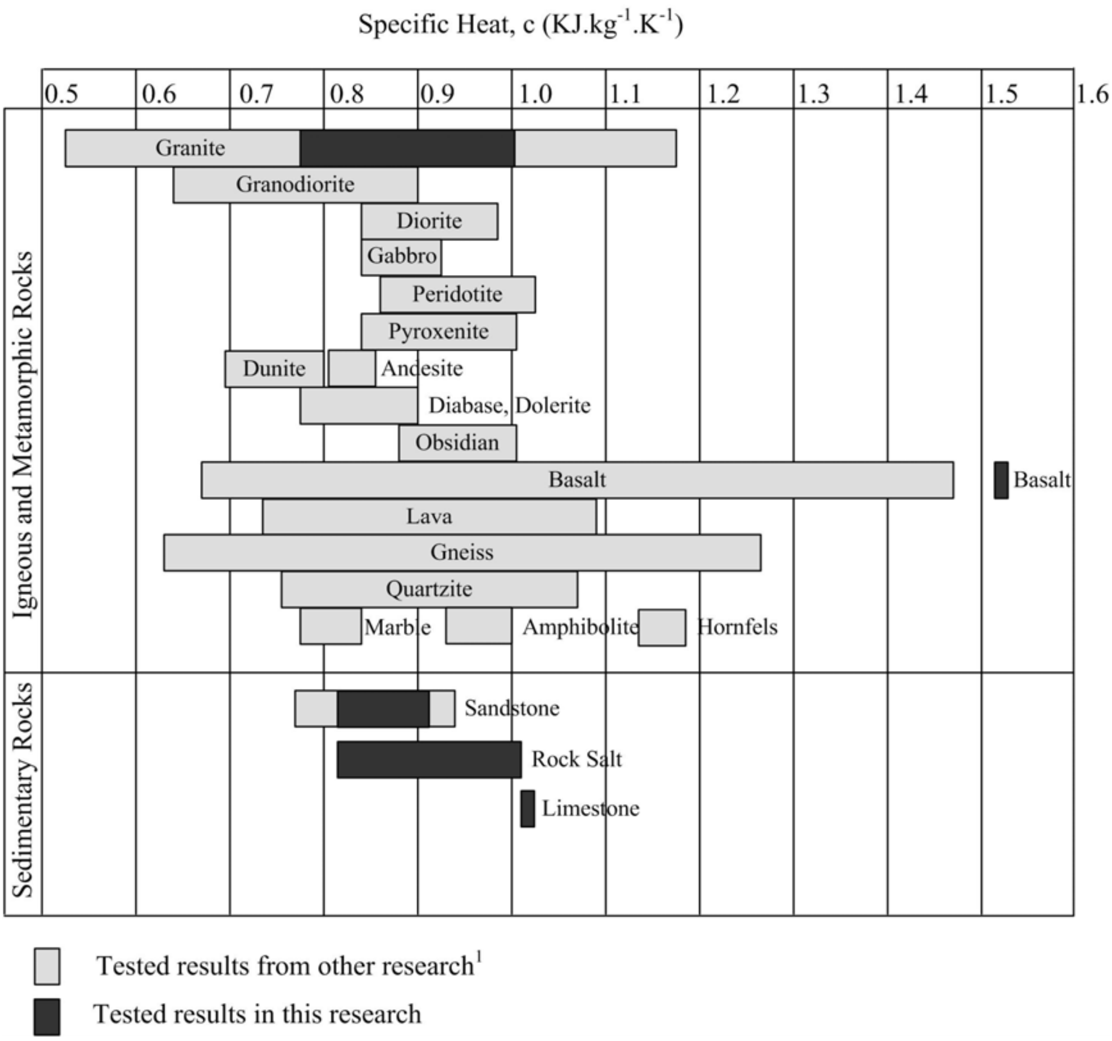

Figure 3.15 Heat capacity of rocks tested here and from other research ([1]Department Angewandte Geowissenschaften und Geophysik, 2006).

CHAPTER IV

MATHEMATICAL MODELING

A mathematical model based on the theory of thermodynamic and heat transfer is developed to predict the change of temperatures of rock, air in storage system, and air in housing model, as a function of time. The results from the mathematical calculation will be used to formulate the relationship between the differences of temperatures in housing model and the surrounding temperature, the volume of housing model, and the collector area of the storage system, and the cross-sectional area of hot-air tube. These relations will be use to determine the proper volume of storage system for the housing model. Here, the numerical finite difference approximation is applied to model the systems used in this study and the computer program with MATLAB 7.0 is used in the calculation. The sensitivity factor for each parameter will be analyzed.

4.1 Description of models

The storage medium (rock fill) in this technology directly receives the solar thermal energy and stores that energy in their mass causing an increase in temperature. The stored energy is released during nighttime to warm up the air in the housing model. An energy balance is performed on the fluid (air) and solid (rock) phases, yielding a coupled set of partial differential equations.

Figure 4.1 shows the schematic sketch of the physical model for thermal storage system. The solar thermal storage system consists of rock fragments, a cover plate (acrylic sheet), hot pipe (heat transfer pipe), and housing model (room to be heated). The rock fragments are approximately 5 through 10 cm in diameter and are arranged in each rock basket. The acrylic sheet reinforced with steel frame is used to prevent heat losses under convective mode at the top of the storage system.

The pilot scale solar thermal storage system are divided into three systems including, rocks in the pit (CV1), air in storage bed (CV2) and air in housing (CV3), which is illustrated in Figure 4.2. In daytime or during the hot pipe closure phase, the system can be considered closed because the mass in the system is constant. In night time when the hot pipe is opened, the system is considered open or controlled volume because of the mass transfer between the systems.

4.2 Basis assumptions

The mathematical calculations are carried out under the principle of energy balance. Each system is presented with various modes of heat transfer; radiation, convection, and conduction, which result in a more complicated and difficult problem. To minimize the complications and difficulty, the following assumptions are posed: 1) the solar energy (I_s) which is absorbed by the air is neglected, 2) the humidity in the air is neglected, 3) the physical parameters are considered to be constant, 4) the thermal gradient within solid particles is neglected, 5) radiation effects are neglected, 6) radial heat transfer does not occur, 7) losses to the environment are ignored, and 8) internal heat generation is absent.

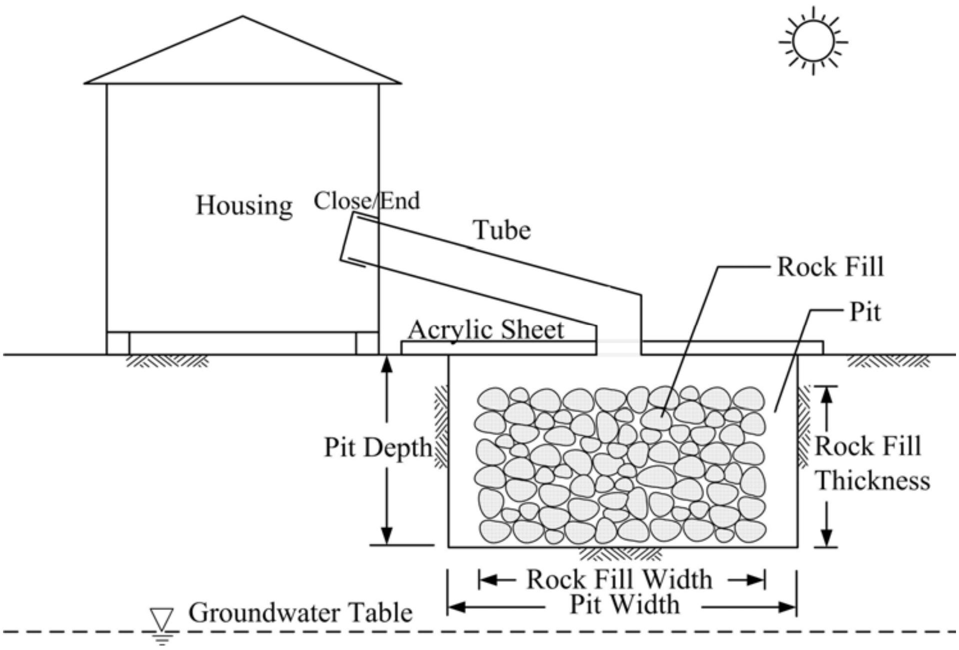

(a) Solar heat collected during daytime

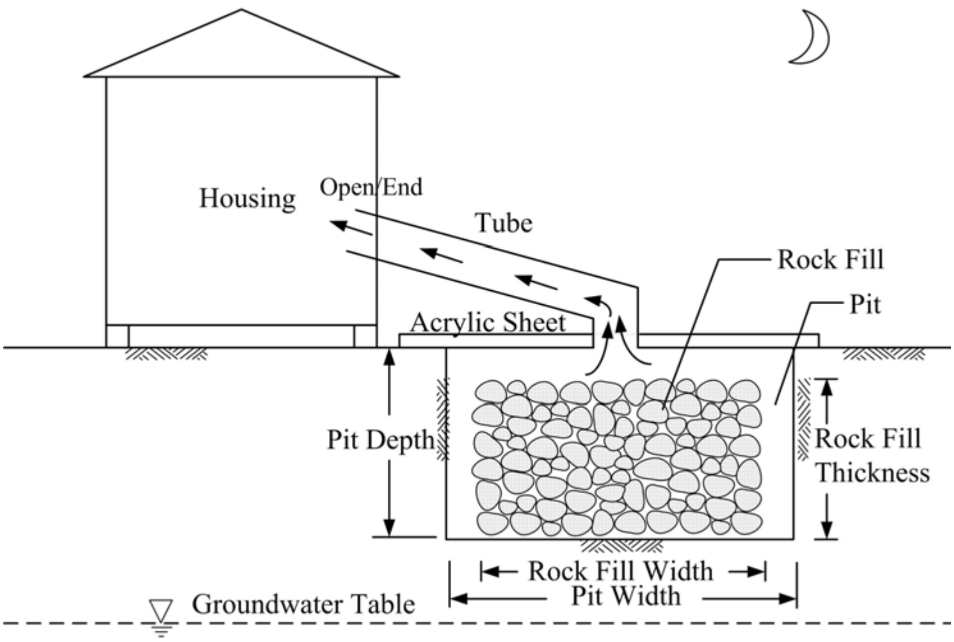

b) Heated air released to warm up room or housing

Figure 4.1 Conceptual thermal energy storage in rock fills.

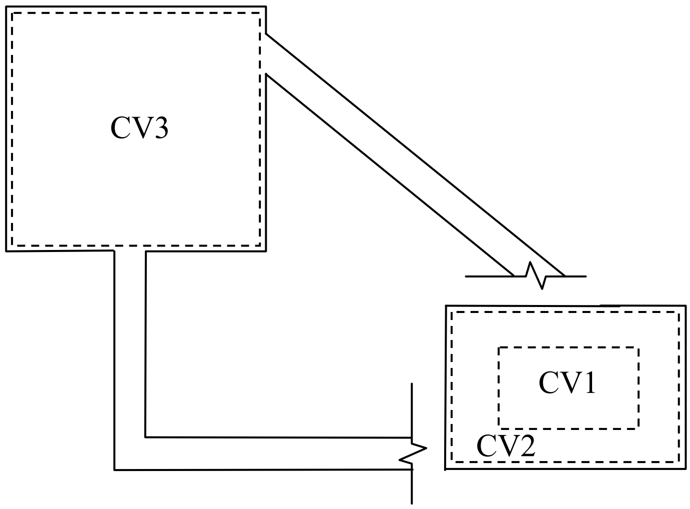

(a) Daytime: Closed System

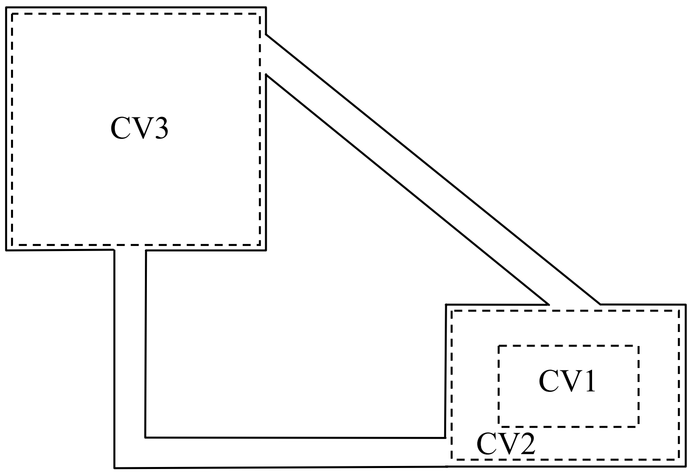

(b) Nighttime: Open System

Figure 4.2 Systems for solar thermal energy storage in rock fill.

4.3 Daytime equivalent models

In the daytime, the calculations are based on two functions 1) rock bins and 2) air in storage system. Income of solar energy is obtained from the theoretical calculation based on the direction of the sun on the earth surface. Figure 4.3 shows the heat transfer in the storage system. Rocks received the energy from the sun (I_s). The ability of rocks in the storing the energy depend on the thermal absorbability (α_r). There are the energy loses by diffusion to the surrounding. A percentage of energy in the rock is lost or transferred through convection and radiation modes to the air in the storage system. A percentage of energy is also lost through radiation to the surroundings. A percentage of energy in the air mass is also lost to the soils and the surrounding air at the top.

4.3.1 Heat transfer within rocks

The temperature of rocks in storage system will increase through the absorbtion of solar energy. The energy changes in the rocks (ΔE_{CV1}) will be derived in terms of the income energy or solar radiation energy ($\sum \dot{Q}_{in}$) and energy lost to the surroundings ($\sum \dot{Q}_{out}$). The energy in the rocks can be lost by convection and radiation. The governing equation can be presented as follows:

$$\Delta E_{CV1} = \sum Q_{in} - \sum Q_{out} = Q_{in,sun} - (Q_{rad,r\_c} + Q_{rad,r\_s} + Q_{con,r\_s}) \qquad (4.1)$$

Eq. (4.1) can be rewritten in the form of transient state or unsteady state as:

$$\frac{dE_{CV1}}{dt} = \dot{Q}_{in,sun} - \dot{Q}_{rad,r\_c} - \dot{Q}_{rad,c\_s} - \dot{Q}_{conv,r\_s} \qquad (4.2)$$

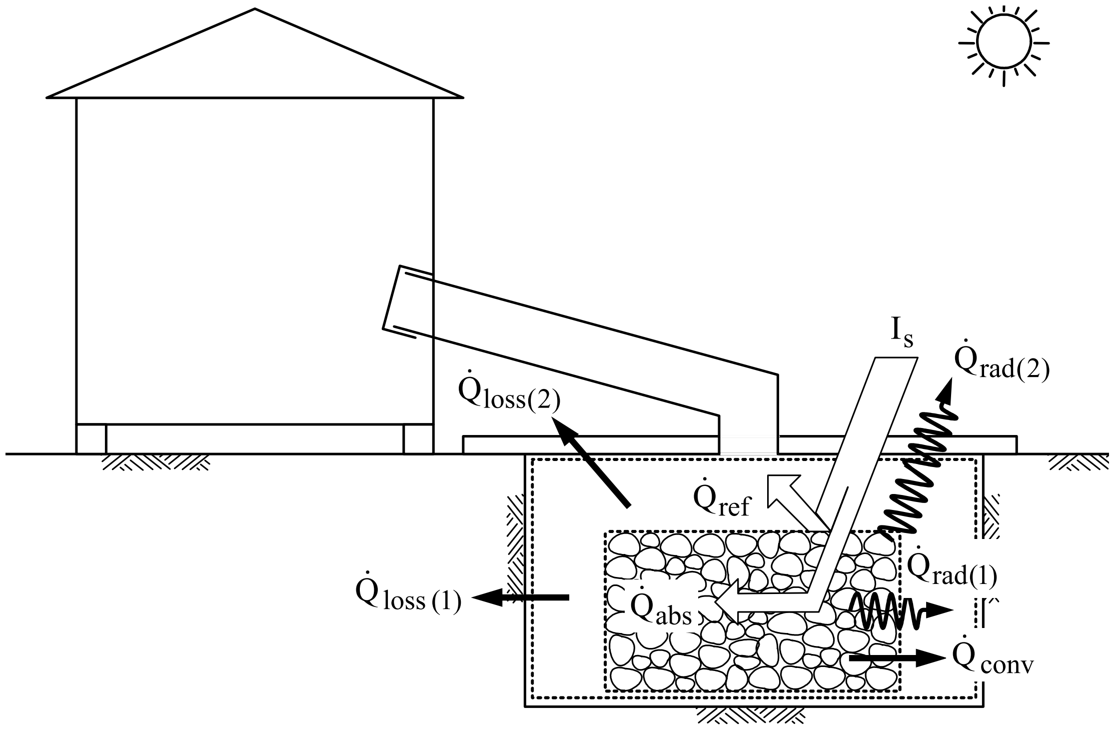

Figure 4.3 Heat transfer within rocks in storage system during daytime.

when $\dot{Q}_{in,sun}$ is the energy gained from the solar irradiation (heat flux), $\dot{Q}_{rad,r\_c}$ is the energy loss from the rock to the chamber or pit wall in form of radiation, $\dot{Q}_{rad,r\_s}$ is the energy loss from the rocks to the surrounding air in mode of radiation, and $\dot{Q}_{conv,r\_s}$ is the energy loss (heat flux) from the rocks surface to the air in the pit in form of convective air transfer. It is assumed that the temperature of the pit wall is the same as that of the air in the pit. Eq. (4.2) can be written

$$m_r C_r \frac{dT_r}{dt} = \alpha_r I_s A_{r,top} - \sigma\varepsilon_r A_{rad}\left(T_r^4 - T_c^4\right) - \sigma\varepsilon_r A_{r,top}\left(T_r^4 - T_{sur}^4\right) - hA_r\left(T_r - T_c\right) \tag{4.3}$$

where m_r is the mass of rocks in pit (kg)

C_r is the specific heat or heat capacity of rocks (J/kg.K)

α_r is absorptivity coefficient of rocks

I_s is solar radiation or heat flux (W/m^2)

$A_{r,top}$ is solar collection area which equivalent with the area of rocks on the top exposed to the air (m^2)

σ is the Stefan-Boltzmann constant equal to 5.67×10^{-8} W/m^2.K^4

ε_r is emissivity or heat exchanger effectiveness of rock

A_{rad} is surface of emissivity (m^2)

T_r is the temperature of rocks (K)

T_c is the temperature of air in pit (K)

T_{sur} is surrounding temperature or air outside the housing (K)

h_r is convective heat transfer coefficient from rocks to air in storage system (W/m^2.K)

A_r is the area of all rock fragments in storage system (m^2).

Because the integration of these equations is complicated and difficult, the Euler's method (Chapra and Canale, 2002; Chapra, 2005) is applied to obtain the solution. Eq. (4.3) can be written as

$$m_r C_r \left(\frac{T_r^n - T_r}{\Delta t} \right) = \alpha_r I_s A_{r,top} - \sigma \varepsilon_r A_{rad} \left(T_r^4 - T_c^4 \right) - \sigma \varepsilon_r A_{r,top} \left(T_r^4 - T_{sur}^4 \right) - h_r A_r \left(T_r - T_c \right) \quad (4.4)$$

Here, T_r^n is the temperature of the rock at the next time step (K). Δt is the time interval between each step. Rearranging Eq. (4.4) we obtain;

$$T_r^n = T_r + \frac{\Delta t}{m_r C_r} \left[\alpha_r I_s A_{r,top} - \sigma \varepsilon_r A_{rad} \left(T_r^4 - T_c^4 \right) - \sigma \varepsilon_r A_{r,top} \left(T_r^4 - T_{sur}^4 \right) - h_r A_r (T_r - T_c) \right] \quad (4.5)$$

For the calculations in the following time step, T_r is taken as T_r^n, and the calculations continued till the required final time.

Assuming that the mode of heat transfer from the rocks to the surrounding air is by natural convection and the rock fragments are spherical shape, the convective heat transfer coefficient (h_r) is a function of Nusselt number (Nu), characteristic length (δ) and thermal conductivity coefficient (k) of rocks as shown below:

$$h_r = \left(\frac{k}{\delta} \right) Nu \quad (4.6)$$

For spherical shape with diameter D, δ is equal to ½ πD and Nu is dependent of the characteristic of surface

$$Nu = 2 + \frac{0.589Ra^{1/4}}{\left[1 + \left(\frac{0.469}{Pr}\right)^{9/16}\right]^{4/9}} \tag{4.7}$$

where Ra is Rayleigh number ($\leq 10^{11}$ when the Prandtl number (Pr) ≥ 0.7) and Pr is Prandtl number of dry air under atmospheric pressure (equal to 0.71 under temperature 0 through 300 degrees Celsius (Raznjevic, 1976)). They are defined as

$$Ra = Gr_L\ Pr = \frac{g\beta(T_s - T_\infty)\delta^3}{\nu^2} \cdot Pr \tag{4.8}$$

$$Pr = \frac{\nu}{\alpha_a} \tag{4.9}$$

where Gr_L is Grashoff number, ν is kinematics viscosity of air (equal to 15.7×10^6 through 19.4×10^6 m^2/s under temperature of 20 through 60 degree Celsius (Raznjevic, 1976)), β is volumetric thermal expansion coefficient of air, α_a is thermal diffusivity of the air, and g is gravitational acceleration (equal to 9.807 m/s^2). Gr_L and β are defined as

$$Gr_L = \frac{g\beta(T_s - T_\infty)\delta^3}{\nu^2}, \tag{4.10}$$

$$\beta = \frac{1}{T_c(K)} = \frac{1}{T_c(^\circ C) + 273} \tag{4.11}$$

4.3.2 Heat transfer within air in storage system

Air in the storage system (CV2) is the gain in solar energy ($\dot{Q}_{in}$) from the sun and the energy lost from the rocks under radiation ($\dot{Q}_{rad,r\_c}$) and convection ($\dot{Q}_{conv,r\_c}$) heat transferred to the air in storage system. The energy lost to the surrounding air above the acrylic sheet by heat convection and to the pit wall under heat conduction is calculated as:

$$\frac{dE_{CV2}}{dt} = \dot{Q}_{in} + \dot{Q}_{rad,r\_c} + \dot{Q}_{conv,r\_c} - \dot{Q}_{loss1} - \dot{Q}_{loss2} \tag{4.12}$$

where, $\dot{Q}_{loss1}$ is the heat loss from the air in storage system to the surrounding air and $\dot{Q}_{loss2}$ is heat loss from the air in storage system to the pit wall. Eq. (4.12) can be rearranged as:

$$\begin{aligned} m_c C_a \frac{dT_c}{dt} &= f_{ab}(1-\alpha_r) I_s A_{r,top} + \sigma\varepsilon_r A_{rad}\left(T_r^4 - T_c^4\right) + h_r A_r \left(T_r - T_c\right) \\ &\quad - U_1 A_{acr}\left(T_c - T_{sur}\right) - U_2 A_{cham}\left(T_c - T_{soil}\right) \end{aligned} \tag{4.13}$$

where m_c is mass of air in storage system (kg)

C_a is specific heat of air in storage system (J/kg.K), ranging from 1,012 J/kg.K through 1,017 J/kg.K

f_{ab} is heat loss factor from reflected radiation of rock

A_{acr} is area of acrylic sheet (m^2)

A_{cham} is area of pit wall (m^2)

U_1 is overall heat transfer coefficient of air in pit to surrounding air ($W/m^2.K$)

U_2 is overall hear transfer coefficient of air to pit wall ($W/m^2.K$)

Rearrange Eq. (4.13) we obtain:

$$T_c^n = T_c + \frac{\Delta t}{m_c C_a}\Big[f_{ab}(1-\alpha_r)I_s A_{r,top} + \sigma\varepsilon_r A_{rad}\left(T_r^4 - T_c^4\right) \\ + h_r A_r\left(T_r - T_c\right) - U_1 A_{acr}\left(T_c - T_{sur}\right) - U_2 A_{cham}\left(T_c - T_{soil}\right)\Big] \tag{4.14}$$

when $$U_1 = \frac{1}{\frac{1}{h_{ic}} + \frac{\Delta x}{k_{acr}} + \frac{1}{h_{exc}}} \text{ and } U_2 = \frac{1}{\frac{1}{h_i} + \frac{\Delta x}{k_{acr}}} \tag{4.15}$$

here, Δx is the thickness of acrylic sheet (m)

h_{ic} is convective heat transfer coefficient of air in pit (W/m^2.K)

h_{exc} is convective heat transfer coefficient of air outside the pit or air above cover sheet (W/m^2.K)

k_{acr} is thermal conductivity of acrylic sheet (W/m^2.K)

The value of h_{ic} and h_{exc} can be evaluated by using Eqs. (4.6) through (4.11).

The mass of air (m_c) in storage system can be calculated from the cross product between the density of air (ρ_{air}) and the volume of pit (V_c). The density of air is a function of temperature; it decreases when the temperature increases. The density of air is 1.197 kg/m^3 at temperature of 22 degrees Celsius and decrease to 1.054 kg/m^3 at temperature of 62 degrees Celsius. Because the change of air density is not specific, it is assumed constant at 1.103 kg/m^3.

4.4 Nighttime equivalent models

The systems during nighttime when the stored energy is used are divided into three subsystems including rocks in the pit (CV1), air in the pit (CV2) and air in the housing model (CV3). When the lid of the hot tube is opened, the hot air immediately flows through the tube to the housing model. The thermal energy from hot air is transferred to cold air in housing causing an increase in temperature. Figure 4.4 shows the energy transfer from storage system to the housing during nighttime.

4.4.1 Heat transfer within rocks

The heat transfer in the system during the nighttime is similar to the system during daytime without the external energy source (solar energy). The heat loss from solar radiation in the rocks to the surroundings is nil because of the acrylic sheet and the isolated cover. The energy equation of rocks in storage system is transformed from Eq. (4.5) to:

$$T_r^n = T_r + \frac{\Delta t}{m_r C_r}\left[-\sigma\varepsilon_r A_{rad}\left(T_r^4 - T_c^4\right) - h_r A_r\left(T_r - T_c\right)\right] \tag{4.16}$$

4.4.2 Heat transfer within air in storage system

The heat transfer to air within the storage system during nighttime is similar to that of daytime transfer. There is no solar energy. The energy within the air in the storage system is transferred to air in housing (CV3) in form of air mass which flowed through the tubing to housing space. It is equal to $\dot{m}C_a(T_c - T_h)$. The energy equation of air in storage system from Eq. (4.12) can be rearranged as:

$$\frac{dE_{CV2}}{dt} = \dot{Q}_{rad,r\_c} + \dot{Q}_{conv,r\_c} - \dot{Q}_{loss,1} - \dot{Q}_{loss,2} - \dot{m}C_a\left(T_c - T_h\right) \tag{4.17}$$

$$\begin{aligned} m_c C_c \frac{dT_c}{dt} = {} & \sigma\varepsilon A_{rad}\left(T_r^4 - T_c^4\right) + h_r A_r\left(T_r - T_c\right) - U_1 A_{acr}\left(T_c - T_{sur}\right) \\ & - U_2 A_{cham}\left(T_c - T_{soil}\right) - \dot{m}C_a\left(T_c - T_h\right) \end{aligned} \tag{4.18}$$

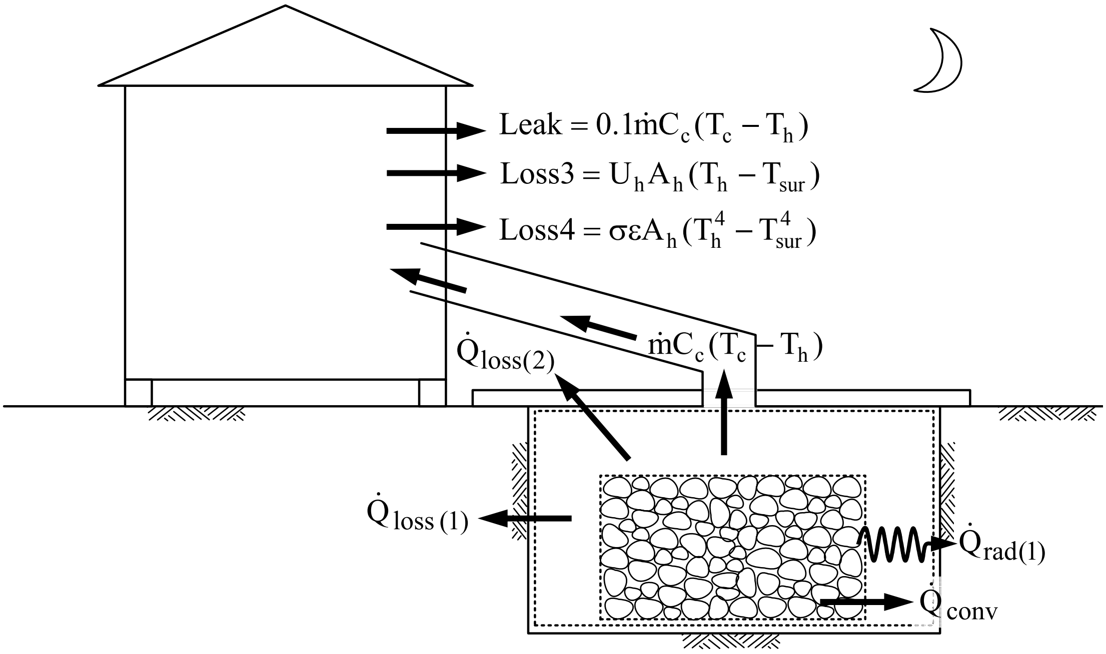

Figure 4.4 Schematic view of energy change within rock in storage system during nighttime.

Rearrange Eq. (4.18) we obtain;

$$T_c^n = T_c + \frac{\Delta t}{m_c C_c}\left[\sigma\varepsilon A_{rad}\left(T_r^4 - T_c^4\right) + h_r A_r\left(T_r - T_c\right) - U_1 A_{acr}\left(T_c - T_{sur}\right)\right.$$
$$\left. - U_2 A_{cham}\left(T_c - T_{soil}\right) - \dot{m}C_a\left(T_c - T_h\right)\right] \tag{4.19}$$

where $\dot{m}$ is an air mass flow rate from the pit to the housing model (kg/s) under stack effect when the hotter air (in storage system) flowed to the cooler area (air in housing model). Bansal et al. (1993) and Anderson (1995) proposed the equation to determine the air mass flow rate as follow;

$$\dot{m} = \frac{\rho_C C_D A_o}{\sqrt{1 + (A_o / A_i)}}\sqrt{2gH\left(\frac{T_C - T_H}{T_C}\right)}, \text{ when } \rho_c = \frac{P}{RT_C} \tag{4.20}$$

where, P is air pressure equal to 101,300 Pa

C_D is discharge coefficient equal to 0.60 through 0.75

R is gas constant equal to 287 J/ Kg.K

C_a is specific heat of air (kJ/kg K)

T_h is temperature of air in housing (K)

A_o, A_i is cross-sectional area of tube (m^2)

A_r is ratio of A_o/A_i

H is elevation head of tube (different between the elevation of entrance and exit (m)

4.4.3 Heat transfer within air in housing

When the end of the hot tube is opened, the mass of hot air in storage system ($\dot{m}C_a(T_C - T_H)$) will flow to the housing space which will cause an increase in the temperature of air in housing. At the same time, there is heat loss to the surroundings through convection ($\dot{Q}_{loss3}$) and radiation ($\dot{Q}_{loss4}$) from air in housing to surroundings and leaks ($\dot{Q}_{leak}$) of air in housing through the rift of the wall or between the connected walls, bars, ceiling, floor, and columns. The energy loss in form of air leaks are assumed to be 0 through 15 percentage of energy from mass of air that flowed from storage system. The energy equations of air in housing are shown below:

$$\frac{dE_{CV3}}{dt} = \dot{m}C_a\left(T_c - T_h\right) - \dot{Q}_{loss3} - \dot{Q}_{loss4} - \dot{Q}_{leak} \tag{4.21}$$

$$\begin{aligned} m_h C_a \frac{dT_h}{dt} = {} & \dot{m}C_a\left(T_c - T_h\right) - U_h A_h\left(T_h - T_{sur}\right) - \sigma\varepsilon_h A_h\left(T_h^4 - T_{sur}^4\right) \\ & - 0.1\dot{m}C_a\left(T_c - T_h\right) \end{aligned} \tag{4.22}$$

$$\begin{aligned} T_h^n = {} & T_h + \frac{\Delta t}{m_h C_a}\Big[\dot{m}C_a\left(T_c - T_h\right) - U_h A_h\left(T_h - T_{sur}\right) \\ & - \sigma\varepsilon_h A_h\left(T_h^4 - T_{sur}^4\right) - 0.1\dot{m}C_a\left(T_c - T_h\right)\Big] \end{aligned} \tag{4.23}$$

when $$U_h = \frac{1}{\dfrac{1}{h_{i,h}} + \dfrac{\Delta x}{k_w} + \dfrac{1}{h_{ex,h}}} \tag{4.24}$$

U_h is overall heat transfer coefficient of air in housing to surrounding ($W/m^2.K$)

m_h is mass of air in housing (kg)

$h_{i,h}$ is convective heat transfer coefficient of air in housing ($W/m^2.K$)

$h_{ex,h}$ is convective heat transfer coefficient of air outside housing ($W/m^2.K$)

k_w is thermal conductivity coefficient of housing wall (W/m.K)

A_h is area of housing wall for thermal loss (m^2)

Δx is thickness of housing wall (m)

The values of $h_{i,h}$ and $h_{ex,h}$ can be determined from Eq. (4.6) through (4.11).

4.5 Computer software development

Even though the energy equations are nonlinear and time invariant, these equations can not solve exactly in simple analytical forms so digital computer solutions are usually sought. Direct numerical simulation (finite difference method) of the entire heat transfer process in basaltic rock fill will be applied to calculate the variation of temperature. This computer program will be developed by using MATLAB 7 which is based on the mathematical equation mentioned above.

This computer program can be used to analyze the changes in the variety of designed parameter including rock type, quantity of rock, storage characteristic (the dimension of storage unit), housing volume (the dimension of housing), and characteristics of hot pipe (cross section area and the difference between inlet and outlet).

The results of the calculations will be plotted to show the variation of temperature of rocks, air in storage system, air in housing, and surrounding as a function of time through 24 houses. This data will be used to analyze the sensitivity of each parameter on the changing of temperature. The results from sensitivity analysis will be used to optimize the solar thermal energy storage system.

CHAPTER V

PILOT SCALE FOR SOLAR THERMAL ENERGY STORAGE SYSTEM

The objectives of the development of a pilot scale for solar thermal energy storage system (or physical model) are to verify the efficiency of the designed solar thermal storage system and to determine its suitable design parameters. To do so, a scaled down model was built and the thermocouples were equipped to monitor the temperature changes in the components of the system at all time. The measurement results were used to compare with the results calculated by the equations derived in Chapter IV. The influence factors were tested and the model were modified and improved to achieve the optimum efficiency system.

5.1 Construction of pilot scale for solar thermal energy storage system

The pilot scale for solar thermal energy storage system consists of two main components: 1) a storage pit and 2) a housing model (Figure 5.1). The storage pit is packed with predefined fragment-sized basalt. Insulator sheets are placed around the pit walls and floor. The pit floor is excavated in soil mass above the groundwater table. Top of the pit is covered with a transparent acyclic sheet. The housing model is made of wood and covered with a tile roof.

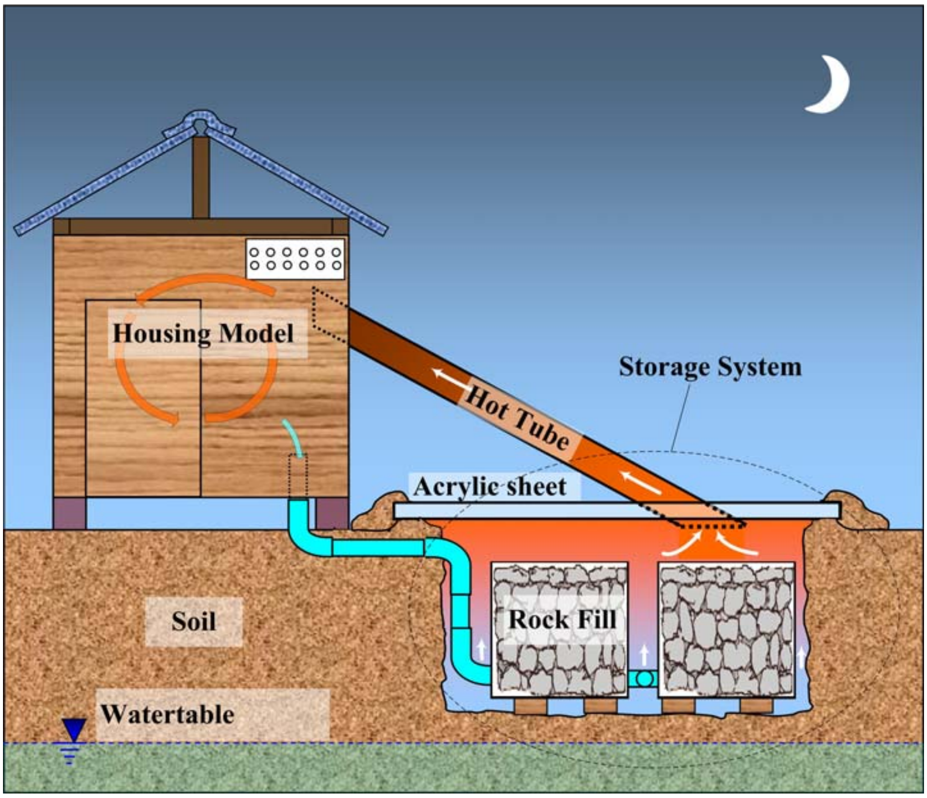

Figure 5.1 Pilot scale for solar thermal energy storage system.

5.1.1 Storage pit

The pit is excavated with size approximately of 1.75×1.75×0.75 m (width×length×depth) with a total volume (V_p) of 3.25 m^3. Four chain-link baskets with a dimension of 0.5×0.5×0.5 m were placed in the pit. Each basket contained about 230 pieces of 10-20 cm fragments of basalt. The bulk volume (V_{bed}) is about 0.5 m^3. This is equivalent to a total mass of rocks (m_r) of about 743 kg with a total volume (V_r) of 0.26 m^3. The insulator sheets were applied around the pit walls and floor to prevent heat loss through the pit walls and floor. The transparent acrylic sheets reinforced by steel frames were placed on top of the storage pit. This allows the solar energy to directly transmit to the rocks and to prevent the heat loss under mode of the force convection by wind (Figure 5.2). The concept of this model is to use the air in the pit heated by the rock fragments as a medium for heat transfer from one piece of rock to the adjacent rock fragments. The construction method is illustrated in Figure 5.3.

The system has a ratio of the storage pit (V_p) to the housing volume (V_h), V_p:V_h, of about 1:1, the bulk volume of rock (or packed rock volume) to the housing volume, V_{bed}:V_h, of about 1:6.5, and the rock volume (V_r) to the housing volume, V_r:V_h, of about 1:16 (V_{rock}:V_{house}). The porosity of rock fill calculated from the ratio of rock volume to bulk volume is about 0.53 and void ratio about 0.90.

5.1.2 Housing model

The housing model having a dimension of 1.5×1.5×1.5 m (the total volume, V_p, of about 3.5 m^3) was constructed with plywood. The walls, ceiling and floor were sealed with 1.5-cm thick foam to prevent heat loss. The house and storage pit were connected with an air tube. Several sizes of the air tubes were trials, circular

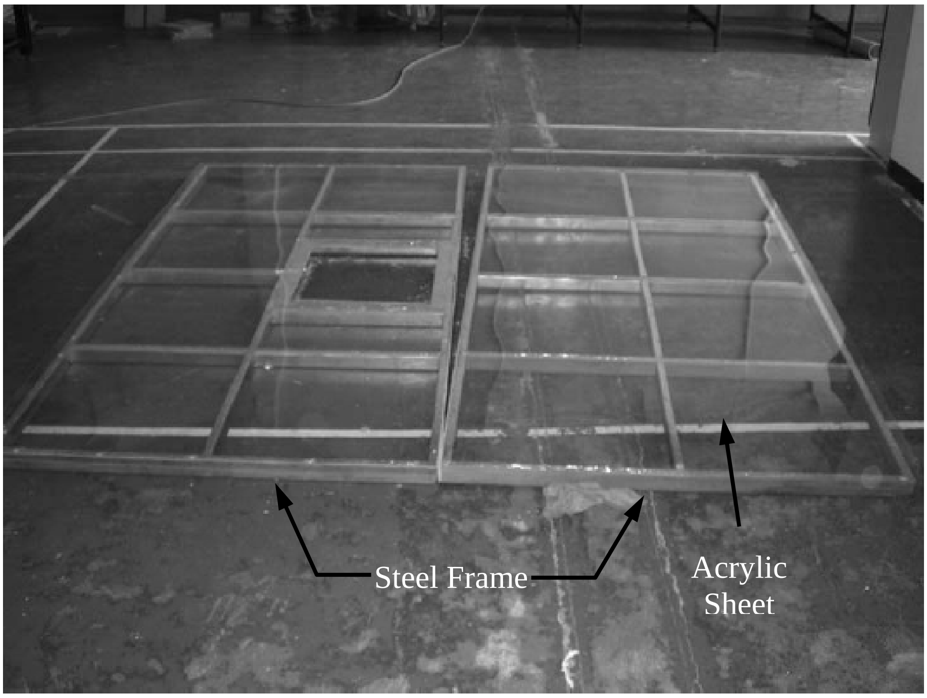

Figure 5.2 Acrylic sheets reinforced by steel frames were used for covering the storage pit.

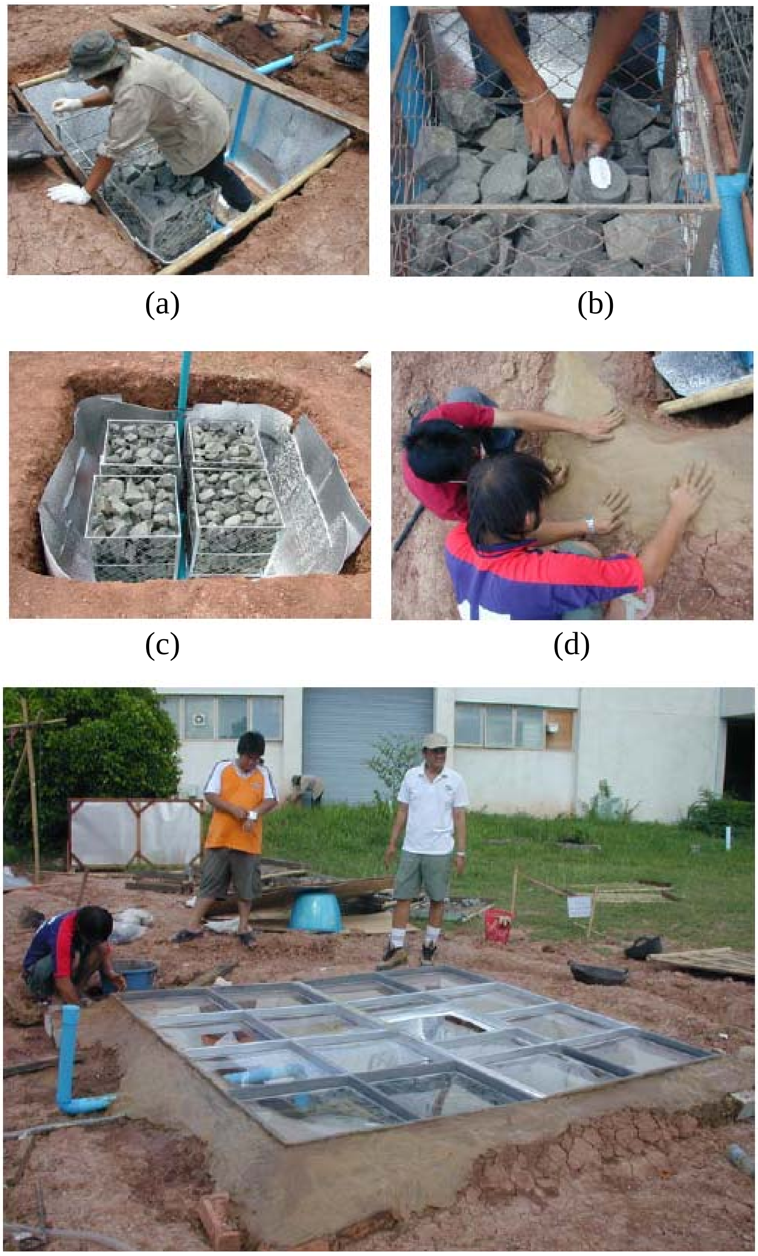

Figure 5.3 Storage pit construction: (a) placing of rock baskets, (b) packing rock fragments in the baskets and installing thermocouples, (c) placing insulator sheets around pit walls and floor, (d) shaping the pit rim with clay, and (e) installing acrylic sheets reinforced by steel frames.

tubes with diameters varying from 5 to 20 cm, and a squared vent with dimension of 0.6×0.6 m. Cold air tubing with a diameter of 5 cm was connected to circulate cold air from the bottom of the house to the bottom of the storage pit.

5.1.3 Thermocouples installation

Several thermocouples were installed to monitor the changes of rock temperature at the center of pit (Figure 5.4), air in the pit (Figure 5.5), air at the end of the tube in the housing model (Figure 5.6), air in the housing model (Figure 5.7), and the surrounding air outside the housing (Figure 5.8). Reading and recording were made for every 30 minutes.

5.2 Measurement results

The temperatures were measured from the 20th of November 2005 through the 20th of April 2006 and again from the 28th of November 2008 through the 28th March 2007. The results are given in Appendix A. To optimize the system efficiency, the system was modified and improved several times. The sizes hot-air tube were varied, the housing walls were sealed with insulator sheet (foam sheet), the opening and closing time for the housing model, tubes, and pit were changed, the mass of rock in pit was changed, and a ventilator was installed. The results are explained below.

5.2.1 Testing with 5.1 cm diameter hot-air tube

The storage system was connected to the housing model by a 5.1-cm (2 inches) diameter hot-air tube. One end was placed on the top of the pit (the pyramid shaped box with base size of 0.6×0.6 m). The other end was inserted into the housing wall (Figure 5.9). The pit was not covered by any insulator on the top at all time. During charging period, 6:00 am-6:00 pm, the housing model was opened and

Figure 5.4 Thermocouple (the upper left) is installed onto the polished surface of rock sample using protective glue (the upper right) and placed into the middle of chain-link basket to measure the temperature of rock fragments (bottom).

Figure 5.5 Thermocouple was mounted on a glass sheet and hung in the air to monitor the temperature of pit air.

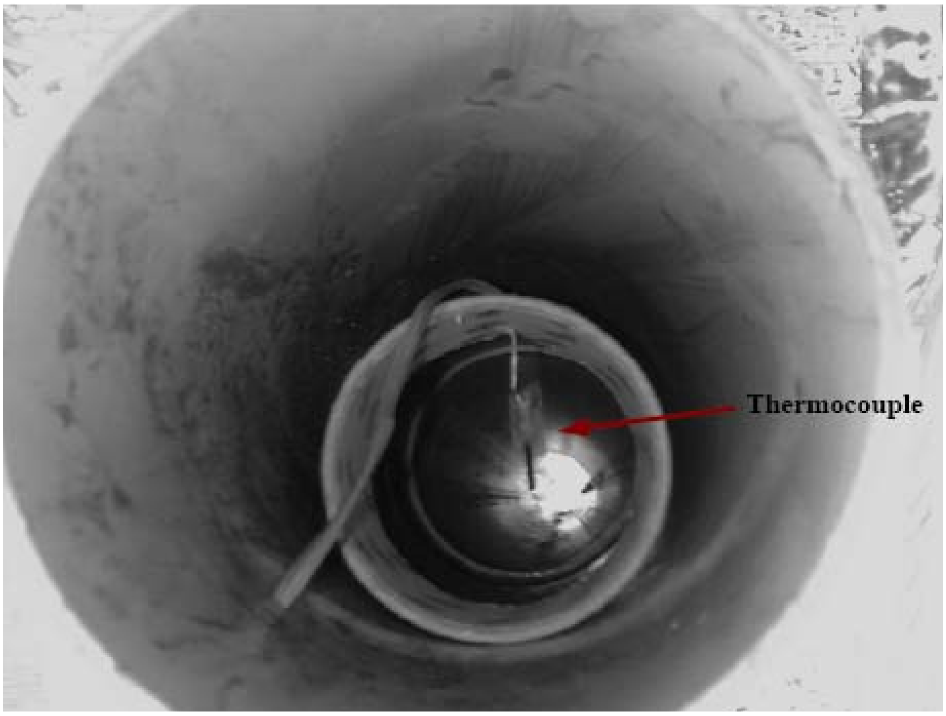

Figure 5.6 Thermocouple was hung in the center of the hot-air tube to measure the temperature of the air flow to the housing model.

Figure 5.7 Thermocouple was hung in the housing model to monitor its temperature.

Figure 5.8 Thermocouple was hung under the roof to monitor the surrounding air temperature.

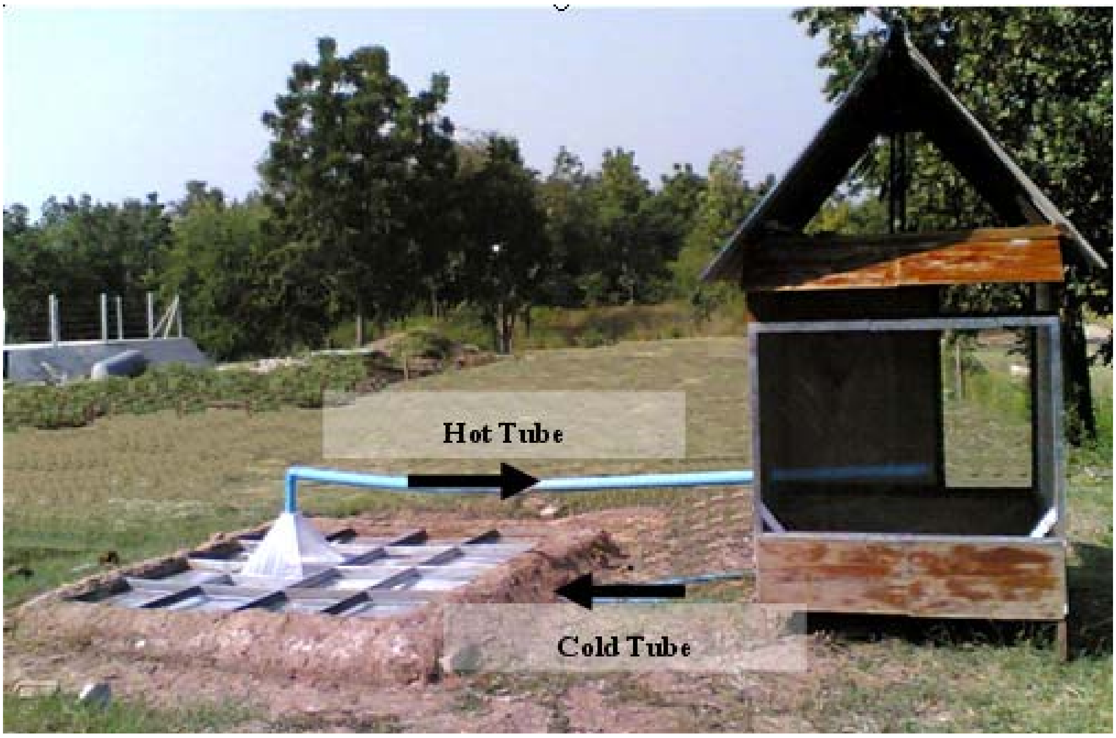

Figure 5.9 The storage pit (left) connected to the housing model (right) by a 5.1-cm (2 inches) diameter hot-air tube. The hot-air and cold-air tubes are horizontal.

the hot-air and cool-air tubes were closed. After 6:00 pm, the housing model was closed and the hot-air and cool-air tubes were opened to allow the hot-air in the pit circulated to the housing model and the cool-air in housing model circulated to the pit.

Figure 5.10 shows the records of representative measured temperatures. The temperatures of air in the storage pit, in the tube, in the housing, and ambient air increased with the solar energy, which had a highest value at about 42, 36, 34, and 34 °C at 2:00 pm. After 2:00 pm, these temperatures decreased until 6.00 am. The temperature of rock increased with highest value of about 38.5 °C at 6:00 pm. The housing temperature did not increase while the tubes were opened.

Results of the temperature measurements indicated that the heat flow through the pipe to the housing space was quite minimal, probably caused by excessive heat loss through the acrylic sheet, improper size and inclination of tube, and leakage of heat energy of the housing model.

5.2.2 Testing with 10.2 cm diameter hot-air tube

In an attempt to enhance the heat flow, the hot-air tube with a diameter of 10.2 cm (4 inches) was installed. It was inclined at an angle of 30 degrees with difference elevations between the inlet and outlet of about 1.5 m (Figure 5.11). The outer tube surface was covered with an isolator sheet to prevent the heat loss by conduction to the surrounding. The opening and closing time for the pit, tubes, and housing was set at same period as the previous testing. The housing model was opened and the tubes were closed after 6:00 am. After 9:00 pm the housing was closed and the tubes were opened.

The results of temperatures measured from this model were not different from the results from using 5.1-cm diameter hot-air tube. This is probably

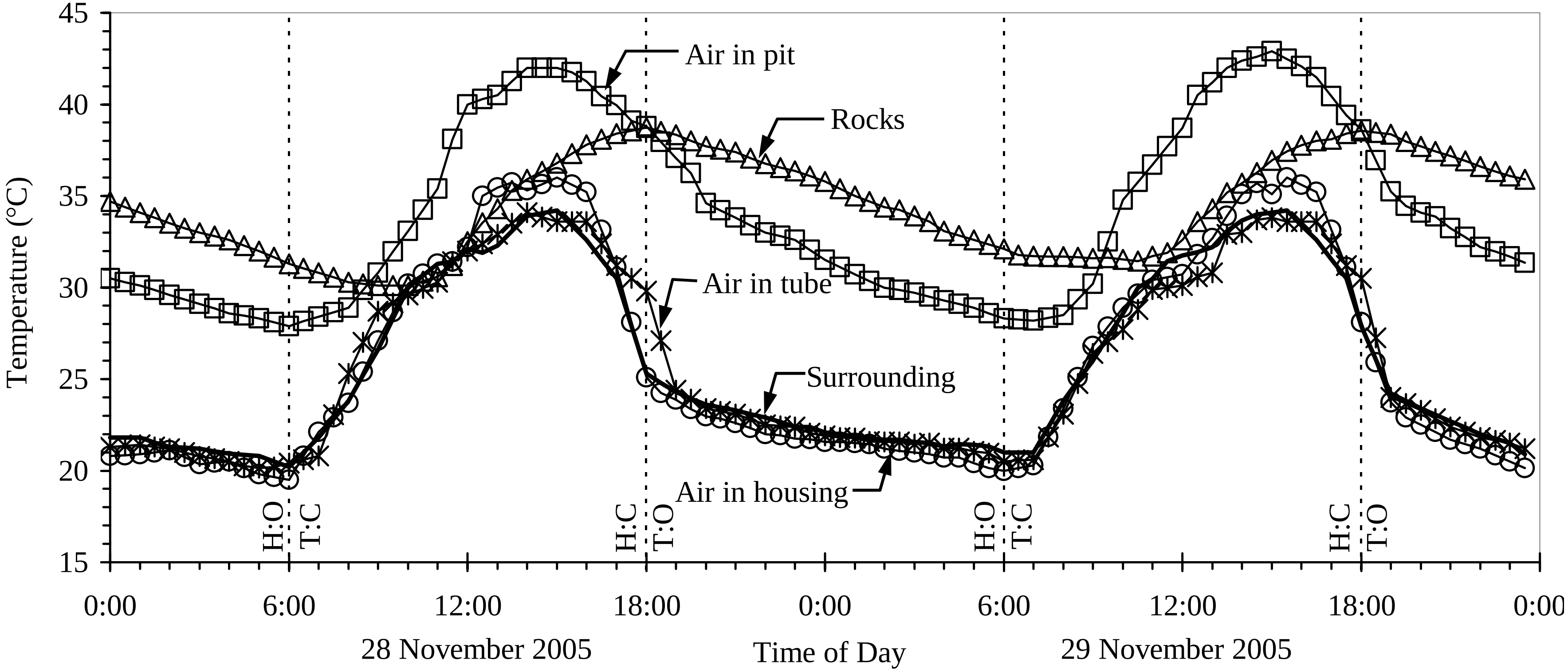

Figure 5.10 Temperature as a function of time measured from the system using 5.1-cm diameter hot-air tube. At 6:00 am, the housing model is opened (H:O) and the hot-air tube is closed (T:C). At 6:00 pm, the housing model is closed (H:C) and the hot-air tube is opened (T:O).

Figure 5.11 The storage pit (front) was connected to the housing model (back) with 10.2-cm diameter hot-air tube. The tube was inclined at an angle of 30 degrees with the vertical height of 1.5 m.

because there were energy losses on the top of the pit. To prevent the energy loss from the housing model, the top of pit was covered by gunny-bags after 3:00 pm. The temperature in housing model was slightly increased by about 1^{o}C higher than that of the surrounding temperature. Then the housing walls, ceiling and floor were sealed with 2-cm thick foam sheets to minimize the heat loss and leakage. After the tubes were opened, the temperature in the housing model rapidly increased within the first 60 minutes then its slightly decreased which was similar to the increasing rate of air in the hot-air and surroundings. The results showed that more heat energy was transferred to the housing model as evidence by the temperature in the housing model was nearly 5^{o}C higher than the surrounding air temperature (Figure 5.12).

At 6:00 when the pit was opened the rock temperature continued to decrease. Before 9:00 am and after 3:00 pm the energy level from the sun was getting low and loss of the energy from the storage pit was higher than the energy gain. This evidence indicated that the opening time of storage pit was improper. The opening time of the storage pit was therefore changed from 6:00 am to 9:00 am and the closing time was changed from 6:00 pm to 3:00 pm. The hot-air tube was opened at 9:00 pm and closed at 9:00 am.

5.2.3 Testing with 20.3 cm diameter hot-air tube

The storage pit was connected to the housing model with 20.3-cm (8 inches) diameter hot-air tube. The tube was inclined at an angle of 60 degrees on the first half and 20 degrees on the second half. The elevation difference between the inlet and outlet was about 1.5 m. The opening and closing times of the pit, housing model, and tubes were the same as the previous.

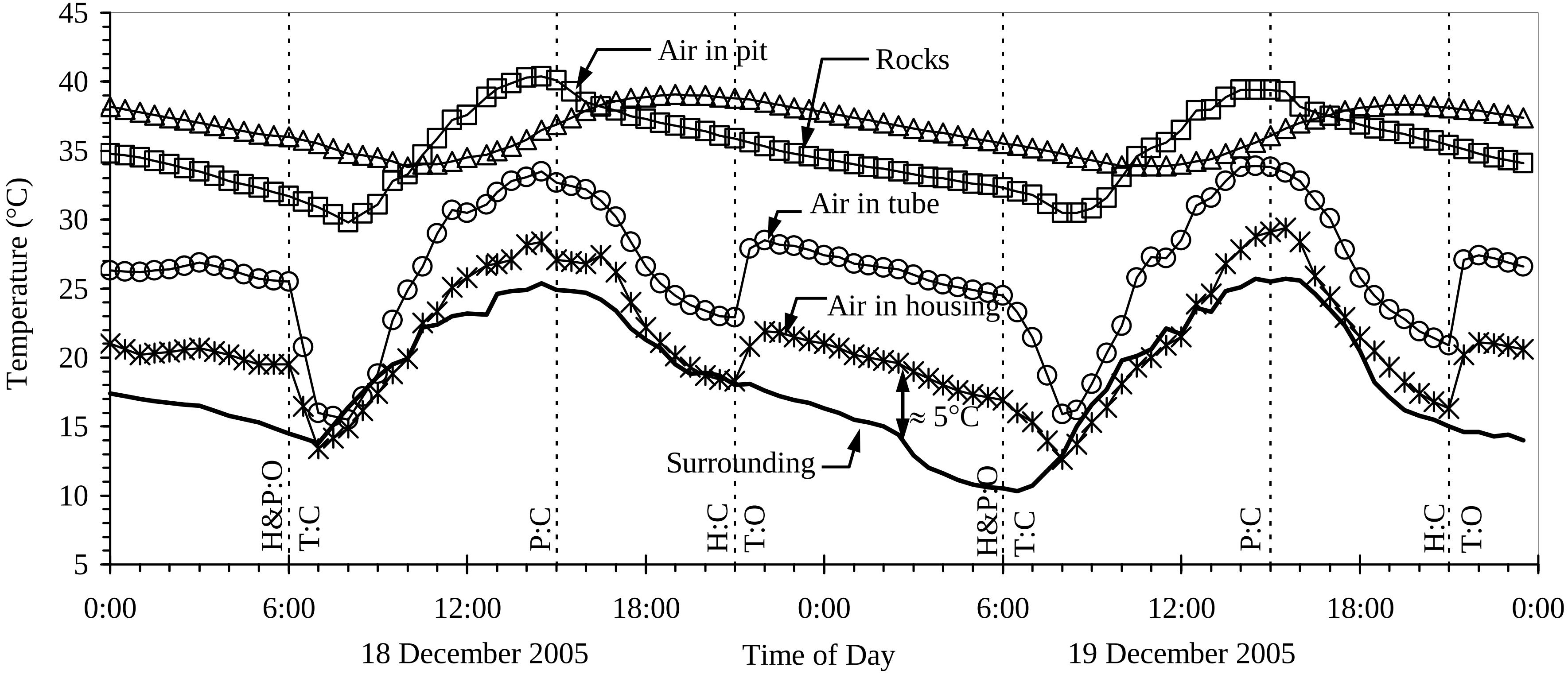

Figure 5.12 Temperature as a function of time measured from the system using 10.2-cm diameter hot-air tube. At 6:00 am, the housing model and pit are opened (H&P:O) and the hot-air tube is closed (T:C). At 3:00 pm, the pit is closed (P:C). An 9:00 pm, the housing model is closed (H:C) and the hot-air tube is opened (T:O).

The temperature changes were similar to the results obtained from the system with 10.3-cm diameter hot-air tube. The results indicated that the temperature increasing in the housing model was greater than 5^{o}C (Figure. 5.13).

An AC-12 Volt ventilator was used in an attempt to circulate the air in the housing model by placing it on top of a 5.1-cm diameter cold-air tube. The cold-air in the house was presumably sucked by the ventilator and flow into the pit, and hence that the heat energy stored in the rocks was accelerated into the housing model. Although the temperature measurements indicated that this method could help increasing the temperature in the housing model, the intention of this research was to avoid using other sources of energy except that from the sun. Thus the ventilator was temporary installed just to test the ability of circulatory system through the provided tubes. A detailed analysis on this experiment was not the intention of this study.

5.2.4 Testing with 20.3 cm diameter hot-air tube and 370 kg rocks

This testing used 20.3-cm diameter hot-air tube and took about 50% of the rock fragment out off the pit; the remaining weight was approximately 370 kg. The housing model was opened at 9:00 am and the storage pit was also opened at 9:00 am. After 3:00 pm, the pit was closed again and the hot-air tube was opened at 9:00 pm. The measured temperature in the housing model increased around 2-3^{o}C (Figure 5.14) over the surrounding temperature which was about 50% of the temperature increasing compared to the previous model where the rock fragments was not removed.

5.2.5 Testing with 0.6×0.6 m cross-sectional area vent and 370 kg rocks

The housing model was connected to the storage pit by a hot-air vent with a cross-sectional area of 0.6×0.6 m, the largest used in this study. The air vent was made from zinc sheet and insulated with 2-cm thick foam sheet as shown in

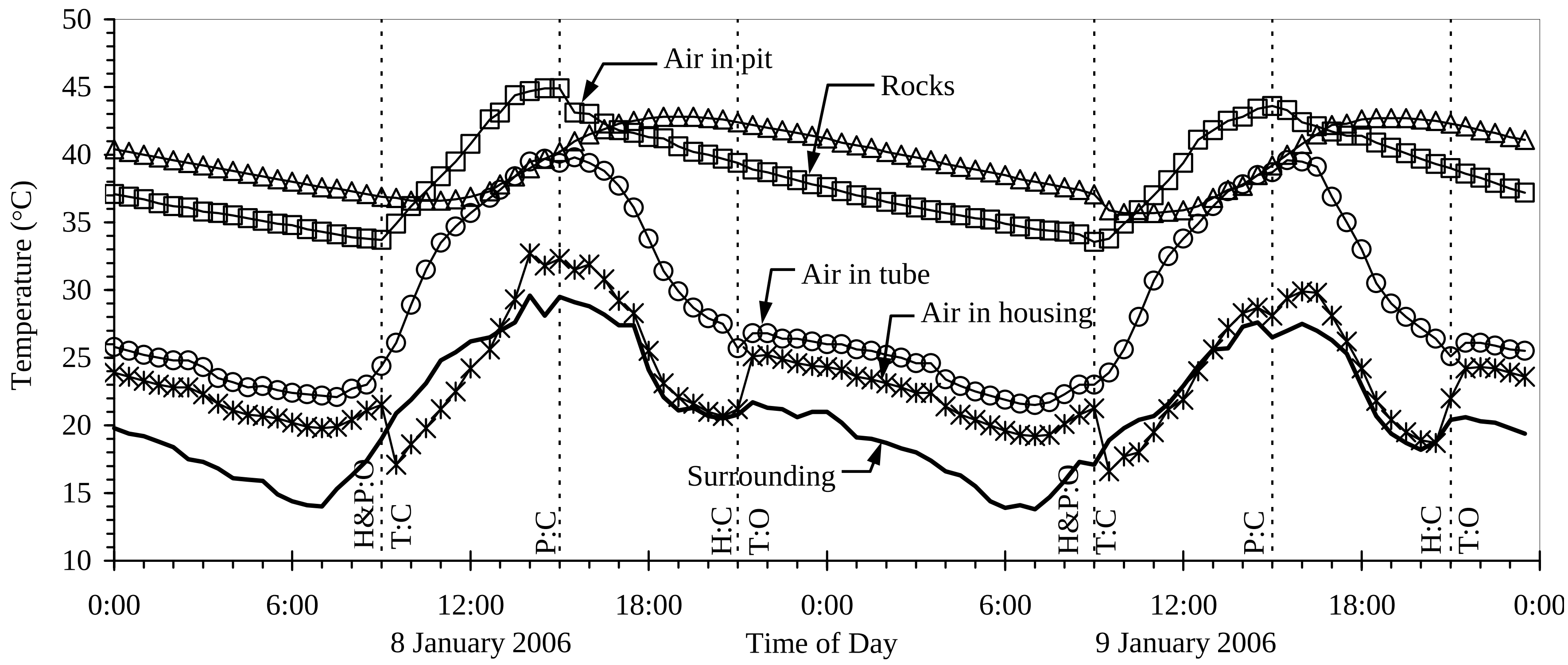

Figure 5.13 Temperature as a function of time measured from the system using 20.3-cm diameter hot-air tube. At 9:00 am, the housing model and pit are opened (H&P:O) and the hot-air tube is closed (T:C). At 3:00 pm, the pit is closed (P:C). At 21:00 pm, the housing model is closed (H:C) and the hot-air tube is opened (T:O).

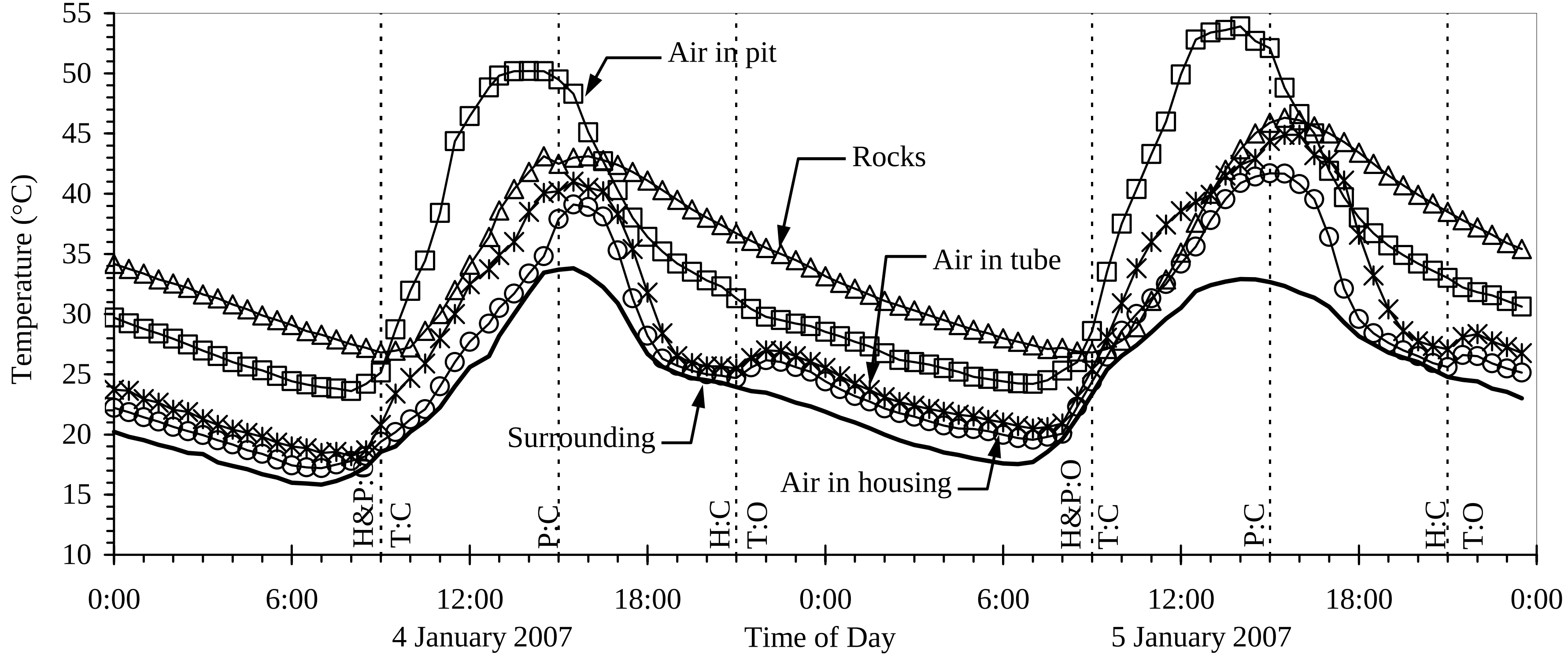

Figure 5.14 Temperature as a function of time measured from the system using 20.3-cm diameter hot-air tube and 370-kg rock fragment. At 9:00 am, the housing model and pit are opened (H&P:O) and the hot-air tube is closed (T:C). At 3:00 pm, the pit is closed (P:C). At 9:00 pm, the housing model is closed (H:C) and the hot-air tube is opened (T:O).

Figure 5.15. The remaining weight of rock fragments in the pit was approximately 370 kg. The opening and closing time of the pit, housing model and tubes were the same as the previous testing.

Figure 5.16 shows the temperature measurements from this testing. The temperature in the housing model increased by 2-3^{o}C compared to the surrounding temperature. The temperature increase was lower than that using the smaller tube. Because of the vent may block the solar energy which resulted in smaller heat energy absorbed by the rock fragment.

5.3 Discussions and conclusions

The storage system efficiency depends on the level of energy, size and inclination of hot-air tube, the heat loss in pit, and the heat loss. In comparison, it seems that the most suitable model was the system which the storage pit connected to housing model with over 10.2-cm (4 inches) diameter hot-air tube and inclined at an angle about 30 degrees. The top of storage pit should be covered with the isolator sheet (a textile, gunny-bags or fabric sheet). This system resulted in a temperature increase as high as 5^{o}C in the housing model. When the heat energy was allowed to transfer to the housing model until 9:00 am, the temperature in the storage pit is still higher than that in the housing model. This implies that the efficiency of the heat transfer was not optimized. Mathematical equations will be employed to improve efficiency of the system for the next stage of this study. The mathematical equations will be used to improve the system efficiency by producing comparable temperatures in the housing and storage pit, during the heat transfer time from the storage pit. The behavior of the heat transfer system will be simulated to compare with the actual temperature measured in the model.

Figure 5.15 The storage pit (left) connected to the housing model (right) by a 0.6×0.6 m cross-sectional area vent. The vent made from zinc sheet and covered by 2-cm thick foam sheet.

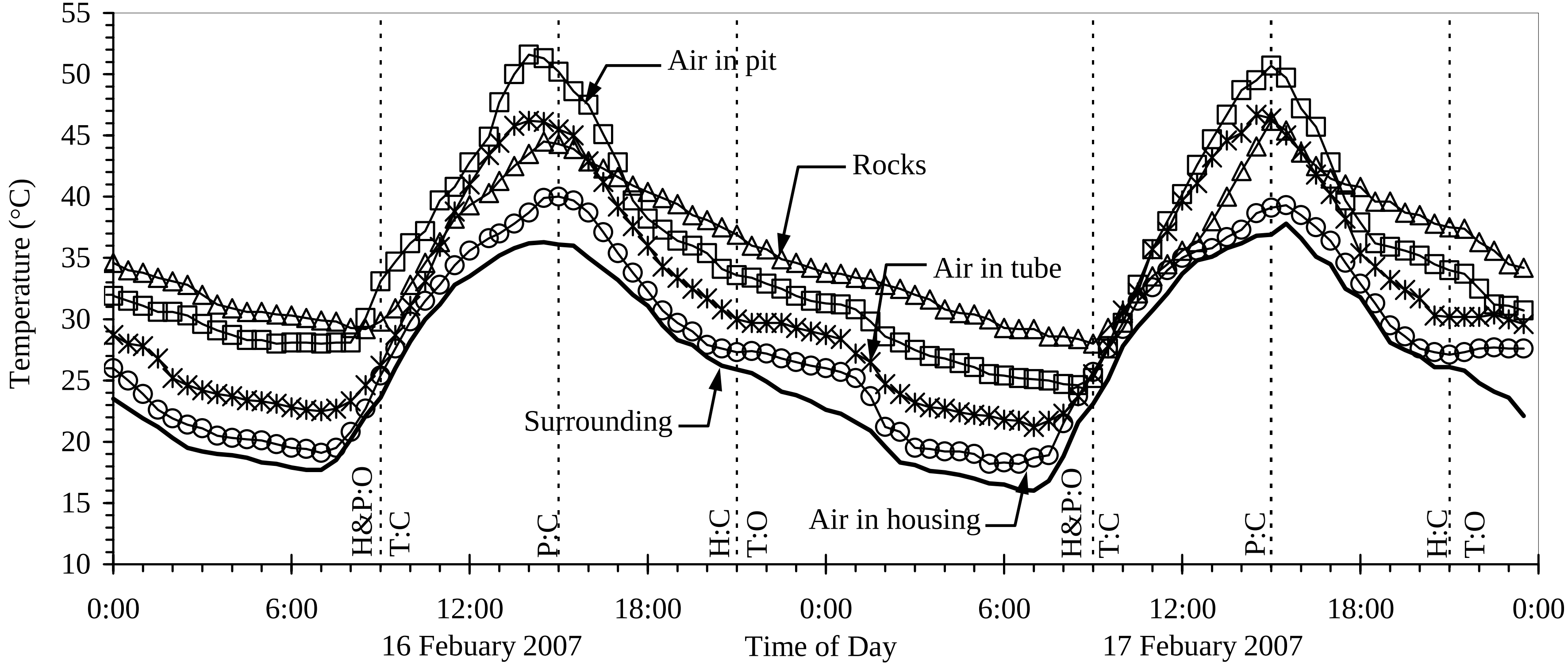

Figure 5.16 Temperature as a function of time measured from the system using 0.36 m^2 of cross-sectional area hot-air tube and 370-kg rock fragment. At 9:00 am, the housing model and pit are opened (H&P:O) and the hot-air tube is closed (T:C). At 3:00 pm, the pit is closed (P:C). At 9:00 pm, the housing model is closed (H:C) and the hot-air tube is opened (T:O).

CHAPTER VI

COMPARISONS BETWEEN CALCULATIONS AND MEASUREMENTS

This chapter compares the temperatures measured from the storage system with those calculated from the mathematical model. The objective is to study the reliability, the agreement, and the variability of the results from the two methods.

6.1 Input parameters

The input parameters for the calculation include the constants and variables related to the characteristics of the storage pit, hot-air tube, and housing model of the pilot scale. The constant parameters used here include the surrounding air and soil mass temperature and the solar radiation (Table 6.1), the air properties (density, Nusselt number, and Prandtl number, specific heat and thermal conductivity) as shown in Table 6.2, the rock properties (a specific heat and thermal conductivity, emissivity, absorbtion coefficient, effective diameter), and the acrylic sheet properties (a specific heat and thermal conductivity, thickness, area). Table 6.3 summaries the input parameters of the rock and acrylic sheet. The surrounding air temperature was averaged from the measured data from year 2000 to 2003 recorded by the Thai Meteorological Department (2003). The solar energy on the collected surface was averaged from the solar energy during winter season (November through January) using the equation proposed by Exell and Kumar (1981). The changing of soil

Table 6.1 Input data for the calculation: solar radiation, temperature of soil mass and surrounding air (Exell and Kumar, 1981; Thai Meteorological Department, 2003).

Time of Day	Solar Radiation (W/m^2)		Temperature (°C)		
			Soil Mass	Surrounding Air	
	Average	Minimum		Average	Minimum
6:00	58.4	19.5	28.5	19.2	10.4
7:00	185.2	133.7	28.4	20.2	10.7
8:00	323.8	258.4	28.8	22.4	12.8
9:00	457.3	364.9	29.3	24.6	15.9
10:00	567.0	450.8	29.8	26.8	18.8
11:00	636.2	496.0	30.3	28.9	21.3
12:00	653.8	493.8	30.8	31.0	23.9
13:00	617.2	446.2	31.3	32.7	25.9
14:00	532.1	361.9	31.9	33.7	26.9
15:00	411.9	256.5	32.3	33.9	27.3
16:00	274.5	147.8	32.4	32.3	26.8
17:00	138.3	51.8	32.2	29.4	25.1
18:00	21.2	0	31.9	26.0	22.5
19:00	0	0	31.7	23.5	20.2
20:00	0	0	31.4	22.4	18.5
21:00	0	0	31.1	22.0	17.0
22:00	0	0	30.8	21.6	15.6
23:00	0	0	30.5	21.3	14.6
24:00	0	0	30.2	20.9	14.0
1:00	0	0	29.9	20.6	13.4
2:00	0	0	29.6	20.1	12.8
3:00	0	0	29.4	19.7	12.2
4:00	0	0	29.1	19.4	11.6
5:00	0	0	28.8	19.0	11.3

Table 6.2 Input parameters of air properties for mathematical calculation (Cengel, 1998).

Temperature (K)	Air Density (kg/m^3)	Nusselt Number	Prandtl Number
250	1.413	1.14×10^5	0.724
280	1.271	1.40×10^5	0.717
290	1.224	1.48×10^5	0.714
298	1.186	1.55×10^5	0.712
300	1.177	1.57×10^5	0.712
310	1.143	1.67×10^5	0.711
320	1.11	1.77×10^5	0.71
330	1.076	1.86×10^5	0.708
340	1.043	1.96×10^5	0.707
350	1.009	2.06×10^5	0.706

Table 6.3 Constant parameters of rock and acrylic sheet used in the calculation.

Parameters	Unit	Value
a) Rock fragment		
- Specific heat, C_r	J/kg.K	1,174
- Thermal conductivity, k_r	W/m.K	1.70
- Effective diameter, D_{eff}	m	0.08
- Emissivity, ε_r	-	0.8
- Absorbtion coefficient, α_r	-	0.8
- Density, ρ_r	kg/m^3	2,760
b) Acrylic sheet		
- Specific heat, C_a	J/kg.K	1,470
- Thermal conductivity, k_a	W/m.K	0.20
- Thickness, t_a	m	0.003
- Density, ρ_a	kg/m^3	1,150

temperature obtained from the measurement results. The variable parameters included the characteristics of the storage pit (width, length, and depth), packed rock fragment properties (weight, collector surface and thickness), characteristics of the hot-air tube (diameter, inclination, length and elevation head between inlet and outlet), and volume of housing model. These parameters are used to simulate the pilot scale solar energy storage system. An unknown for this study is the percentage of heat energy leaking from the housing model. This unknown was systematically trialed to fit the measurement results. The computer program, MATLAB version 7.0, is used in the calculation. Euler's method for the integration of mathematical equation is applied.

6.2 Comparisons of the results

The comparisons are made for different sizes and shapes of the hot-air tube: circular tubes with diameter of 5.1, 10.2, and 20.3 cm and a squared vent with a cross-section of 0.6×0.6 m. The weight of the rocks in the pit has been changed twice; 370 and 743 kg. The heat energy loss from the hot-air tube was negligible and hence ignored.

Figures 6.1 through 6.3 compare the changes of temperatures of the rocks and the pit when using circular tubes and 743 kg of rock fragments. It has been found that during the daytime, the highest temperature of the rocks given by the calculation was at 4:00 pm (approximately 4 hours after the time of the highest solar energy). However, the results from the actual measurements indicate that the rocks had the highest temperature at 6:00 pm (approximately 6 hours after the time of the highest solar energy). This is due to the delay time before the energy transfers to the

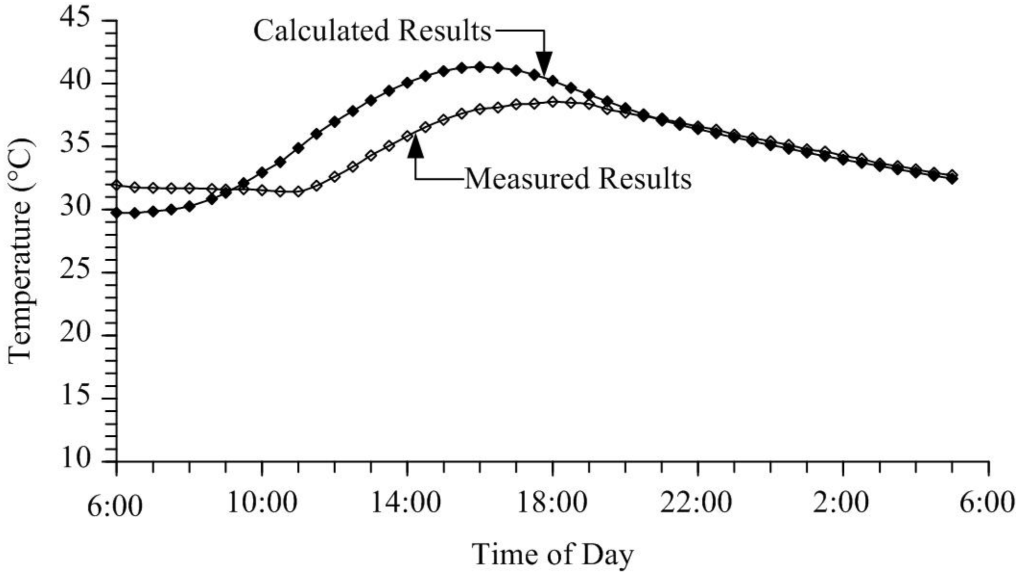

(a) Rock Fragments

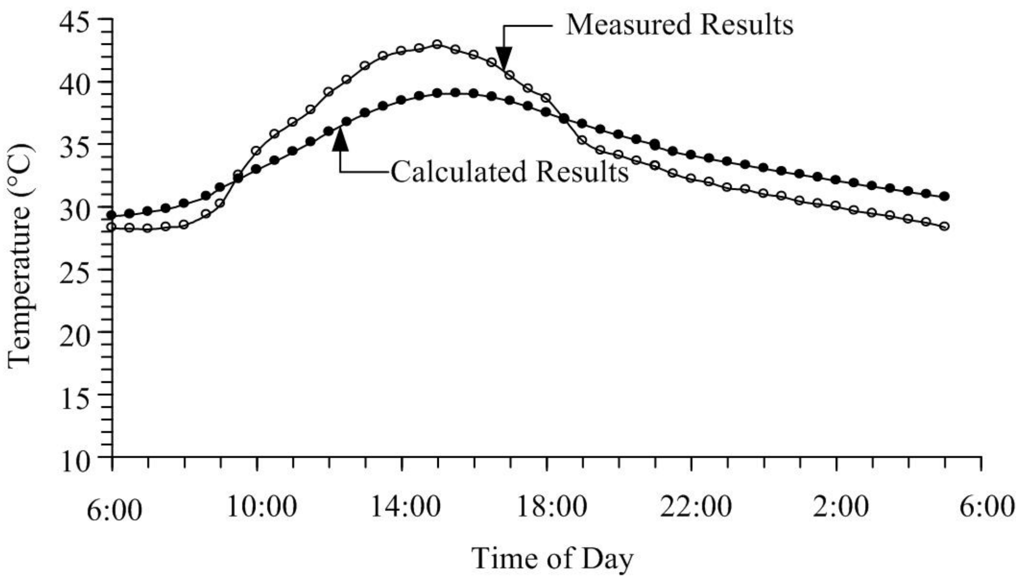

(b) Pit Air

Figure 6.1 Changes of temperature of the rock fragments (a) and the air in storage pit (b) for the measured results at November 28th, 2005 and the calculated results using 5.1-cm diameter hot-air tube.

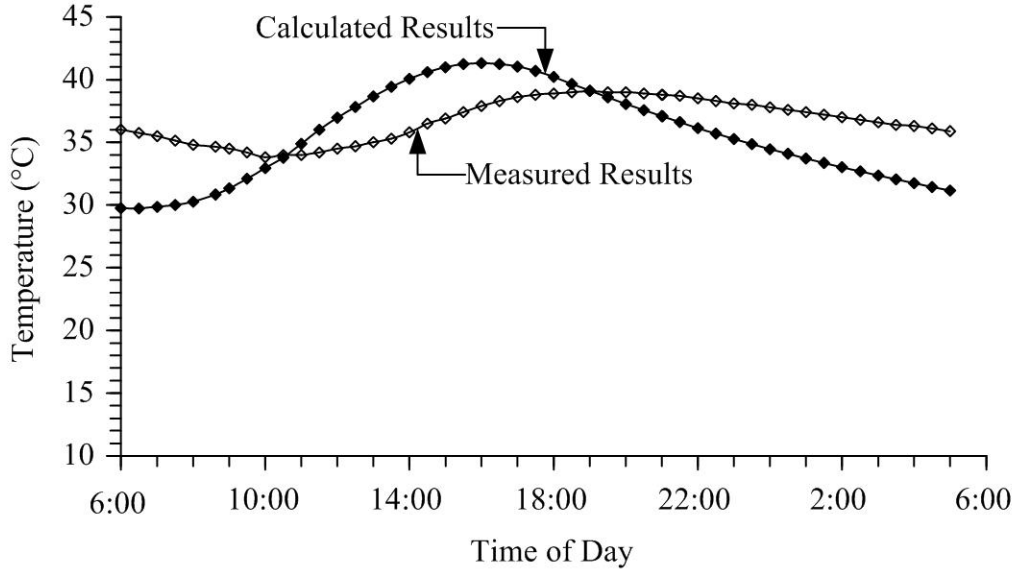

(a) Rock Fragments

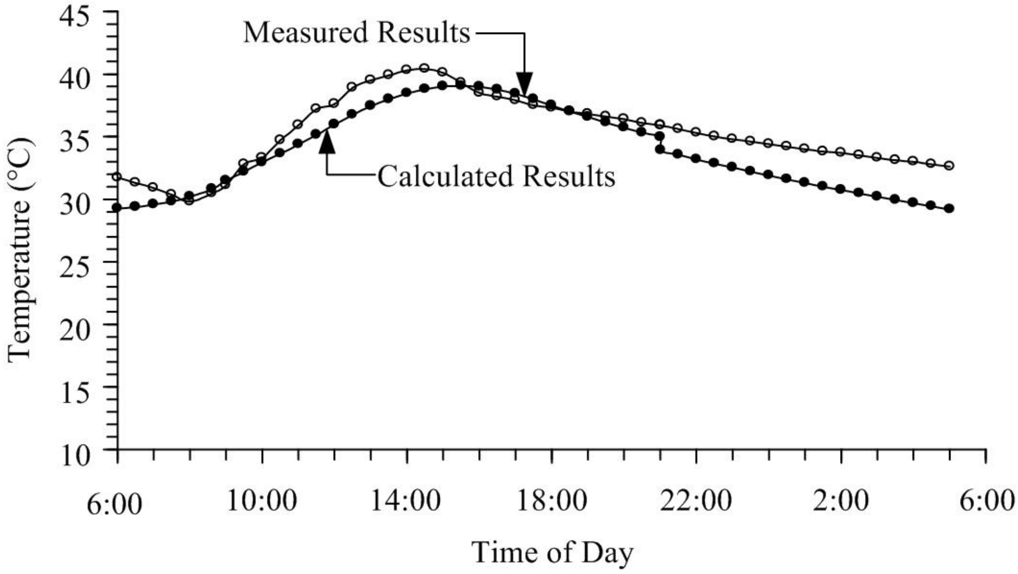

(b) Pit Air

Figure 6.2 Changes of temperature of the rock fragments (a) and the air in storage pit (b) for the measured results at December 18th, 2005 and the calculated results using 10.2-cm diameter of hot-air tube.

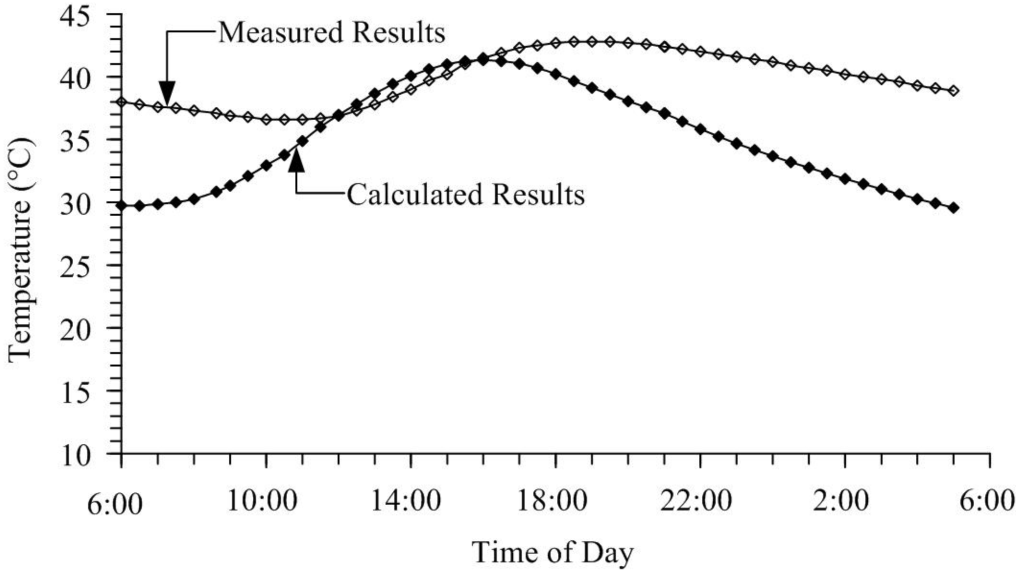

(a) Rock Fragments

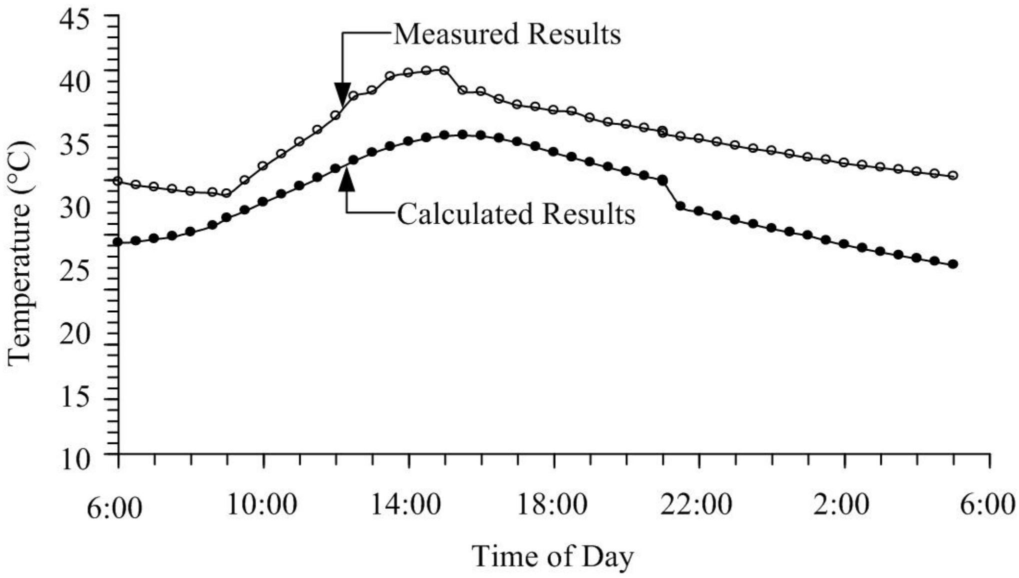

(b) Pit Air

Figure 6.3 Changes of temperature of the rock fragments (a) and the air in the storage pit (b) for the measured results at January 8th, 2006 and the calculated results using 20.3-cm diameter of hot-air tube.

measured point. Since the calculation is based on the assumption that all rock fragments have the same temperature, the rocks did not have the delay time to increase its temperature. For the changes of air temperature in the storage system obtained from the actual measurements and from the calculation was similar. The air temperature in the storage system during the daytime reached its highest at 3:00 pm. For the night time, temperature changes for the air and rock in storage system were slightly different. The system with a larger hot-air tube released the heat energy to the housing model at the higher rate than that with the smaller size. Therefore the cooling rate of the air temperature and rock for a larger hot-air tube was higher than that with the smaller hot-air tube.

Figures 6.4 through 6.6 compare the changes of air temperature in the housing model and the surrounding air. The 743 kilograms of rock fragments and circular tubes are used. The results given by the two methods were similar. The larger hot-air tube gives a higher temperature for the housing model. The housing temperature was about 3 – 6°C higher than that of the surrounding air.

Figures 6.7 and 6.8 compare the changes of temperature of the rock and air in the storage system with 370 kilograms of rock fragments and two different sizes of hot-air tube (20.3-cm diameter and 0.6×0.6 m sectional area vent). The results indicate that the rock temperatures obtained from the measurements and the calculations were at their peaks at 4:00 pm (approximately 4 hours after the time of the highest solar energy). It was also found that the delay time for the rocks to increase their temperature to the peak was shorter compared with the system with 743 kilograms of rock fragments. This could be due to the shorter distance of the measuring point (which was only 12 cm deep from the surface) was exposed to the

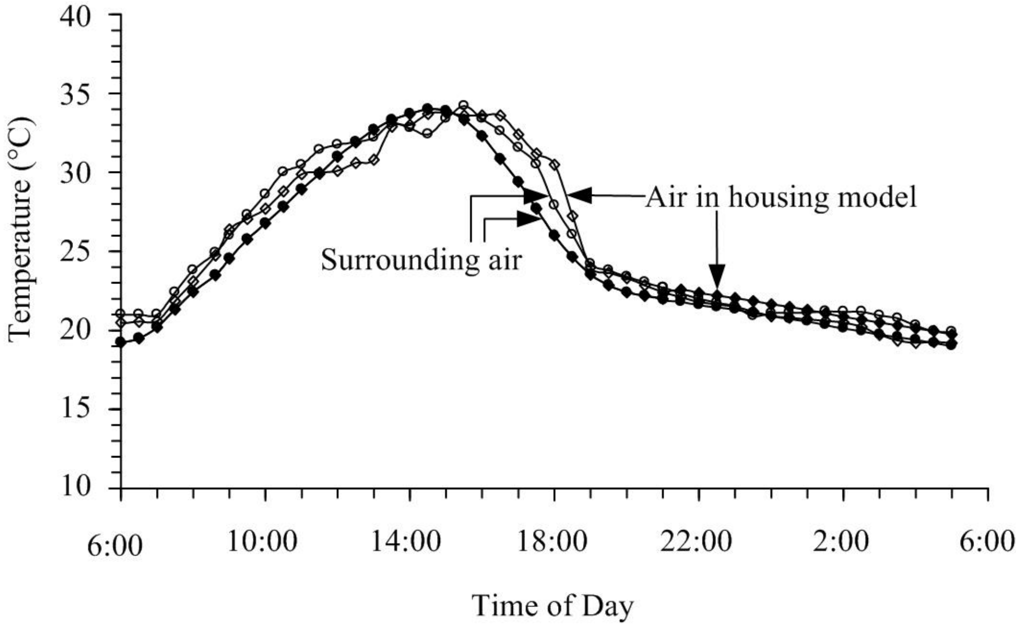

Figure 6.4 Changes of temperature of the air in housing model and the surrounding air for the measured results at November 28th, 2005 (white dots) and the calculated results (black dots) using 5.1-cm diameter hot-air tube.

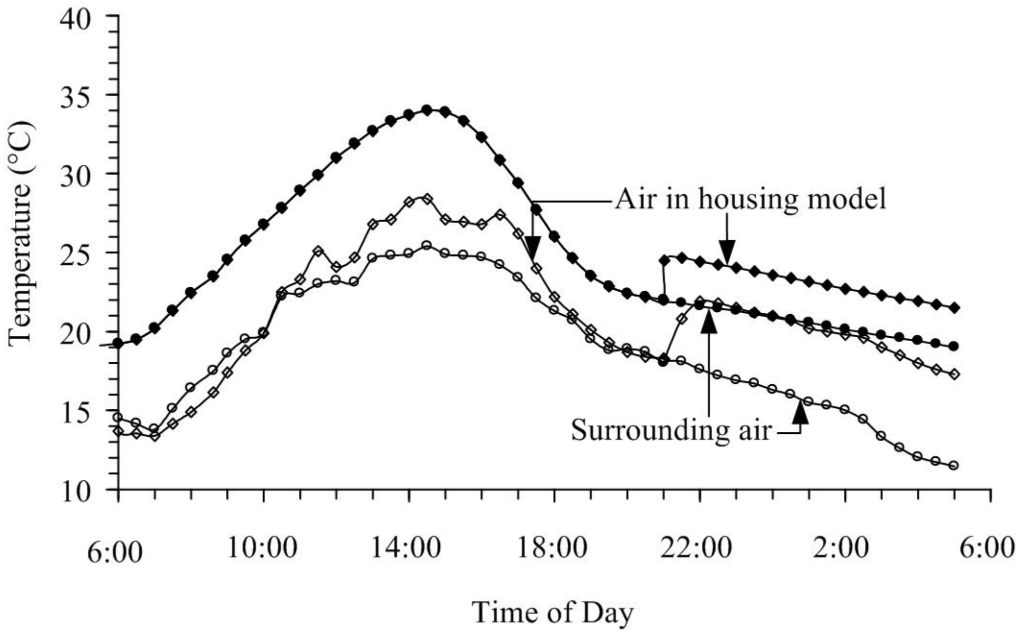

Figure 6.5 Changes of temperature of the air in housing model and the surrounding air for the measured results at December 18th, 2005 (white dots) and the calculated results (black dots) using 10.2-cm diameter hot-air tube.

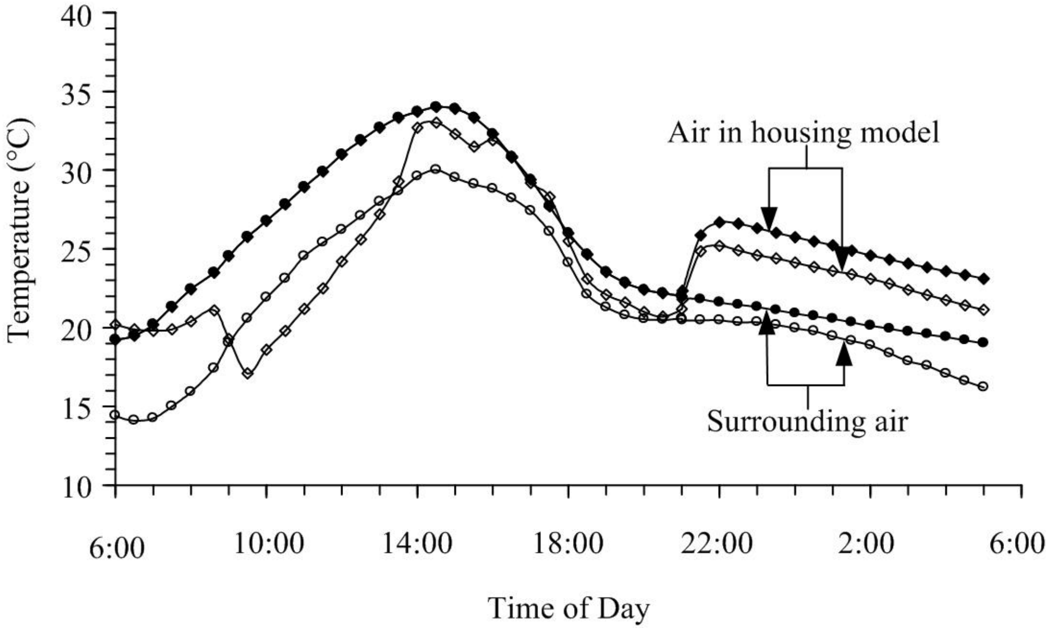

Figure 6.6 Changes of temperature of the air in housing model and the surrounding air for the measured results at January 8th, 2006 (white dots) and the calculated results (black dots) using 20.3-cm diameter hot-air tube.

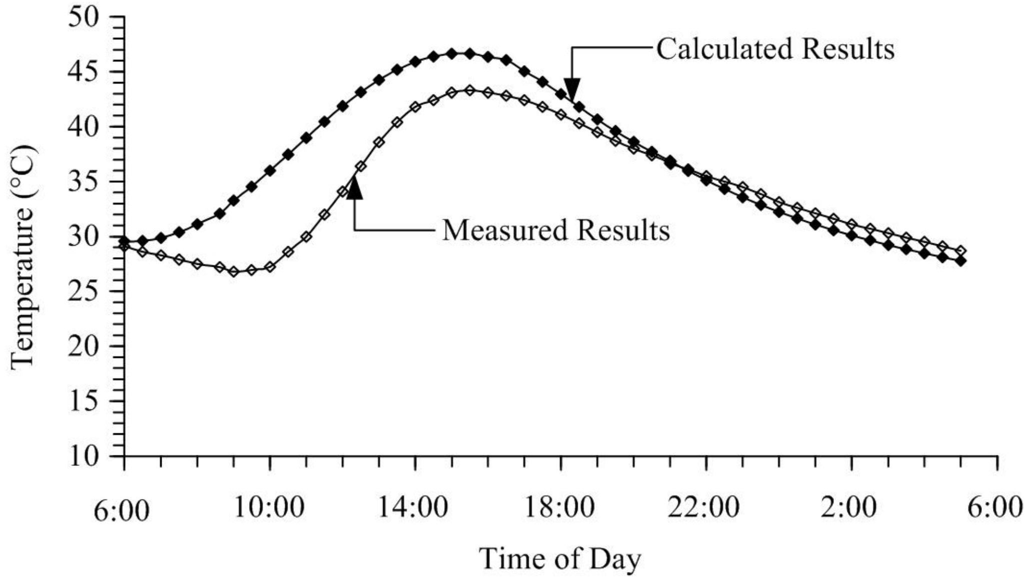

(a) Rock Fragments

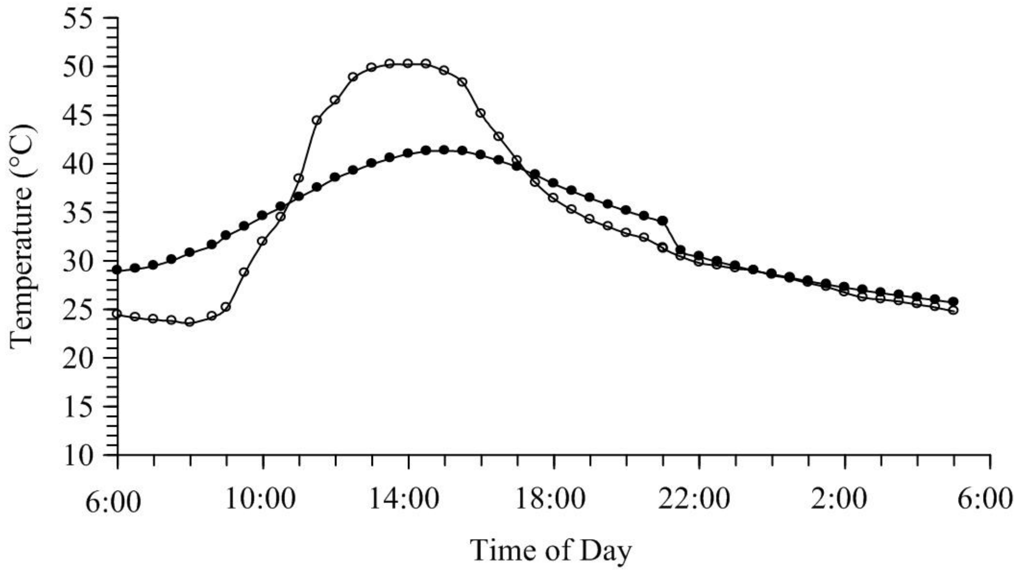

(b) Pit Air

Figure 6.7 Changes of temperature of the rock fragments (a) and the air in storage pit (b) for the measured results at January 4th, 2007 and the calculated results using 20.3-cm diameter of hot-air tube and 370 kg of rock fragments.

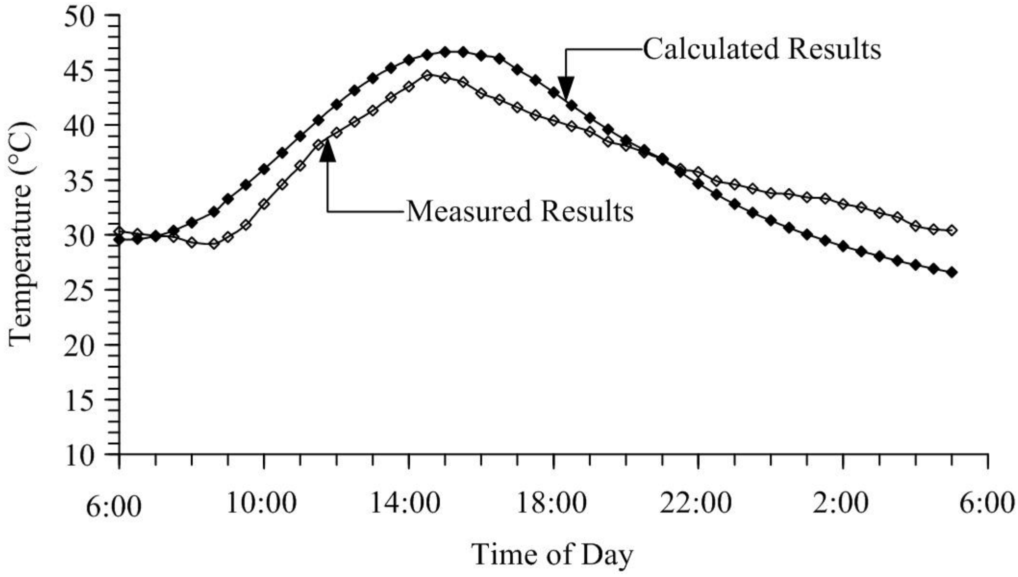

(a) Rock Fragments

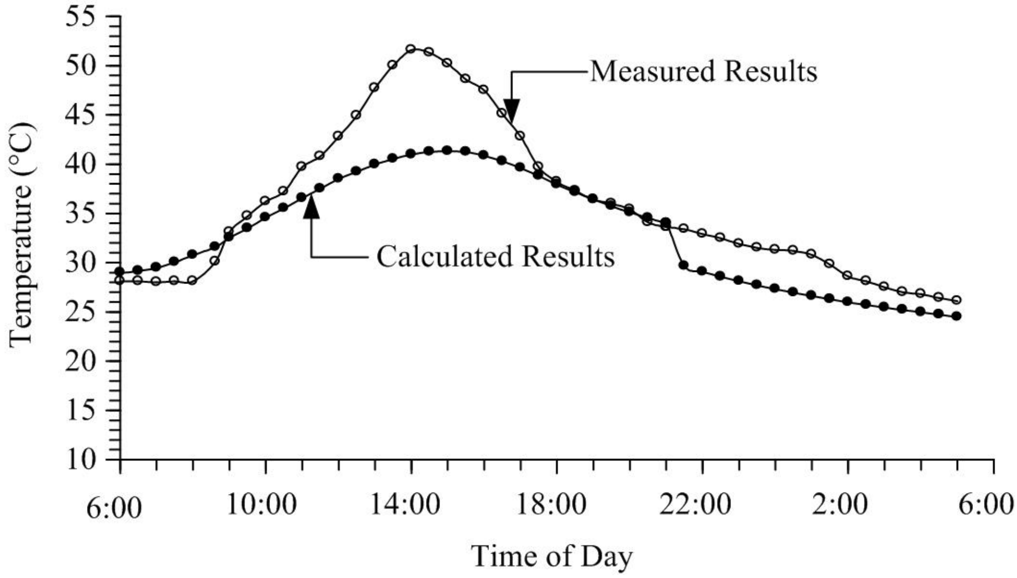

(b) Pit Air

Figure 6.8 Changes of temperature of the rock fragments (a) and the air in storage pit (b) for the measured results at February 16th, 2007 and the calculated results using the hot-air vent with cross-sectional area of 0.6×0.6 m and 370 kg of rock fragments.

solar energy. Although the quantity of the rocks in the rock-fill system was decreased, the heat energy was still the same.

Figures 6.9 and 6.10 compare the changes of air temperature in the housing model with the surrounding air temperatures. The storage system had 370 kilograms of rock fragments and two different sizes of hot-air tube (30.2-cm diameter and 0.6×0.6 m sectional area vent). The results from the two methods were similar: the temperature in the housing model increased for about 3-4°C after opening the hot-air tube. The comparison also indicates that decreasing quantity of the rock fragments in half (from the total of 734 kilograms) has lowered the temperatures of the housing model by only about 1-2°C. The decrease of rock fragments by 50% reduces the temperature increase by only 20-30%.

The calculation results suggest that about 10 percent of heat energy was leaked from the housing model. The calculated results agree with the measurement results which can be concluded that the mathematical equations were reliable and suitable for the temperature predictions under different parameters.

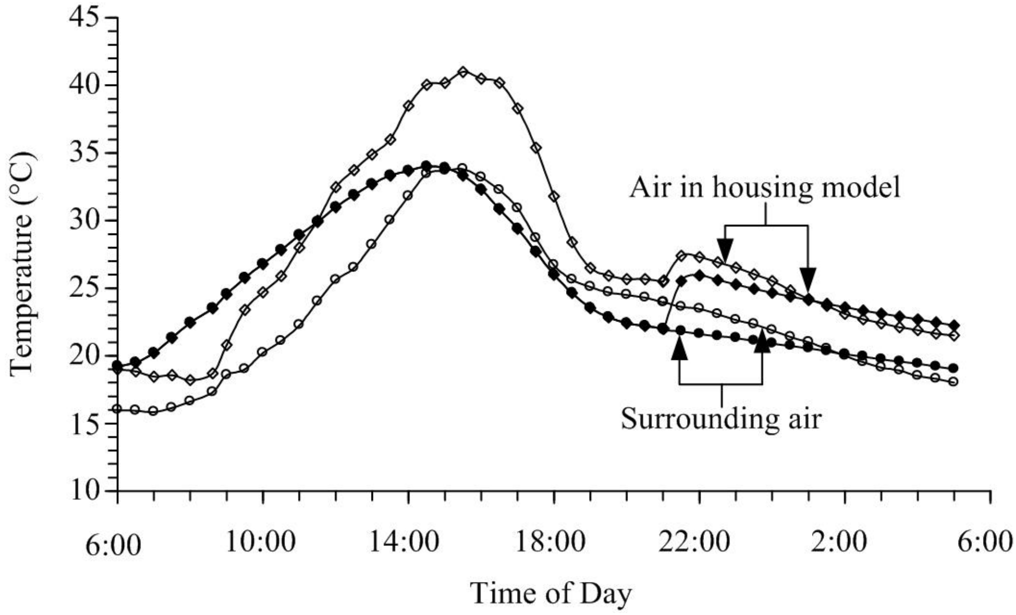

Figure 6.9 Changes of temperature of the air in housing model and the surrounding air for the measured results at January 4th, 2007 (white dots) and the calculated results (black dots) using 20.3-cm diameter hot-air tube and 370 kg of rock fragments.

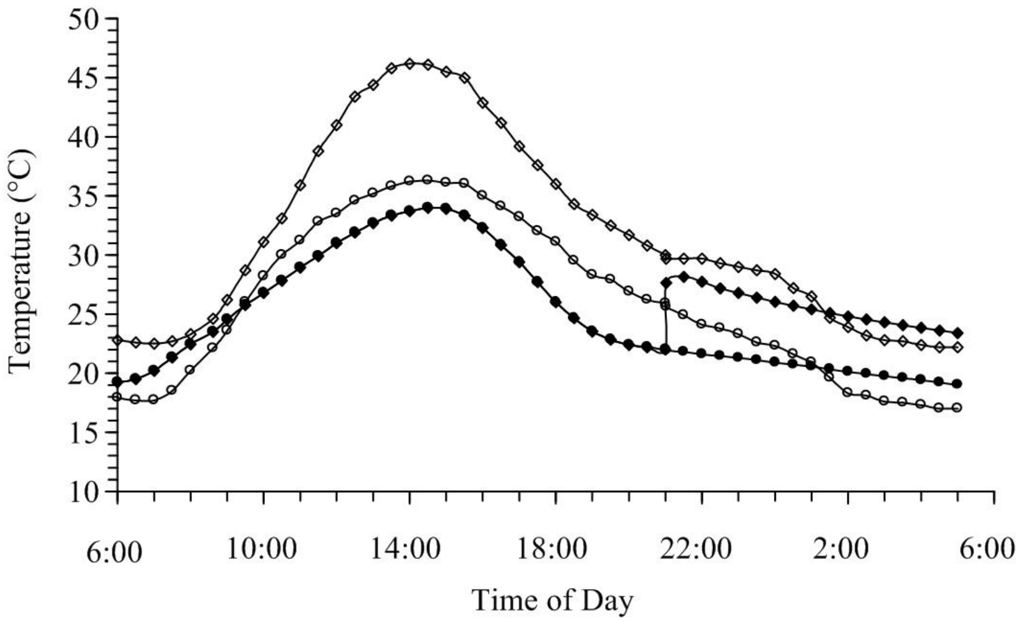

Figure 6.10 Changes of temperature of the air in housing model and the surrounding air for the measured results at February 16th, 2007 (white dots) and the calculated results (black dots) using the hot-air pipe with cross-sectional area of 0.6×0.6 m and 370 kg of rock fragments.

CHAPTER VII

DESIGN RECOMMENDATIONS

Relationships are derived between the temperature and volume of the housing and the weight of rock fragments to develop a guideline for the design of the suitable size of the storage pit for a given size of the housing model. The storage system efficiency and the heat energy gained in the housing model in form of the electrical energy are determined.

7.1 Sensitivity analysis of variables

The sensitivity analyses of variables are performed in order to investigate the effect of various parameters on the performance of storage system. Table 7.1 summarizes the variable ranges for the sensitivity analysis. They are divided into two groups: 1) an internal factors, i.e. the size of hot-air tube (ϕ), the volume of housing model (V_h), the collector area (A_{top}), and the types of rock fragments (in term of the heat capacity, C_r, and thermal conductivity, k_r), and 2) an external factors, i.e. the leakage of heat energy from the housing model (%leak), the surrounding air temperature (T_{sur}), and the level of solar energy (I). Each variable is set up based on assumptions that: the volume of housing model of 56 m^3, the size of hot-air tube is 10 cm in diameter, the volume of rock-fill is 1/6 times of the volume of housing model, the collector area is 16 m^2, the lowest temperature of surrounding air is 10°C (at 6.00 am),

Table 7.1 Variables of the housing model, tube, and storage system used in the calculation.

Variables	Unit	Range
a) Housing model		
- Volume, V	m^3	30 – 90
- Height , H	m	2.5
- Leakage	%	0 – 100
b) Tube		
- Diameter, D	m	0.1 – 0.5
- Length, L	m	2.5
- Elevation head, ΔH	m	1.5
- Inclination ($\Delta H/L$)	degrees	30
3) Storage pit		
- Collector area, A_{top}	m^2	6.25 – 16
- Rock fill thickness, t_{bed}	m	0.1 – 5.0

and the minimum solar energy as mentioned in the previous chapter. The results of the analyses are given below.

1) Effects of solar energy level

Two levels of solar energy have been applied: the highest energy of 4,734 W/m^2 and the lowest energy of 3,480 W/m^2. Figure 7.1 shows the energy level distributed over the northern part of Thailand during the winter. The results indicate that the temperature increases in the housing model under the lowest and the highest energy levels are 3.0°C and 3.4°C. This suggests that the solar energy levels have only small effect on the efficiency of the storage system which is negligible. On the conservation basis, the lowest energy level has been applied for the further analysis.

2) Effects of climate

For this aspect, the lowest surrounding air temperatures of the day (at 6:00 am) have been divided into 4 levels: 0-5°C, 5-10°C, 10-15°C, and 15-20°C as shown in Figure 7.2. The results show that the temperature increases (ΔT) in the housing model dropped when the surrounding air temperature became higher (Figure 7.3). This indicates that the efficiency of heat transfer depends on the difference between the temperature in the storage system and in the housing model. It could be noticed that the air mass flow rate (as mentioned in Eq. (4.20)) increases with increasing the temperatures difference.

3) Effect of rock types

The heat capacity of 12 rock types tested in the laboratory are applied in this study. Figure 7.4 plots the temperature increases in the housing model with the heat capacities of rock. The temperature increases tends to be similar (between 3.02–

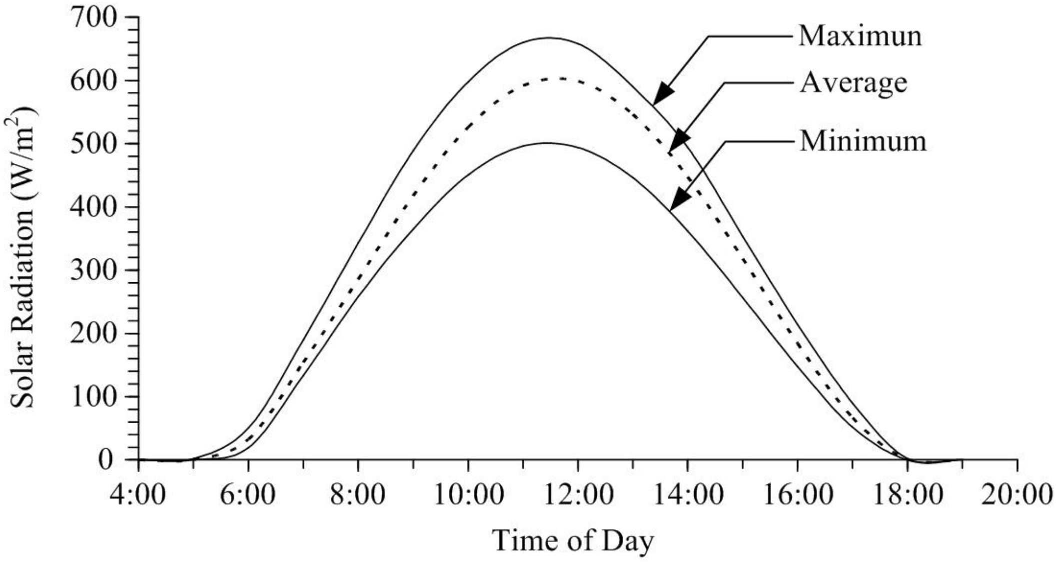

Figure 7.1 Mean of the highest and the lowest solar energy in the north of Thailand during winter (calculated by using equations given by Exell and Kumar, 1981).

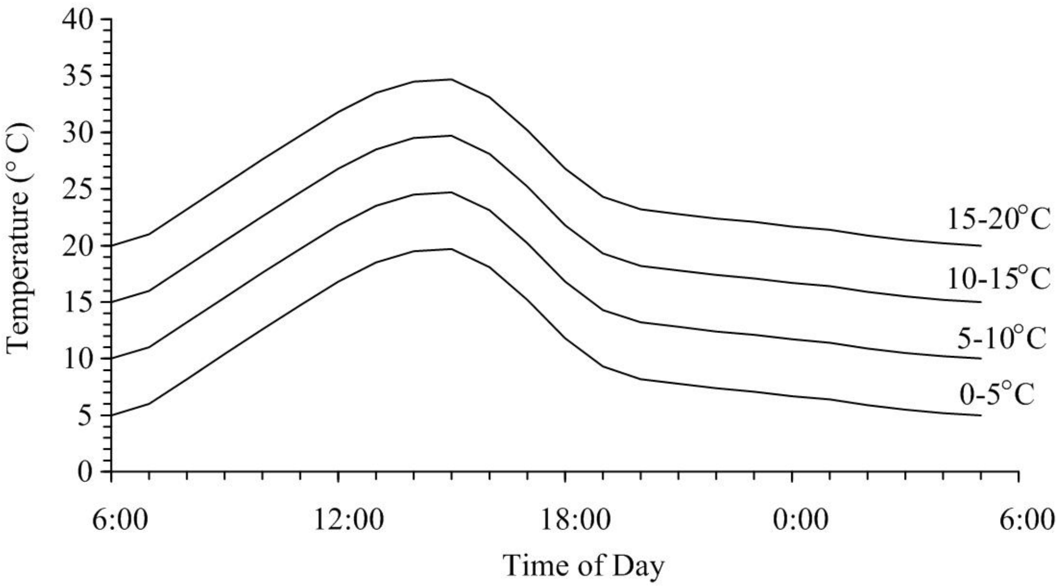

Figure 7.2 Four levels of the surrounding air temperatures used to analyze the effect of surrounding air temperature on the performance of the heat transfer.

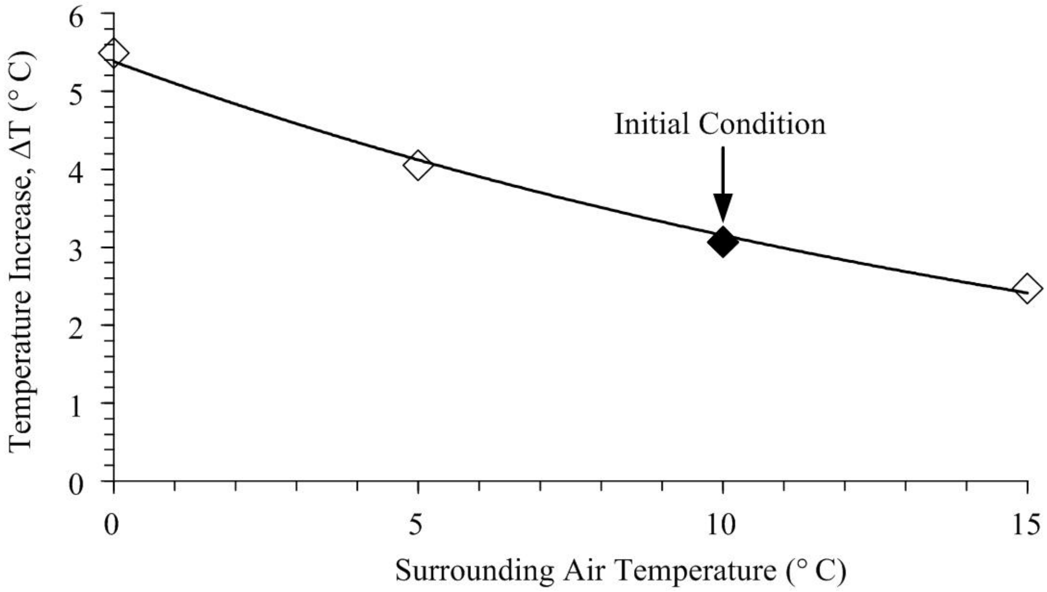

Figure 7.3 Temperature increase of the air in housing model under several surrounding air temperatures.

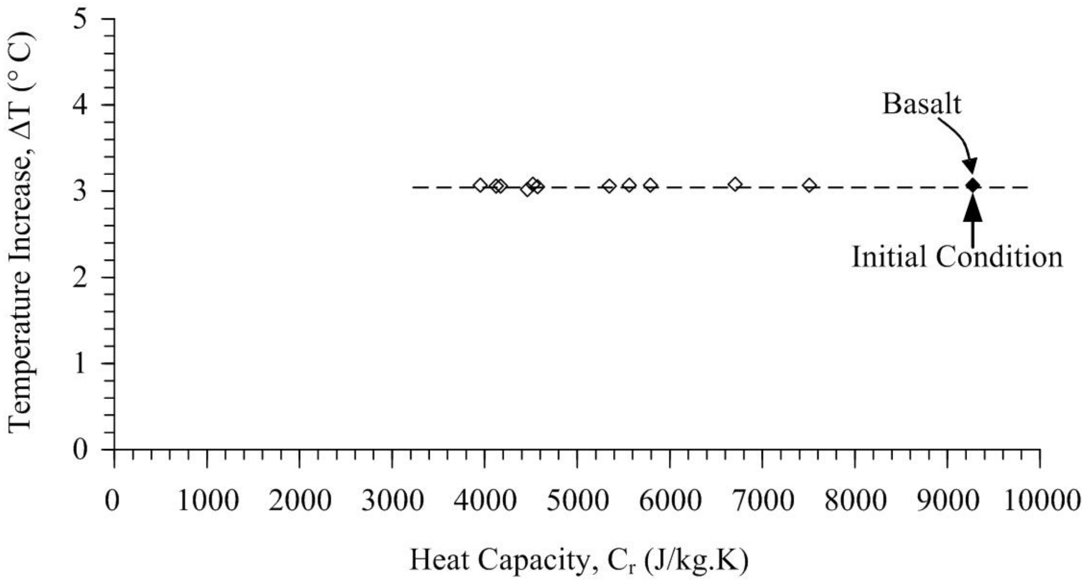

Figure 7.4 Temperature increase in the housing model predicted by using the heat capacities from 12 rock types.

3.08°C) for all rock types and hence no effect occurs when changing the rock types in the storage system.

4) Effects of housing model volume

The ratios of the housing model volume (V_h) to the bulk volume of rock-fill or packed rock volume (V_b) have been varied from 1:1 to 1:12. The volume of rocks-fill was fixed at 9.33 m^3 (the cross-sectional area of 4.0×4.0 m with a thickness of 0.58 m). The results indicate that the temperature increases (ΔT) in the housing model decreases as increasing the V_h/V_b ratio (Figure 7.5), primarily due to the larger volume of air in the housing model. This relation can be shown in equation as follows:

$$\Delta T = 5.08 \left(\frac{V_h}{V_b} \right)^{-0.376} \tag{7.1}$$

5) Effect of the collector area

The collector area (A_{top}) exposed to the solar energy has been varied from 4 to 25 m^2 while the packed rock volume was fixed at 9.33 m^3. The results suggest that a larger size of the collector area produces a higher temperature in the housing model (Figure 7.6). This could be due to the larger collector area allows a higher solar energy for the storage rock fragments. This can be presented by an equation as follows:

$$\Delta T = 0.043\ A_{top} + 2.40 \tag{7.2}$$

6) Effects of hot-air tube

The diameter of the hot-air tube has been varied from 0.1 m to 1.0 m. The results show that the temperature in the housing model will be increase when a

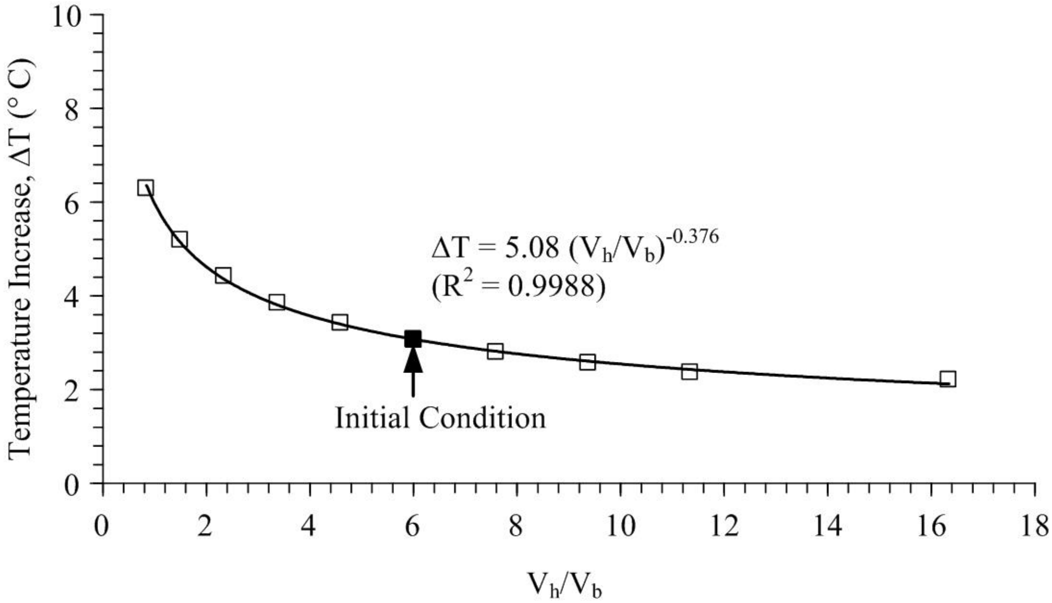

Figure 7.5 Temperature increase in the housing model plotted as a function of the ratio of housing volume (V_h) to bulk volume of rock fill (V_b).

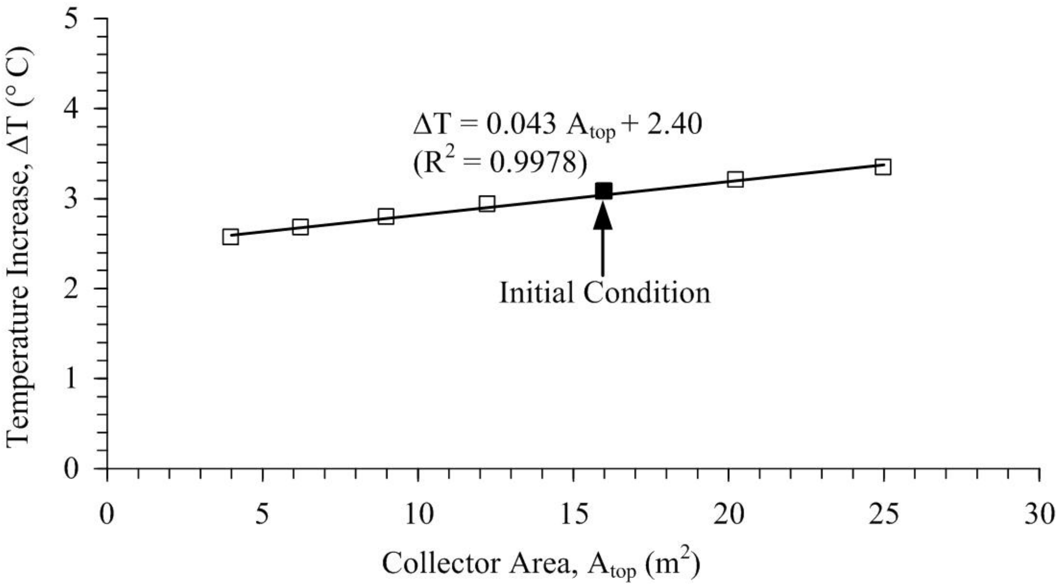

Figure 7.6 Relationship between the temperature increase (ΔT) in the housing model and the collector area (A_{top}).

larger hot-air tube is used. The larger hot-air tubes help increasing the mass flow rate of the heated air. Figure 7.7 shows the relationship between the temperature increases in the housing model and the size of hot-air tubes.

7) Effects of heat loss from the housing model

The leakage of heat energy from the housing model affects the system performance. The leakage depends from the types of construction material, the gaps in walls, and between the components. The energy leakage is assumed here with the ranges from 0 to 100 percent. Figure 7.8 shows the temperature increases in housing model and the percentage of the heat energy leak. This relation can be shown by the following:

$$\Delta T = [1 - 0.01(\%leak)]\ T_0 \qquad (7.3)$$

where T_0 is the temperature increases when have no leakage from the housing model.

The results of sensitivity analysis suggest that the main variables that affected the efficiency of the rock fill system are the collector area, the hot-air tube size, the housing model volume, and the volume of rock fill. These variables are considered for the calculation on the design recommendations.

7.2 Design guidelines of rock-fill system

The design guidelines of the rock-fill system have been developed under the assumption that no heat energy leaks from the housing model and the lowest surrounding air temperature at 6:00 pm is about 0°C. The variables include the

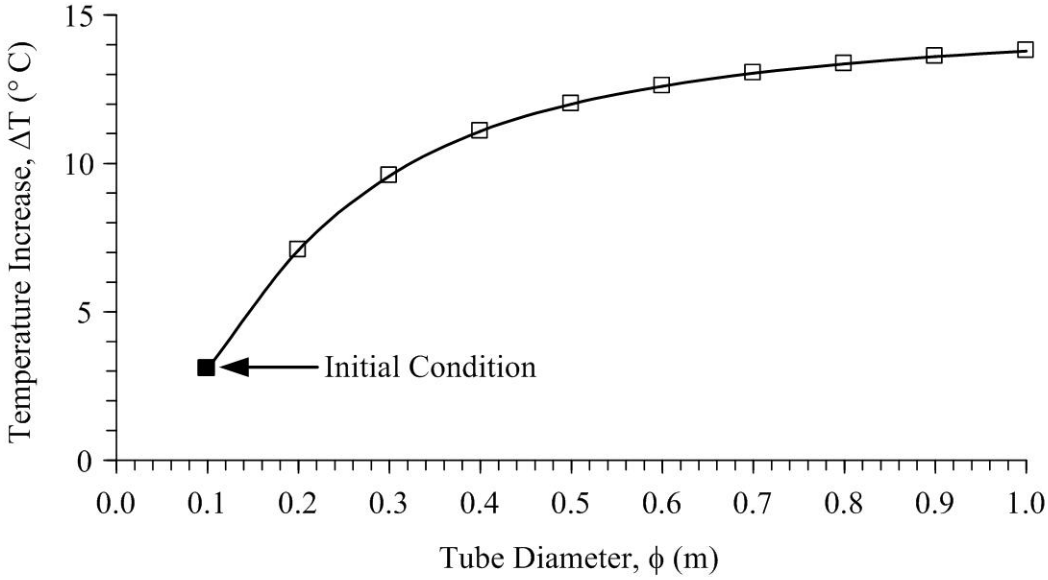

Figure 7.7 Relationship between the temperature increase (ΔT) in the housing model and the sizes of hot-air tube.

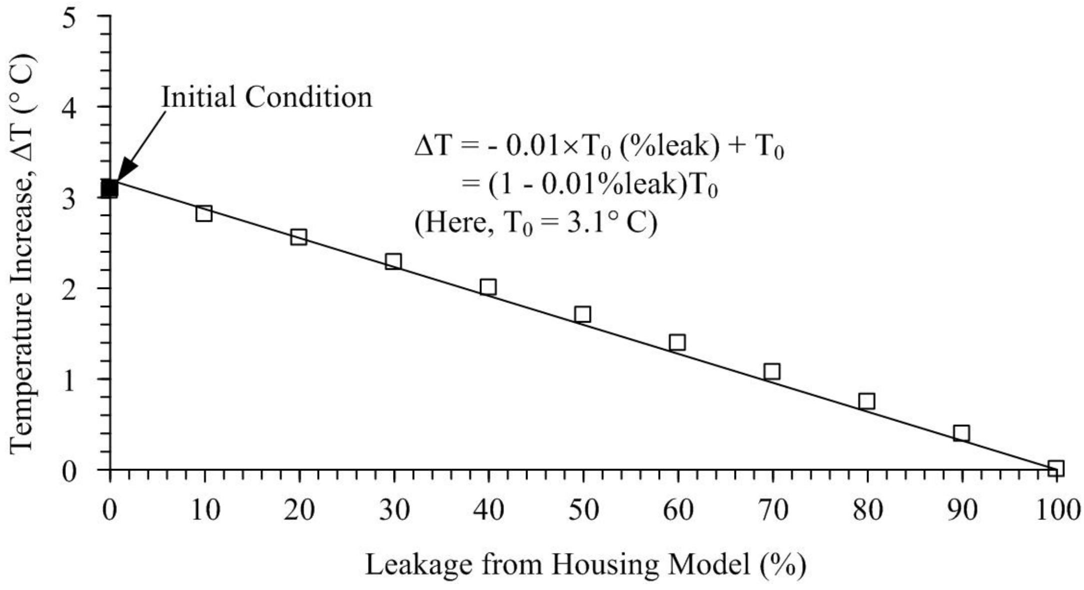

Figure 7.8 Relationship between the temperature increase in the housing model and the heat loss from housing model.

volume of housing model (V_h), the packed rock volume (V_b), and the collector area (A_{top}), and the size of the hot-air tubes (ϕ).

Forty sizes of rock fill volume with four sizes of the collector area (6.25, 9.00, 12.25 and 16 m^2), ten rock fill thickness (0.1 to 1.0 m), three sizes of the housing model with the volume of 31.1, 56.0, and 87.5 m^3, and five sizes of hot-air tube with the diameter of 0.1 to 0.5 m are used as variables.

Figures 7.9 through 7.11 show the relationship between the temperature increase in 31.5 m^3, 56.0 m^3 and 87.5 m^3 housing models and the rock fill thickness using four sizes of collector area. The results indicate that the larger rock-fills volume and its collector area give the higher temperature increase due to the rock-fills could be store more heat energy. It is also discovered that the suitable thickness of rock fills is about 30-70 cm (Figure 7.12). These results provide a design recommendation which is presented in form of a graphic representation.

The user can apply the required temperature increase (ΔT) in the housing on the charts prepared for 6.25 m^2 (Figure 7.13), 9.00 m^2 (Figure 7.14), 12.25 m^2 (Figure 7.15), and 16 m^2 (Figure 7.16) of collector area. The provided size of hot-air tube is then selected. The V_h/V_b ratio can be obtained.

The temperature increase applied on the previous step would be minimized due to the effect of surrounding air temperature by three times the surrounding air temperature (Figure 7.17) and due to the effect of leakage of housing one percentage of the heat loss (Figure 7.18). The net temperature increase in the housing ($\Delta T'$) is:

$$\Delta T' = \Delta T - 3T_{sur} - (\%leak). \qquad (7.4)$$

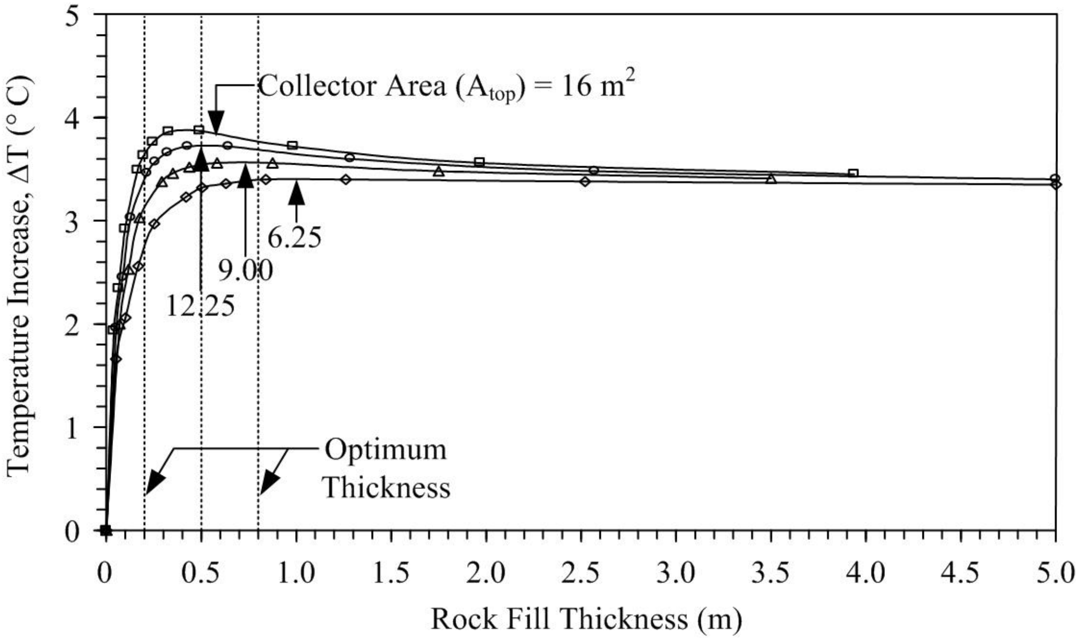

Figure 7.9 Temperature increase in the 31.5 m^3 housing model with four sizes of collector areas and the rock fill thicknesses of 0 to 5 m.

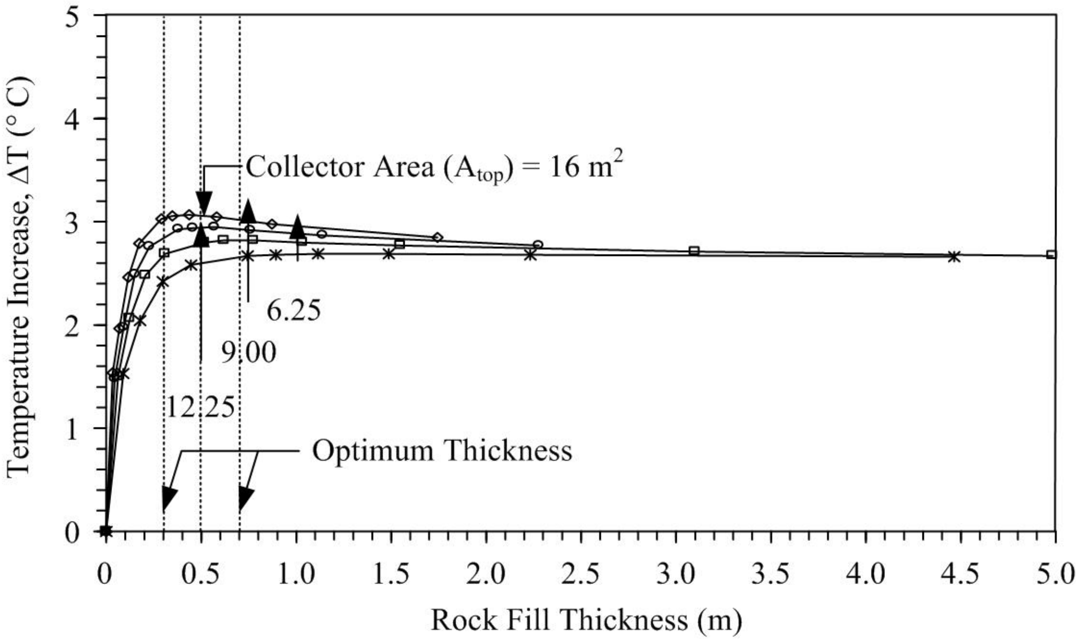

Figure 7.10 Temperature increase in the 56.0 m^3 housing model with four sizes of collector areas and the rock fill thicknesses of 0 to 5 m.

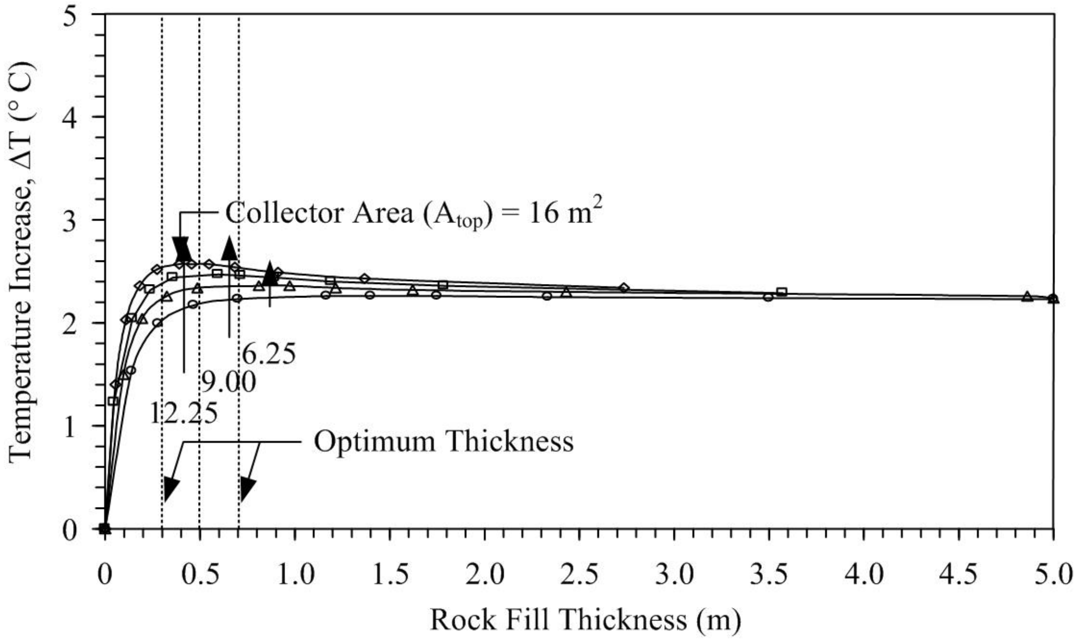

Figure 7.11 Temperature increase in the 87.5 m^3 housing model with four sizes of collector areas and the rock fill thicknesses of 0 to 5 m.

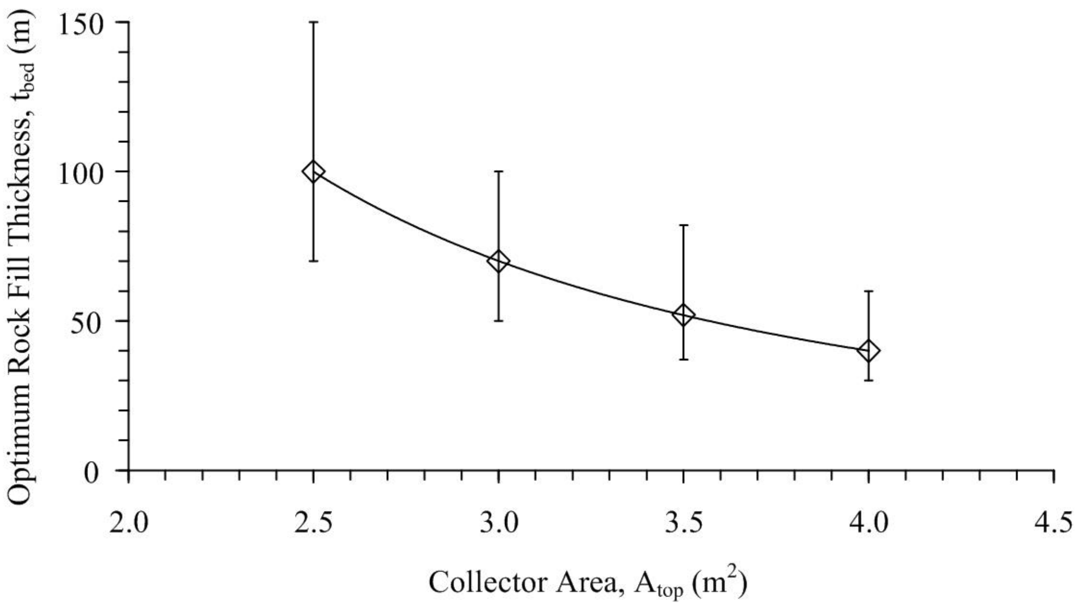

Figure 7.12 Relationship between the optimum rock fill thickness and the collector area that could be produced the highest increasing of temperature in the housing model.

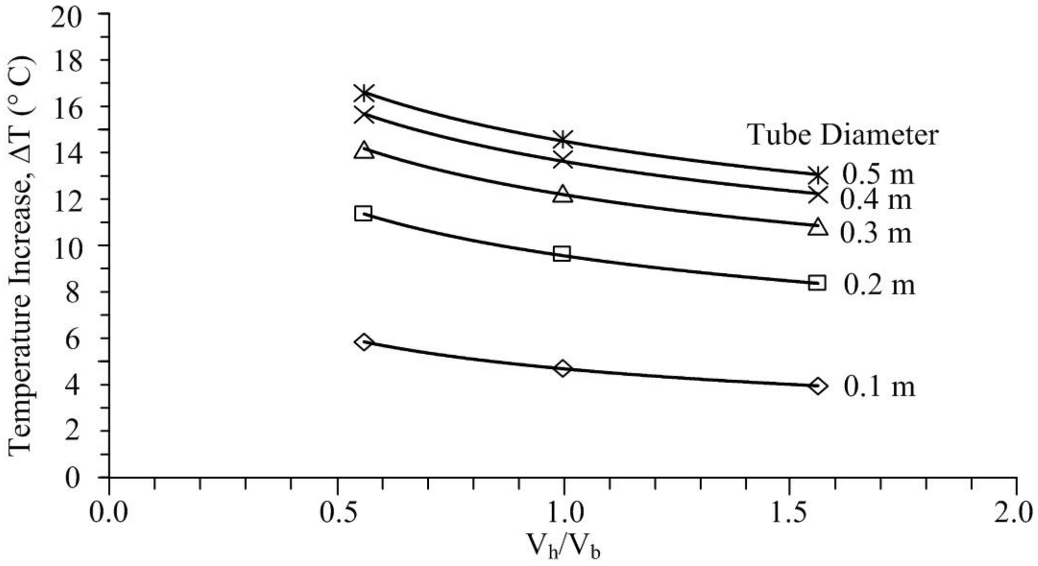

Figure 7.13 Relationship between the temperature increase in the housing model and the ratio of housing volume to rock fill volume with 6.25 m^2 collector area and the hot-air diameter of 0.1-0.5 m.

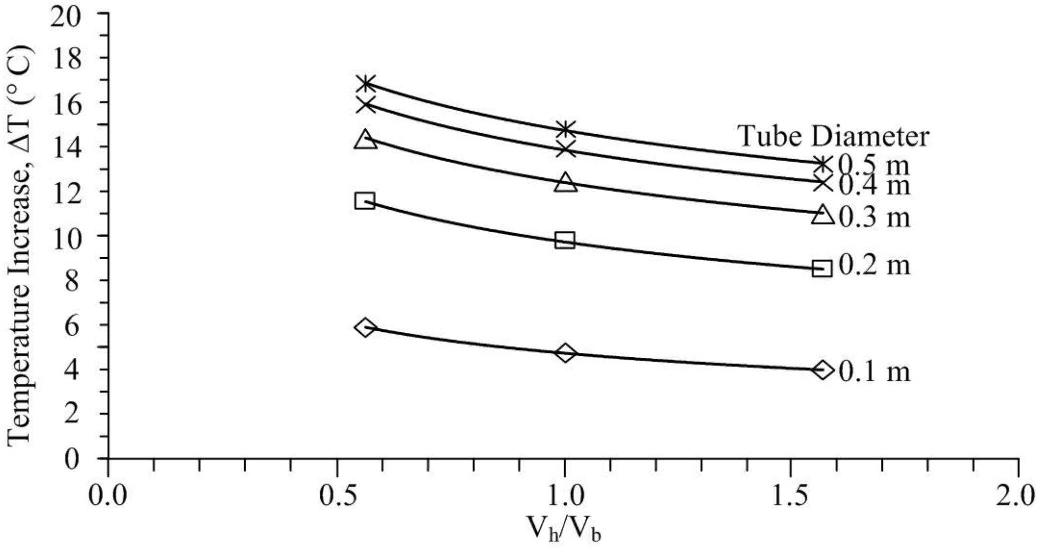

Figure 7.14 Relationship between the temperature increase in the housing model and the ratio of housing volume to rock fill volume with 9.00 m^2 collector area and the hot-air diameter of 0.1-0.5 m.

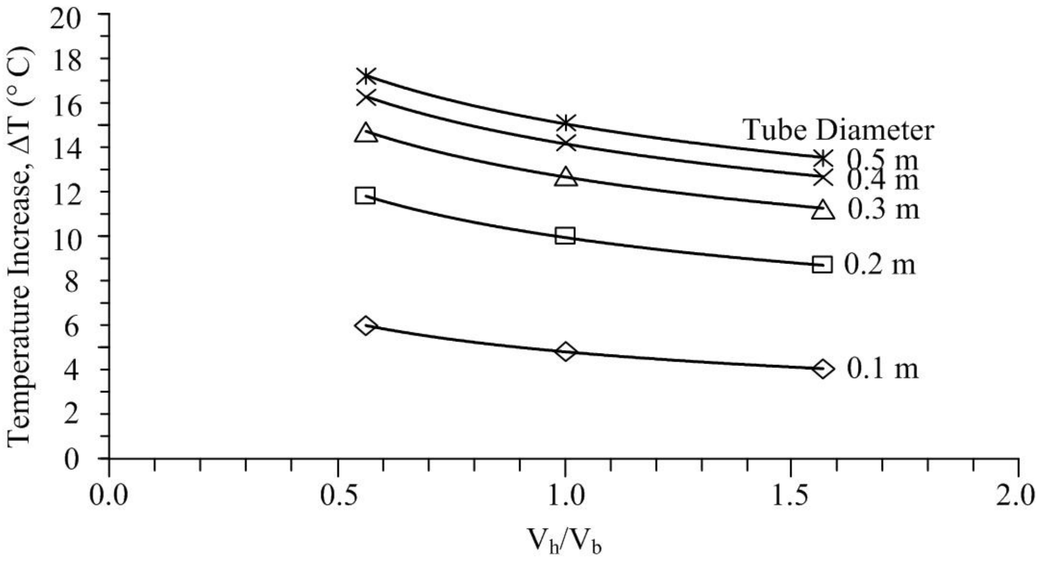

Figure 7.15 Relationship between the temperature increase in the housing model and the ratio of housing volume to rock fill volume with 12.25 m^2 collector area and the hot-air diameter of 0.1-0.5 m.

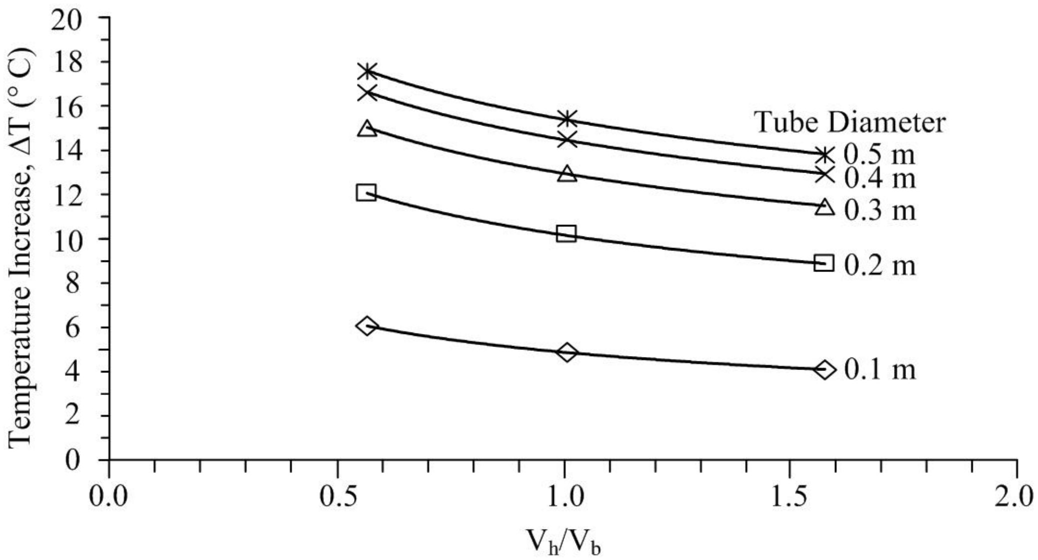

Figure 7.16 Relationship between the temperature increase in the housing model and the ratio of housing volume to rock fill volume with 16.00 m^2 collector area and the hot-air diameter of 0.1-0.5 m.

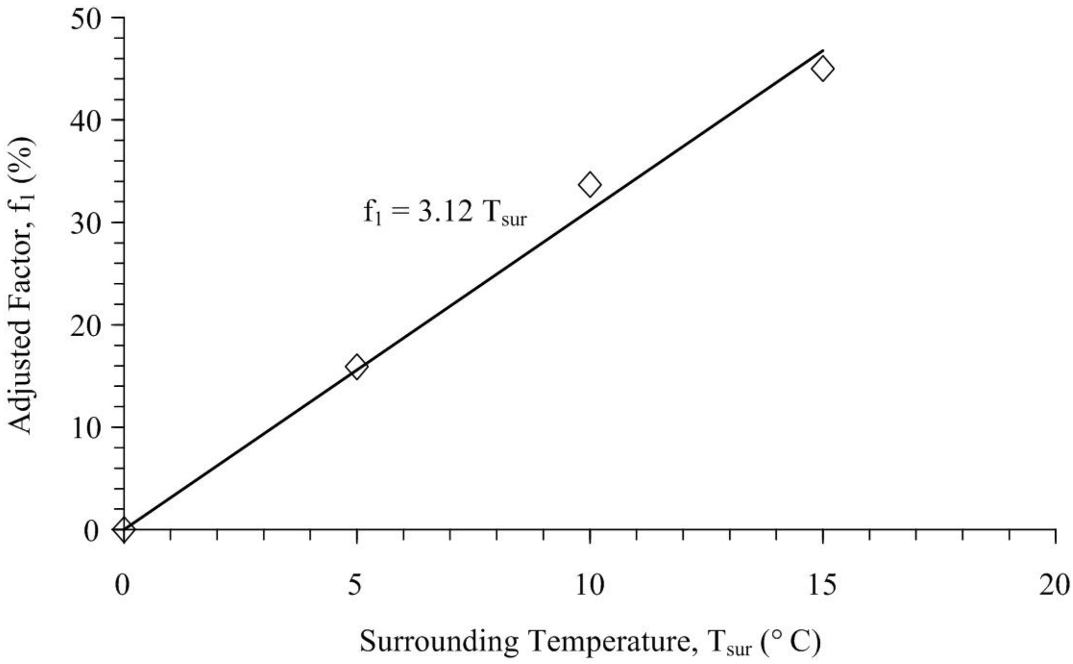

Figure 7.17 The adjusted factor (f_1) use to minimize the temperature increase in the housing model as an effect of the surrounding air temperature.

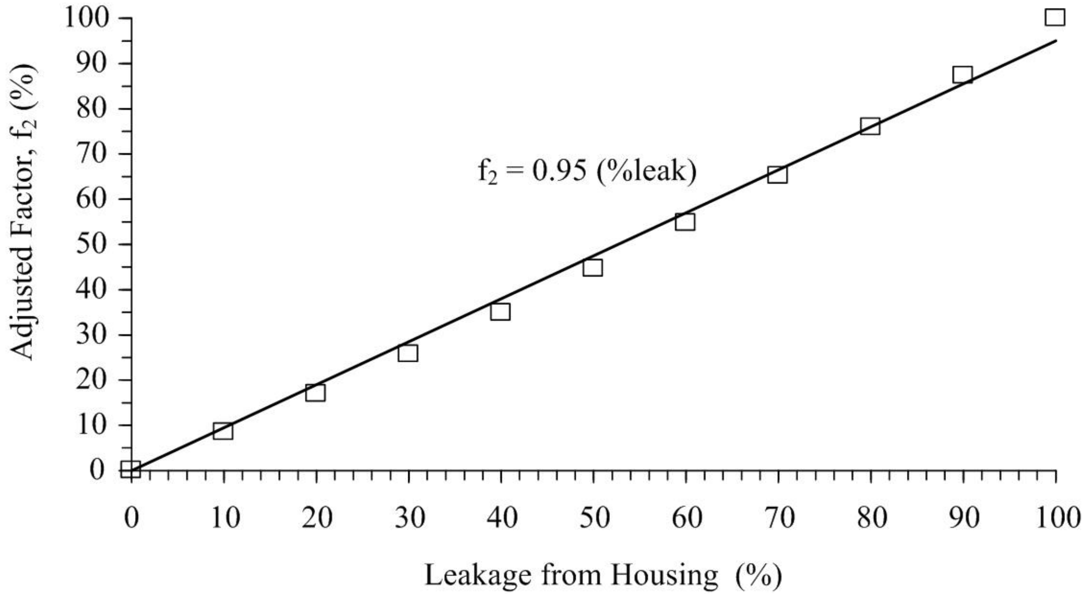

Figure 7.18 The adjusted factor (f_2) use to minimize the temperature increase in the housing as an effect of heat loss from the housing.

7.3 Storage system efficiency

An attempt is made here to assess the storage system efficiency and to determine the heat energy gained in the housing in form of the electrical energy. The housing model with 10.2 cm diameter hot-air tube is considered here as an example.

The amount of solar energy stored Q_r in the rock fill due to the direct gain of solar energy, with the mass flow rate of air being zero, is given by:

$$Q_r = m_r C_r \Delta T \tag{7.5}$$

where ΔT is the rock fragments temperature increase over a specified period of time; C_r is the specific heat of the rocks and m_r is the weight of the rock fragment which is given by:

$$m_r = V_{bed} (1 - \varepsilon) \rho_r \tag{7.6}$$

where V_{bed} is the bulk volume of rock or the packed rock volume; ε is the void fraction of rock fill (0.50) and ρ_r is the density of rocks (2,760 kg/m^3). The storage efficiency (η) of the rock fill is given by:

$$\eta = Q_r/I \tag{7.7}$$

where I is the amount of solar radiation received over a specified period of time.

From the observations in the scale-down model, the average temperature increase of rock fragments is about 5°C. From equations (7.4) and (7.5), the solar energy stored in the rock fill is estimated as 4.28 MJ (where m_r = 730 kg, C_r = 1,174 J/kg.K, and ΔT = 5 K). The amount of solar radiation received over a specified period of time (during 9.00 am – 3.00 pm for this study as shown in Figure 7.19) is estimated as 12.4 MJ. The efficiency of this storage system is about 35 percent.

The heat energy absorbed by the air in housing model can be calculated by using an equation (Sonntag al., 1998),

$$Q_a = \sum_{i=1}^{n} \left(m_a \cdot C_a \cdot \Delta T_i \cdot \Delta t_i \right) \tag{7.8}$$

where Q_a is the absorbed energy by air mass in housing model (J), m_a is the weight air mass (kg), C_a is the specific heat capacity of air (J/kg.K), ΔT_i is the temperature increase of the air mass (K), t_i is time interval of energy absorption (hour) and n is number of hours.

The measured results using the 10.2 cm diameter hot-air tube produces the temperature increase in the 3.38 m^3 housing model about 5°C (278.15 K) for a period of 10 hours (from 9.00 pm to 6.00 am). This has a ratio of housing volume to rock fill volume of 1:1. The temperature increase (ΔT) is used to calculate the equivalent electrical energy by using Equation (7.8). Here, the weight of air (m_a) is approximately 4 kg ($m = \rho \times V$; when $\rho = 1.186$ kg/m^3 and $V = 3.378$ m^3), the specific heat capacity of air is 1,015 J/kg.K (ranging from 1,012 J/kg.K through 1,017 J/kg.K), $\Delta T_i = 5$ K, and $\Delta t_i = 10$ hours. The gained heat energy in housing is equivalent to the electrical energy of 203.3 kJ·hr.

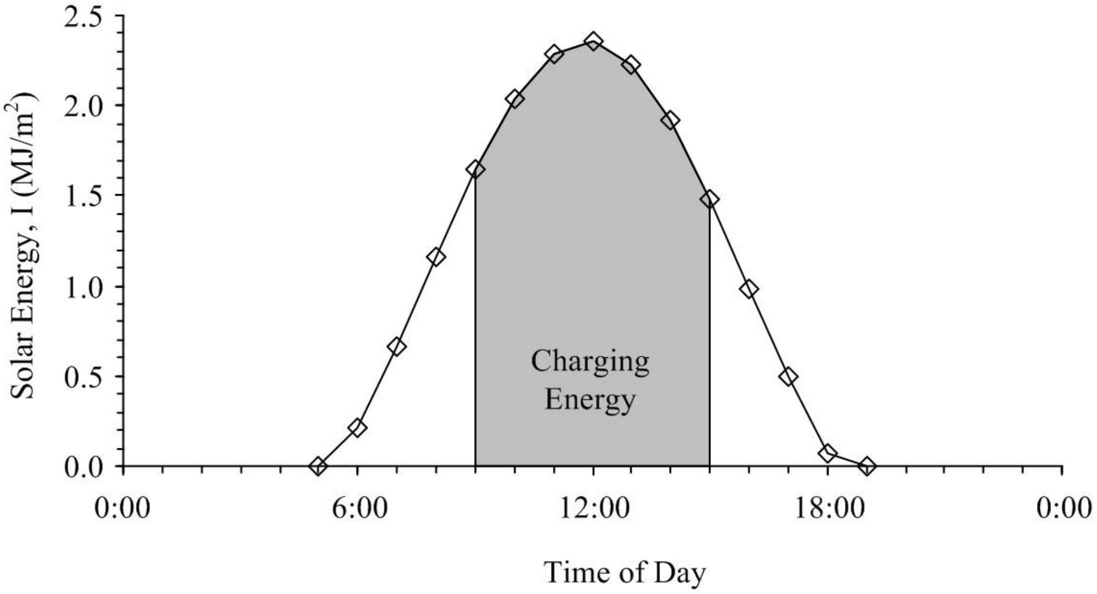

Figure 7.19 The amount of solar radiation received over a specified period of time. (9.00 am – 3 pm).

CHAPTER VIII

CONCLUSIONS AND RECOMMENDATIONS FOR FUTURE STUDIES

8.1 Conclusions

The objective of this research is to design the optimum thermal energy storage system by using rock fills for household space warming. This research determines experimentally the transient behavior of the thermal energy storage system using a scaled-down physical model. The heat transfer is analyzed by a simple model (mathematical equation) to describe the system performance and comparing the results with the experimental results. The relationships are developed between the increased temperatures in household space during nighttime (differences between the temperatures in the housing and surrounding), volume of household space, and size of rock fill. The system deals with storage of heat or solar thermal energy during sunny day and releasing it to warm up household space during nighttime when the weather cools down without using external electricity or fossil fuel.

The research has been carried out in eight states: 1) literature review, 2) sample collection and preparation, 3) laboratory testing, 4) developed the mathematical model, 5) constructed the pilot scale solar thermal energy storage system (physical model), 6) comparison between the calculated and measured results, 7) developed design guideline for storage system, and 8) thesis writing and presentation.

The results suggested that the locals in the north and northeast of Thailand suffer by the cold weather about four months (mid-October through mid-February). The lowest temperature is about 14 to 23 Celsius. The solar radiation in the winter is about 15 to 20 MJ/m^2.day which have a potential for solar thermal technology. The storage medium should have high thermal conductivity, density, and absorptivity (hence dark color).

The laboratory test results imply that the thermal conductivity and heat capacity of rock tend to be independent of their density because rocks contain various mineral compositions (each minerals show difference in thermal properties). From all rock types tested here, basalt which can be found in the northern and the northeastern parts of Thailand was primarily considered to be a storage medium because it has the highest of thermal conductivity and absorptivity.

A mathematical model based on the theory of thermodynamic and heat transfer is developed to predict the change of temperatures of rock, air in the storage system, and air in the housing model, as a function of time. Here, the numerical finite difference approximation is applied to model the systems, and the computer program with MATLAB 7.0 is used in the calculation. Three systems (controlled volume) considered include rock fragment in the storage pit, air in the storage pit, and air in the housing model. Daytime equivalent model, the storage medium (rock fragments) directly receives the solar thermal energy and stores that energy in their mass causing an increase in temperature. Air in the storage pit increase the temperature by receives the transferring energy from the heated rock fragments. Nighttime equivalent model, when the hot-air tube is opened, the hot air immediately flows through the tube to the housing model. The heat energy from hot air is transferred to cold air in housing causing an increase in temperature.

The pilot scale for solar thermal energy storage system (or physical model) are constructed to verify the efficiency of the designed solar thermal storage system and to determine its suitable design parameters. The pit is excavated with size approximately of 1.75×1.75×0.75 m (width×length×depth). Four chain-link baskets with a dimension of 0.5×0.5×0.5 m were placed in the pit. Each basket contained about 230 pieces of 10-20 cm fragments of basalt with the weight of 743 kg. The insulator sheets were applied around the pit walls and floor to prevent heat loss through the pit walls and floor. The transparent acrylic sheets reinforced by steel frames were placed on top of the storage pit. This allows the solar energy to directly transmit to the rocks and to prevent the heat loss under mode of the force convection by wind. Several thermocouples were installed to monitor the changes of rock temperature at the center of pit, air in the pit, air at the end of the tube in the hosing model, air in the housing model, and the surrounding air outside the housing.

The temperatures were measured from the 20th of November 2005 through the 20th of April 2006 and again from the 28th of November 2008 through the 28th March 2007. Several sizes and shapes of the hot-air tube: circular tubes with diameter of 5.1, 10.2, and 20.3 cm and a squared vent with a cross-section of 0.6×0.6 m were tried. The weight of the rocks in the pit has been changed twice; 370 and 743 kg. The measured results indicated that the storage system efficiency depends on the level of energy, size and inclination of hot-air tube, the heat loss in pit and in housing model. In comparison, it seems that the most suitable model was the system which the storage pit connected to housing model with over 10.2-cm (4 inches) diameter hot-air tube and inclined at an angle about 30 degrees. The top of storage pit should be covered with the isolator sheet (a textile, gunny-bags or fabric sheet). This system resulted in a temperature increase as high as 5^{o}C in the housing model.

The mathematical equations were used to improve the system efficiency by producing comparable temperatures in the housing and storage pit, during the heat transfer time from the storage pit. The behavior of the heat transfer system was simulated to compare with the actual temperature measured in the model. These results suggest that the calculated results agree with the measurement results which can be concluded that the mathematical equations were reliable and suitable for the temperature predictions under different parameters. The heat loss from housing model is calibrated as 10 percent of heat energy transferring from the storage pit.

The sensitivity analyses of variables are performed in order to investigate the effect of various parameters on the performance of storage system. The results suggest that the main variables that affected the efficiency of the rock fill system are the collector area, the hot-air tube size, the housing model volume, and the volume of rock fill. These variables are considered for the calculation on the design recommendations. The design guidelines of the rock-fill system have been developed under the assumption that no heat energy leaks from the housing model and the lowest surrounding air temperature at 6:00 pm is about 0°C. The variables include the volume of housing model, the packed rock volume, and the collector area, and the size of the hot-air tubes. The results indicate that the larger rock-fills volume and its collector area give the higher temperature increase due to the rock-fills could be store more heat energy. It is also discovered that the suitable thickness of rock fills is about 30-70 cm. These results provide a design recommendation which is presented in form of a graphic representation. The user can apply the required temperature increase (ΔT) in the housing on the charts prepared for 6.25 m^2, 9.00 m^2, 12.25 m^2, and 16 m^2 of collector area. The provided size of hot-air tube is then selected. The V_h/V_b ratio can be obtained.

The storage system efficiency and the heat energy gained in the housing in form of the electrical energy are determined. The housing model with 10.2 cm diameter hot-air tube is considered here as an example. The average temperature increase of rock fragments is about 5°C. The solar energy stored in the rock fill is estimated as 4.28 MJ. The amount of solar radiation received over a specified period of time is estimated as 12.4 MJ. The efficiency of this storage system is about 35 percent. The measured results using the 10.2 cm diameter hot-air tube produces the temperature increase in the 3.38 m^3 housing model about 5 K for a period of 10 hours (from 9.00 pm to 6.00 am). The gained heat energy in housing is equivalent to the electrical energy of 203.3 kJ·hr.

8.2 Recommendations for future studies

From the observations on the pilot scale solar thermal energy storage system it seems that the soil mass around the pit was not completely dry. The permeated water would be evaporated and suspended in the hot air mass and then transferred to the housing model. When the air in the housing cooled down in the morning, the vapor is condensed to be the drop of water on the ceiling. To solve this problem, the pit walls and floor should be covered with the impermeable material such as concrete, steel sheet, or rubber. This can increase the efficiency of rock fragments to store the heat energy due to the heat loss to soil mass was minimized.

The efficiency of the storage pit and the increasable of housing temperature can be improved by several ways such as installation of ventilator at the hot-air tube increases the mass flow rate from the storage and temperature in the housing model, installed double layers of acrylic sheet on the top of pit, cover the pit walls and floor with impermeable material with also can prevent the heat loss. Some housing with the wall made from bamboo should be covered with the isolator.

REFERENCES

Abbud, I. A., Löf, G. O. G., and Hittle, D. C. (1995). Simulation of solar air heating at constant temperature**. Solar Energy** 54 (2): 75-83.

Abu-Hamdeh, N. H. and Reeder, R. C. (2000). Soil thermal conductivity: Effects of density, moisture, salt concentration, and organic matter. **SOIL SCI. SOC. AM. J.** 64: 1285-1290.

Anderson, G. M. (2005). **Thermodynamics of natural systems**. New York: Cambridge University Press.

ASTM C351-92b, Standard test methods for mean specific heat of thermal insulation. In Annual Book of ASTM Standards, 04.08, American Society for Testing and Materials, Philadelphia.

ASTM D2487-00, Standard Classification of Soils for Engineering Purposes (Unified Soil Classification System). In Annual Book of ASTM Standards, 04.08, American Society for Testing and Materials, Philadelphia.

ASTM D4611-86, Standard test methods for specific heat of rock and soil. In Annual Book of ASTM Standards, 04.08, American Society for Testing and Materials, Philadelphia.

ASTM D5334-92, Standard test methods for determination of thermal conductivity of soil and soft rock by thermal needle probe procedure. In Annual Book of ASTM Standards, 04.08, American Society for Testing and Materials, Philadelphia.

Bansal, N. K., Mathur, R., and Bhandari, M. S. (1993). Solar chimney for enhanced stack ventilation. **Building and Environment** 28: 373–377.

Barr, S.M. and Macdonal, A.S. (1979). Paleomagnetism age and geochemistry of the Denchai basalts, Northern Thailand. **Earth Planet Science Letters** 46: 113-124.

Baum, F., Braun, E.V., Hahn, L., Hess, A., Koch, K.E., Kruse, G., Quarch, H. and Siebenhuner, M. (1970). On the geology of Northern Thailand. **Beihefte Geologische Jahrbuch** 102: 23 p.

Beck, A. E. (1988). Methods for determining thermal conductivity and thermal diffusivity. In Haenal, R., Rybach, L. and Stegena, L. (Eds.), **Handbook of Terrestrial Heat-Flow Density Determination**. Kluwer Academic Publishers, Dordrecht.

Bilskie, J. R. (1994). **Dual probe methods for determining soil thermal properties: Numerical and laboratory study.** Ph.D. Dissertation. Iowa State University.

Bristow, K. L. (2002). Thermal Conductivity. In J.H., Dane and G. C., Clarke (Co-eds.) **Methods of Soil Analysis** (pp.1209-1226). Soil Science Society of America, Madi.

Bunopas, S. (1981). **Paleogeographic history of Western Thailand adjacent parts of Southeast Asia-A plate tectonics interpretation**, Ph.D. thesis, Victoria University of Wellington, New Zealand., 810 p.

Campbell, G. S. and Norman, J. M. (1998). **An introduction to environmental biophysics** (2nd ed.). New York: Springer-Verlag.

Cengel, Y. A. (1997). **Introduction to thermodynamics and heat transfer**. New York: McGraw-Hill.

Cengel, Y. A. (2003). **Heat Transfer: A Practical Approach** (2nd ed.). Boston: McGraw-Hill.

Chapra, S. C. (2005). **Applied numerical methods with MATLAB for engineers and scientists**. Boston: McGraw-Hill.

Chapra, S. C. and Canale, R. P. (2002). **Numerical Methods for Engineers**. New York: McGraw-Hill.

Charters, W. W. S. and Pryor, T. (1982). **Theory and Design of Solar Thermal Systems**, Australian Syndicators Pty. Ltd., Melbourne, Australia.

Choudhury, C., Chauhan, P. M., and Garg, H. P. (1995). Economic design of a rock bed storage device for storing solar thermal energy. **Solar Energy** 55(1): 29-37.

Clapp, R. B., Hornberger, G. M. (1978). Empirical equations for some soil hydraulic properties. **Water Resources Research** 14(4): 601-604.

Clauser, C. and Huenges, E. (1995). Thermal conductivity of rocks and minerals. In T. J. Ahrens (ed.). **Rock physics & Phase relations: A handbook of Physical constants** (pp. 105-126). Washington, DC: American Geophysical Union.

Coutier, J. P. and Farber, E. A. (1982). Two applications of a numerical approach of heat transfer process within rock beds. **Solar Energy**. 29 (6): 451-462.

Crandall, D. M. and Thacher**,** E. F. (2004). Segmented thermal storage, **Solar Energy**, 77(4): 441.

Department Angewandte Geowissenschaften und Geophysik. (2006). Chapter 8: Thermal Properties of Rocks [On-line]. Available: http://www.unileoben.ac.at/~geophwww/neu/data/chapter8thermal.pdf

Department of Alternative Energy Development and Efficiency (DEDE) and Silpakorn University. (1999). **Solar energy map of Thailand**. ISBN 974-600-616-9. Bangkok: DEDE and Silpakorn University.

Department of Disaster Prevention and Mitigation of Thailand (2006). **Situation of disaster from cold climate during 2002 through 2006** (in Thai) (On-line). Available: http://www.disaster.go.th/disaster01/page/report00.htm

Department of Disaster Prevention and Mitigation. (2005) Summary of disaster situation in the winter season during 2000 through 2005 [On-line]. Available: http://www.disaster.go.th/ disaster01/ disas_05.xls.

Department of Mineral Resources. (1999). Geological Map of Thailand, Scale 1:250,000.

Department of Mineral Resources. (2003). Surveying and reserves estimation of mineral [in Thai]. Report No. STR 2/2003, Bangkok: Bureau of Mineral Resources.

Department of Mineral Resources. (2003). Surveying and reserves estimation of mineral [in Thai]. Report No. STR 2/2003, Bangkok: Bureau of Mineral Resources.

Department of Primary Industries and Mines of Thailand (2004) Strategy on primary industries and mines, Bangkok, 106 p (in Thai)

Departments of the Army and the Air Force, USA. (1988). **Arctic and subarctic construction calculation methods for determination of depths of freeze and thaw in soils**, Technical manual no. TM 5-852-6/AFR 88-19, volume 6, 12 pp.

DeVries, D. A. (1963). Thermal properties of soils. In W.R. van Wijk (ed.) **Physics of plant environment** (210-235). North-Holland Publishing Company: Amsterdam.

DeVries, D. A. and Peck, A. J. (1958). On the cylindrical probe method of measuring thermal conductivity with special reference to soils: II. Analysis of moisture effects. **Aust. J. Phys.** 11: 409-423.

Dincer, I. (1999). Evaluation and selection of energy storage systems for solar thermal applications. **International Journal of Energy Research** 23(12): 1017-1028.

Dost, S. (1996). Perspective on thermal energy storage systems for solar energy applications. **International Journal of Energy Research** 20(6): 547-557.

Duffie, J. A. and Beckman, W. A. (1991). **Solar Energy of Thermal Processe**s. New York: John Wiley and Sons.

El-Sayed, M. A. H. and Kreusel, J. (1995). Substitution potential of solar thermal power stations in electrical energy systems. **Renewable Energy** 6(7): 849-854.

Eshlemen, W. D., Baird, C. D., and Mears, D. R. (1997). A numerical simulation of heat transfer in rock beds, In **Proceedings on International Solar Energy Society**, Annual Meeting, June 6-10, 1977, Sections 14-25. (A78-11212 01-44) (pp 17-21 – 17-25). Orlando, Fla.

Exell, R. H. B. (1976). The solar radiation climate of Thailand. **Solar Energy** 8(4): 349-354.

Frazer, R. K. (1975). A general application heat transfer computer program, In **Summer Computer Simulation Conference**, July 21-23, 1975, Volume 1. (A76-42076 21-59) (pp 518-523). San Francisco, Calif.: AFIPS Press.

Fricker, H. W. (1991). High-temperature heat storage using natural rock. **Solar Energy Materials** 24(1-4): 249-254.

Garg, H.P., Sharma, V.K., Mahajan R.B., and Bhargave, A.K. (1985). Experimental study of an inexpensive solar collector cum storage system for agricultural uses. **Solar Energy** 35(4): 321-331.

German Geological Mission. (1972). Final report of the German Geological Mission to Thailand 1965-1971 (unpublished report). Bundesanstalt fur Bodenforschung, Hanover, 94 p.

Goswami, D. Y., Kreith, F., and Kreider, J. F. (2000). **Principals of Solar Engineering**. Philadelphia: Taylor and Francis.

Gul, I. H. and Maqsood, A. (2006). Thermophysical properties of diorites along with the prediction of thermal conductivity from porosity and density data. **International Journal of Thermophysics** 27 (2): 614-626.

Halman, J. P. (1990). **Heat transfer** (7th ed.). New York: McGraw-Hill.

Hamdan, M. A. (1998). Investigation of an inexpensive solar collector storage system. **Energy Conversion and Management** 39 (5-6): 415-420.

Hasnain**,** S. M. (1998). Review on sustainable thermal energy storage technologies, Part I: heat storage materials and techniques. **Energy Conversion and Management** 39 (11): 1127-1138.

Hollands, K. G. T. and Sullivan, H. F. (1984). Sullivan Pressure drops across rock bed thermal storage systems. **Solar Energy** 33(2): 221-225.

Hollands, K. G. T., Sullivan, H. F., and Shewen, E. C. (1984). Flow uniformity in rock beds. **Solar Energy** 32(3): 343-348.

Holman J. P. (2002). **Heat Transfer** (9th ed.). New York: McGraw-Hill.

Hudson, J. B. (1996). **Thermodynamics of materials: a classical and statistical synthesis**. New York: J. Wiley.

Hunsavek, R. (1983). **Petrochemical Features of granites associated with tin-tungsten mineralization at Mae Chedi, Wiang Pa Pao, Chiangrai** (unpublished). M.Sc. thesis, Department of Geology, Chulalongkorn University.

Intasopa, S.B. (1993). **Petrology and geochronology of the volcanic rocks of the Central Thailand volcanic belt** (unpublished). Ph.D. thesis, University of New Brunswick, Canada, 242 p.

Ishihara, S., Sawata, H., Shibata, K., Terashima, S., Arykul, S. and Sata K. (1980). Granites and South-West deposits of Peninsular Thailand. **Mining Geology, Special issue** 8: 223-241.

Janjai, S., Laksanaboonsong, J., Nunez, M., and Thongsathitya, A. (2005). Development of a method for generating operational solar radiation maps from satellite data for a tropical environment. **Solar Energy** 78(6): 739-751.

Jittawikul, A., Saito, I., and Ishihara, O. (2004). Climatic Maps for Passive Cooling Methods Utilization in Thailand. **Journal of Asian Architecture and Building Engineering** 3(1): 109-114.

Juluria, Y. (1998) Design and optimization of thermal systems. New York : McGraw-Hill, 626 p.

Juluria, Y. and Torrance, K. E. (1998) Computational heat transfer. New York: Taylor & Francis, 544 p.

Kamil, K. (1999). The viability of thermal energy storage. **Energy Sources** 21: 745-755.

Klompe, Th. H.F. (1962). Igneous and structure features of Thailand, **Monograph of American Geophysics Union** 6: 122-134.

Kotake, S. and Hijikata, K. (1993). **Numerical simulations of heat transfer and fluid flow on a personal computer**. Amsterdam: Elsevier.

Kurklu, A., Bilgin, S., and Ozkan, B. (2003). A study on the solar energy storing rock-bed to heat a polyethylene tunnel type greenhouse. **Renewable Energy** 28: 683-697.

Li, Z., Zhong, H., Tang, R., Liu, T., Gao, W., and Zhang, Y. (2006). Experimental investigation on solar drying of salted greengages. **Renewable Energy** 31: 837–847.

Macdonald, A.S. and Barr, S.M. (1978). Tectonic significance of Late Carboniferous volcanic arc in Northern Thailand. In **Proceedings of the Third Regional Conference on Geology and Mineral Resources of S.E. Asia** (pp 151-156). Bangkok, Thailand.

Mahawat, J. (1982). **The petrology and geochemistry of the granitic rocks of the Tak batholith, Thailand** (unpublished). Ph.D. thesis, Liverpool University, 210 p.

Mantajit, N. and Hinthong, C. (1999). Geological Map of Thailand (Scale 1:250,000). Department of Mineral Resources, Thailand.

Meier, A., Winkler, C., and Wuillemin, S. (1991). Experiment for modeling high temperature rock bed storage. **Solar Energy** 24: 255-264.

Miri, R. and Mraoui, S**.** (2007). Electrolyte process of hydrogen production by solar energy. **Desalination** 206(1-3): 69-77.

Mongelli, F., Zito, G., and Loddo, M. (1971). A Method for the Determination of the Thermal Properties of Soil Near the Surface. **Arch. Met. Geoph. Biokl., Ser. A.** 20: 35-42.

Nandwani, S. S. (2006). Uses of solar energy in Costa Rica. **Renewable Energy** 31: 689-701.

Ochsner, T. E., Horton, R., and Ren, T. (2001). A new perspective on soil thermal properties. **Soil Sci. Soc. Am. J.** 65:1641-1647.

Pitakpaivan, K. (1969). Tin bearing and tin barren granite in Thailand. In **Proceedings of the second Technical Conference on Tin, Inst. Tin Council** (p.283-298). Bangkok, Thailand.

Potisat, S. (1996). Geology and mineral resources in Thailand. In **Mining Asia Congress'96**, Singapore, March 20-22m, 18 p.

Puttapiban, P. (2002). Geology and Geochronology of the Igneous Rocks of Thailand. In **Symposium on Geology of Thailand**, Bankok, Thailand.

Ragone, D. V. (1995). **Thermodynamics of material**. New York : Wiley.

Riaz, M. (1978). Transient analysis of packed-bed thermal storage systems. **Solar Energy** 21(2): 123-128.

Robert, F. S. (1994). **Thermal analysis of materials**. New York: Marcel Dekker.

Robertson, E.C. (1988). **Thermal properties of rocks**, open file report 88-441, Reston, VA: U.S. Geol. Survey, 1988.

Rosen, M. A. and Dincer, I. (2003). Energy methods for assessing and comparing thermal storage systems. **International Journal of Energy Research** 27(4): 415-430.

Saiyudthong, C. and Guymer, I. (2005). Simulation of energy loss due to changes in pipe direction across a manhole, In Proceedings of The 10th National Convention on Civil Engineering (pp. Env 5 – Env 9), May 2-4, 2005. Pattaya, Thailand.

Salaron Corporation Solar Energy Systems. (1978). **Application engineering manual**. Solaron Corporation, 300 Galleria Tower, 720 South Colorado Blvd., Denver, Colorado, 80222.

Saricali, K. (1974). **Solar radiation in Thailand**. M.S. thesis, Asian Institute of Technology, Bangkok, Thailand.

Sass, J. H., Lachenbruch, A. H., Moses, T., Morgan, P. (1992). Heat flow from a scientific research well at Cajon Pass, California. **J. Geophys. Res.**, 97: 5017-5030.

Scharli, U. and Rybach, L. (2001). Determination of specific heat capacity on rock fragments. **Geothermics** 30(1): 93-110.

Seipold, U. (1998). Temperature dependence of thermal transport properties of crystalline rocks – a general law. **Tectonophysics** 291: 161-171.

Sharma, S. P., Saini, J. S., and Varma, H. K. (1991). Thermal performance of packed-bed solar air heaters. **Solar Energy** 47(2): 59-67.

Sharma, V. K., Rizzi, G., and Garg, H. P. (1991). Design and development of an augmented integrated solar collector with rock storage system for heating applications. **Energy Conversion and Management** 31(4): 369-377.

Somerton, W. H. (1992). **Thermal properties and temperature related behavior of rock/fluid systems**. Amsterdam: Elsevier.

Sonntage, R.E., Borgnakke, C., and VanWylen, G.J. (1998) **Fundamentals of Thermodynamics** (5th ed.). John Wiley & Son, New York, 783 p.

Sontag, E. D. (1998). **Mathematical control theory: deterministic finite dimensional systems** (2nd ed.). New York: Springer.

Suansilpong, S. and Putthapiban, P. (1978). Some aspects of tin granite and its relatiohship to tectonic setting, Geological paper presented in the Second Meeting on Tin, Manaus, Brazil.

Suryanarayana, N. V. and Arici, O. (2004). **Design and simulation of thermal system**. Boston: McGraw-Hill.

Swartman, R. K. and Ogunlade, O. (1966). An investigation on packed-bed collectors. **Solar Energy** 10(3): 106-110.

Teggin, D.E. (1975). **The granites of Northern Thailand** (unpublished). Ph.D. thesis, University of Manchester, U.K.

Thai Meteorological Department (2002). **Climate of Thailand** [Online]. Available: http://www.tmd.go.th/

Thai Meteorological Department (2003). **Climate Information Service**, CD.

Thanasuthipitak, T. (1978). Geology of Uttaradit area and its implications on tectonic history of Thailand. In P. Nutalaya (ed.). **Proceedings of the Third Regional Conference on Geology and Mineral Resources of Southeast Asia** (pp 87-197). Bangkok, Thailand.

The Schumacher Center for Technology & Development. (n.d.). Technical brief: Solar thermal energy. Hourton Hall, Bourton-on-Dunsmore, Rugby, Warwickshire CV23 9QZ, UK.

Vichit, P., Vudthichatvanich, S. and Hansawek, P. (1978). The distribution and some characteristics of corundium-bearing basalt in Thailand. **Journal of Geological Society of Thailand** 3: 1-8.

Vosteen, H-D. and Schellschmidt, R. (2003). Influence of temperature on thermal conductivity, thermal capacity and thermal diffusivity for different types of rock. **Physicals and Chemistry of the Earth** 28:499-509.

Waples, A. W. and Waples, J. S. (2004). A review and evaluation of specific heat capacities of rock, minerals, and subsurface fluids, Part 1: Minerals and nonporous rocks. **Natural Resources Research** 13(2): 97-122.

Zoth, G. and Hänel, R. (1988). Appendix, in Handbook of Terrestrial Heat Flow Density Determination, edited by Hänel, R, Rybah, L., and Stegena, L., Kluwer, Dordrecht, pp. 449-466.

APPENDIX A

MEASURED RESULTS FROM PILOT SCALE MODEL

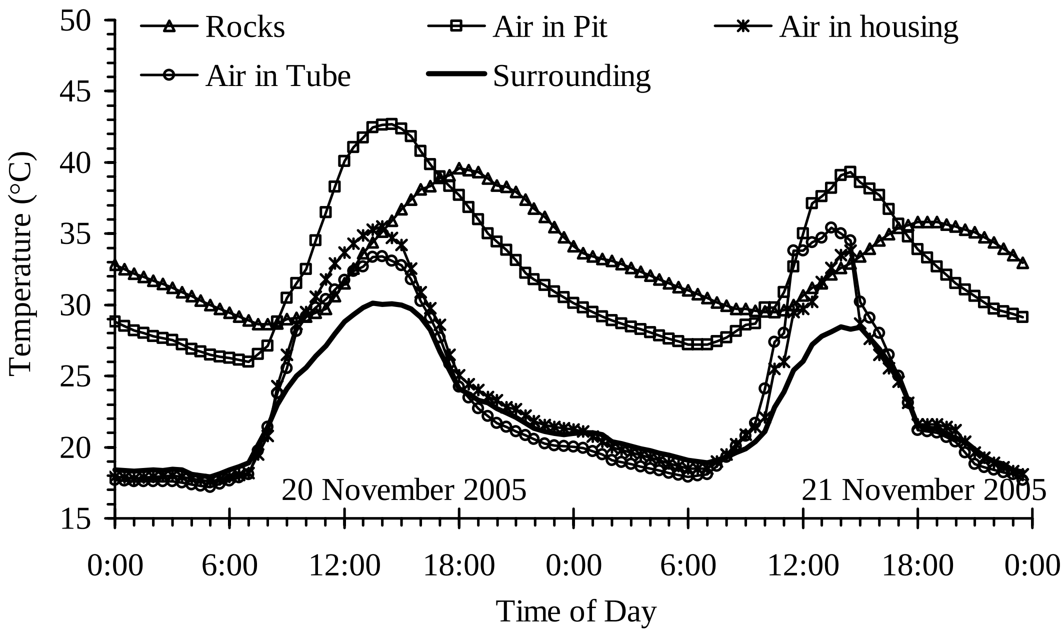

Figure A.1 Temperature as a function of time at November 20-21, 2005 measured from the system using 5.1-cm diameter hot-air tube.

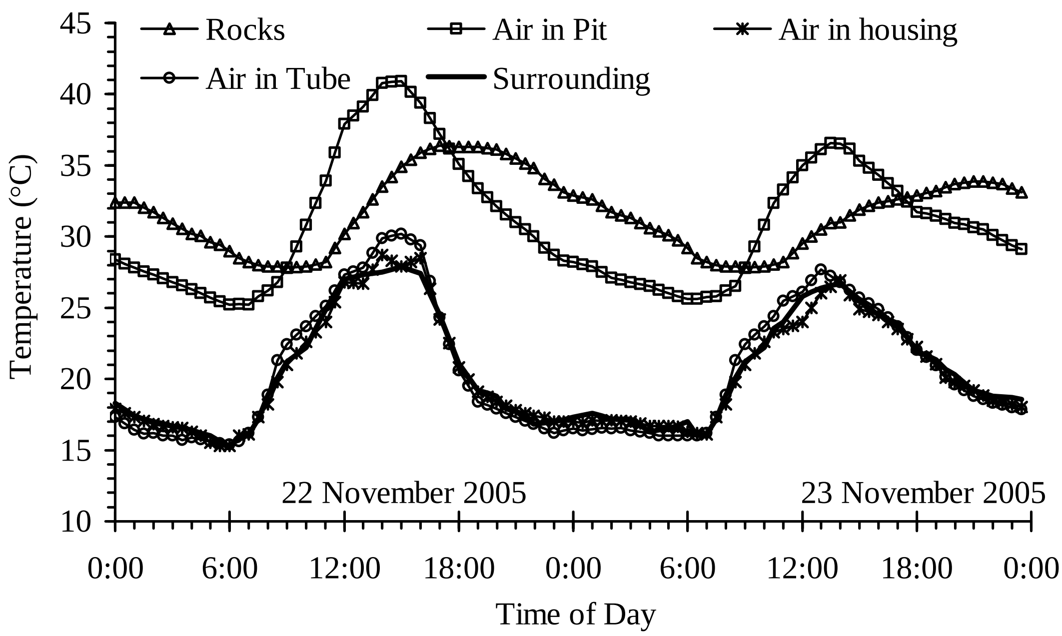

Figure A.2 Temperature as a function of time at November 22-23, 2005 measured from the system using 5.1-cm diameter hot-air tube.

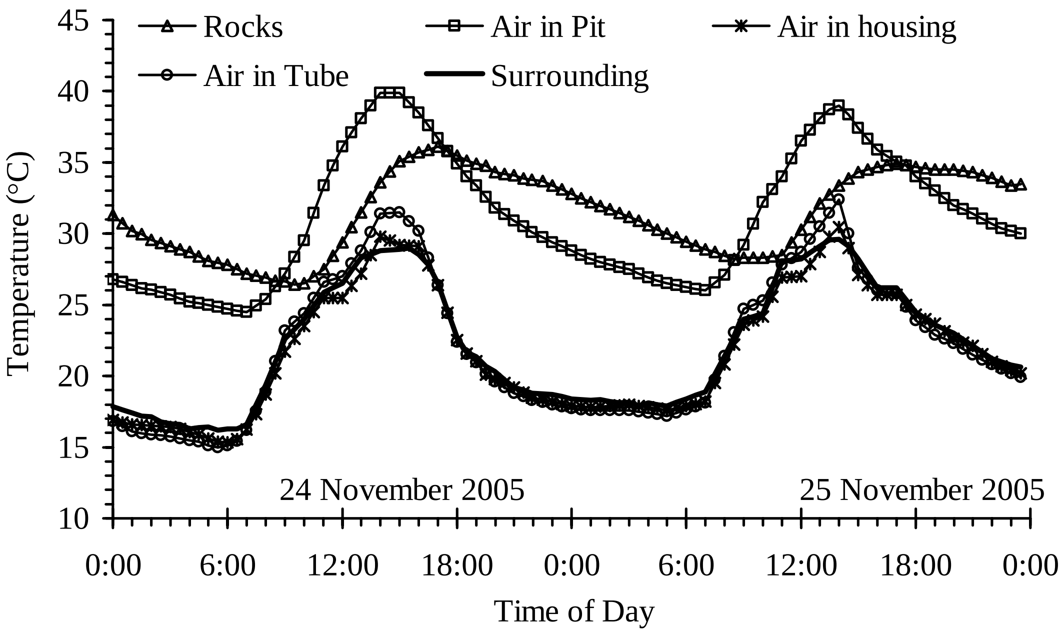

Figure A.3 Temperature as a function of time at November 24-25, 2005 measured from the system using 5.1-cm diameter hot-air tube.

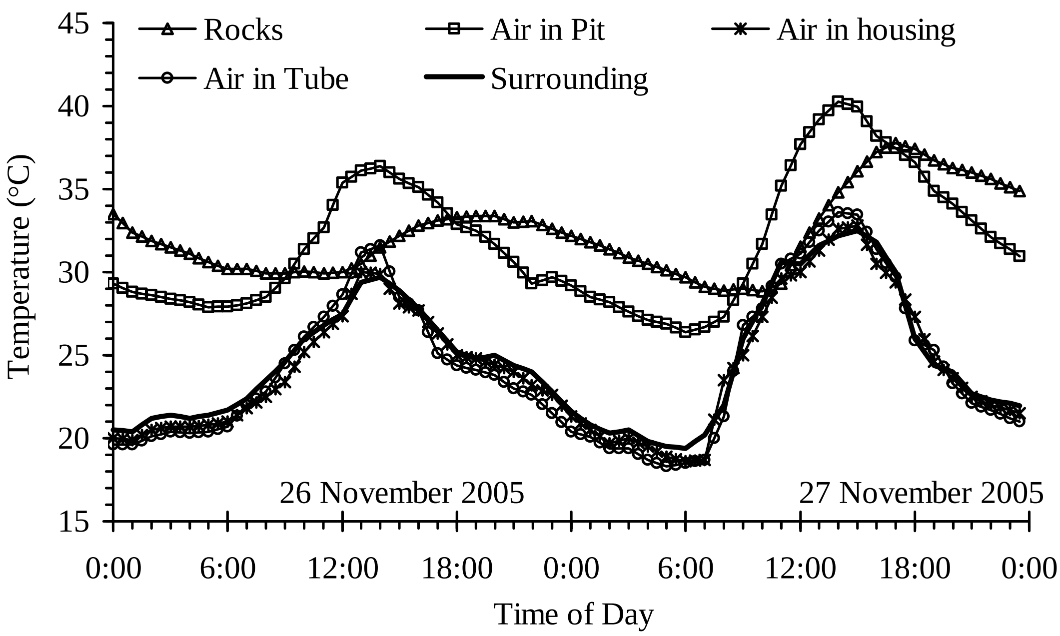

Figure A.4 Temperature as a function of time at November 24-25, 2005 measured from the system using 5.1-cm diameter hot-air tube.

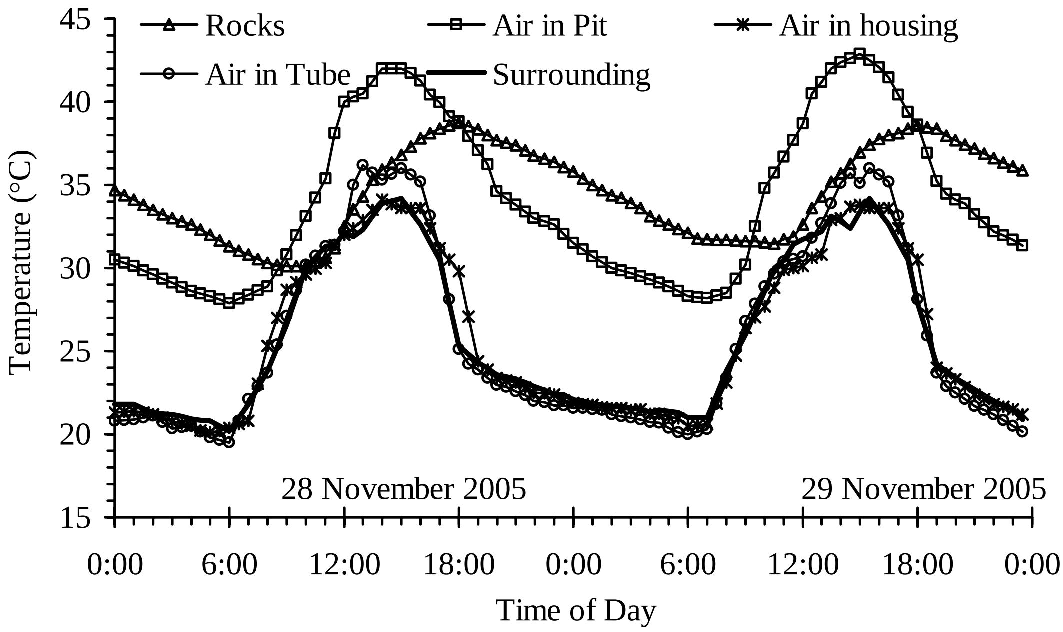

Figure A.5 Temperature as a function of time at November 28-29, 2005 measured from the system using 5.1-cm diameter hot-air tube.

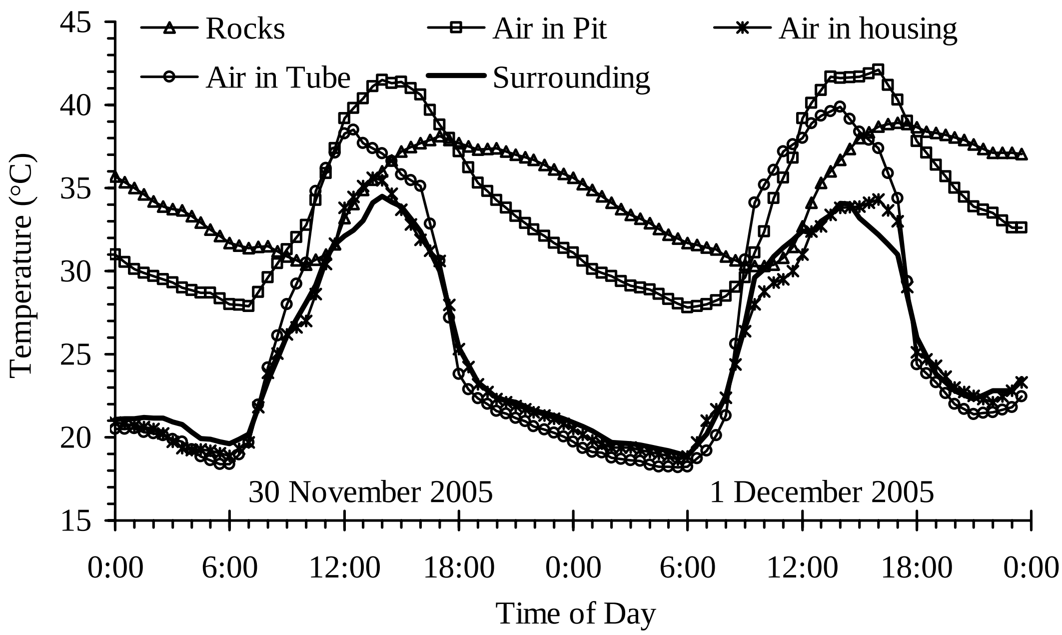

Figure A.6 Temperature as a function of time at November 30 – December 1, 2005 measured from the system using 5.1-cm diameter hot-air tube.

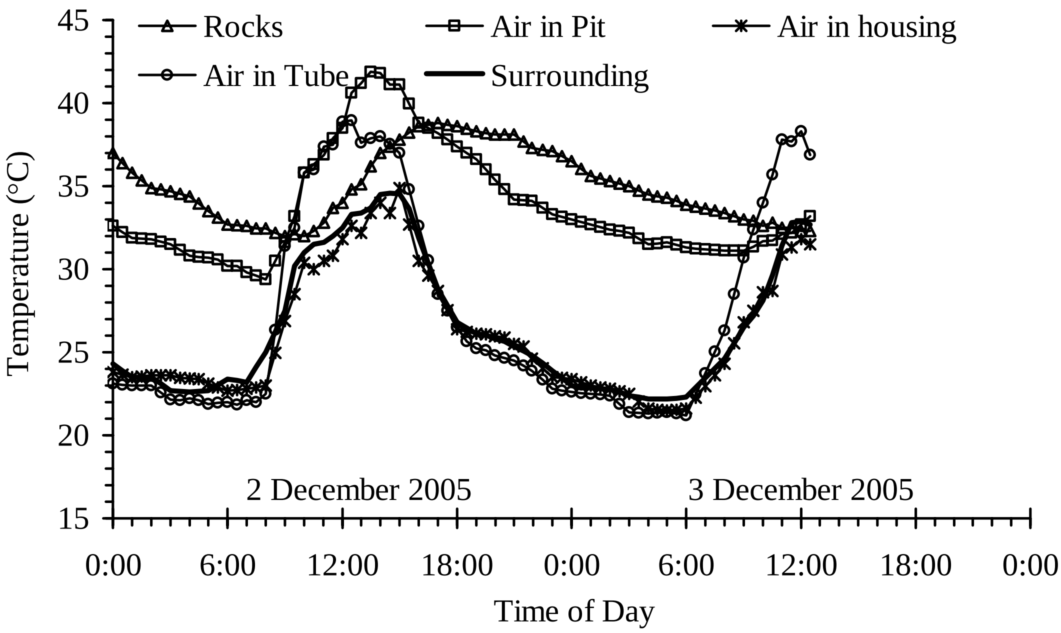

Figure A.7 Temperature as a function of time at December 2-3, 2005 measured from the system using 5.1-cm diameter hot-air tube.

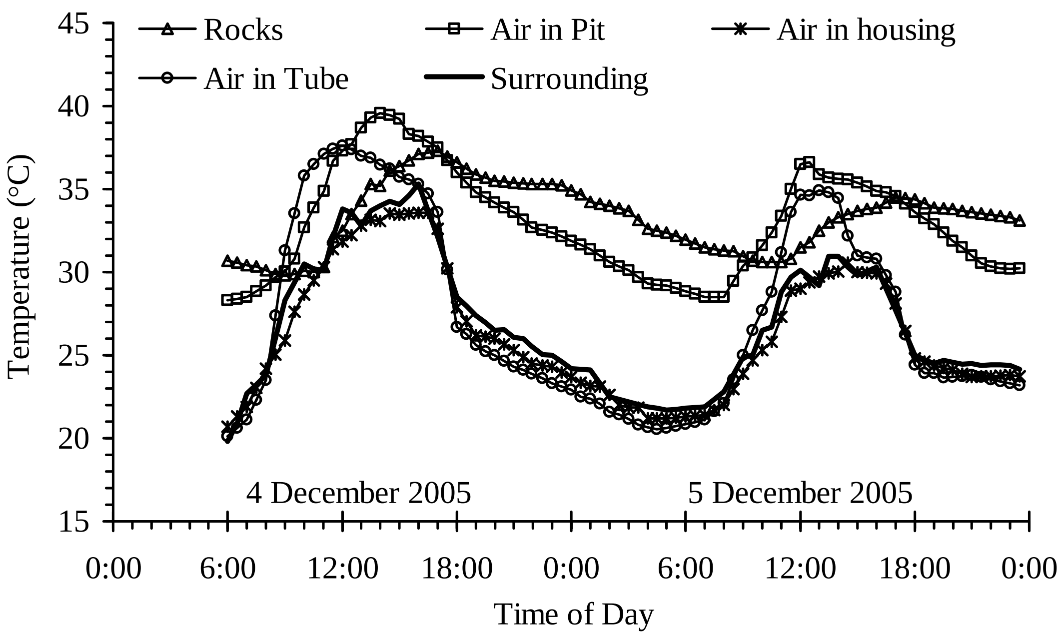

Figure A.8 Temperature as a function of time at December 4-5, 2005 measured from the system using 5.1-cm diameter hot-air tube.

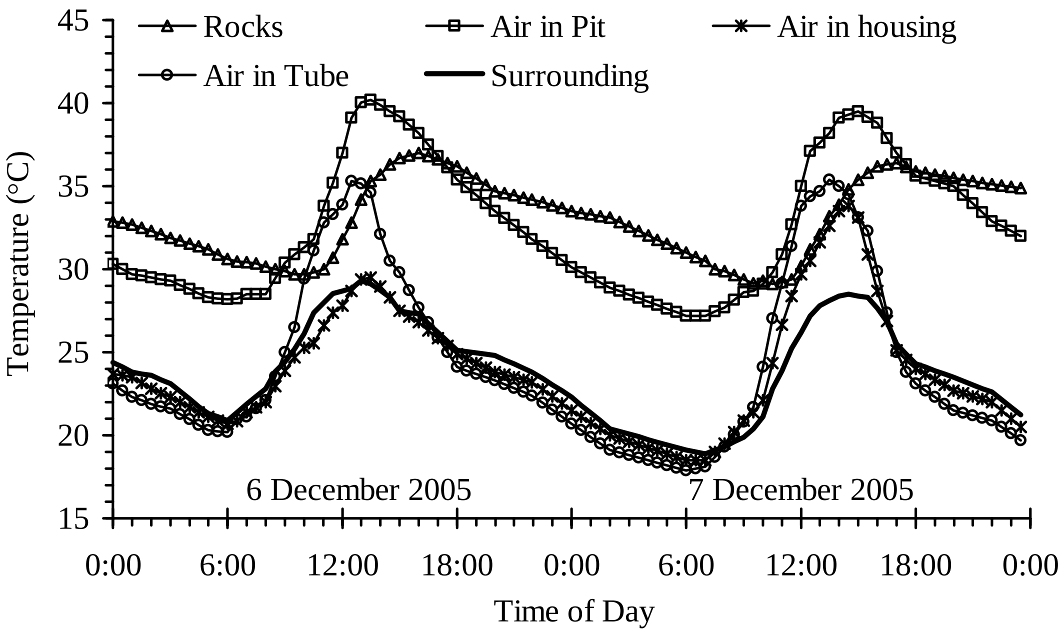

Figure A.9 Temperature as a function of time at December 6-7, 2005 measured from the system using 5.1-cm diameter hot-air tube.

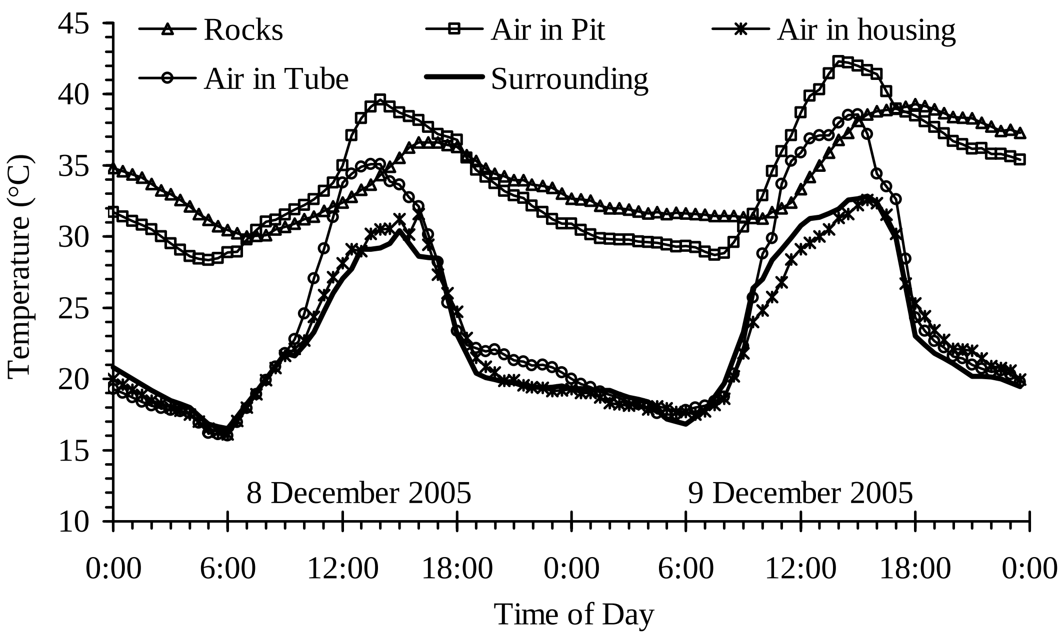

Figure A.10 Temperature as a function of time at December 8-9, 2005 measured from the system using 5.1-cm diameter hot-air tube.

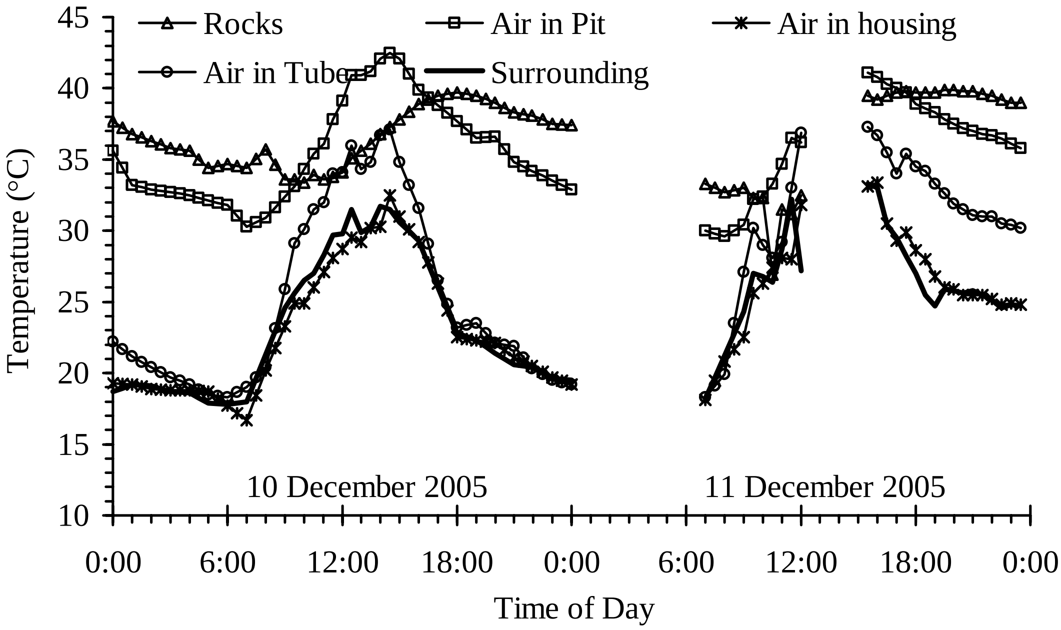

Figure A.11 Temperature as a function of time at December 10-11, 2005 measured from the system using 5.1-cm diameter hot-air tube.

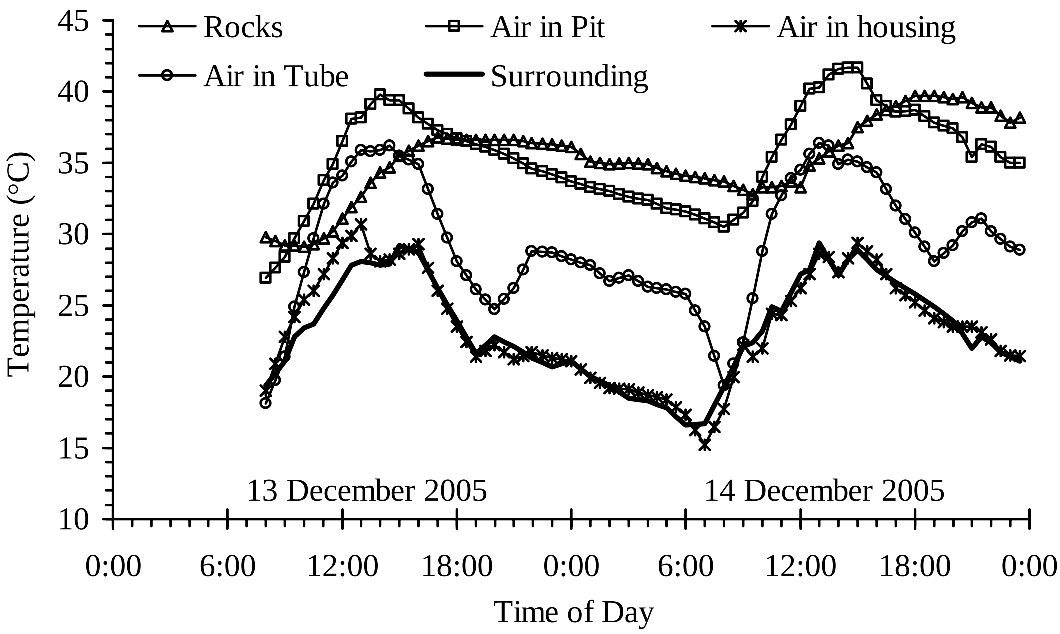

Figure A.12 Temperature as a function of time at December 13-14, 2005 measured from the system using 5.1-cm diameter hot-air tube.

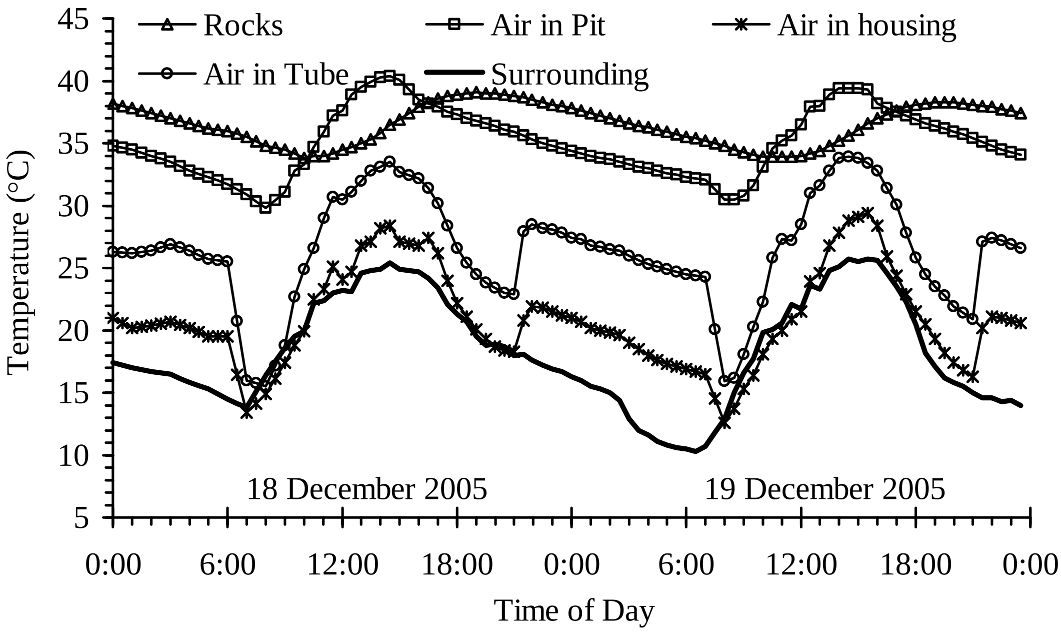

Figure A.13 Temperature as a function of time at December 18-19, 2005 measured from the system using 10.2-cm diameter hot-air tube.

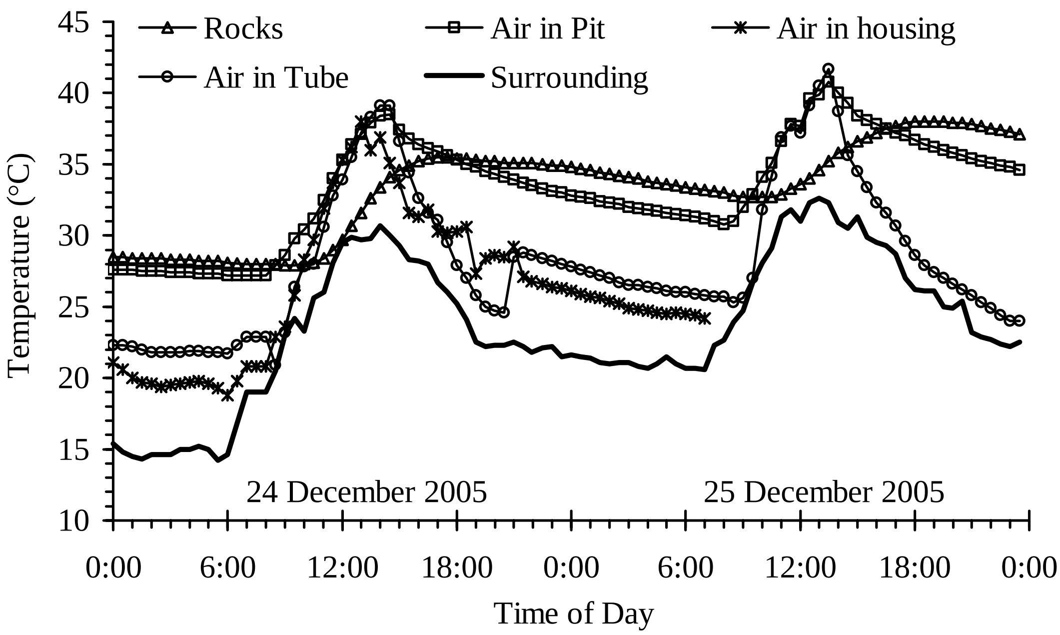

Figure A.14 Temperature as a function of time at December 24-25, 2005 measured from the system using 10.2-cm diameter hot-air tube.

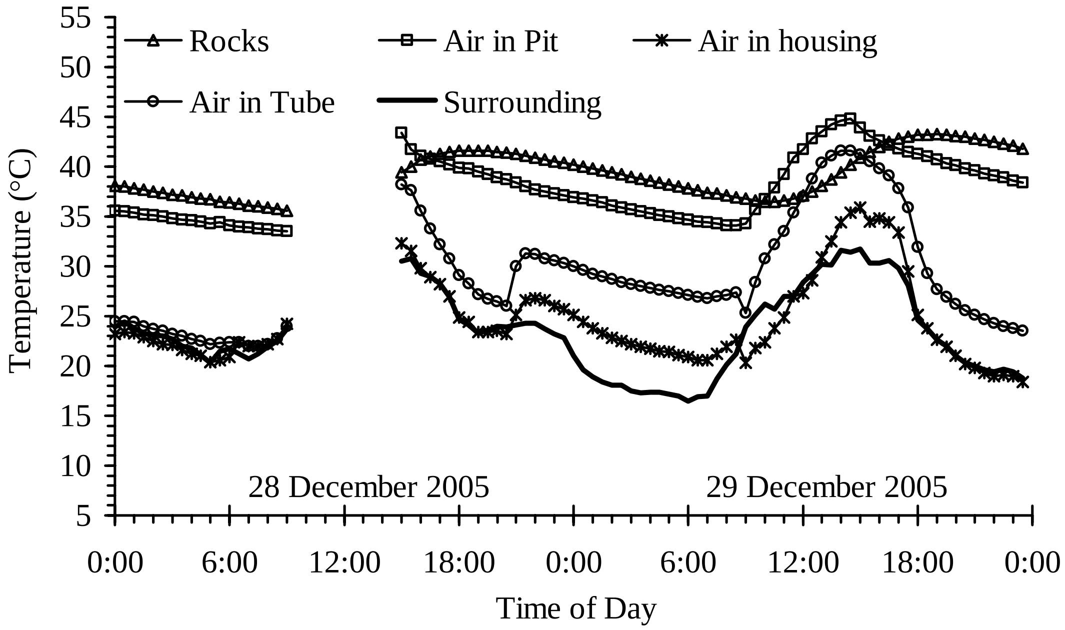

Figure A.15 Temperature as a function of time at December 28-29, 2005 measured from the system using 10.2-cm diameter hot-air tube.

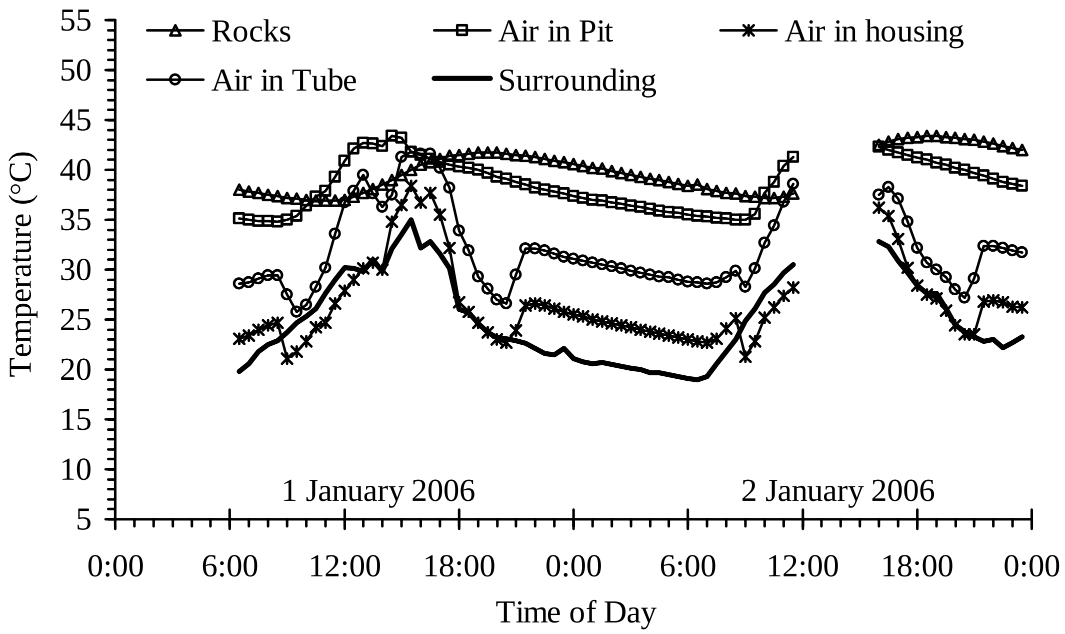

Figure A.16 Temperature as a function of time at January 1-2, 2006 measured from the system using 10.2-cm diameter hot-air tube.

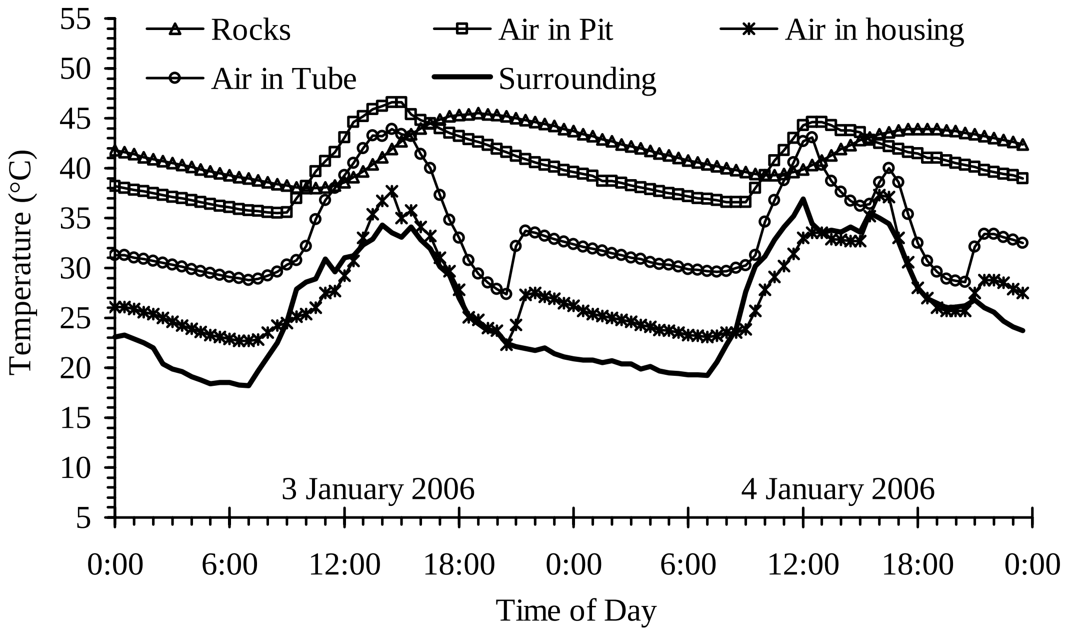

Figure A.17 Temperature as a function of time at January 3-4, 2006 measured from the system using 10.2-cm diameter hot-air tube.

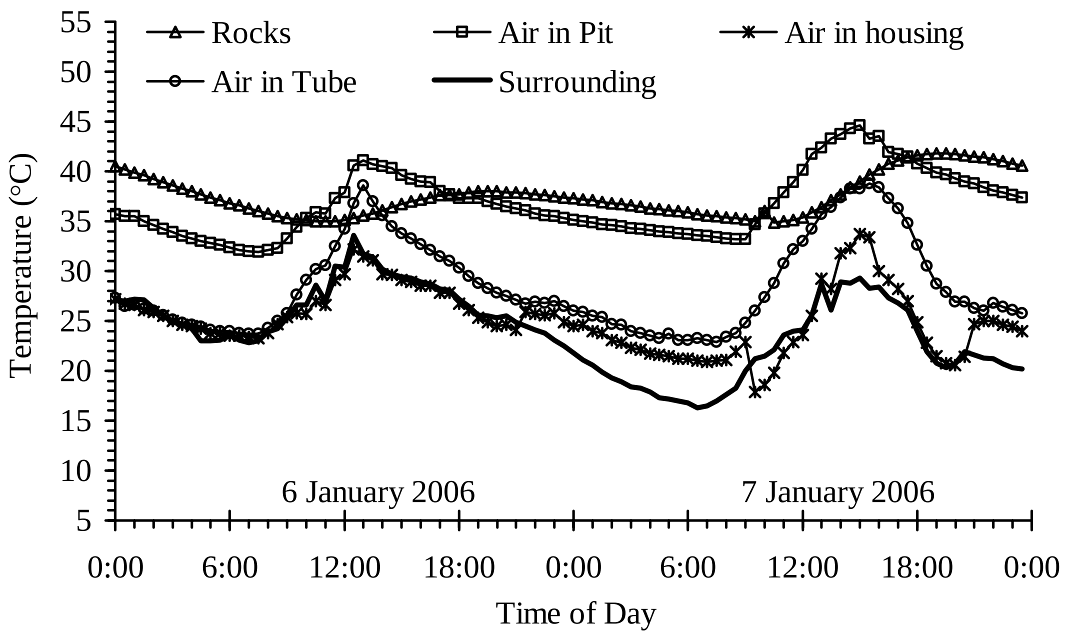

Figure A.18 Temperature as a function of time at January 6-7, 2006 measured from the system using 20.3-cm diameter hot-air tube.

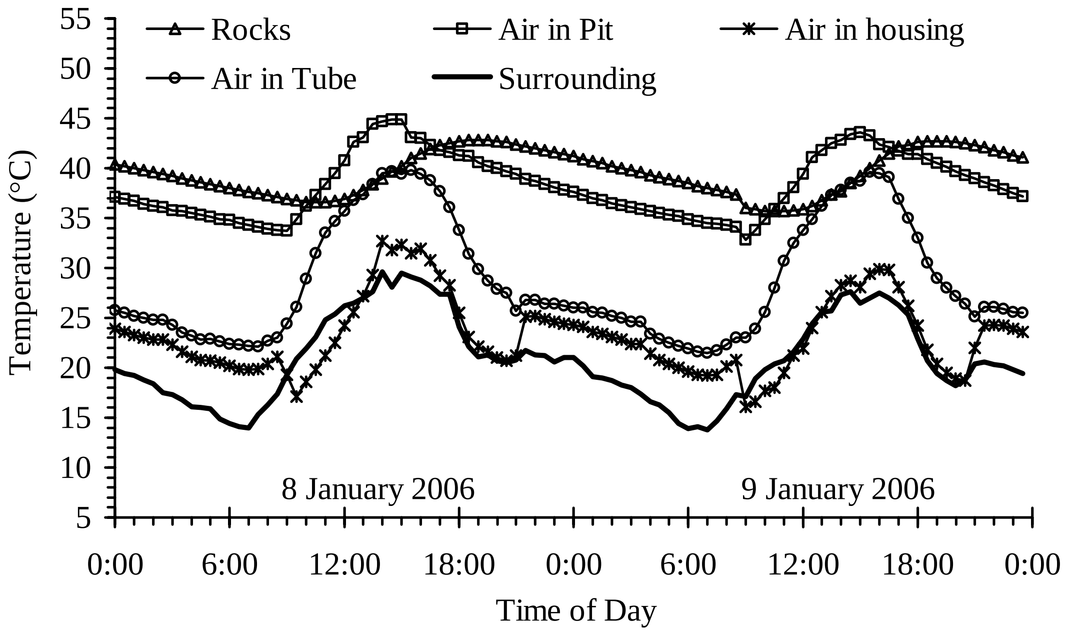

Figure A.19 Temperature as a function of time at January 8-9, 2006 measured from the system using 20.3-cm diameter hot-air tube.

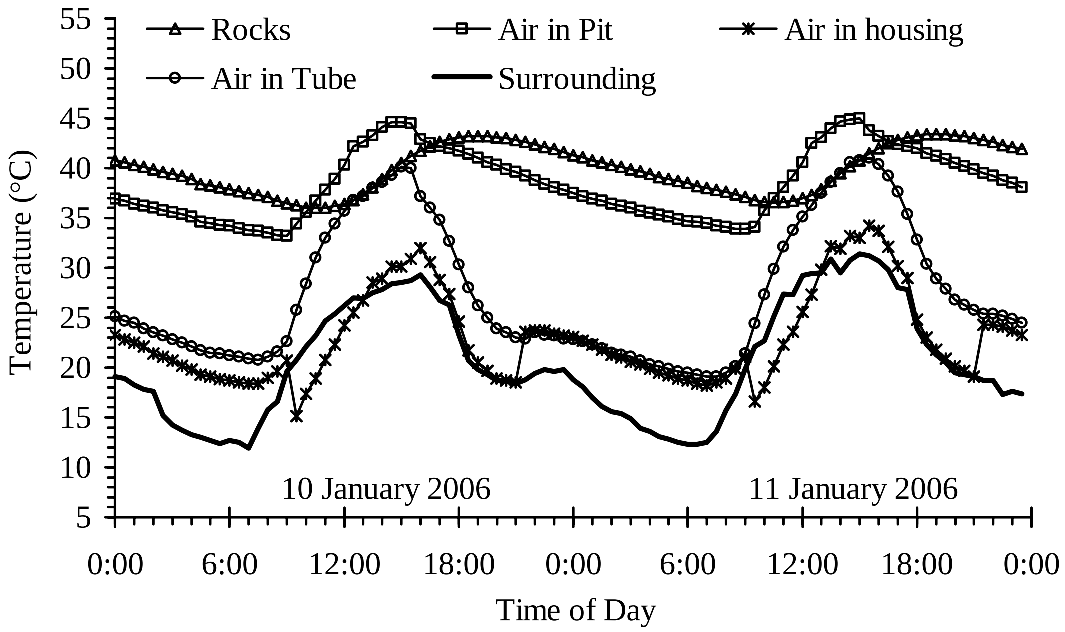

Figure A.20 Temperature as a function of time at January 10-11, 2006 measured from the system using 20.3-cm diameter hot-air tube.

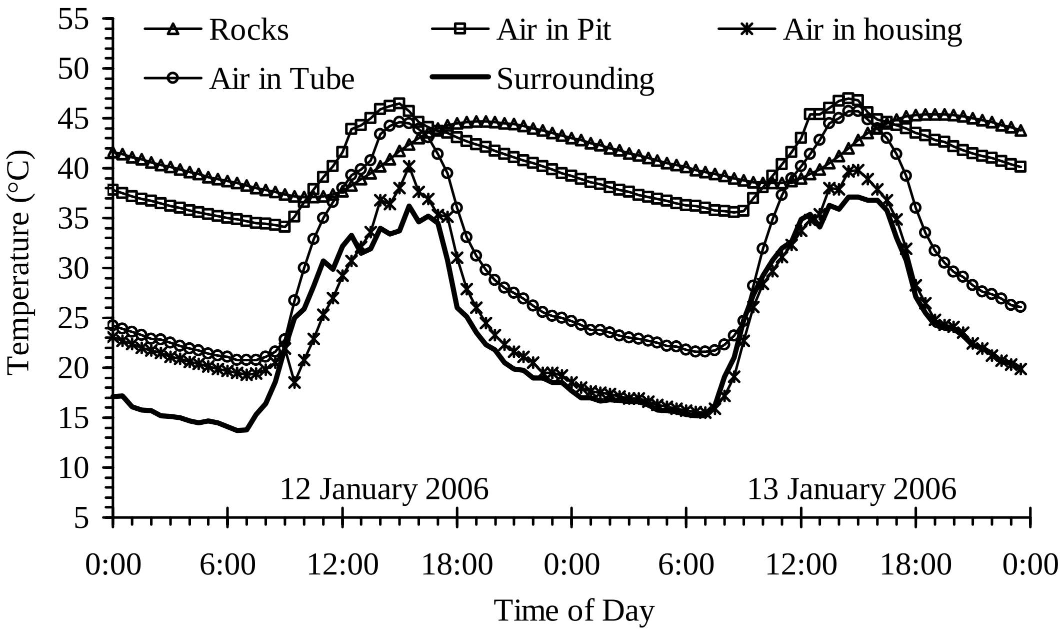

Figure A.21 Temperature as a function of time at January 12-13, 2006 measured from the system using 20.3-cm diameter hot-air tube.

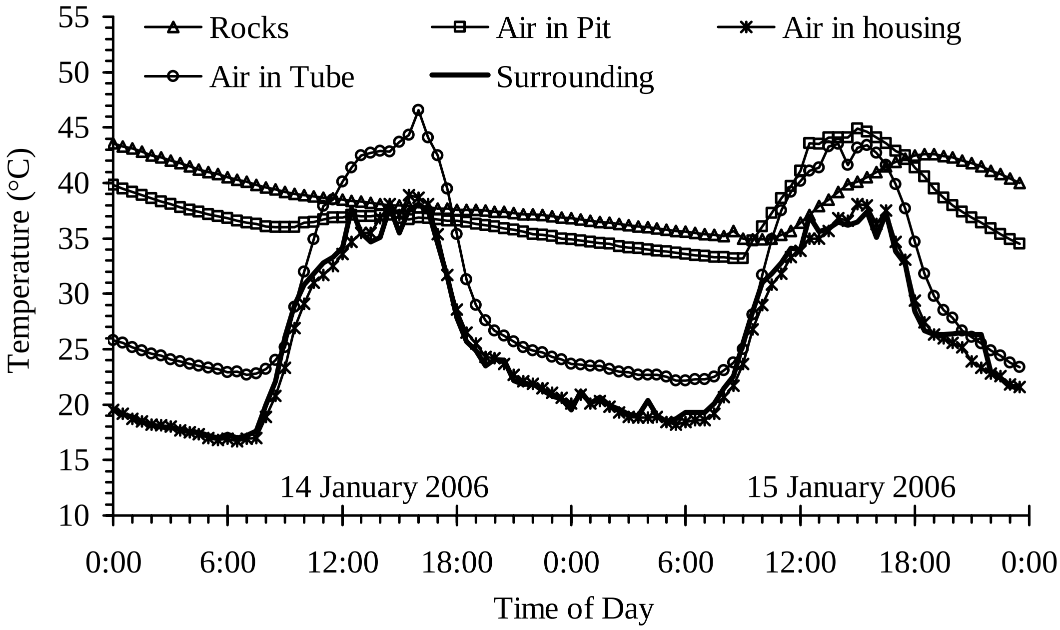

Figure A.22 Temperature as a function of time at January 14-15, 2006 measured from the system using 20.3-cm diameter hot-air tube.

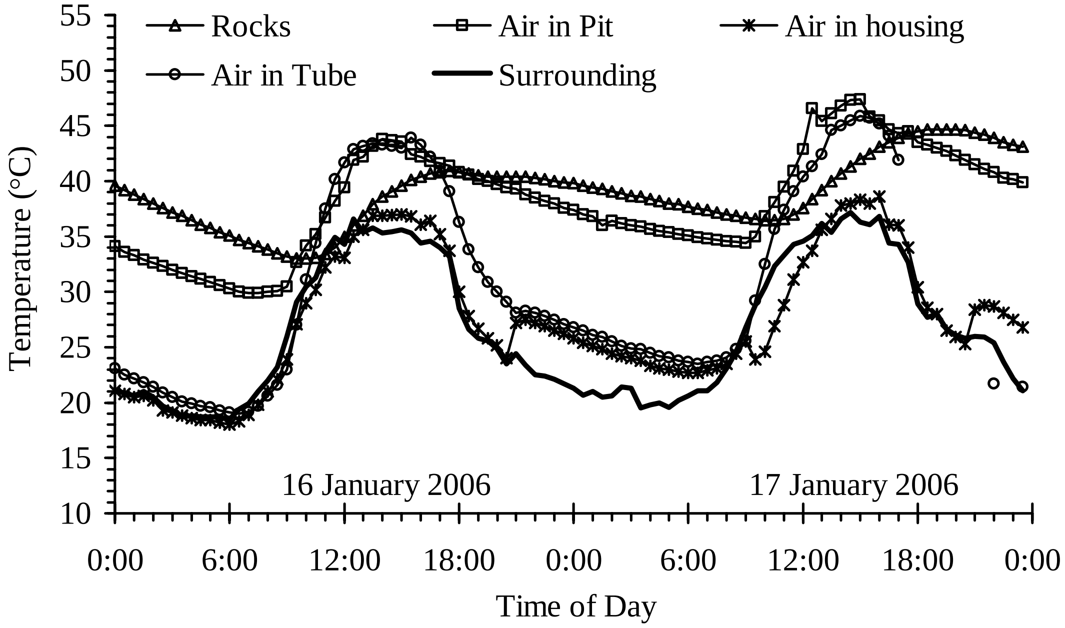

Figure A.23 Temperature as a function of time at January 16-17, 2006 measured from the system using 20.3-cm diameter hot-air tube.

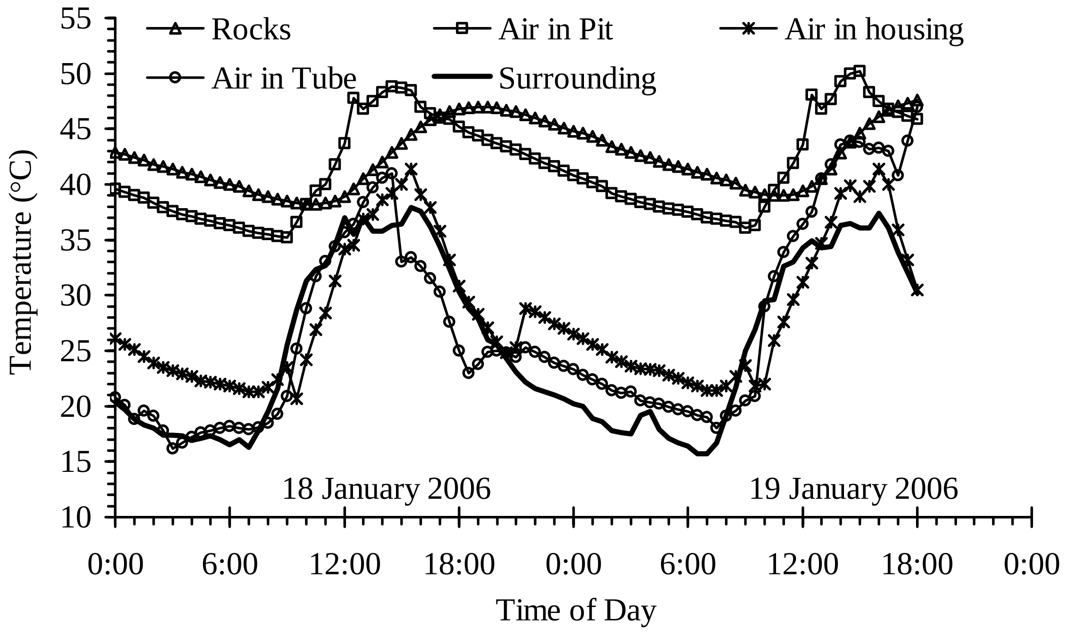

Figure A.24 Temperature as a function of time at January 18-19, 2006 measured from the system using 20.3-cm diameter hot-air tube.

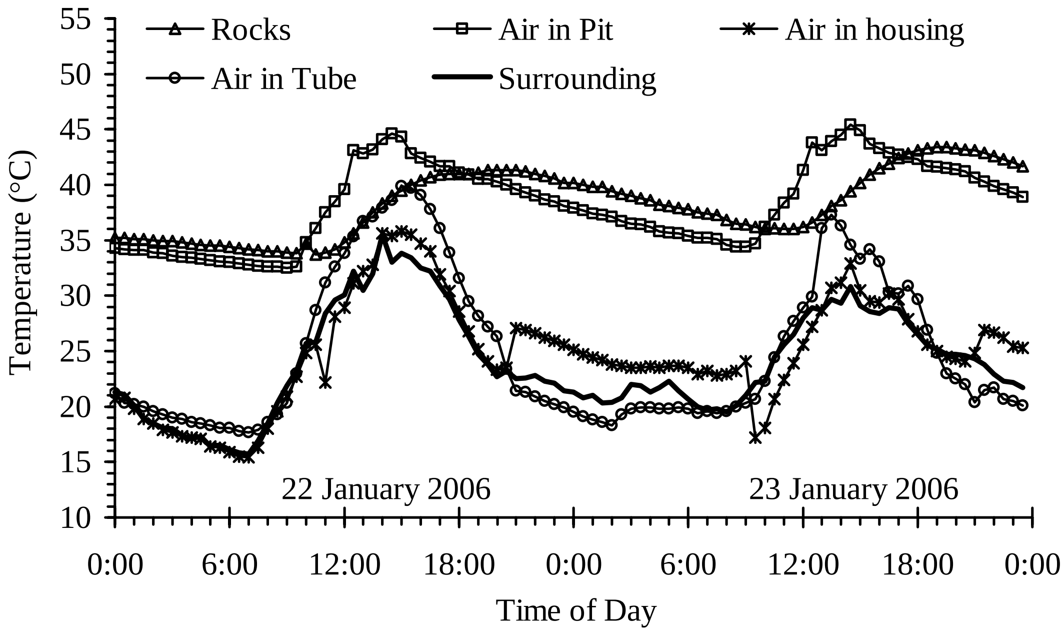

Figure A.25 Temperature as a function of time at January 22-23, 2006 measured from the system using 20.3-cm diameter hot-air tube.

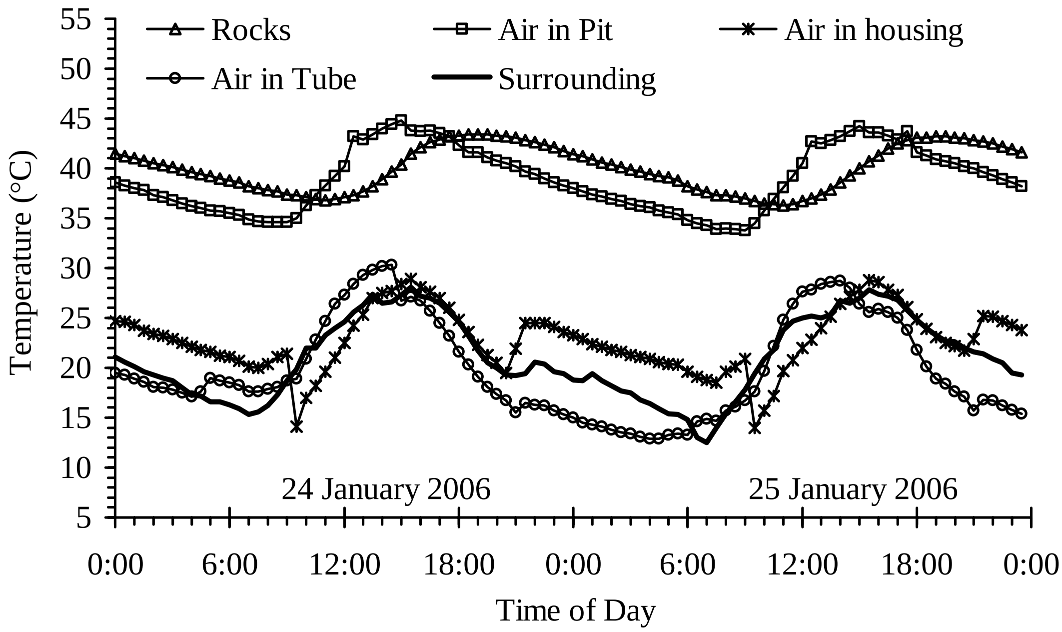

Figure A.26 Temperature as a function of time at January 24-25, 2006 measured from the system using 20.3-cm diameter hot-air tube.

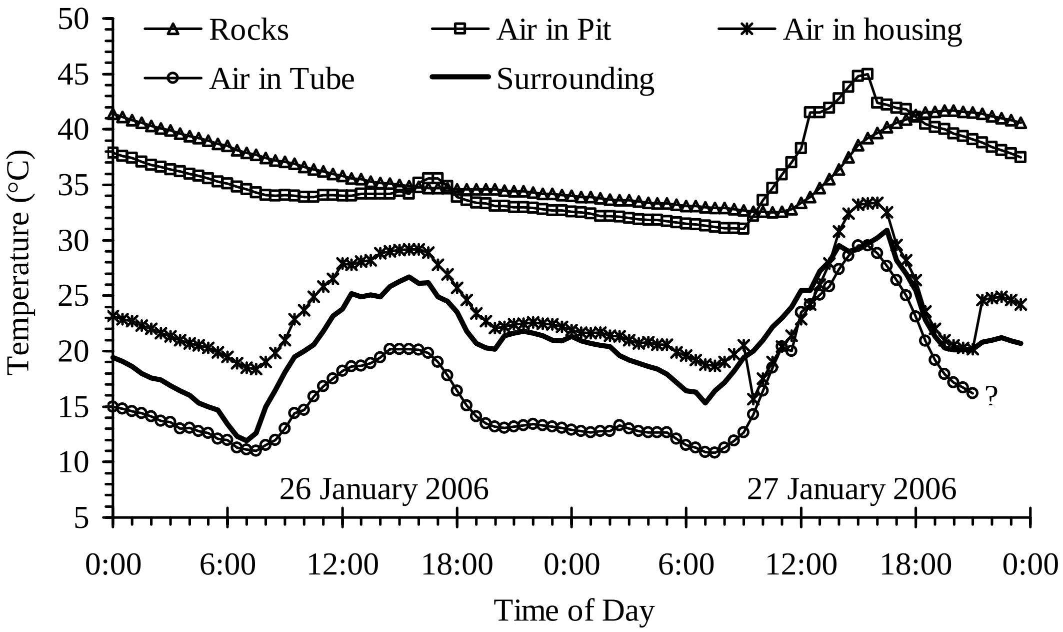

Figure A.27 Temperature as a function of time at January 26-27, 2006 measured from the system using 20.3-cm diameter hot-air tube.

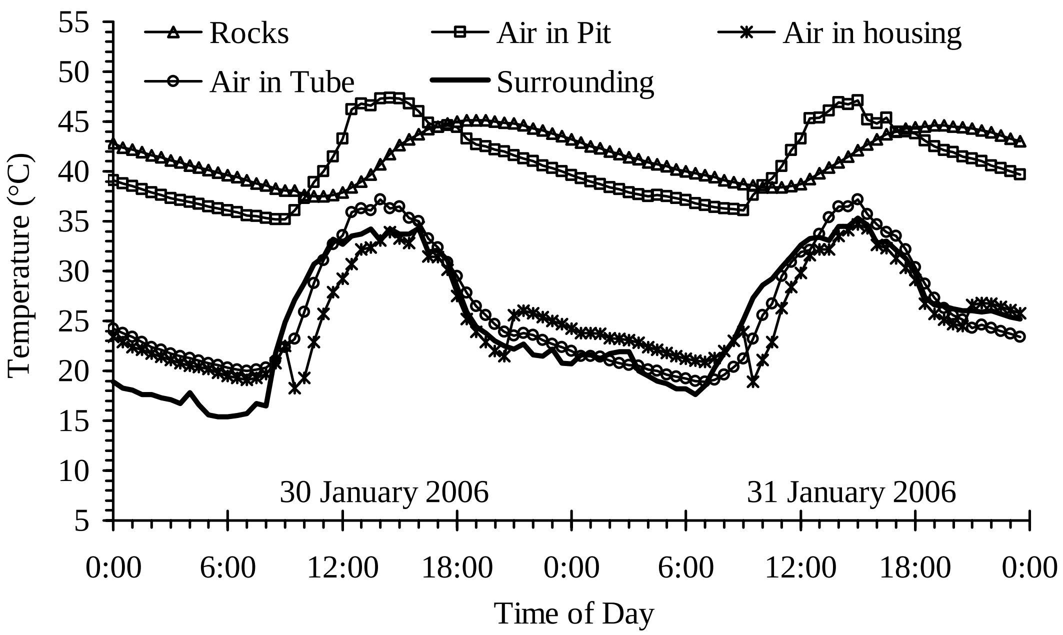

Figure A.28 Temperature as a function of time at January 30-31, 2006 measured from the system using 20.3-cm diameter hot-air tube.

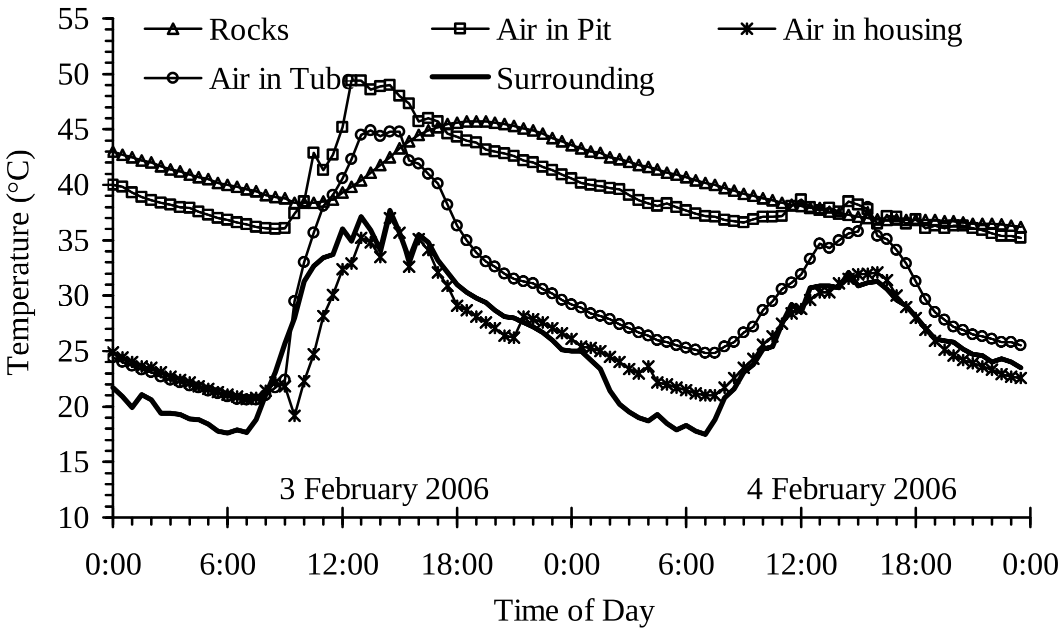

Figure A.29 Temperature as a function of time at February 3-4, 2006 measured from the system using 20.3-cm diameter hot-air tube.

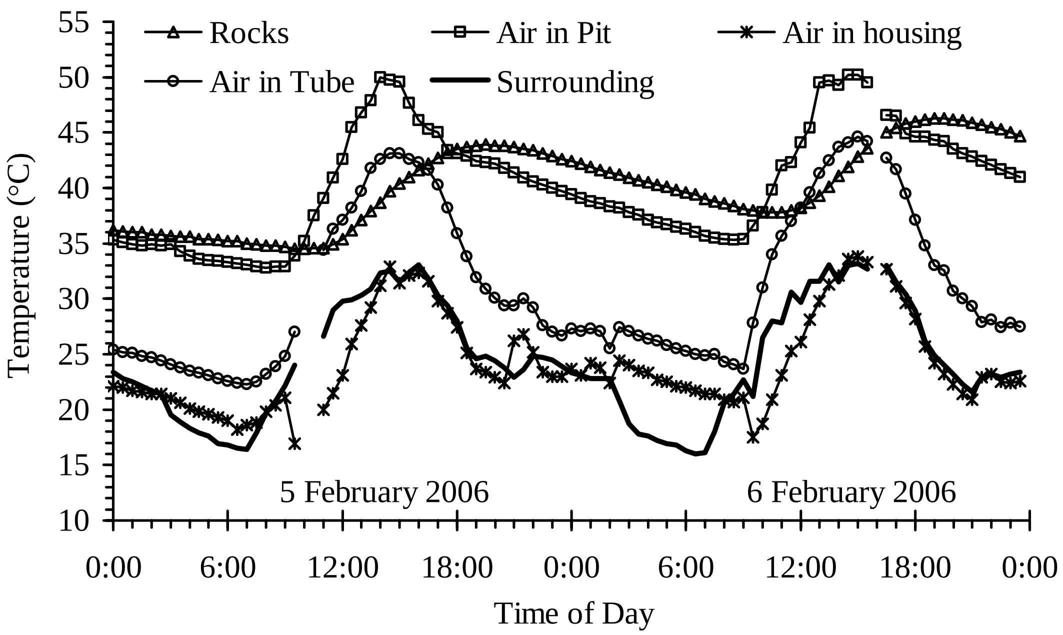

Figure A.30 Temperature as a function of time at February 5-6, 2006 measured from the system using 20.3-cm diameter hot-air tube.

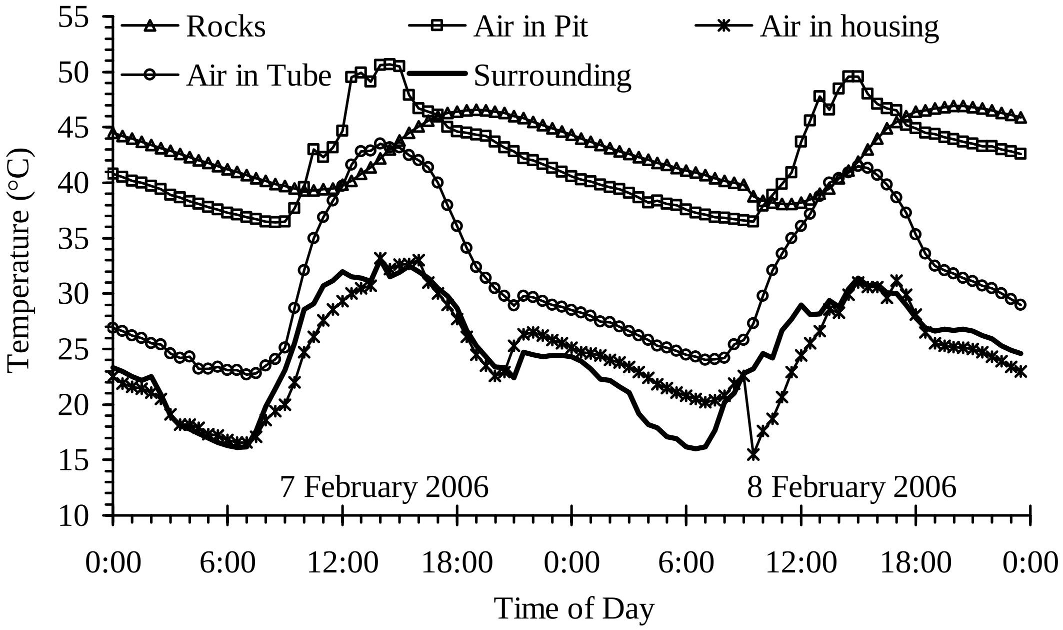

Figure A.31 Temperature as a function of time at February 7-8, 2006 measured from the system using 20.3-cm diameter hot-air tube.

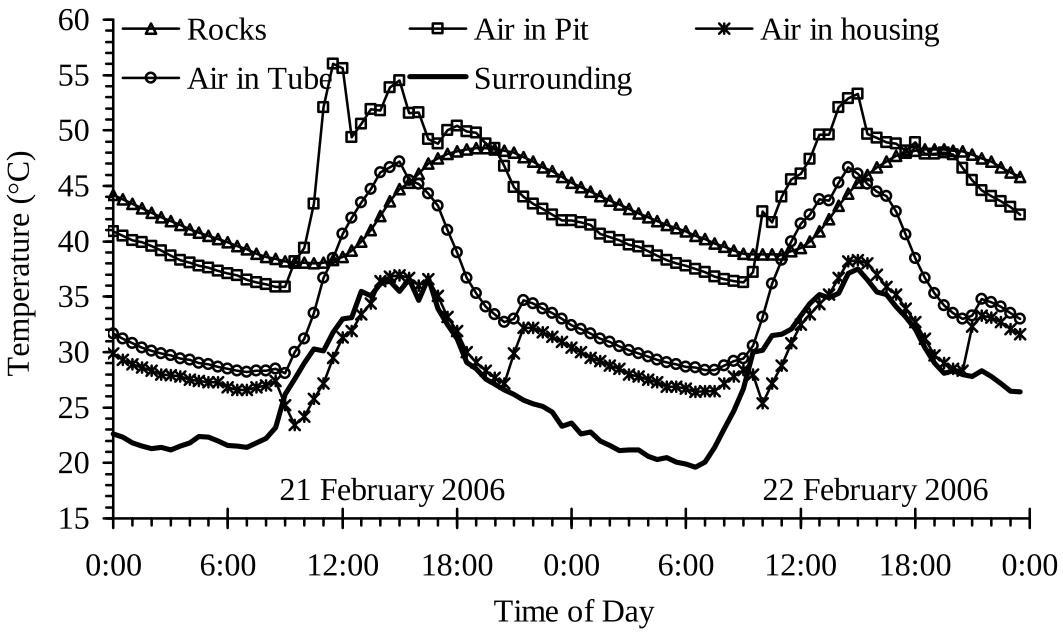

Figure A.32 Temperature as a function of time at February 21-22, 2006 measured from the system using 20.3-cm diameter hot-air tube.

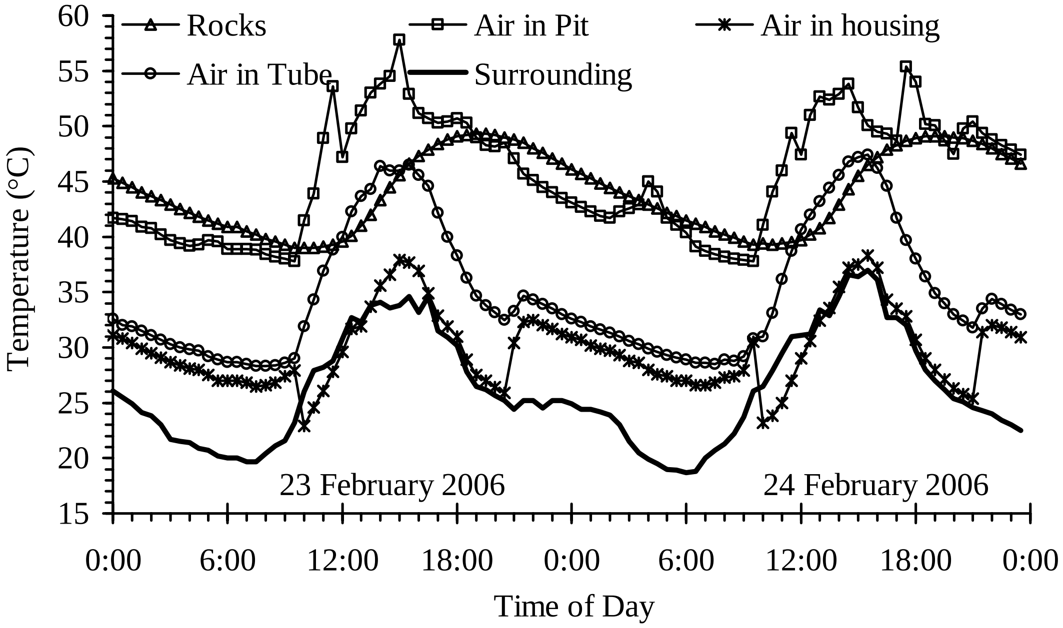

Figure A.33 Temperature as a function of time at February 23-24, 2006 measured from the system using 20.3-cm diameter hot-air tube.

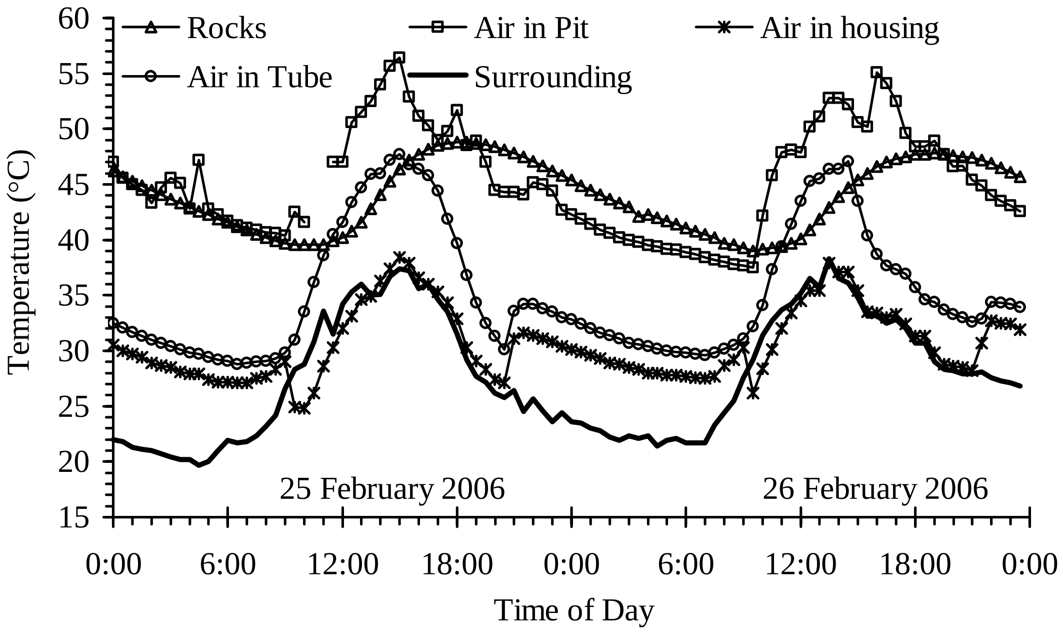

Figure A.34 Temperature as a function of time at February 25-26, 2006 measured from the system using 20.3-cm diameter hot-air tube.

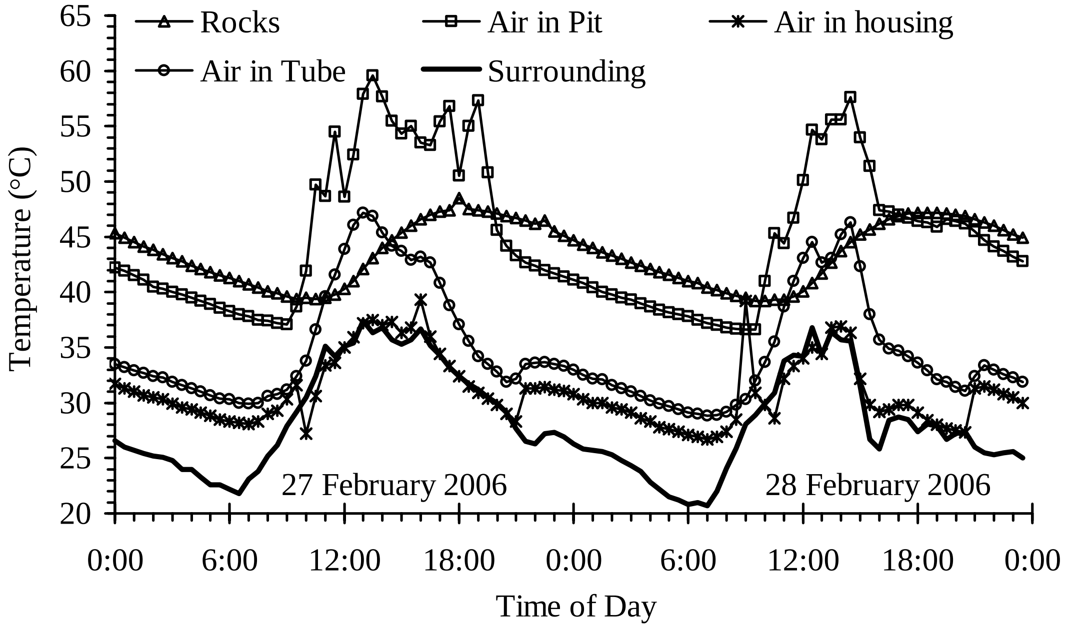

Figure A.35 Temperature as a function of time at February 27-28, 2006 measured from the system using 20.3-cm diameter hot-air tube.

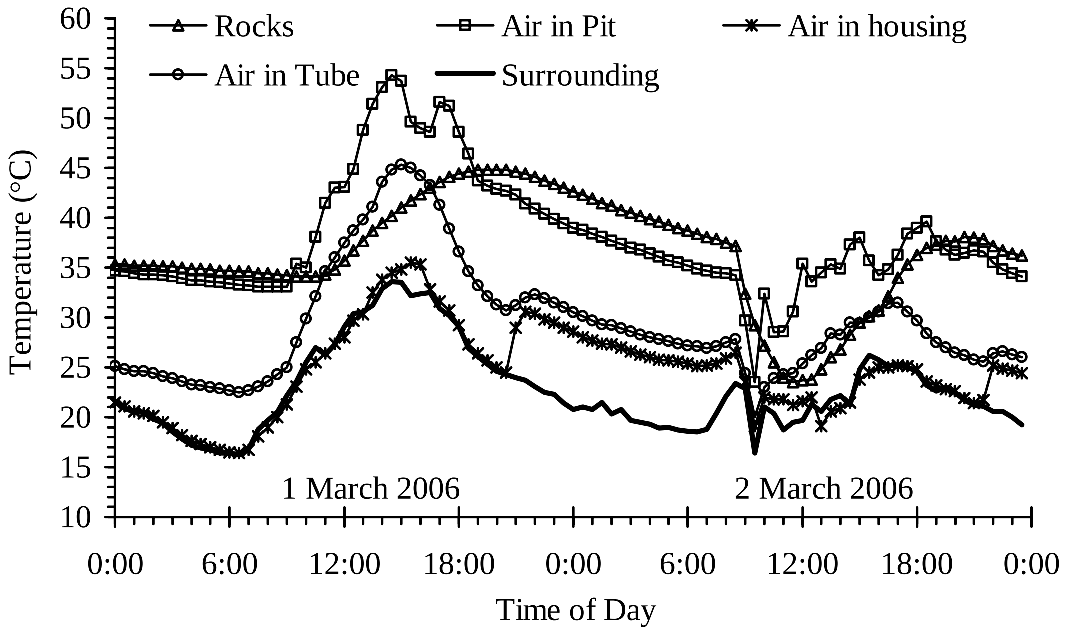

Figure A.36 Temperature as a function of time at March 1-2, 2006 measured from the system using 20.3-cm diameter hot-air tube.

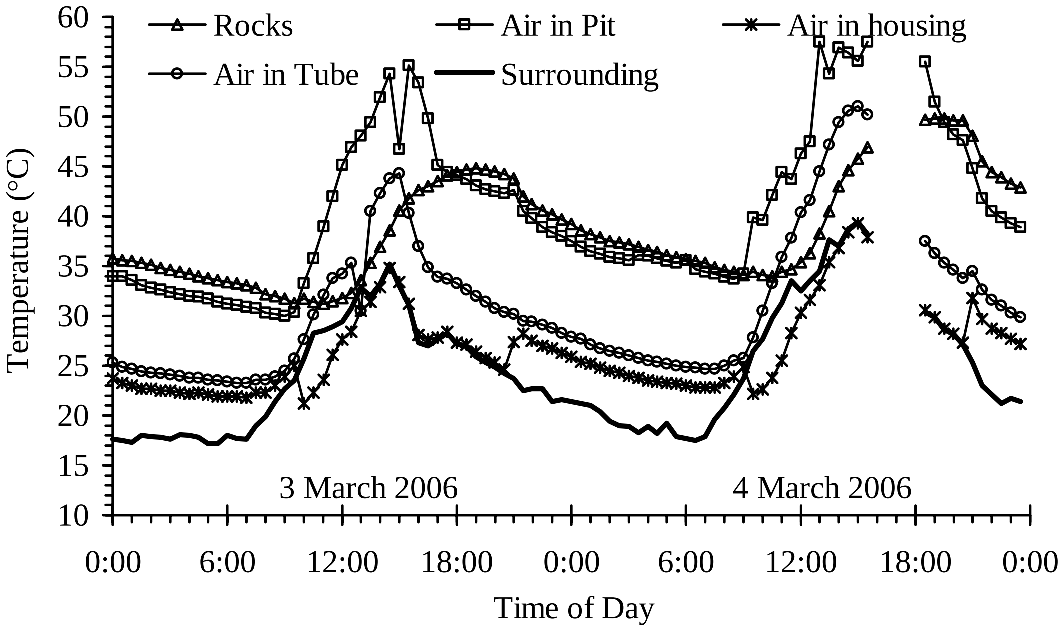

Figure A.37 Temperature as a function of time at March 3-4, 2006 measured from the system using 20.3-cm diameter hot-air tube.

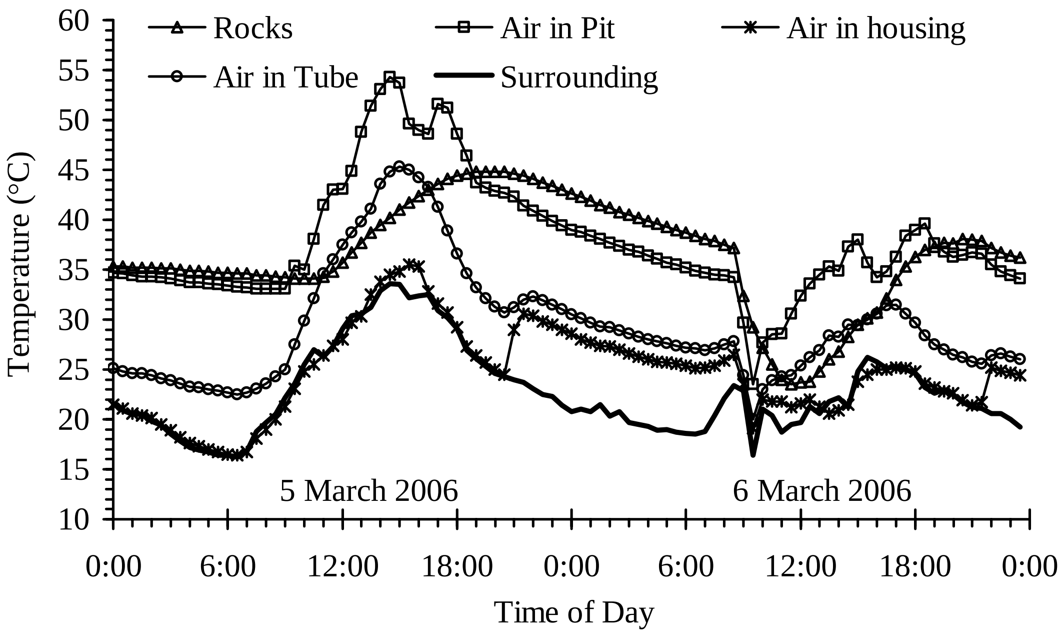

Figure A.38 Temperature as a function of time at March 5-6, 2006 measured from the system using 20.3-cm diameter hot-air tube.

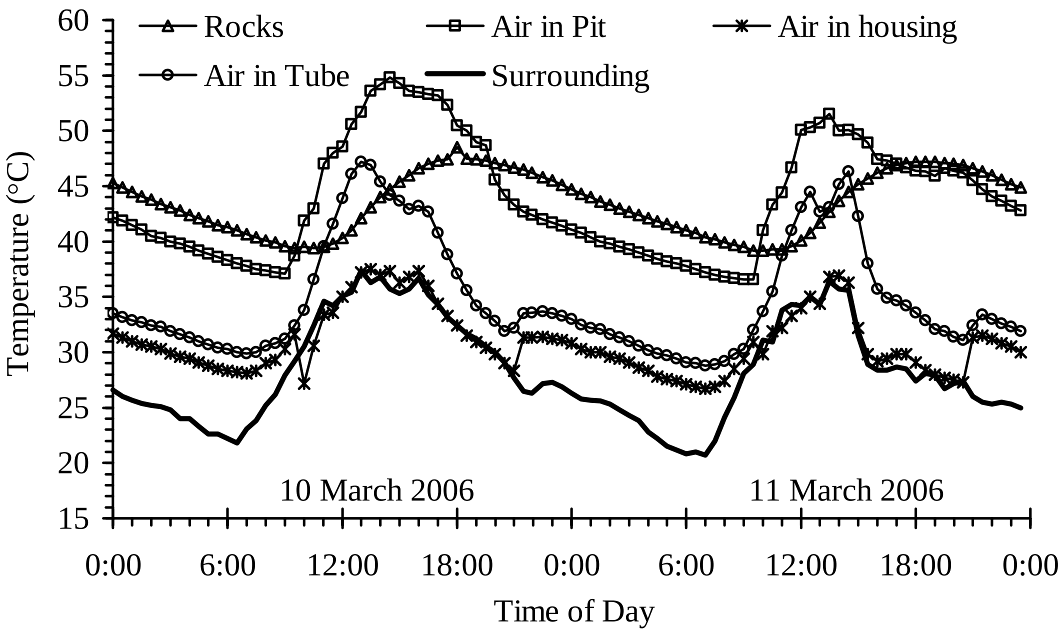

Figure A.39 Temperature as a function of time at March 10-11, 2006 measured from the system using 20.3-cm diameter hot-air tube.

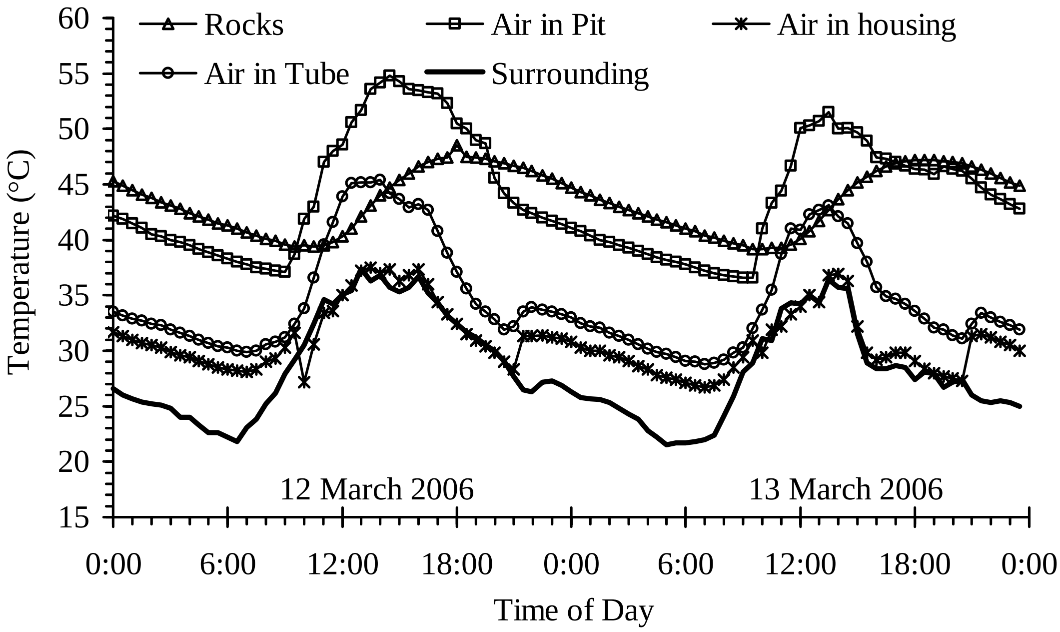

Figure A.40 Temperature as a function of time at March 12-13, 2006 measured from the system using 20.3-cm diameter hot-air tube.

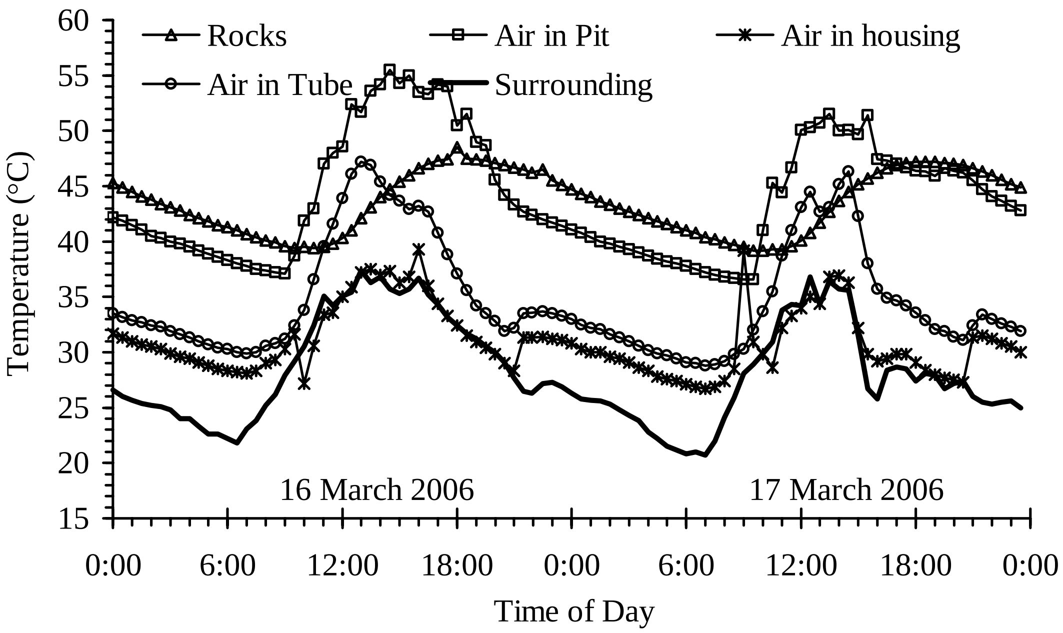

Figure A.41 Temperature as a function of time at March 16-17, 2006 measured from the system using 20.3-cm diameter hot-air tube.

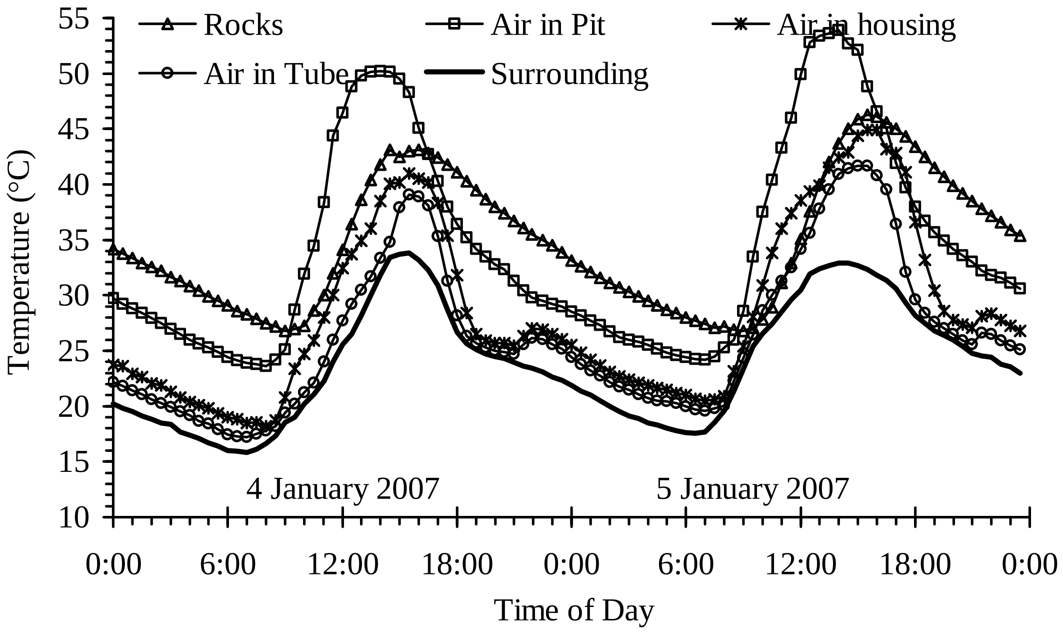

Figure A.42 Temperature as a function of time at January 4-5, 2007 measured from the system using 20.3-cm diameter hot-air tube and 347-kg rocks.

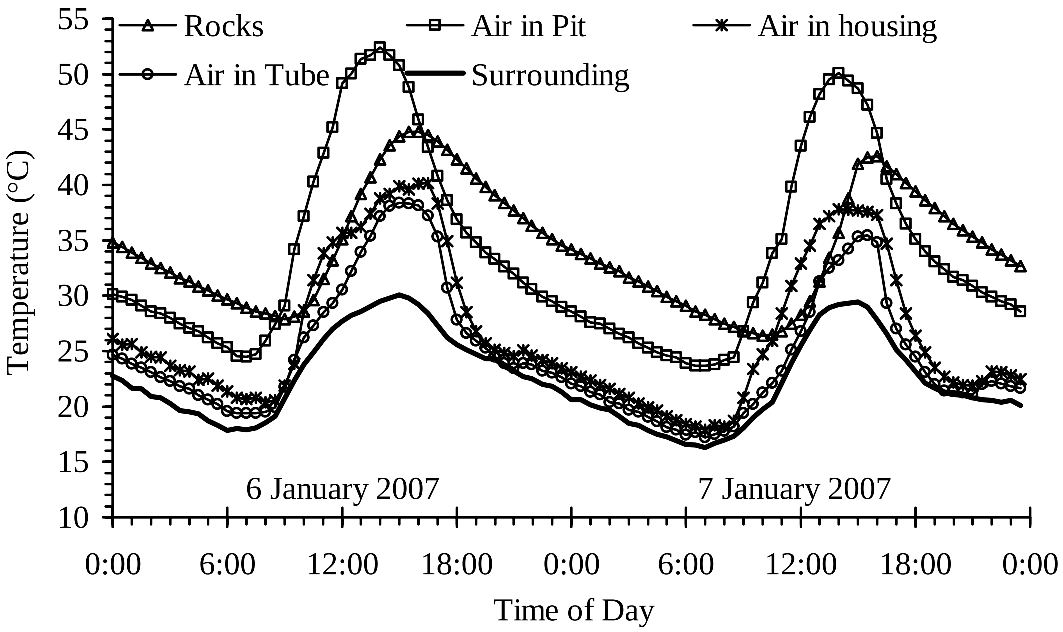

Figure A.43 Temperature as a function of time at January 6-7, 2007 measured from the system using 20.3-cm diameter hot-air tube and 347-kg rocks.

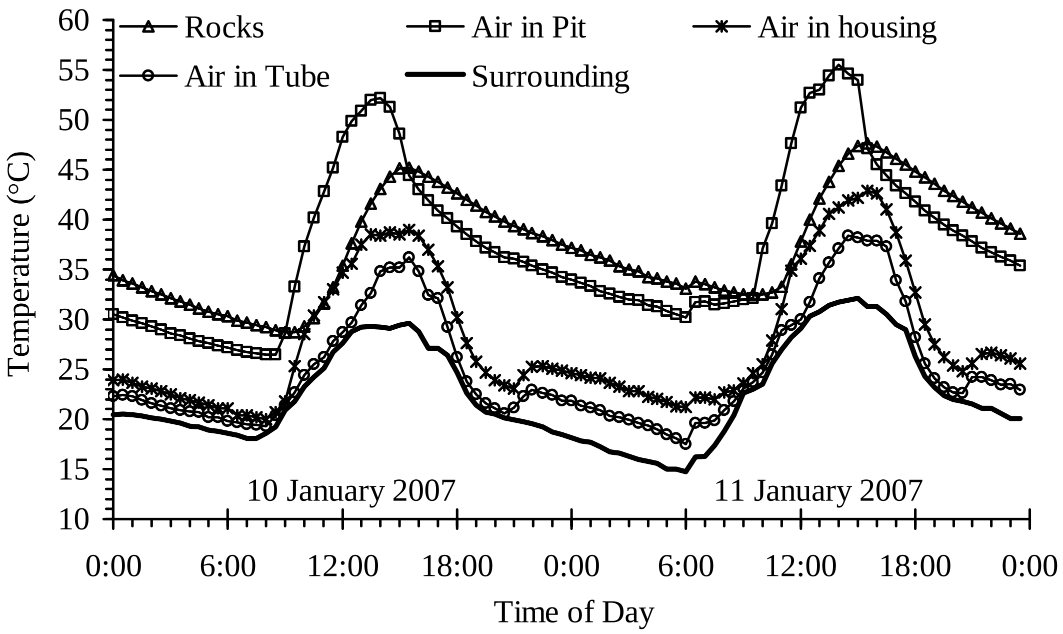

Figure A.44 Temperature as a function of time at January 10-11, 2007 measured from the system using 20.3-cm diameter hot-air tube and 347-kg rocks.

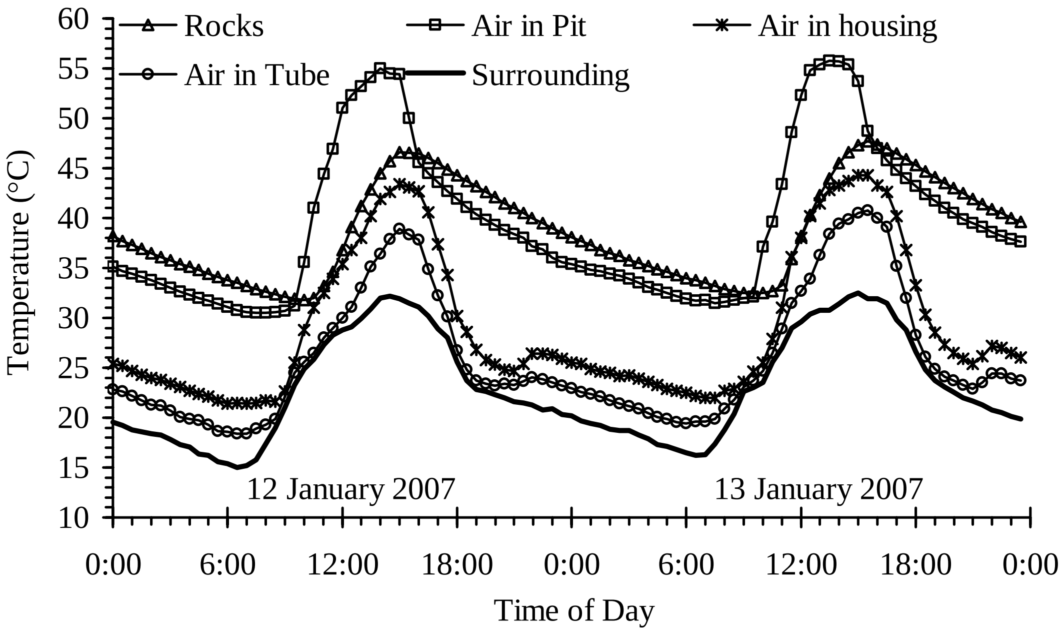

Figure A.45 Temperature as a function of time at January 12-13, 2007 measured from the system using 20.3-cm diameter hot-air tube and 347-kg rocks.

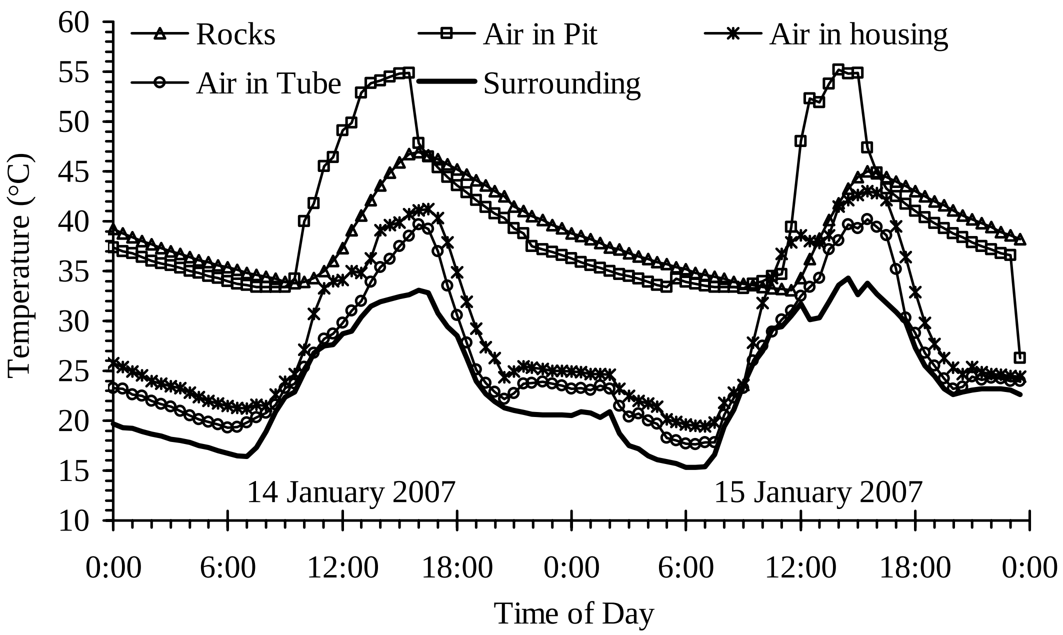

Figure A.46 Temperature as a function of time at January 14-15, 2007 measured from the system using 20.3-cm diameter hot-air tube and 347-kg rocks.

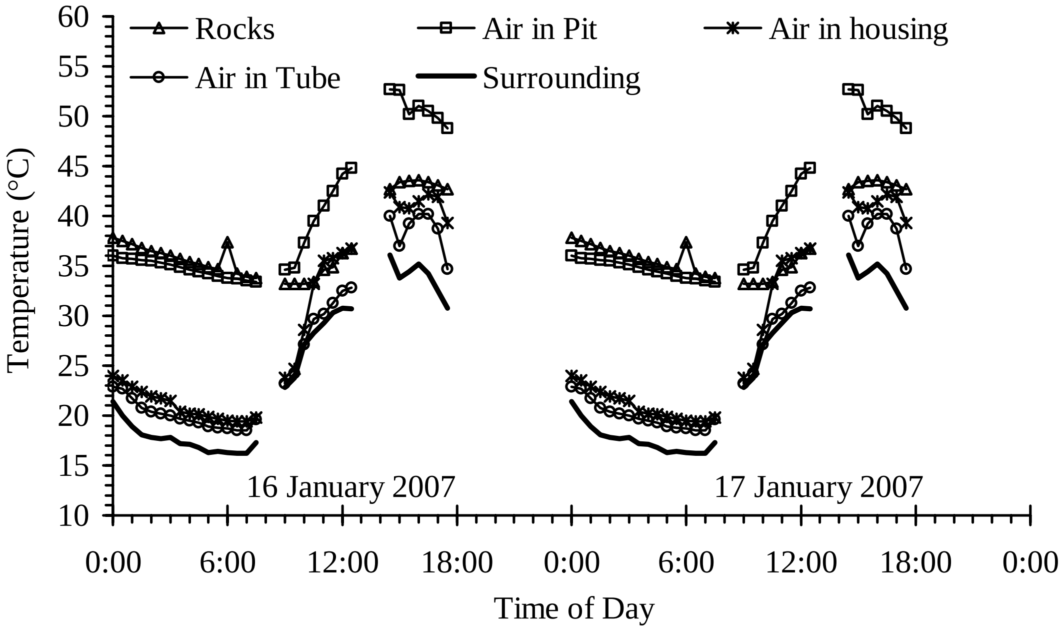

Figure A.47 Temperature as a function of time at January 16-17, 2007 measured from the system using 20.3-cm diameter hot-air tube and 347-kg rocks.

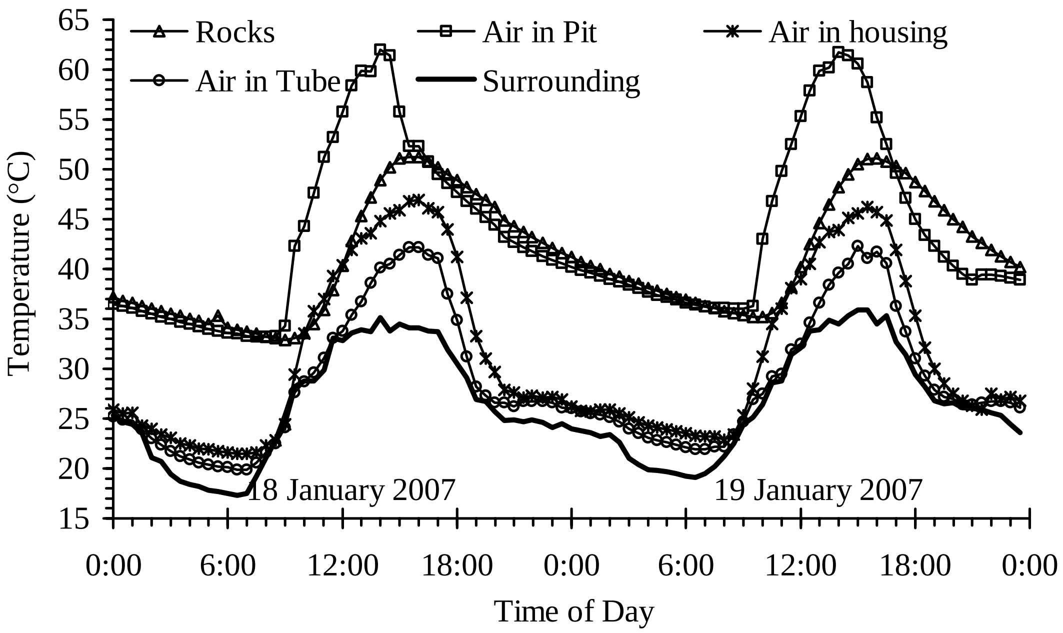

Figure A.48 Temperature as a function of time at January 18-19, 2007 measured from the system using 20.3-cm diameter hot-air tube and 347-kg rocks.

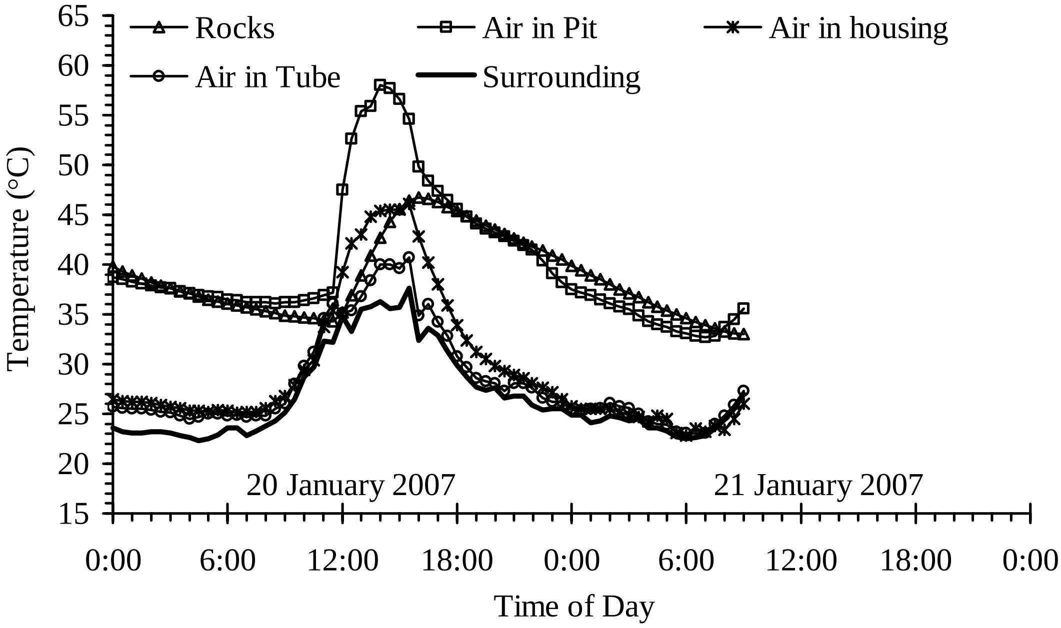

Figure A.49 Temperature as a function of time at January 20-21, 2007 measured from the system using 20.3-cm diameter hot-air tube and 347-kg rocks.

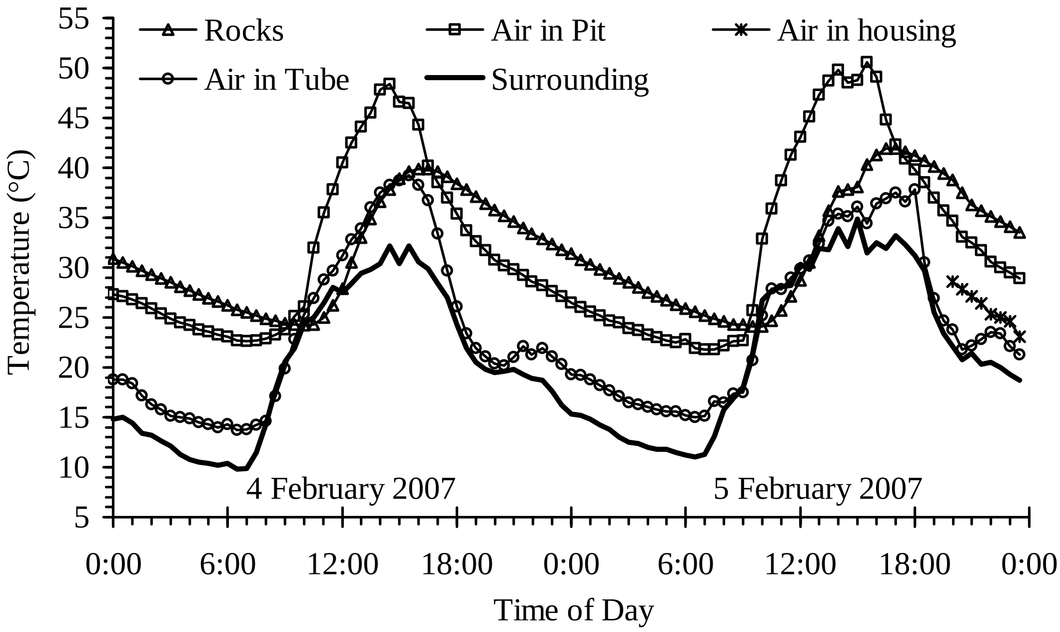

Figure A.50 Temperature as a function of time at February 4-5, 2007 measured from the system using 0.6×0.6 m cross-sectional area vent and 347-kg rocks.

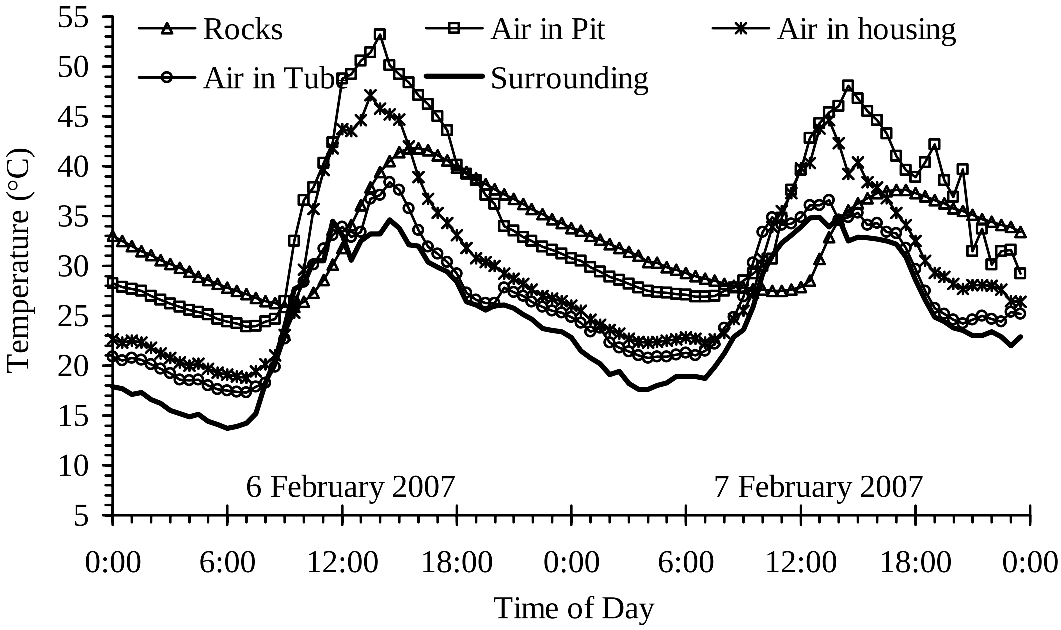

Figure A.51 Temperature as a function of time at February 6-7, 2007 measured from the system using 0.6×0.6 m cross-sectional area vent and 347-kg rocks.

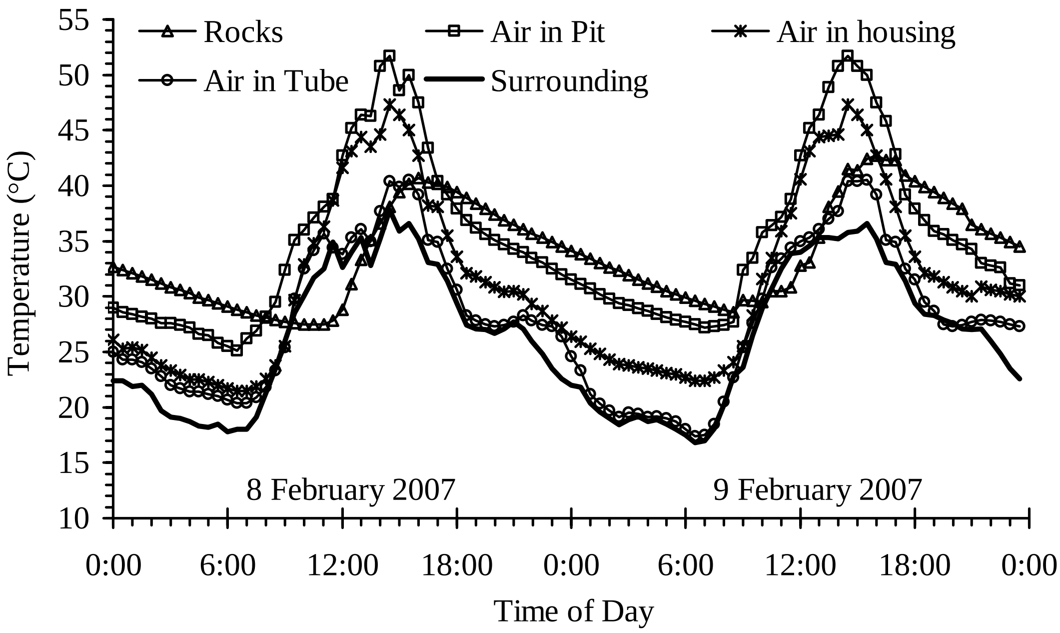

Figure A.52 Temperature as a function of time at February 8-9, 2007 measured from the system using 0.6×0.6 m cross-sectional area vent and 347-kg rocks.

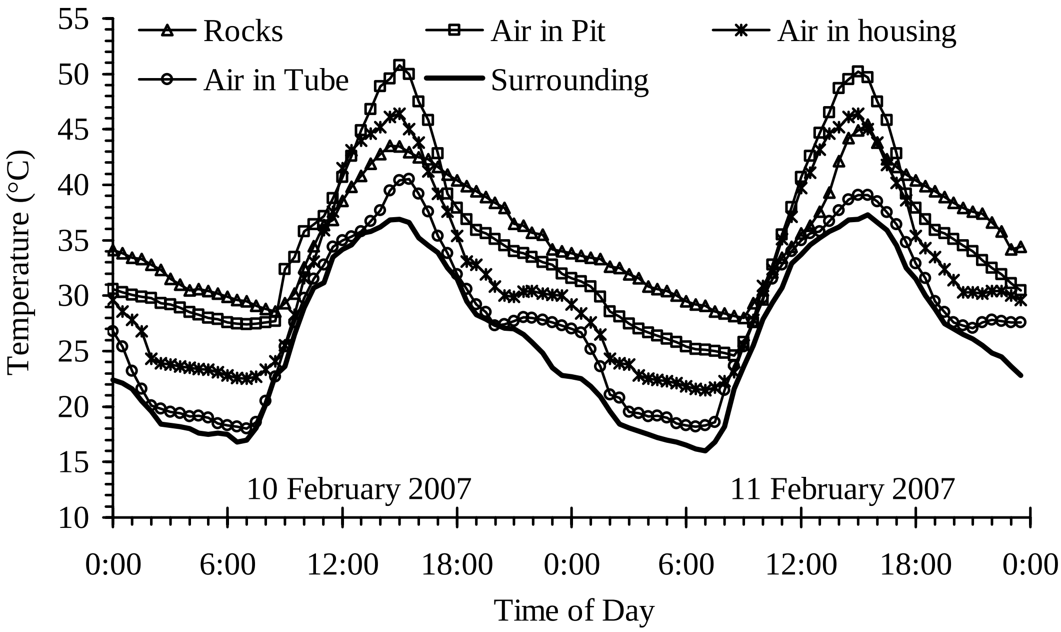

Figure A.53 Temperature as a function of time at February 10-11, 2007 measured from the system using 0.6×0.6 m cross-sectional area vent and 347-kg rocks.

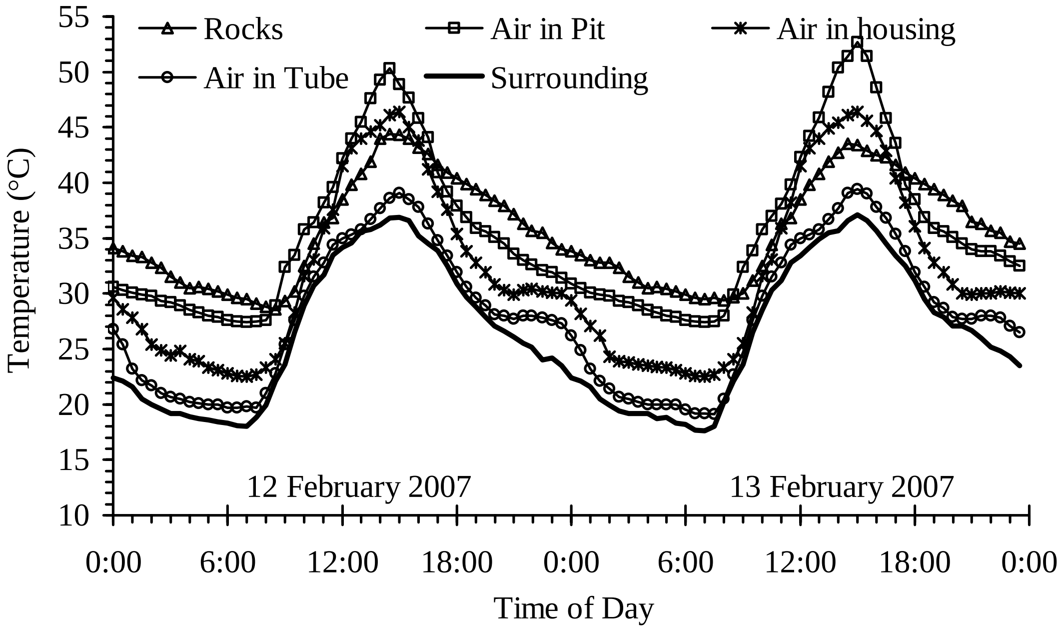

Figure A.54 Temperature as a function of time at February 12-13, 2007 measured from the system using 0.6×0.6 m cross-sectional area vent and 347-kg rocks.

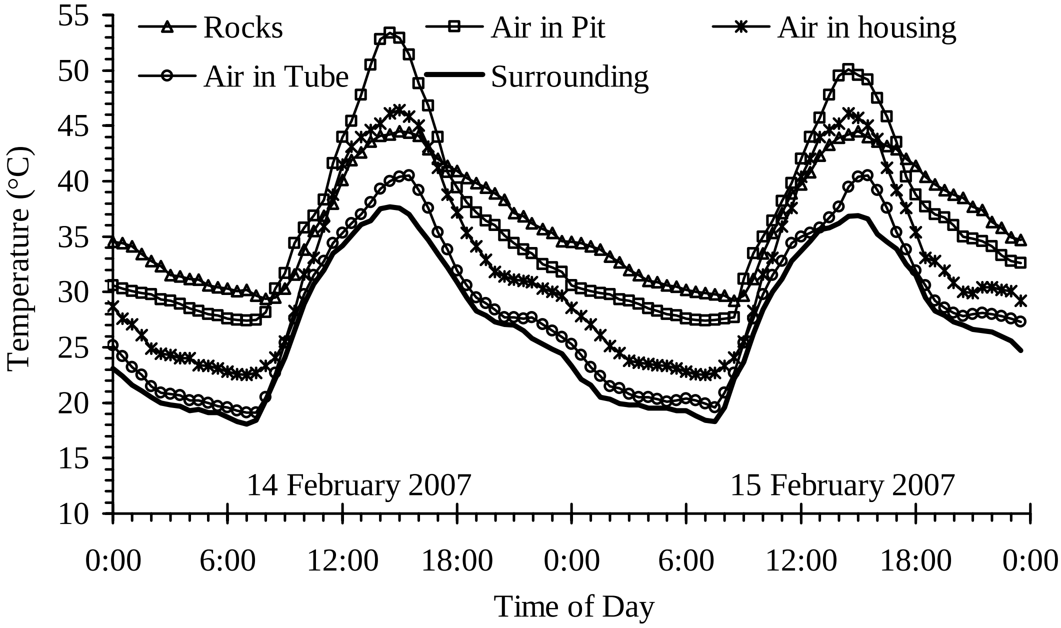

Figure A.55 Temperature as a function of time at February 14-15, 2007 measured from the system using 0.6×0.6 m cross-sectional area vent and 347-kg rocks.

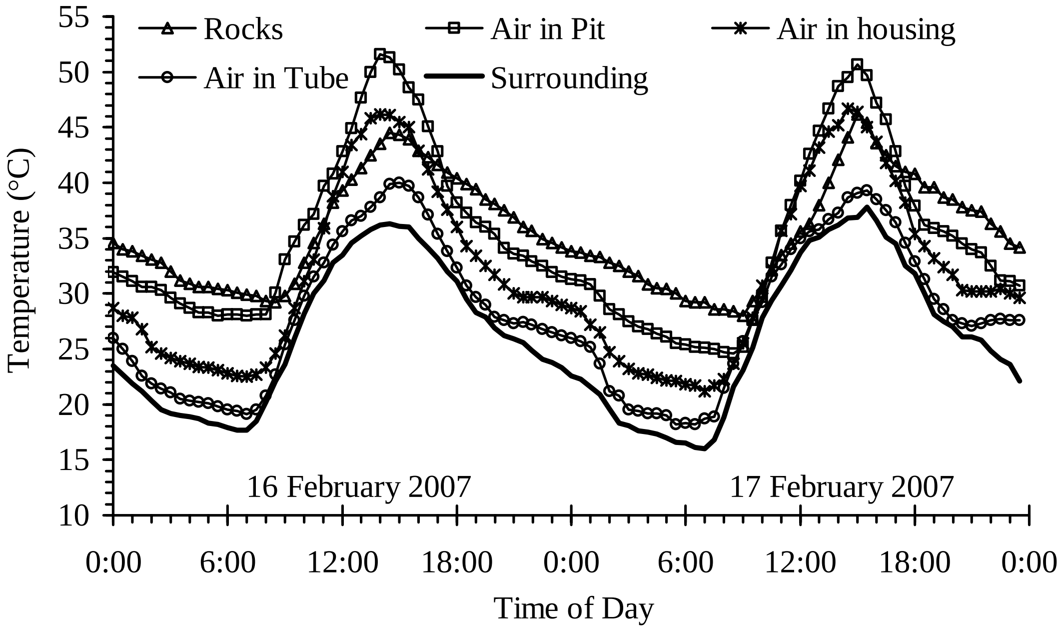

Figure A.56 Temperature as a function of time at February 16-17, 2007 measured from the system using 0.6×0.6 m cross-sectional area vent and 347-kg rocks.

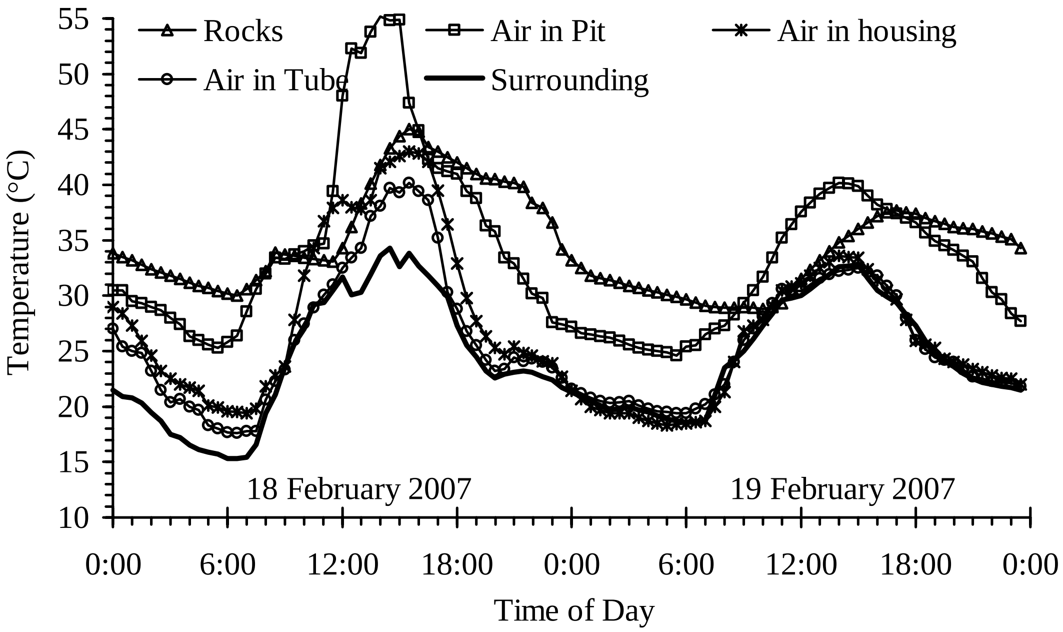

Figure A.57 Temperature as a function of time at February 18-19, 2007 measured from the system using 0.6×0.6 m cross-sectional area vent and 347-kg rocks.

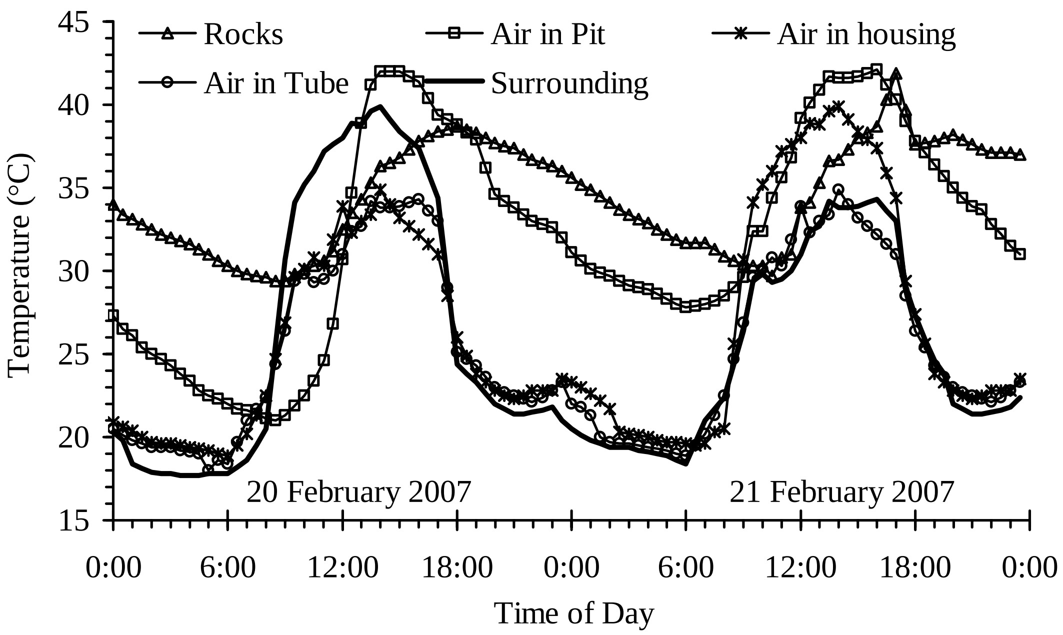

Figure A.58 Temperature as a function of time at February 20-21, 2007 measured from the system using 0.6×0.6 m cross-sectional area vent and 347-kg rocks.

APPENDIX B

SOURCE CODE ON MATLAB 7.0 USING FOR

MATHEMATICAL CALCULATION

```
clear all;
%-----INPUT DATA PROCESS-----%
%Temperature of environment and soil mass
%time   envi    soil
data =[
5.0    10.93   28.80
5.5    10.57   28.65
6.0    10.39   28.50
6.5    10.39   28.46
7.0    10.70   28.42
7.5    11.56   28.61
8.0    12.83   28.80
8.5    14.29   29.06
9.0    15.92   29.32
9.5    17.45   29.57
10.0   18.80   29.80
10.5   19.98   30.05
11.0   21.27   30.26
11.5   22.54   30.54
12.0   23.90   30.81
12.5   25.08   31.05
13.0   25.90   31.30
13.5   26.44   31.60
14.0   26.89   31.90
14.5   27.17   32.14
15.0   27.26   32.30
15.5   27.12   32.35
16.0   26.80   32.40
16.5   26.03   32.30
17.0   25.08   32.20
17.5   23.90   32.05
18.0   22.54   31.90
18.5   21.30   31.80
19.0   20.20   31.70
19.5   19.27   31.54
20.0   18.46   31.38
20.5   17.55   31.23
21.0   16.96   31.08
21.5   16.24   30.93
22.0   15.60   30.77
22.5   15.10   30.64
23.0   14.60   30.50
23.5   14.33   30.37
24.0   13.97   30.23
24.5   13.70   30.09
25.0   13.40   29.94
25.5   13.10   29.79
```

```
26.0   12.80   29.63
26.5   12.50   29.50
27.0   12.20   29.37
27.5   11.90   29.24
28.0   11.60   29.10
28.5   11.45   28.95
29.0   11.30   28.80
];
ndat1=49;

%SOLAR RADIATION (HEAT FLUX) DATA
solar=[
%t  Heat flux
5        0.0000
6        19.510
7        133.68
8        258.40
9        364.91
10       450.80
11       495.99
12       493.82
13       446.20
14       361.90
15       256.52
16       147.79
17       51.760
18       0.0000
19       0.0000
23       0.0000
];
ndat2=16;

%AIR PROPERTIES
air=[
% Temp  density    nu       Pr
250   1.413   1.14e-5    0.724
280   1.271   1.40e-5    0.717
290   1.224   1.48e-5    0.714
298   1.186   1.55e-5    0.712
300   1.177   1.57e-5    0.712
310   1.143   1.67e-5    0.711
320   1.110   1.77e-5    0.710
330   1.076   1.86e-5    0.708
340   1.043   1.96e-5    0.707
350   1.009   2.06e-5    0.706
];
ndat3=10;
```

```
%PROCESS DATA%
for n=1:ndat1
   t1(n)=data(n,1);
   Tenvi(n)=data(n,2);
   Tsoil(n)=data(n,3);
end

for n=1:ndat2
   St(n)=solar(n,1);
   Sheat(n)=solar(n,2);
end

for n=1:ndat3
   aTemp(n)=air(n,1);
   aDen(n)=air(n,2);
   anu(n)=air(n,3);
   aPr(n)=air(n,4);
end

%INPUT CONSTANT PROPERTIES
Cpr=1174.38;            %Heat capacity of rock (J/kg.K)
Cpc=1014.0;             %Heat capacity of air in pit (J/kg.K)
Cph=1014.0;             %Heat capacity of air in housing model (J/kg.K)
g=9.807;                %Acceleration (m/s^2)
k=0.0268;               %Thermal conductivity of air (W/m.K)
rho_a=1.2;              %Air density (kg/M^3)

%ROCK IN STORAGE SYSTEM CHARECTERISTIC
Mr=11560.5;             %Weight of rock fragments (kg)
Deff=0.08;              %Effective diameter of rock (m)
fab=0.99;               %Assumed correction factor
Ar_top=16.0;            %Collector area (top face, m^2)
Ar=302.95;              %Total surface of all pieces of rock fragments (m^2)
Aradc=23.88;            %Total area of rock fill radiate to the air in pit (5 plane)(m^2)
delta=0.5*pi()*Deff;    %Delta of rock using to calculate value of Nu
sigma=5.669e-8;         %Stefan-Boltzmann constant
epsi=0.8;               %Rock emissivity
alphar=0.8;             %Rock Absorbtion coefficient

%ACRYLIC SHEET PROPERTY
ka=0.2;                         %Thermal conductivity (W/m.K)
delta_a=(4.0*4.0)/4/4.0;        %delta =Area/Perimeter
thick=0.003;                    %plate thickness (m)
Atop=4.0*4.0;                   %Top plate area (m^2)
```

```
%PIT CHARACTERISTIC
Cwide=4.00;                              %Pit Length: Square (m)
Chigh=0.99;                              %Pit Depth (m)
delta_c=(Chigh*Cwide)/2/(Chigh+Cwide);   %delta =Area/Perimeter
Acham=4*(Chigh*Cwide);                   %chamber face area 4 side-plane
Mc=rho_a*Cwide*Cwide*Chigh;              %Mass of air in chamber

%HOUSING MODEL CHARECTERISTIC
Hwide=3.0000;                       % House dimension, WxLxH (m)
Hlong=3.0000;
Hhigh=3.5000;
Volh= Hwide * Hlong * Hhigh ;       %Housing volume (m^3)
Ar_toph=2*Hhigh*(Hwide+Hlong);      %House side surface area (m^2)
hh=4.35;                            %Heat transfer coefficient
UA3=hh*Ar_toph;                     %Overall heat transfer coefficient (W/m^2.K)
Mh=rho_a*Volh;                      %Mass of air in housing (kg)

%HOT-TUBE CHARACTERISTIC
CD=0.65;                  %discharge coefficient
L=4;                      %pipe long (m)
H=4;                      %pipe high
Pdim=0.3000;              %Pipe diameter (m)
Ap=pi()/4*Pdim^2;         %pipe cross section area (m^2)

%TIME INTERVAL
dt=5;                     %dt in seconds
tall=16;                  %tall in hours
tstart=5;                 %Starting time for calculations
lass=tall*3600/dt;
time(1)=tstart;

%INITIAL TEMPERATURE%
Tr(1)=26.65;
Tc(1)=24.43;
%Tr(1)=36;
%Tc(1)=32;
Th(1)=interp1(t1,Tenvi,tstart);

%-----CALCULATON PROCESS-----%

%DAYTIME CALCULATION%
for i=1:lass;
   Tsur = interp1(t1,Tenvi,time(i));   % interpolate surround temp @time
   Tgnd = interp1(t1,Tsoil,time(i));   % interpolate ground temp @time

  %Convective heat transfer from rocks to the air in pit
   Tf=(Tc(i)+Tr(i))/2+273  ;
```

```
    beta_r=1/(Tf);
    Pr_r = interp1(aTemp,aPr,Tf);
    nu_r = interp1(aTemp,anu,Tf);
    Ra_r=g*beta_r*(Tr(i)-Tc(i))*delta^3*Pr_r/nu_r^2;
    Ra_r=abs(Ra_r);
    Nu_r=2+0.589*Ra_r^0.25/( 1+(0.469/Pr_r)^(9/16))^(4/9);
    hrc=k*Nu_r/delta; % h of rock-air

    %Convective heat transfer calculation of side chamber face
    beta_c=1/Tc(i);
    Pr_c = interp1(aTemp,aPr,Tc(i)+273);
    nu_c = interp1(aTemp,anu,Tc(i)+273);
    Ra_c=g*beta_c*(Tc(i)-Tgnd)*delta_c^3*Pr_c/nu_c^2;
    Ra_c=abs(Ra_c);
    Nu_c=0.59*Ra_c^(1/4);
    hic=k*Nu_c/delta_c;  % h of air-soil
    UA2=hic*Acham;

    %Convective heat transfer calculation on the top pit
    Ra_a=g*beta_c*(Tc(i)-Tsur)*delta_a^3*Pr_c/nu_c^2;
    Ra_a=abs(Ra_c);
    Nu_a=0.27*Ra_c^(1/4);
    hi=k*Nu_a/delta_a;
    Ua=1/(1/hi+thick/ka);
    UA1=Ua*Atop;

    rho=101300/287/(Tc(i)+273);                %air density in chamber
                                               %Mp=rho*L*Ap;  %mass in pipe
    Is = interp1(St,Sheat,time(i));            % interpolate solar heat flux @time

    Th(i+1)=Tsur;                              %set house temp. = surround
    loss_cs=UA1*(Tc(i)-Tsur);                  % loss from chamber to  surround
    loss_cg=UA2*(Tc(i)-Tgnd);                  % loss from chamber to  ground
                                               %loss_cg=0;
    rad_rs=sigma*epsi*+Ar_top*((Tr(i)+273)^4-(Tsur+273)^4); %radiation from
                                                             rock to surround
                                                             (loss)
    rad_rc=sigma*epsi*Aradc*((Tr(i)+273)^4-(Tc(i)+273)^4);    %radiation from rock
                                                             to chamber

    %....Calculate 2 major equations .......%
    Tr(i+1)=Tr(i)+dt/Mr/Cpr*(alphar*Is*Ar_top-hrc*Ar*(Tr(i)-Tc(i))-rad_rs-rad_rc);
    Tc(i+1)=Tc(i)+dt/Mc/Cpc*(fab*(1-alphar)*Is*Ar_top+hrc*Ar*(Tr(i)-
Tc(i))+rad_rc-loss_cs-loss_cg) ;

    Tc(i+1)=(Tc(i+1)+Tc(i))/2; % average temp from 2 time step for reduce
discontinuity
```

```
        time(i+1)=time(i)+(dt/3600); % set next time step
    end
%END OF DAYTIME CALCULATION%


%NIGHTTIME CALCULATION%

for i=lass:lass+8*3600/dt-1;

    Tsur = interp1(t1,Tenvi,time(i));
    Tgnd = interp1(t1,Tsoil,time(i));

    Tf=(Tc(i)+Tr(i))/2+273  ;
    beta_r=1/(Tf);
    Pr_r = interp1(aTemp,aPr,Tf);
    nu_r = interp1(aTemp,anu,Tf);
    Ra_r=g*beta_r*(Tr(i)-Tc(i))*delta^3*Pr_r/nu_r^2;
    Ra_r=abs(Ra_r);
    Nu_r=2+0.589*Ra_r^0.25/( 1+(0.469/Pr_r)^(9/16))^(4/9);
    hrc=k*Nu_r/delta; % h of rock-air

    beta_c=1/Tc(i);
    Pr_c = interp1(aTemp,aPr,Tc(i)+273);
    nu_c = interp1(aTemp,anu,Tc(i)+273);
    Ra_c=g*beta_c*(Tc(i)-Tgnd)*delta_c^3*Pr_c/nu_c^2;
    Ra_c=abs(Ra_c);
    Nu_c=0.59*Ra_c^(1/4);
    hic=k*Nu_c/delta_c;  % h of air-soil
    UA2=hic*Acham;

    Ra_a=g*beta_c*(Tc(i)-Tsur)*delta_a^3*Pr_c/nu_c^2;
    Ra_a=abs(Ra_c);
    Nu_a=0.27*Ra_c^(1/4);
    hi=k*Nu_a/delta_a;
    Ua=1/(1/hi+thick/ka);
    UA1=Ua*Atop;

    rho=101300/287/(Tc(i)+273);  %air density in chamber
    %Mp=rho*L*Ap;  %mass in pipe


    loss_cs=UA1*(Tc(i)-Tsur);     % Loss from chamber to surrounding
    loss_cg=UA2*(Tc(i)-Tgnd);     % Loss from chamber to ground

    rad_rs=sigma*epsi*+Ar_top*((Tr(i)+273)^4-(Tsur+273)^4);   %radiation from
rock to surround (loss)
```

```
    rad_rc=sigma*epsi*Aradc*((Tr(i)+273)^4-(Tc(i)+273)^4);    %radiation from rock
to chamber

    mdot=rho*CD*Ap*(2*g*H*(Tc(i)-Th(i))/Tc(i))^.5;

    %....Calculate 2 major equation .......%
    Tr(i+1)=Tr(i) +dt/Mr/Cpr*( -hrc*Ar*(Tr(i)-Tc(i))-rad_rc );
    Tc(i+1)=Tc(i) +dt/Mc/Cpc*( hrc*Ar*(Tr(i)-Tc(i))+rad_rc-mdot*Cpc*(Tc(i)-Th(i))-
loss_cs-loss_cg );
    Tc(i+1)=(Tc(i+1)+Tc(i))/2;
    Th(i+1)=Th(i) +dt/Mh/Cph*( mdot*Cpc*(Tc(i)-Th(i)) -UA3*(Th(i)-Tsur)-
0.4*mdot*Cpc*(Tc(i)-Th(i)) );
    %Th(i+1)=(Th(i+1)+Th(i))/2;

    time(i+1)=time(i)+(dt/3600);

end


%-----PLOTTING PROCESS-----%
%plotyy(time,Tc,St,Sheat);
plot(time,Tr,'-k',time,Tc,'-.k',time,Th,'--k','LineWidth',2);
%grid on;
xlabel('Time (hr)');
ylabel('Temperature (Celsius)');
title('Thermodynaics analysis of Rock Bed');
text(14,1.5,'This Text start at point (14,1.5)');
%legend('Rock','Chamber','House',0);
hold on;
plot(t1,Tenvi,'-k','LineWidth',2);
text(14,1.5,'This Text start at point (14,1.5)');
```

APPENDIX C

LIST OF PUBLICATIONS

Article in Journal (1)

[1] Phueakphum, D. Sri-In T., and Fuenkajorn, K. (2008). **Strength and stiffness of claystone specimens tested with neoprene capping**, *Research and Development Journal*, Volume 19, No. 4, pp. 1 – 7.

Article in Conference Proceedings (7)

[1] Phueakphum, D. and Fuenkajorn, K. (2009). **Effects of cyclic loading on mechanical properties of Maha Sarakham salt**, In *Proceedings of the Second Thailand Symposium on Rock Mechanics (ThaiRock 2009)*, Jomtien Palm Beach Hotel & Resort, Chonburi, 12-13 March 2009, pp. 107 – 120.

[2] Intaraprasit, C., Phueakphum, D., Tepnarong, P. and Fuenkajorn, K. (2009). **Modified point load testing of volcanic rocks from Chartree gold mine**, In *Proceedings of the Second Thailand Symposium on Rock Mechanics (ThaiRock 2009)*, Jomtien Palm Beach Hotel & Resort, Chonburi, 12-13 March 2009, pp. 309 – 318.

[3] Phueakphum, D. and Fuenkajorn, K. (2009). **Effects of cyclic loading on mechanical properties of salt**, In *Proceedings of International Symposium on Rock Mechanics "Rock Characterization, Modelling and Engineering Design Methods"*, The University of Hong Kong, 19-22 May 2009.

[4] Kensakoo, T., Phueakphum, D. and Fuenkajorn, K. (2007). **Mechanical properties of Maha Sarakham salt as affected by inclusions**, In *Proceedings of the First Thailand Symposium on Rock Mechanics (ThaiRock 2007)*, The Greenery Resort, Khao Yai, 13-14 September 2007, pp. 103 – 117.

[5] Phueakphum, D. and Sri-In T. (2007). **End effect on strength and stiffness of Maha Sarakham siltstone specimens**, In *Proceedings of the First Thailand Symposium on Rock Mechanics (ThaiRock 2007)*, The Greenery Resort, Khao Yai, 13-14 September 2007, pp. 161 – 169.

[6] Phueakphum, D. and Fuenkajorn, K. (2006). **Experimental Assessment of Solar Thermal Energy Storage in Rock Fills**, In *Proceedings of the Second Conference on Energy Technology Network of Thailand; E-NETT*, Suranaree University of Technology, Nakhon Ratchasima, July 27-29, 2006

[7] Fuenkajorn, K., Phueakphum, D. and Jandakaew, M. (2003). **Healing of Rock Salt Fractures**, In *Proceedings of the 38th Symposium on Engineering Geology and Geotechnical engineering*, University of Nevada, Reno, Nevada, March 19-21, pp. 393-408.

BIOGRAPHY

Mr. Decho Phueakphum was born on the 7th of June 1977 in Surat Thani province. He earned his Bachelor's degree in Engineering (Civil Engineering) in 1999 and Master's degree in Engineering (Geological Engineering) in 2003 from Suranaree University of Technology (SUT). He continued with his Doctor's degree in the School of Geotechnology, Institute of Engineering, SUT with the major in Geological Engineering. During his graduate studies, he was a research assistant and special lecturer at SUT. In 2009, he has published thee technical papers, two papers at the Proceeding of the Second Thailand Symposium on Rock Mechanics (ThaiRock 2009), Jomtien Palm Beach Hotel & Resort, Chonburi, March 12-13; 1) Effects of cyclic loading on mechanical properties of Maha Sarakham salt and 2) Modified point load testing of volcanic rocks from Chartree gold mine, and the other at Proceedings of International Symposium on Rock Mechanics "Rock Characterization, Modelling and Engineering Design Methods", The University of Hong Kong, May 19-22; Effects of cyclic loading on mechanical properties of salt. In 2007, he has published two technical papers at the Proceeding of the First Thailand Symposium on Rock Mechanics, The Greenery Resort, Khao Yai, September 13-14; 1) End effect on strength and stiffness of Maha Sarakham siltstone specimens and 2) Mechanical properties of Maha Sarakham salt as affected by inclusions. In 2003, he has published paper at Proceedings of the 38th Symposium on Engineering Geology and Geotechnical engineering, University of Nevada, Reno, Nevada, March 19-21; Healing of Rock Salt Fractures. His expertises are in the areas of soil and rock mechanics, hydrology, and foundation engineering.